https://ntrs.nasa.gov/search.jsp?R=19880020270 2020-03-20T05:15:20+00:00Z

NASW- 4066

STAR not AIAA

MEVTV WORKSHOP ON NATURE AND COMPOSITION OF SURFACE UNITS ON MARS

MEVTV

(NASA-CR-183075) MEVTV WORKSHOP ON NATURE AND COMPOSITION OF SURFACE UNITS ON MARS (Lunar and Planetary Inst.) 148 p CSCL 03B

N88-29654
--THRU--
N88-29703
Unclas
G3/91 0154900

LPI Technical Report Number 88-05

LUNAR AND PLANETARY INSTITUTE 3303 NASA ROAD 1 HOUSTON, TEXAS 77058

MEVTV WORKSHOP ON
NATURE AND COMPOSITION OF SURFACE UNITS ON MARS

Edited by
J. R. Zimbelman, S. C. Solomon, and V. L. Sharpton

December 4–5, 1987

Held at
Napa, California

Sponsored by
Lunar and Planetary Institute
NASA/MEVTV Study Project

Lunar and Planetary Institute 3303 NASA Road 1 Houston, Texas 77058-4399

LPI Technical Report Number 88-05

Compiled in 1988 by the
LUNAR AND PLANETARY INSTITUTE

The Institute is operated by Universities Space Research Association under Contract NASW-4066 with the National Aeronautics and Space Administration.

Material in this document may be copied without restraint for library, abstract service, educational, or personal research purposes; however, republication of any portion requires the written permission of the authors as well as appropriate acknowledgment of this publication.

This report may be cited as:
Zimbelman J. R., Solomon S. C., and Sharpton V. L., eds. (1988) *MEVTV Workshop on Nature and Composition of Surface Units on Mars*. LPI Tech. Rpt. 88-05. Lunar and Planetary Institute, Houston. 144 pp.

Papers in this report may be cited as:
Author A. A. (1988) Title of paper. In *MEVTV Workshop on Nature and Composition of Surface Units on Mars* (J. R. Zimbelman, S. C. Solomon, and V. L. Sharpton, eds.), pp. xx–yy. LPI Tech Rpt. 88-05. Lunar and Planetary Institute, Houston.

This report is distributed by:

ORDER DEPARTMENT
Lunar and Planetary Institute
3303 NASA Road 1
Houston, TX 77058-4399

Mail order requestors will be invoiced for the cost of shipping and handling.

Contents

OMIT P3

Introduction

The first workshop of the MEVTV (Mars: Evolution of Volcanism, Tectonics, and Volatiles) study project was held in Napa, California, on December 4–5, 1987. The subject of the workshop, "Nature and Composition of Surface Units on Mars," had been selected by the study group participants at an organizational meeting held earlier in the year. Sean Solomon, the MEVTV Project Chairman, convened the December workshop in an effort to provide a common starting point for the diverse research efforts represented by the project membership. The workshop was organized around tutorial presentations designed to assess the current understanding of the composition, distribution, and origin of martian surface materials. Stimulation of interdisciplinary discussions was one of the primary goals of this first workshop.

The morning session on the first day dealt with the SNC meteorites and their potential for providing information about the geochemical evolution of Mars. While most researchers seem to accept the likelihood that these rocks came from Mars, the precise location from which the materials were excavated remains an important unknown. The intriguing results obtained from analyses of the SNC meteorites point out the need for obtaining documented samples from Mars. The afternoon session concentrated on the compositional information that can be derived from remote-sensing results. Remote-sensing techniques cannot provide detailed chemical information about natural materials, as can laboratory analysis of a sample, yet useful constraints on certain minerals result from quantitative measurements of reflected or emitted energy. Present results are at least compatible with the compositions observed in the SNC meteorite group.

The second day started with a session devoted to photogeological inferences of martian surface compositions. The Viking images are being used to update the geologic maps of Mars that were based primarily on Mariner 9 information. The new information allows finer subdivisions to be made of various rock units, but surface morphology does not provide a unique solution to the possible compositions of many materials. Even the morphology of individual lava flows leads to rather broad limits on the lava's possible compositions. While the compositional constraints inferred from photogeology are admittedly quite broad, the geo-

logic maps serve the useful purpose of providing a regional and global framework for understanding the developmental history of the martian surface. The final session of the workshop dealt with the interaction of the surface with volatiles in either the surface or the atmosphere. One significant result from this discussion was that most of the martian surface materials have undergone varying degrees of alteration. In addressing compositional problems on Mars, one needs to evaluate how the compositional information may be affected by products that are far from pristine in nature.

It is likely that most people went away from the workshop with a new appreciation of the limitations that must be applied to the diverse techniques being used to address compositional questions for martian materials. Researchers may hope that some very different approach will provide the panacea for problems encountered in their particular field, but nature in general, and Mars in particular, does not allow that to happen very often. The entire MEVTV community can only benefit from a concise and honest appraisal of what we know and what we do not know about Mars. The four session summaries and the abstracts provided in this volume are the result of this appraisal process.

James R. Zimbelman
Washington, DC

Program

Friday, December 4

8:30 a.m.–12:00 noon

SNC Meteorites and Implications for the Composition of Mars
J. Longhi and E. Stolper, Chairmen
Tutorial: J. Longhi

1:30 p.m.–5:00 p.m.

Remote Sensing of the Martian Surface
J. Adams and R. Greeley, Chairmen
Tutorial: J. Adams, R. Singer, and R. Arvidson

5:00–7:30 p.m.
Poster Presentations of Contributed Papers
(all accepted papers except those designated as print only were presented as posters)

Saturday, December 5

8:30 a.m.–12:00 noon
Photogeological Inferences on Martian Surface Composition
J. E. Guest and J. Adams, Chairmen
Tutorial: R. Greeley

1:30 p.m.–5:00 p.m.
Volatiles and Surface-Atmosphere Interactions
F. Fanale and S. Clifford, Chairmen
Tutorial: F. Fanale

Print Only Abstracts

Intercrater Plains Deposits and the Origin of Martian Valleys
G. R. Brakenridge

Small Martian Volcanoes
P. A. Davis and K. L. Tanaka

Progress in Determining the Thickness and Distribution of Volcanic Materials on Mars
R. A. De Hon

Some Probable Characteristics of the Martian Regolith
E. A. King

Documenting Volcano-Tectonic Episodes in Mars' Stratigraphic Record
D. H. Scott and K. L. Tanaka

SUMMARY

Workshop Summaries

SESSION I:

SNC METEORITES AND IMPLICATIONS FOR THE COMPOSITION OF MARS

E. Stolper

The first session of the workshop, co-chaired by John Longhi (Yale University) and Edward Stolper (California Institute of Technology), was devoted to discussion of the so-called SNC meteorites. These igneous meteorites—the shergottites (S), nakhlites (N), and chassignites (C)—have been suggested to be fragments of Mars blasted off the planet by impact. The goal of this session was to describe the features of these meteorites and, if a martian provenance is accepted, to explore what they tell us about the composition and differentiation of Mars.

John Longhi presented an extended tutorial on the petrology and geochemistry of these meteorite groups, followed by brief presentations by John Jones (NASA Johnson Space Center) on their chronology and radiogenic isotope geochemistry, by Alan Treiman (Boston University) on aspects of their textures and analogies to terrestrial komatiites, and by Lucy McFadden (University of California, San Diego) on their alteration products and martian soils.

The principal message delivered during this phase of the workshop was that the SNC meteorites came from a complex, highly evolved planet with igneous activity spanning most of solar system history. In this respect they are more similar to terrestrial igneous rocks than to other igneous meteorites that come from simpler, presumably much smaller parent bodies that differentiated soon after the formation of the solar system and then shut down. Both Longhi and Jones stressed the interpretation that the shergottites represent relatively recent ($\leq$1.3 b.y.) melts of a mantle source previously depleted by melting early in the planet's history; geochemical and petrological evidence suggests that these magmas were contaminated by passage through the planet's incompatible element enriched crust. Strong analogies were drawn to terrestrial Archean magmas, including komatiites, many of which show geochemical and petrological evidence of similar histories. The analogy to komatiites was made directly by Treiman who showed that some of the textures of SNC meteorites are similar to those of terrestrial ultramafic lava flows.

Many questions were raised that remain unanswered: Why are nearly all of the SNC meteorites crystal cumulates? What was the role of volatiles in the evolution of these igneous rocks? If, as has been suggested, they were somewhat hydrous, why are no vesicles observed? Could impact-induced melting have played a role in the evolution of these meteorites? If these meteorites come from Mars, does the extensive planetary differentiation they imply tell us anything about the presence and/or characteristics of an early atmosphere?

It would be difficult to overemphasize the futility of trying to accurately reconstruct the evolution of a complex planet even to zeroeth order from a handful of random samples taken out of geological context. Nevertheless, if the SNC meteorites are from Mars, they tell us of a complex, highly evolved planet, more similar to Earth in composition, internal evolution, and gross structure than the parent planet of any other nonterrestrial igneous rocks yet studied. Even if these meteorites are from Mars, the consensus and probably the unanimous sense of the participants was that as tantalizing as these meteorites are, they are no substitute for a sample return mission to Mars.

SESSION II:

REMOTE SENSING OF THE MARTIAN SURFACE

J. B. Adams, R. E. Arvidson, and R. B. Singer

This session was co-chaired by John B. Adams (University of Washington) and Ron Greeley (Arizona State University), and contained reviews by Adams, Robert B. Singer (University of Arizona), and Raymond E. Arvidson (Washington University).

Much of our current information about the composition of Mars comes from Earth-based spectral measurements. While no single technique is without some uncertainty, reflectance spectroscopy has been very productive for exploring Mars. To first order Mars has two classes of surface materials: bright, heavily

PRECEDING PAGE BLANK NOT FILMED

PAGE 4 INTENTIONALLY BLANK

altered materials and dark, less altered materials. Their distributions generally have no simple correlation with regional geomorphologic units. While spectral interpretation of the martian surface is complicated by effects of atmosphere and dust, there is still a wealth of information present. On the scale of telescopic spatial resolution (>300 km) regional variations have been observed within both bright and dark units.

All surface regions on Mars have an intense but relatively featureless Fe^{3+} absorption edge from the near-UV to about 0.75 μm. The slope is steeper for bright regions than dark regions, indicating more ferric iron in the former. This absorption edge is attributed to combinations of Fe^{3+} crystal-field and charge transfer absorptions. Mars does not exhibit the distinct absorption features characteristic of well-crystallized ferric oxides and Fe^{3+}-bearing clay minerals. The best (but not perfect) spectral analogs are amorphous iron-silica gels (certain palagonites) that form by low-temperature alteration of mafic volcanic glass. Recent work indicates that extremely fine-grained hematite might be the coloring agent in these palagonites and on Mars. Regional and temporal variations in observed bright regions also indicate that at least some of the nonmobile weathered deposits also contain unweathered mafic components.

The martian surface certainly contains some molecular water and OH, as attested to by a deep "3-μm" absorption envelope. The surface is nevertheless quite desiccated relative to Earth. Structural OH and molecular water features near 1.4 and 1.9 μm have not been seen for Mars. Although complicated by atmospheric CO_2 absorptions, deep water/OH bands should be apparent if present. At 2.36 μm there is a very weak absorption generally attributed to structural Mg-OH bonds, but with at least a factor of 3 less band depth than expected for a well-crystallized clay (or other OH-bearing) mineral. Either crystalline clays are a minority phase mixed with other materials (e.g., palagonite), or the bright soils are homogeneous but structurally intermediate between amorphous palagonites and crystalline clays. New telescopic observations throughout the 3-μm region indicate that observed soils are at least somewhat more crystalline than the most amorphous palagonite analogs.

There has been much interest in the possible occurrence of carbonates and other salts such as sulfates and nitrates. A variety of telescopic and spacecraft observations has yet to find any absorptions due to these minerals, placing a rough upper limit of a few weight percent carbonate if well mixed in the regolith. Orbital mapping spectroscopy (e.g., Mars Observer VIMS) is required to look for possible small regional exposures of these minerals.

From a variety of spectral observations the martian crust appears to be dominated by basaltic, but not necessarily ultramafic, rock. There is no indication of more silicic crust, although reflectance spectroscopy is less sensitive to such materials. Much of the observed mafic material is crystalline and relatively unaltered, as evidenced by unambiguous pyroxene absorptions near 0.95–0.99 μm for most dark region observations. For some regions a characteristic pyroxene band somewhat above 2 μm has also been observed. The most straightforward interpretation indicates a high-iron subcalcic augite as the most common pyroxene, although further refinement is necessary. Olivine and/or basaltic glass is also possibly evident in some observations, but is more controversial. The prospects for more detailed study of crustal composition from Mars Observer are excellent.

Viking Lander images (six bandpasses) and Orbiter images (three bandpasses) have insufficient spectral resolution to make unique mineral or rock identifications on Mars; however, the image spectra place constraints on possible materials, and provide a rich spatial context for interpretation. When Mars is viewed through the Viking Lander spectral bandpasses there is a remarkable similarity of the materials at both of the Lander sites and in an Orbiter mosaic that includes the Lander 1 site. Nearly all of the spectral variation in these images is explained by the presence of two main materials, a bright dust similar to some terrestrial palagonites, and dark, gray rock similar to terrestrial basalts/andesites. These results are broadly consistent with the telescopic spectra that cover much larger areas at higher spectral resolution.

The Lander images reveal a few small patches of the surface that are redder than the bright dust, and that have been interpreted as being enriched in hematite. The origin of this material is not known. Other spectral variations in the dust and in the rocks are indistinguishable from mixtures of dust and rock, textural differences caused by shading and shadow, or lighting artifacts such as spectral phase-effects.

Textural changes in the dust include rough dust/soil in trenches dug by the Landers and duricrust, which is consistent with compacted very fine-grained soil. The spectral class of gray rock includes the prominent rocks on the surface and those areas of the soil that have a rougher texture as revealed by the higher fraction of shade/shadow. The rougher, rock-like soil has been interpreted as unweathered rock or tephra that may be locally derived. The bright dust, in contrast, coats the rocks and appears to be moved and deposited by wind. No spectral or contextual evidence links the origin of the dust to the rocks in the Lander images; therefore

the palagonitic dust is likely to have been formed elsewhere, perhaps in the geologic past.

A mosaic of Viking Orbiter images that includes the Lander 1 site has been calibrated and compared to Lander images and telescopic spectra. Spectral variations in the Orbiter images can be explained by the presence of the same materials, dust and dark rock, that are present in the Lander 1 and 2 images, along with differences in the surface topography and texture as expressed by the amount of subpixel shade/shadow. Three main spectral units are present.

Dark gray unit. This unit is exposed in Acidalia Planitia against topographic barriers and within Kasei Valles, and as dark splotches and streaks in Xanthe Terra and Oxia Palus. It has high thermal inertia. The spectrum is similar to laboratory reference spectra of mafic rock with minor palagonite and a significant fraction of shade/shadow.

Dark red unit. This unit is exposed south of Acidalia, in Lunae Planum, Xanthe Terra, and Oxia Palus. It has intermediate thermal inertia. The spectrum is similar to a mixture of mafic rock and palagonite and a major fraction of shade/shadow.

Bright red unit. This unit is exposed in Tharsis and Arabia, and at borders between dark gray and dark red materials. It has the lowest thermal inertia. The reflectance is that of palagonite with minor shade/shadow.

There is little correlation of surficial units and bedrock geology. Rather, distribution of these materials is correlated with topography at regional and local scales. Regionally, dark gray materials are at lowest elevations, dark red materials are at intermediate elevations, and bright red materials are at highest elevations. Locally, bright red and dark gray materials are associated with craters, cliffs, and other topographic obstacles.

These Orbiter units can be geologically interpreted as: *bright red* materials are dust deposits—aeolian suspension load; *dark gray* materials are saltation and traction load, along with some immobile deposits. Lower entrainment velocities associated with lower elevations (high atmospheric densities) ensure self-cleansing of dust and continual exposure of lithic fragments; *dark red* materials are part of an immobile substrate over which dark gray and bright red materials migrate. Dark red material is perhaps aeolian lag, but thermal inertias are less than those for dark gray exposures. Dark red exposures are perhaps rough, indurated, deflated dust deposits. Induration may be associated with formation of duricrust. Rougher topography at microscale associated with disrupted duricrust plates may lead to accumulation of dust as dust-laden winds traverse from dark gray to dark red exposures. This hypothesis would explain the bright red borders found between dark gray and dark red materials. Aeolian processes appear to dominate the distribution of the geologic units. Topographic control is important on regional, local and perhaps even microscales.

SESSION III:

PHOTOGEOLOGICAL INFERENCES ON MARTIAN SURFACE COMPOSITION

R. Greeley and J. E. Guest

This session was chaired by John Guest and John Adams and involved reviews by R. Greeley, Steve Baloga (Jet Propulsion Laboratory), J. Guest, and Peter Mouginis-Mark (University of Hawaii). Presentations included an overview of various photogeological mapping programs for Mars, mechanisms of lava flow emplacement, and discussions of how one could assess the composition of materials as inferred from volcanic landforms and lava flows.

The most recent global, systematic geologic mapping of the planet is by David Scott, Kenneth Tanaka (both from the U.S. Geological Survey), Greeley, and Guest, coordinated by the U.S. Geological Survey. The mapping uses the new 1:15-million-scale base maps and will serve as a key frame of reference for other studies and for the Mars Observer Mission in the early 1990s. About 90 different units have been distinguished on these maps. From this and other mapping it is shown that more than half the surface of Mars appears to involve volcanic materials derived from a wide variety of volcanic eruptions.

An assessment of the general morphology of terrestrial volcanoes and their compositions shows a potential simplistic correlation. For many years, it has been recognized that volcanoes composed of high-silica lavas have steep flanks, whereas mafic flows produce low-profile volcanoes. For example, volcanic domes are usually composed of rhyolitic or dacitic flows, and shields and lava plains typically are basaltic. This is explained in part as a consequence of lava viscosities. High-silica lavas typically are more viscous and do not spread far from their vents; mafic lavas are generally more fluid and travel a longer distance from their vent. However, there are many exceptions to this correlation and a wide variety of morphologies can be found for even a narrow range of compositions. For example, basalts can include not only lava plains and shields, but also steep-sided volcanoes, domes, and pyroclastic plains. On the other hand, silicic lavas seldom form large, low-profile volcanoes.

During the last 15 years various empirical and theoretical models have been formulated to explain lava flow development and the final morphology. Empirical

models relate, for example, effusion rate to maximum length of flow. Theoretical models treat lava as a non-Newtonian material and are used to determine such characteristics as yield strength and other rheological properties. However, because many complex factors control the flow of lavas, no theoretical model has yet been developed to take all parameters into account. Composition is only one of the critical parameters and thus knowledge of the rheological behavior of a lava does not necessarily specify the composition.

Several investigators have studied possible correlations between composition and the morphology of individual flow features, such as lava channel levees. As reviewed by Baloga, most of these studies are based on the influence of silica content on the flow properties of lavas and development of certain features such as levees. Although the models that have been developed appear to be valid for application on Earth, lack of adequate data make the application to other planets difficult. For example, most inferences of lava composition based on the morphology of lava levees apply only to those levees formed by single-stage flows. However, many levees are accretionary and result from multiple overflow of the channel banks. Unfortunately, image resolution is inadequate to assess single- versus multiple-stage levee formation on martian lava flows.

Other models to derive composition (i.e., silica content) from flow morphology depend on knowledge of levee height, flow margin thickness, flow-festoon dimensions, or other features. These models have been applied to the study of some martian lava flows. Although there are limitations in the data that cause uncertainties, the general results for Mars predict low-silica lavas such as basalts, which is consistent with other predictions.

In addition to assessing the morphology of volcanoes and individual lava flows in recent years, attention has focused on studying sets of lava flow or *lava flow fields*. As discussed by Guest, Mt. Etna is a good laboratory for such studies because it has a long historical record. Since the mid-18th century the output of lava at Etna has been remarkably constant, indicating that the "plumbing" conditions in the volcano have remained the same during this period. It has been pointed out by Geoff Wadge (University of Reading) that during this time, the long duration eruptions have all occurred on the east and southeast sector of the volcano. Flank eruptions elsewhere have tended to be less than 25 days duration. Correspondingly, in the south and southeast sector the volumes of individual flow fields are large and the eruptions have had low effusion rates. Examination of the morphology of flow fields on Mt. Etna shows a wide range despite the fact that the composition of the flows has been the same and they are broadly similar in their petrography. Thus, the different forms of flow fields are likely to have developed from lava of similar rheological properties and it appears that the flow field morphology may result more from the eruptive conditions than the rheology. The two most common forms of flow during the last 250 years have been either long thin flows or broad complex flows. These two forms appear to be more related to the "plumbing" system than to any other characteristic of the erupting lava. Thus, on Mars, different flow-field morphologies may be a useful way of assessing "plumbing" conditions, but not necessarily lava composition.

Theoretical studies show that explosive volcanism is a likely style of activity to have occurred on Mars. Volcanism almost certainly has occurred on Mars from the earliest stages of crustal evolution and there is abundant evidence for the presence of water early in martian history. Consequently, phreatic eruptions very likely occurred. Moreover, ground ice and ground water probably have been present through much of Mars' history and would provide ample opportunity for hydromagnetic eruptions, as presented by Mouginis-Mark. Certain volcanic areas on Mars show erosional channel networks, indicating the presence of material that was readily eroded; such materials may well be pyroclastic deposits. However, even with explosive activity driven by juvenile volatiles, a wide variety of eruptions could have been involved, including Strombolian, Plinian, and other activity—all relatively independent of magma composition.

In conclusion, photogeologic mapping shows that a wide variety of materials are present on Mars, many of which appear to be of volcanic origin. However, the knowledge of the composition of this material is very poorly constrained. Based on present knowledge, volcanic morphology is not a definitive means to determine the composition of the lavas, but it can place broad constraints and provide clues. The large shield volcanoes and the extensive flows on Mars (e.g., those of several hundred kilometers length) are most likely to have been formed from relatively fluid lavas, which on Earth are mafic in composition. Inferences drawn from the morphology of individual flows, flow fields, and total accumulations suggest that most of the martian materials had rheological properties similar to basaltic or other mafic magmas at the time of their emplacement.

SESSION IV:

VOLATILES AND SURFACE-ATMOSPHERE INTERACTIONS

S. M. Clifford

This session began with an overview by session co-chairman Fraser Fanale (University of Hawaii). To assess the role of volatiles in weathering, Fanale identified a number of key questions: What was the original state and distribution of volatiles on Mars and how has it changed through time? By what processes and to what extent has primary rock been weathered by direct contact with the atmosphere? How might impacts and endogenic magmatism alter a volatile-rich crust? What mineral phases are likely to be produced by these interactions and how would they be distributed? Finally, how do volatiles and weathering products interfere with remote sensing?

Fanale led off the discussion by reviewing our current understanding of the volatile history of Mars. Evidence that the early climate may have differed substantially from that of today comes from the dissection of the planet's heavily cratered terrain by integrated networks of small valleys. If these valleys are ancient runoff channels, then calculations indicate that the early atmosphere must have contained between 2 and 3 bars of CO_2. Although evidence for such a massive early atmosphere is scarce, it is clear that if a massive atmosphere did exist, it could not have persisted for long. Mass loss from hydrodynamic escape, atmospheric erosion by large impacts, carbonate formation, and adsorption by the regolith would have quickly reduced the surface pressure to something approaching its present value. Thus, with the exception of periodic fluctuations forced by time-varying orbital and rotational parameters, the martian climate has apparently undergone little change over the past 4 b.y.

Although conditions may have once favored the global distribution of regolith H_2O on Mars, those conditions did not survive the transition to the present climate. At equatorial latitudes, current mean annual temperatures exceed the frost point temperature of the atmosphere by as much as 20 K. As a result, equatorial ground ice will sublime, resulting in an inexorable transfer of H_2O from the comparatively warm equatorial region to the colder latitudes poleward of 40°. Confirmation of the desiccated state of the equatorial regolith may come from the distribution of softened terrain, a type of landform degradation attributed to ice-enhanced creep that is found only at high latitudes.

Atmosphere-surface interactions were discussed by Bruce Fegley (Massachusetts Institute of Technology). Because of differences in atmospheric composition and surface pressure, the weathering of exposed rock on Mars is expected to be qualitatively different from that occurring on Earth. To understand this interaction, the physical properties and mineralogy of the exposed rock must be characterized, as well as the reactive atmospheric constituents (e.g., O_3, H_2O_2, Co, etc.). Although some analyses, such as atmospheric compositional measurements, can be performed *in situ* by automated landers, Fegley concluded that any serious attempt to characterize the nature of the surface must await the return of samples for study in terrestrial labs.

Horton Newsom (University of New Mexico) spoke on the potential role of impact weathering on Mars. Studies of terrestrial impact sites, such as the Ries crater in West Germany, indicate that postimpact hydrothermal alteration of ejecta and fallback can result in the production of an appreciable quantity of clay (10–20 wt%). Therefore, if Mars is indeed water-rich, impact-generated clays should constitute a significant fraction of the regolith. This conclusion is consistent with the results of several Viking Lander experiments, which indicated that smectite clays might dominate the composition of the soil.

Volcanism has also clearly played an important role in the geologic evolution of Mars. As discussed by Mouginis-Mark, an important consequence of the interaction of iron-rich basaltic magma with ground ice is the production of palagonite, an altered volcanic glass rich in smectite clay. One location that may have witnessed such activity is Elysium Mons. Northwest of the volcano and approximately 250 km downslope, several major channels emerge from structural features located at the volcano's periphery. The most probable origin for the water that carved these channels is ground ice melted by volcanism.

Roger Burns (Massachusetts Institute of Technology) discussed the geochemical implications of sulfide oxidation in an aqueous martian environment. Groundwater that participates in this type of reaction will become highly acidic, ultimately developing high concentrations of dissolved silica, Fe, Ca, Al, Mg, Ni, and sulfate ions through interaction with the host rock. Subsequent hydrolysis and oxidation could then result in the precipitation of clay silicates, silica, ferric sulfate, and iron oxyhydroxides. On Earth, such reactions frequently produce rust-colored iron-rich oxidized coatings on sulfide-bearing rocks. Martian surface rocks and duricrust have a similar appearance, a possible result of the same geochemical process.

However, a multispectral analysis of the martian surface suggests that its appearance may have a simpler explanation. By treating each pixel of a Viking Lander image as a potential mixture of spectrally distinct materials, Adams described how he and his colleagues used the six Lander bandpasses to establish that only three spectral endmembers—rock, soil, and shade—were necessary to reproduce the observed pixel-to-pixel spectral variation. Comparisons with laboratory reference spectra reveal that the characteristics of the rock component are similar to those of Hawaiian basalt, while the soil component most closely resembles palagonite. This analysis further suggests that the oxidation and hydration of old flows that happen on Earth do not occur on Mars, although this interpretation may need revision once the visual and infrared mapping spectrometer aboard the Mars Observer spacecraft begins its operation in 1992.

ABSTRACTS

5/-91
N88-29655 13

SURFACE COMPOSITION OF MARS: A VIKING MULTISPECTRAL VIEW

[1]John B. Adams, [1]Milton O. Smith, [2]Raymond E. Arvidson, [2]Mary Dale-Bannister, [2]Edward A. Guinness and [3]Robert Singer
[1]University of Washington, Seattle, WA 98195
[2]Washington University, St. Louis, MO 63130
[3]University of Arizona, Tucson, AZ 85721

NF835159
NG032961
AX852975

A new method of analysing multispectral images [1] takes advantage of the spectral variation from pixel to pixel that is typical for natural planetary surfaces, and treats all pixels as potential mixtures of spectrally distinct materials. For Viking Lander images, mixtures of only three spectral endmembers - rock, soil and shade - are sufficient to explain the observed spectral variation to the level of instrumental noise.

Inferences about the composition of martian rocks and soil can be constrained by using mixtures of reference spectra; however, interpretations comparing image pseudospectra in terms of single reference spectra may be ambiguous. For example, spectra of a single rock viewed at different illuminations or orientations can be different. These spectra may be fit by different reference spectra. Also, if the rock is smaller than a pixel, then the spectrum may be influenced by adjacent materials such as soil. The possible modifications of a pure rock spectrum can be specified by mixtures with other spectral endmembers.

The endmember rock at the Viking 1 site is consistent with a broad class of andesites/basalts (H190), and the endmember soil fits the spectrum of weathered palagonitic basalt tephra (H34)[1]. Further work shows that these results with minor modifications also hold for the Lander 2 site, corroborating the remarkable similarity of the two sites on the basis of surface chemistry and other properties. The spectral mixing volume defined by these endmembers and shade includes some other rocks and minerals that have been proposed for Mars. For example, nontronite cannot be distinguished from mixtures of the above endmembers using the six Lander bandpasses.

In the Viking Lander images it is possible to use the image context to select pixels that are relatively pure compositionally. Many scenes show smooth, clean rock, areas of pure soil, and shadows cast by the rocks. This type of image facilitates selection and evaluation of endmember spectra.

PRECEDING PAGE BLANK NOT FILMED
PAGE 12 INTENTIONALLY BLANK

Viking Orbiter images, however, present a more challenging problem. The Lander 1 site in Chryse Planitia imaged by Orbiter includes within each pixel the spectral contributions of rock, soil and shade. From the context of the Lander images, we know that these endmembers must be present; however, none has sufficient areal extent to be spatially resolved by Orbiter. Even if compositionally pure areas occur elsewhere in Orbiter images at the pixel scale, there probably will be topographic and textural effects of shade and shadow. To compare spectra taken at the scale of Orbiter (or telescopic spectra) with pure reference spectra, it is necessary at the minimum to allow for the presence of spatially unresolved shade. It probably is necessary to treat pixels as mixtures of rock, soil and other potential endmembers, also.

Image endmembers were determined for a 1978 Orbiter mosaic that includes the Lander 1 site. After initial calibration of the image, the image endmembers were calibrated to reflectance using a method that simultaneously solves for endmember fractions and for gains and offsets. The image-derived endmembers - ideal shade, blue unit, white unit, and Lunae Planum - are contained within the volume defined by pure reference spectra - ideal shade, H34-63 (<63 μm) and H190 (Fig.1). These results are consistent with the view that the mixing volume for any Orbiter image cannot lie outside the mixing volume defined by the pure endmembers that would correspond to reference samples. The reference endmembers also encompass the mixing volume of the Viking Lander images, therefore, they meet the constraints imposed by the six Lander bandpasses, as well as the three Orbiter bandpasses.

We conclude from Fig. 1 that the Lander materials and the laboratory reference spectra fit the spectral variation in the Orbiter image that includes parts of Chryse Planitia, Acidalia Planitia, Kasei Valles, and Lunae Planum. The major compositional differences among the Orbiter spectral units are consistent with mixtures of rock and soil, and shade/shadow. Different fractions of shade imply topographic and/or textural variations. There is no way of knowing from the spectral data what the scale is of the shade component. It could be caused by spatially unresolved topographic elements, large boulders, rocks similar to those seen at the Lander sites, or opaque sand grains.

We interpret the Orbiter "blue" unit (prominent in Kasei Valles) as a mixture of a class of rock represented by H190 (Hawaii basalt) and shade, with little or no soil component. The scale of the shade, and therefore, the texture of the surface is unspecified. Photogeologic

evidence, however, shows that some portions of the blue unit are located against topographic barriers and in crater floors, implying that the material is wind-deposited, possibly tephra sand. The "white" unit (prominent at the margin of Lunae Planum) is interpreted as a mixture of soil similar to H34 (palagonite) and H190 (basalt), with little or no shade component. This suggests a mixture of weathered and unweathered fine soil or tephra. The Lunae Planum unit is interpreted as a mixture of soil, rock, and shade. It is somewhat darker than the Chryse Plains unit, which includes the Viking Lander 1 site. Chryse also is consistent with a mixture of soil, rock, and shade, but appears to be smoother and to have less rock. This interpretation of the Orbiter data is consistent with what is observed spectrally and contextually in the Lander images.

We conclude that a large portion of the martian surface consists of only two spectrally distinct materials, basalt and palagonitic soil. We emphasize, however, that as viewed through the three broad bandpasses of Viking Orbiter, other materials cannot be distinguished from the mixtures discussed. It remains possible that the surface composition, as manifested spectrally, is indeed simple. Images of Mars with additional bandpasses coupled with telescopic, thermal and photogeologic evidence, should clarify interpretations.

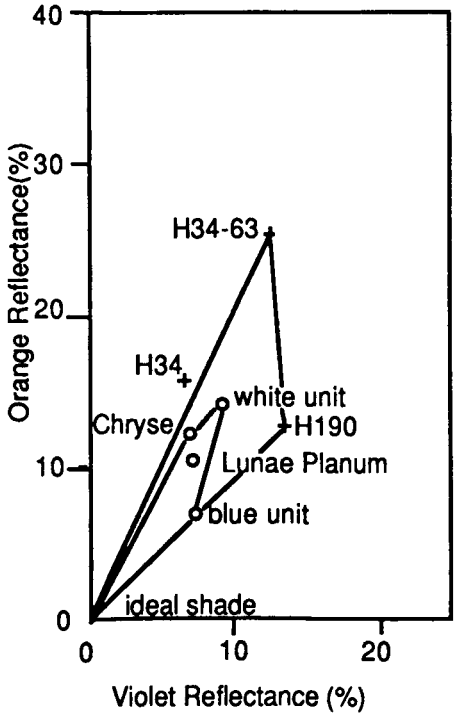

Figure 1. Viking Orbiter image endmembers (open circles) and laboratory reference spectra (crosses) in two dimensional projection (orange/violet) of the Orbiter three bandpasses. Image endmembers lie within the mixing volume defined by the pure reference endmembers.

Reference
1. Adams, J. B., M. O. Smith, and P. E. Johnson (1986), J. Geophys. Res. 91, 8098-9112.

NATURE AND DISTRIBUTION OF SURFICIAL DEPOSITS IN CHRYSE PLANITIA AND VICINITY, MARS; R.E. Arvidson, M.A. Dale-Bannister, E.A. Guinness, McDonnell Center for the Space Sciences, Department of Earth and Planetary Sciences, Washington University; J. Adams and M. Smith, University of Washington; P.R. Christensen, Arizona State University; and R. Singer, University of Arizona

Viking Lander 1 blue, green, and red channel image data acquired for bright red soils during the morning and afternoon of Sol 611 (subsolar longitude ~70°, northern spring season) were used to extract values for the single scattering albedo (0.34, 0.50, 0.82, respectively) and single particle phase function asymmetry factor (-0.06, -0.08, -0.12, respectively). The atmospheric multiplicative term was removed using solar optical depth values (~0.5) from the Lander cameras and the additive term was removed using shadows cast by rocks. Results were used to check radiometric calibrations for a mosaic of four violet, green, and red Viking Orbiter image triplets acquired on Sol 609 over the landing site and surroundings. Radiance factors predicted from the Lander for the Orbiter image lighting and viewing geometries are indistinguishable (to within 10% error) from atmosphere-corrected radiance factors extracted from the Orbiter images for an area surrounding the most probable landing site. Thus, soil exposures must dominate the Orbiter image data at least for this area. The bright red soils at Lander 1 are typical of materials exposed in Chryse Planitia and surrounding areas. The material appears to be dust (i.e., aeolian suspension load) eroded by high winds from the classical dark area, Acidalia Planitia, accumulating in the younger volcanic terrains that dominate Chryse, and against topographic barriers such as craters and cliffs in adjacent regions. The soil three-point radiance factor spectra (violet, green, red) are most like laboratory spectra for fine-grained palagonite, with radiance factor values of 0.08, 0.14, and 0.35, at a 20° incidence and 0° emission angle. The data also are indistinguishable from Earth-based spectra for classical bright areas. Dark gray materials are exposed on the floor and against north-facing cliffs within Kaseii Valles, and as dark streaks downwind of craters in Xanthe Terra. Dark gray materials are probably outliers of wind-blown sands (i.e., aeolian saltation and traction loads) from Acidalia Planitia. The dark gray material has three point spectra indicative of basalt fragments with a minor amount of palagonite cover. Dark red deposits occur in Lunae Planum to the west, Xanthe Terra to the south, and Oxia Palus to the east. The dark red material has a noticeable lack of aeolian features. It is a substrate (e.g., aeolian lag or other indurated materials) over which bright red and dark gray materials migrate. Dark red three point spectra are most like palagonite mixed with a few weight percentage of opaque materials such as dark basalt fragments or basaltic glass. The regional pattern of red, dark red, and dark gray material follows topography and is locally modulated by surface roughness. The lowest areas (Acidalia, Chryse) have highest thermal inertias and are darkest, except for red dust in Chryse that on average must be optically thick (100s μm), but thin as compared to the diurnal skin depth (centimeters). Areas with intermediate elevation (Lunae Planum, Xanthe, Oxia) have intermediate inertias and dark red materials. Highest areas (Tharsis, Arabia) have lowest inertias and are dominated by bright red materials. The broad correlation with topography and the lack of correlation with geology implies meteorological controls on the outcrop patterns of surficial materials. Slope winds may play a role. Low threshold friction velocities in lowlands may be able to keep surfaces swept clean of bright red, low inertia dust. Intermediate elevations have been stripped to some extent, leaving dark red, immobile exposures, but not exposing extensive fresh bedrock or extensive areas with fresh lithic fragments. Highest areas are sites of accumulation of dust because of high threshold friction velocities associated with low atmospheric densities. The dominance of aeolian control of exposures of surface material will make identification and characterization of materials derived locally from bedrock a challenge for Mars Observer.

JJ 574450 N88-29656 52-91 17

A REVIEW QUANTITATIVE MODELS FOR LAVA FLOWS ON MARS; S. M. Baloga

The purpose of this abstract is to review and assess the application of quantitative models of lava flows on Mars. These theoretical models have usually been applied to Martian flow data to aid in establishing the composition of the lava or to determine other eruption conditions such as eruption rate or duration. There are four general categories [3] of lava flows observed in the Viking images: 1) channel-fed flows featuring obvious and prominent lateral levees; 2) tube-fed flows, often with central ridges and collapse features; 3) broad flood-like plains flows; and 4) well-defined, lobate sheet flows that sometimes exhibit regular and irregular wave-like surface structures. All models require dimensional data on the specific flows to develop quantitative inferences. This dimensional data typically consists of thickness, width, length and any profiles, either in the direction of flow or transverse to it. The most difficult dimensional information to obtain is the local slope and the thickness or thickness profile of the flow. The thickness of a flow must be determined by comparison of the flow edge or front with nearby craters, photoclinometry or measurements of the shadows cast on the adjacent surface.

There are two distinct classes of models that have been developed to describe the emplacement of lava flows. "Local" models describe the features and dimensions of the lava that occur at a single point along the path of the lava and infer local rheological properties, usually apparent viscosity or yield stress. "Global" models examine the overall dimensions and character of the flow in an attempt to develop quantitative constraints or compositional indicators.

The *Gratz number correlation model* is a thermal model based on Walker's suggestion [14] that the length of a flow is proportional to the eruption rate. This hypothesis is embodied by the dimensionless Gratz number assignment,

$$Gz = \langle Q \rangle h / k L W = 300, \quad (1)$$

where $\langle Q \rangle$ is the eruption rate, h is the thickness of the lava, and L and W are the length and width of the flow, respectively. The appearance of the thermal diffusivity, k, clearly presupposes that thermal diffusion is the key process controlling flow dimensions. Such a correlation could be obtained for any reasonably constant property of lava flows. Numerous authors [3,6,12,13] have, of necessity, resorted to this correlation in studies of lava flows at Olympus, Ascraeus Mons and Alba Patera. Subsequent terrestrial studies [8,15] have suggested that eq. (1) may depend importantly on a number of other factors. There is as yet no compelling theoretical explanation of why any particular Gratz number should appear in eq. (1)

Radiative loss models have also been developed to explain the dimensions of lava flows on Hawaii and sheet flows at Alba Patera [8,16,17]. This model presumes that cooling by Stefan-Boltzmann radiation is the

dominant thermal loss, and further, that such thermal losses determine the plan area of the emplaced flow. Consequently, the predicted correlation takes the similar form,

$$\langle Q \rangle = (\text{const})\ W\ L\ . \qquad (2)$$

The constant prefactor is a sensitive non-linear function of thermal parameters such as initial temperature and specific heat. When Hawaiian flow data is pre-sorted to limit the sensitivities of the prefactor, eq. (2) provides a correlation superior to eq. (1) [8]. However, to predict the actual correlation (*i.e.*, to predict the prefactor in eq. (2)) requires the introduction of an artificial "effective radiation temperature" for lava flows from each volcano. There is as yet no compelling theoretical explanation of effective radiation temperatures for this model. This model, and its application to Hawaiian flows, clearly demonstrates that terrestrial lava flows stop prior to complete solidification of the flowfront.

Yield stress models [5,7,12] have been applied to numerous terrestrial and Martian lava flows featuring central channels and lateral, embanking levees [3,6,7,13,17]. The recurrent theme of these applications is that lava is an isothermal non-Newtonian fluid. The flow expands laterally until the basal stress at the edge of the channel reaches a critical yield strength. With the assumption of a parabolic transverse thickness profile [5], this theory provides the constraint,

$$F = (\text{const})\ \langle Q \rangle\ \nu \qquad (3)$$

where F is purely a function of the widths of the channel and levees, ν is the viscosity of the lava, and the constant prefactor depends on yield strength, gravity and lava density. This formalism is the most widely applied diagnostic for the composition of lava flows on Mars. Results have generally been used to support the concept of basaltic volcanism on Mars. However, eq. (3) requires some knowledge of eruption rate and viscosity, both of which can vary by orders of magnitude in basaltic eruptions. Moreover, the association of yield strength with silica content is somewhat speculative [7] and the model is not completely consistent with terrestrial observations of the levee formation process [9,11].

One *surface structure model* has been successfully applied to silicic and pahoehoe basalt flows on Earth to describe regularly spaced ridges on the upper surface of lava flows [4,18]. Surface ridges are viewed as preferred modes of fluid dynamic instability associated with the contrast in the viscosity of the cooler upper surface and the hotter inner core. When applied to sheet flows at Arcadia Planitia, the high viscosity of the inner core prompted the speculation of a silicic composition. A more recent application of this method to a compositional spectrum of terrestrial flows has also indicated unexpectedly high interior viscosities during the formation of the ridges, even for Icelandic basalts [10]. Application of this model to other sheet flows on Mars with prominent arcuate festoons has been considered supportive of flood-like basaltic volcanism [10].

Kinematic wave models [1,2] describe the time-dependent emplacement of lava flows based on local and global conservation of lava volume. Results have been applied to sheet flows at Alba Patera and, like other studies, infer high and relatively constant apparent viscosities similar to basaltic andesites on Earth. The model has been extended to embrace levee building by several different mechanisms. Compositional inferences from the levee-building models also tend to support somewhat higher crystallinity or silica content than we would expect for basalts. Only limited validation of this type of model has been completed for terrestrial lava flows.

The models that have been developed and applied to lava flows on Mars cannot as yet uniquely discriminate composition. Generally, the applications discussed above have been used to support the notion of basaltic volcanism, a concept that is certainly the most natural one for the Tharsis volcanics on morphologic grounds. These models only provide an approximate constraint on some function of silica content, crystallinity, or lava temperature rather than a direct compositional inference. These are the physical properties that most directly influence the viscosity and yield stress of the lavas and, therefore, the resulting morphologies. Most of the applications to the larger flows on Mars tend to suggest higher viscosities, crystallinity, or silica content than we normally expect for terrestrial basalts, although some applications have resulted in the opposite conclusions. In part, this may be a relection of our incomplete understanding of terrestrial lava flows.

REFERENCES

[1] Baloga, S. (1987). J. Geophys. Res., 92, 9271-9279. [2] Baloga, S. and D. C. Pieri (1986). J. Geophys. Res., 91, 9543-9552. [3] Carr, M. H., R. Greeley, K. R. Blasius, J. E. Guest and J. B. Murray (1977). J. Geophys. Res., 82, 3985-4015. [4] Fink, J. H. (1980). (Abstract) ***LPSC #11***, 285-287. [5] Hulme, G. (1974). Geophys. J. Roy. Astron. Soc., 39, 361-383. [6] Hulme, G. (1976). Icarus, 27, 207-213. [7] Moore, H. J. (1978). ***Proc. Lunar Planet. Sci. Conf. 9th***, 3351-3378. [8] Pieri, D. C. and S. Baloga (1986). J. Volcanol. Geotherm. Res., 30, 29-45. [9] Sparks, R. S. J., H. Pinkerton, G. Hulme (1976). Geology, 4, 269-270. [10] Theilig, E. and R. Greeley (1986). J. Geophys. Res., 91, E193-E206. [11] Greeley, R. (1970). Mod. Geol. 2, 207-223. [12] Wilson, L. and Head, J. W. (1983). Nature, 302, 663-669. [13] Zimbleman, J. R. (1985). (Abstract) ***LPSC #16***, 932-933. [14] Walker, G. P. L. (1973). Phil. Trans. Roy. Soc. London Ser. A., 274, 107-118. [15] Malin, M. (1980). Geology, 8, 306-308. [16] Baloga and Pieri (1985). ***NASA TM-87563***, 245-247. [17] Cattermole, P. (1986). J. Geophys. Res. 92, E553-E560. [18] Fink, J. H. and R. C. Fletcher (1978). J. Volcan. Geotherm. Res., 4, 151-170.

53-91

20

154423

L86-18929

N88-29657

The History of Martian Volcanism Determined from a Revised Relative Chronology. Nadine G. Barlow, Lunar and Planetary Institute, Houston, TX 77058.

The Mariner 9 and Viking images of the martian surface revealed much evidence of volcanic activity, both from early in the planet's history and more recently. The morphology of volcanic features range from plains to a variety of constructs, known as paterae, tholii (domes) and mons (shields). Calculation of the density of superposed impact craters allows determination of the ages of these features relative to each other and to other geomorphic features on the planet's surface (1, 2, 3).

Use of the Relative plotting technique as opposed to the more traditional Cumulative plots allows variations in the slopes of crater size-frequency distribution curves to be easily discernible. The difference between the multi-sloped curves of the heavily cratered regions of the moon, Mercury, and Mars and the single sloped curves of the lunar mare and martian plains is attributed to different size-frequency distributions of two impacting populations responsible for the cratering record within the inner solar system (4). The population recorded in the heavily cratered regions of these three objects is believed to have been emplaced during the period of heavy bombardment whereas the cratering record seen in the lightly cratered lunar and martian plains has formed since the end of heavy bombardment. Thus, use of the Relative plotting technique can provide age information of geologic units relative not only to other units but also to the end of the heavy bombardment period.

The Relative plotting technique recently was used to revise the martian relative chronolgy according to whether units pre- or post-dated the end of heavy bombardment (5). The ages of units of large areal extent ($>10^5$ km^2) were determined from size-frequency distribution data of craters ≥8-km diameter, thus minimizing the effects of secondary craters and obliteration effects on the distribution curves. Impact craters ≥1-km diameter were used to date individual volcanoes since the smaller areal extent of these regions required the inclusion of smaller craters for the results to be statistically significant (6). In both cases, the results cited here should be considered average ages for the regions over which they apply.

The resulting size-frequency distribution curves indicate that volcanic activity of all forms has occurred throughout martian history (Figs. 1, 2). Most of the small volcanic constructs, including many in the Tharsis and Elysium regions, formed during the period of heavy bombardment. Among the oldest volcanic features are Jovis Tholus, Uranius Tholus, Tyrrhena Patera, Ulysses Patera, and Ceraunius Tholus. Also during the period of heavy bombardment, the intercrater plains of the martian highlands formed, followed by formation of Tharsis Tholus, Hecates

Tholus, Albor Tholus, Apollinaris Patera, and the plains south-southwest of the Hellas Basin. The ridged plains show distribution curves similar in shape to the heavy bombardment-aged terrain, but at a lower crater density, indicating formation near the end of heavy bombardment. Hadriaca Patera also formed near the end of heavy bombardment. Since the end of heavy bombardment the order of formation for volcanic features has been as follows: Uranius Patera, Elysium Mons, the plains surrounding Elysium, Biblis Patera, Alba Patera, and the Tharsis plains and four large volanoes. The majority of volanoes exhibiting channeled flanks date from the period of heavy bombardment, indicating that channeling either was an ancient process (7) or that only evolved volcanoes have surface rheologies conducive to channel formation (8).

References: (1) Plesia and Saunders (1979). Proc. 10th LPSC, 2841-2859. (2) Crumpler and Aubele (1978). Icarus, 34, 496-511. (3) Neukum and Hiller (1981). J. Geophys. Res., 86, 3097-3121. (4) Woronow, Strom, and Gurnis (1982). In Satellites of Jupiter, 235-276. (5) Barlow (1987). PhD Dissetation. (6) Katz and Strom (1984). Personal communication. (7) Strom and Barlow (1985). NASA TM 87563, 177-179. (8) Gulick (1987). MS Thesis.

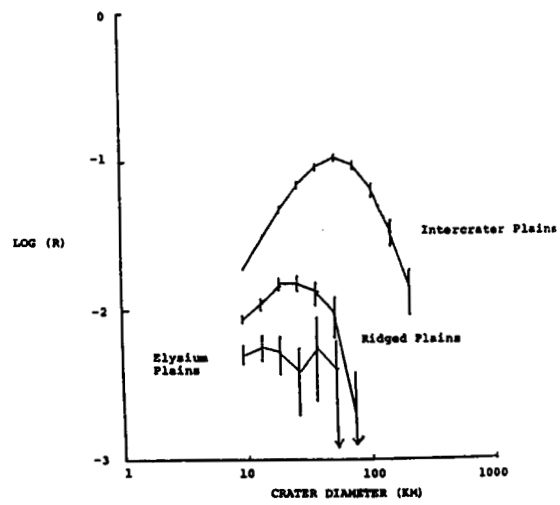

Fig. 1

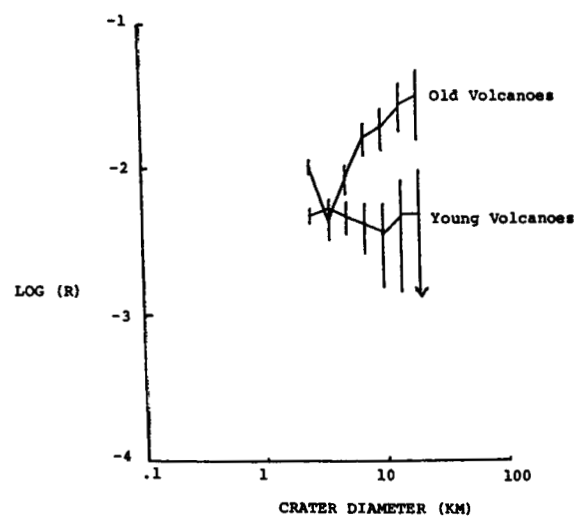

Fig. 2

54-91
154704
22
47

HI 782-556

N88-29658

MARS: NEAR-INFRARED COMPARATIVE SPECTROSCOPY DURING THE 1986 OPPOSITION; **James F. Bell, III and Thomas B. McCord (Planetary Geosciences Division, HIG, Univ. of Hawaii, Honolulu, HI 96822)**

Near-infrared (0.7-2.5 μm) spectral observations of Mars during the 1986 opposition were carried out at the Mauna Kea Observatory utilizing the University of Hawaii 88″ telescope. Spectra were obtained of several martian locations using a continuously variable filter (CVF) spectrometer with a resolution of 1.25% ($\Delta\lambda/\lambda$) (1). During two separate runs in June and August, a number of distinct spots between 354° and 163° longitude and 32° N and 78° S latitude were observed at an angular resolution of $\simeq$ 0.5 to 1.5 arcseconds, corresponding to a spatial resolution on Mars of $\simeq$ 220 to 460 km, varying with nightly seeing conditions. These different spots fall roughly into a set of 8 distinct geologic regions: volcanic regions, ridged plains, ridged volcanic plains, scoured plains, impact basins, channels and canyons, densely cratered regions, and layered terrain and ice (2). The spectra exhibit typical errors of less than 4%.

In order to analyze these spectral data, spot-to-spot ratios were produced between spectra taken in different geologic regions. Spectral features observed in these ratios can act as indicators of mineralogic differences between areas under consideration; this method can also be used to infer the mineralogy of an unknown region which has been compared to one or more well-characterized areas. This exercise produced several interesting results.

In a few of the ratios, weak, broad features were identified which corresponded to Fe^{2+}, Fe^{3+}, or cation—OH absorptions (3,4), however identification of these features was typically the exception rather than the rule. Complications were added to these ratios due to the presence of rapidly variable extinction associated with telluric water bands at 0.718, 0.810, 0.935, 1.130, 1.395, and 1.870 μm (5) as well as martian atmospheric (gas) and surface (frost) CO_2 bands at 1.4, 1.6, and 2.0 μm (5,6) which all exhibited some degree of time- and space-variable behavior. Thus, characterization, by this method, of any features which may exist in close proximity to these bands is difficult except under very stable observing conditions, or when comparing spectra taken close together in time and/or space.

Perhaps the most striking result obtainable from the many ratios taken close in time and under similar viewing geometries was the consistent lack of noticeable differences between spectra taken of areas which, in Viking Orbiter images, appear to have vastly differing morphologies (figures 1 and 2). This observation leads to several possible conclusions: (a) the CVF sensitivity was too low to pick up weak bands or slight differences in band depths between regions. (b) The spatial resolution of spots observed on Mars was not high enough (i.e., the local morphology varies significantly within the aperture region and many units "blur" into one). (c) All of these regions look the same spectrally in the near-IR. It is proposed that conclusions (a) and (b) can be dismissed for a number of reasons and that conclusion (c) is most valid. Additionally, it is proposed that these regions look the same spectrally because a layer of fine dust which represents a single composition global weathering product blankets much of the observed surface, at least down to 200 km resolutions.

MARS: COMPARATIVE SPECTROSCOPY

J.F. Bell, III and T.B. McCord

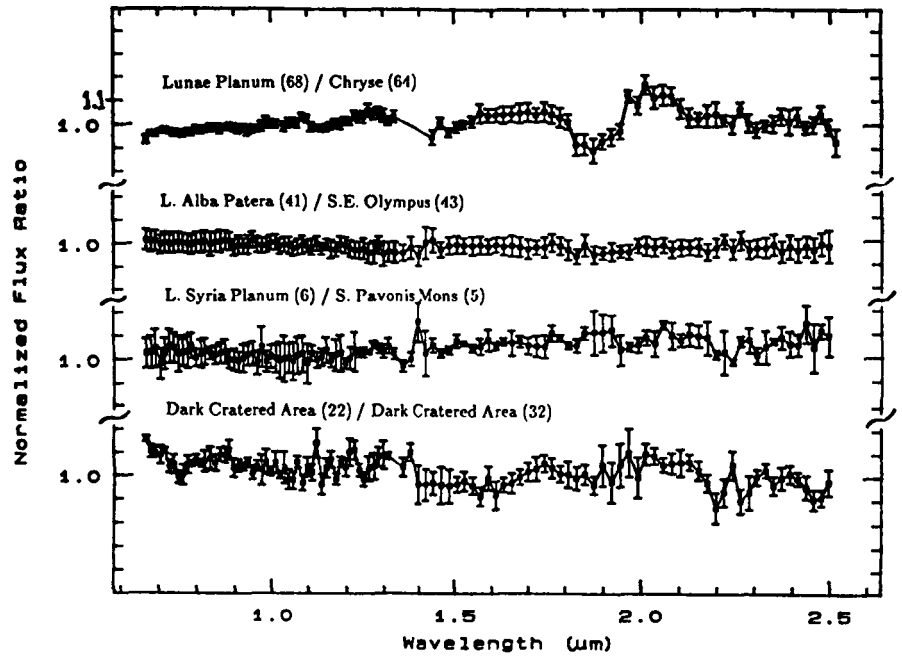

Figure 1: Four ratios of areas exhibiting nearly similar morphology as seen in Viking Orbiter low resolution images. By simple photogeological inference, one would expect that the mineralogy of the areas compared should be grossly similar and thus the ratios should be relatively flat. This is, in fact, what is generally observed. Most features seen in these ratios do not exceed $\simeq$2-3σ of the noise, and thus it is difficult to interpret them as being due to real mineralogical differences.

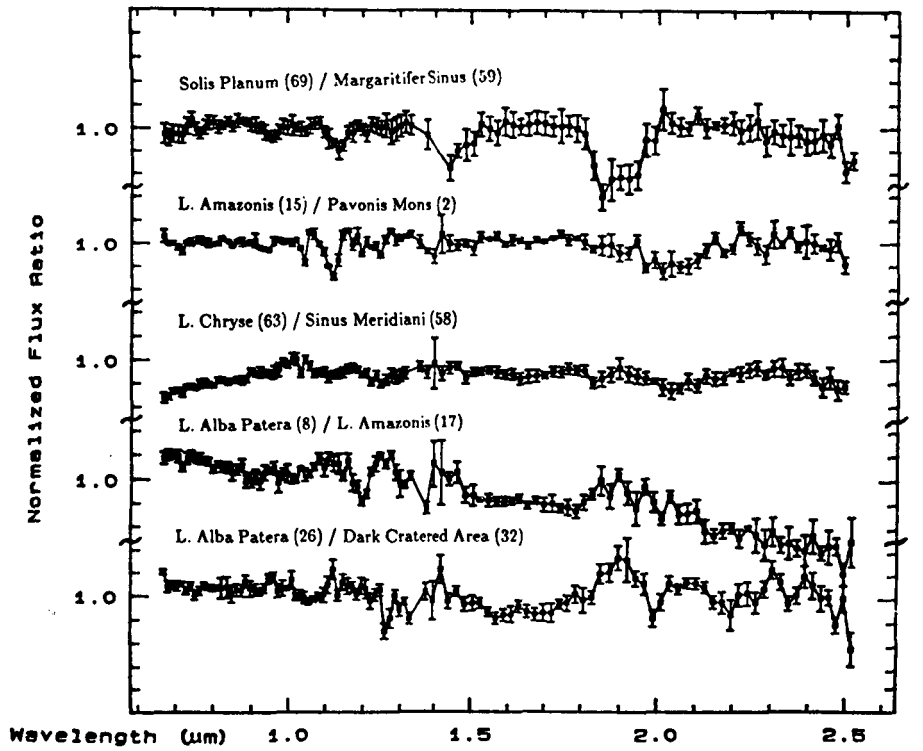

Figure 2: Five ratios of areas, unlike figure 1, exhibiting vastly differing morphology as seen in Viking Orbiter low resolution images. Thus, based on photogeological inferences, one would expect to see noticeable differences in the spectra of the regions compared. In fact, the ratios are just as flat down to the 2-3σ level as those in figure 1. Except for a few mild slope features, gross mineralogic differences do not emerge in these comparisons. This leads us to conclude that a fine layer of dust and/or global weathering product blankets much of the surface which we observed.

MARS: COMPARATIVE SPECTROSCOPY
J.F. Bell, III and T.B. McCord

References

1. McCord, T.B., R.N. CLark, and R.L. Huguenin (1978) *Journal of Geophysical Research, 83,* pp. 5433-5441.
2. Carr, M.H., *The Surface of Mars,* Yale Univ. Press, 1981.
3. Hunt, G.R., J.W. Salisbury, and C.J. Lenhoff (1971) *Modern Geology, 2,* pp 195-205.
4. McCord, T.B., R.N. Clark, and R.B. Singer (1982) *Journal of Geophysical Research, 87,* pp. 3021-3031.
5. Blake, P.L. (1983) Master's Thesis, University of Hawaii.
6. Kieffer, H. (1970) *Journal of Geophysical Research, 75,* pp. 501-509.

Hi 182554
N88-29659
54-91
154905
30

MARS: SPECTRAL SIGNATURES SEEN AND UNSEEN; Diana L.Blaney, Patti A. Walsh, and Thomas B. McCord, Planetary Geosciences Div., Hawaii Inst. of Geophysics, U. of Hawaii, Honolulu, HI 96822.

Interpretation of Mars surface reflectance spectra and geochemical modeling of the surface material are different approaches to the same problem -- determining the compositional nature and evolution of the surface of Mars. This is a report on a study to determine the degree to which these two approaches agree. This study involves: 1) current understanding of the reflectance spectra of Mars, and 2) reflectance spectra of proposed Mars constituents.

Part 1) Reflectance spectroscopy supplies compositional and structural information about the optical surface measured. Spectral measurements of Mars have been made by both groundbased and spacecraft instruments from the visible to the mid-infrared spectral regions (0.3 μm to 5.0 μm). Visible and near-infrared (0.3 μm to 2.6 μm) reflectance spectra obtained from earthbased telescopic measurements (figure 1) show that the reflectance spectra of Mars from 0.3 μm to 0.75 μm region is dominated by broad Fe^{3+} absorptions which lack fine structure, indicating that the Fe^{3+} is in poorly defined crystallographic sites (1,2,3). High albedo regions have stronger Fe^{3+} absorptions than do dark regions, indicating that dark regions may be less oxidized. Dark regions also have Fe^{2+} absorptions in the 1.0 μm region which are interpreted as being due to olivines and pyroxenes (4,5). Absorption features caused by H_2O as a hydrate or ice have been identified between 1.4 μm and 1.7 μm and at 1.9 μm (6). A weak absorption feature at 2.3 μm has been interpreted as being due to the presence of metal cation-OH, indicating clay minerals (7).

The reflectance region at wavelengths longer than 2.7 μm (figures 2 and 3) is dominated by water and hydroxyl absorptions. This wavelength region is especially sensitive to the detection of salts such as carbonates and sulfates which have vibrational absorptions. Calcite is detectable at the 3-5 wt% level in laboratory mixtures with palagonite, a martian dust analog (8). Positive detection of carbonates in the optical surface of Mars has not been made by either groundbased (9,10) or by the Mariner 6 and 7 infrared spectrometer experiments (11,12). However, recent telescopic measurements (13) in the 2.5 to 4.2 μm region show a weak band at approximately 2.85 μm which is unidentified but could be due to salts.

Part 2) Several existing and two new models for Mars surface mineralogy are examined:

A) SNC meteorites -- Reflectance spectra of Nakhla and Chassigny measured (14) and of Shergotty and ALHA 77005 (15);

B) Stable decomposition produces from the weathering of basalt of the same composition as Shergotty (16) which have reached thermodynamic equilibrium with the current martian environment by gas-solid reactions at 240 °K (17); The end product is a composition of 31.75 wt% quartz, 17.16 wt% magnesite, 15.32 wt% calcite, 12.9 wt% Ca-beidellite, 11.03 wt% hematite, 8.67 wt% albite, 1.68 wt% whitlockite, 0.83 wt% corundum, 0.57 wt% iron sulfate, 0.35 wt% orthoclase, and 0.25 wt% ilmenite.

C) Stable decomposition products from the weathering of a dunite of the same composition as Chassigny (18,19), which have reached thermodynamic equilibrium with the current martian environment by gas-solid reactions at 240 °K (17); The end product is a composition of 45.57 wt% hematite, 27.40 wt% quartz, 24.41 wt% magnesite, 1.05 wt% calcite, 1.01 wt% chromite, 0.28 wt% albite, 0.28 wt% Ca-beidellite.

D) Stable decomposition products from the weathering of basalt of the same composition as Shergotty (16) which have reached thermodynamic equilibrium with liquid water containing

dissolved O2 and CO2 (17); The end product is a composition of 25.93 wt% quartz, 17.63 wt% goethite, 15.22 wt% talc, 13.78 wt% calcite, 10.47 wt% Na-beidellite, 10.41 wt% Ca-beidellite, 4.19 wt% sodium carbonate, 0.95 wt% whitlockite, 0.66 wt% corundum, 0.36 K-beidellite, 0.20 wt% ilmenite, 0.10 wt% potassium carbonate, and 0.10 wt% sulfur.

E) Stable decomposition products from the weathering of dunite of the same composition as Chassigny (18,19) which have reached thermodynamic equilibrium with liquid water containing dissolved O2 and CO2 (17); The end product is a composition of 50.54 wt% goethite, 17.83 wt% quartz, 15.62 wt% talc, 13.88 wt% magnesite, 1.02 wt% calcite, 0.41 wt% Na-beidellite, 0.27 wt% Ca-beidellite, 0.16 wt% sodium carbonate, and 0.06 wt% corundum.

F) Interpretation of the Viking X-Ray Fluorescence experiment results (20);

G) Palagonite, an amorphous weathering product of basaltic glass, which is considered a good Martian dust spectral analog (2,3).

H) A mixture of 85 wt% palagonite, 9 wt% magnesium sulfate, 5 wt% calcite, and 1 wt% sodium chloride.

I) A mixture of 60 wt% palagonite, 25 wt% unweathered basalt, 9 wt% magnesium sulfate, 5 wt% calcite, and 1 wt% sodium chloride.

The last two models are proposed by the authors to combine the results of Viking Lander soil measurements with a palagonite model.

The results of this two part analysis and the laboratory spectroscopic measurements of the model materials will be discussed.

References:

1) Adams J. B. and McCord T. B. (1969) *J. Geophys. Res. 74,* p. 4851-4856.
2) Singer R.B. (1982) *J. Geophys. Res. 87,* p. 10159-10168.
3) Evens D. L. and Adams J. B. (1980) *Proc. Lunar Sci. Conf. 11th,* p. 757-763.
4) Huguenin R. L., Adams J. B., and McCord T. B. (1977) *Lunar Sci. VIII,* p. 478-480.
5) Singer R. B., McCord T. B., Clark R. N., Adams J. B., and Huguenin R. L. (1979) *J. Geophys. Res. 84,* p. 8415-8426.
6) McCord T. B., Clark R., and Huguenin R. L. (1978) *J. Geophys. Res. 83,* p. 5433-5441.
7) McCord T. B., Clark R. N. and Singer R. N. (1982) *J. Geophys. Res. 87,* p. 3021-3032.
8) Blaney D. L., Walsh P. A., and McCord T. B. (1987), *Lunar and Planet. Sci. Conf. XVIII,* p. 87-89.
9) Houck J. R., Pollack J. B., . Sagan C., Schack P., and Pecker J. A. (1973) *Icarus18,* p. 470-479.
10) Sinton W.M. (1967) *Icarus 6,* p. 222-228.
11) Nedell S. S. and McKay C. P. (1987) *Lunar Planetary Science Conference XVIII,* p. 712-713.
12) Roush T. L., Blaney D., McCord T.B., Singer R. B. (1986) *Lunar and Planetary Science XVII,* p. 732-733.
13) Blaney D. L. and McCord T.B. (1987) submitted to *J. Geophys. Res.*
14) Gaffey M. J. (1976) *J. Geophys. Res. 81,* p. 905-920.
15) Feierberg M. A. and Drake M.J. (1980) *Science 209,* p. 805-807.
16) Smith M. R., Laul J. C., Ma M. A., Huston T., Verkouteren R. M., Lipschutz M. E., and Schmitt R. A. (1984) *J. Geophys. Res. 84,* p. B229-B236.
17) Gooding J. L. (1978) *Icarus 33,* p.483-513.
18) Nehru C. E., Prinz M., Delaney J. S., Dreibus G., Palme H., Spettel B., and Wånke H. (1983) *J. Geophys. Res. 88,* p. B237-244.
19) Floran R. J., Prinz M., Hlava P. F., Keil K., Nehru C. E., and Hinthorne J. R. (1978) *Geochim. Cosmochim. Acta 42,* p. 1213-1229.
20) Toulmin P., Baird A. K., Clark B. C., Keil K., Rose H. J., Evans P. H., and Kelliher W. C. (1977) *J. Geophys. Res. 82,* p. 4625-4634.

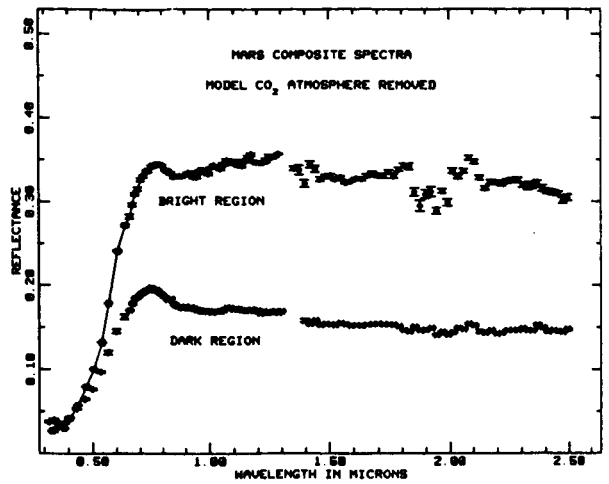

Figure 1. Reflectance spectra from 0.33 to 2.50 for typical bringht and dark regions scaled appoximately to normal reflectance. A model CO_2 atmosphere has been removed. From McCord et al. 1982.

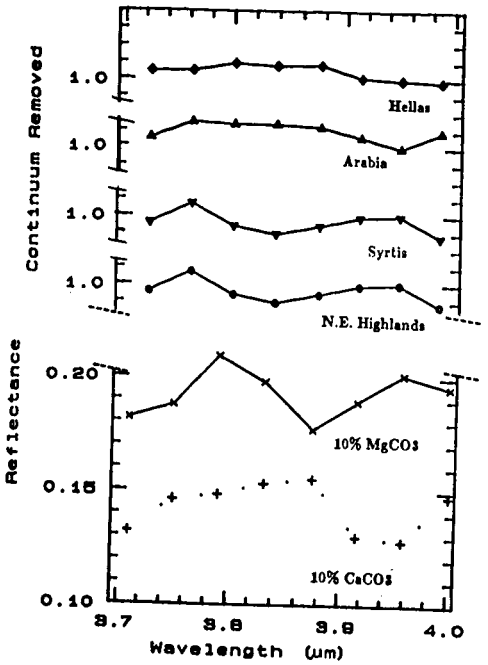

Figure 2. Spectra with straight line continuum removed for four Mars regions. Continuum calculated using values at 3.75 μm and 4.0μm. From Blaney and McCord 1987.

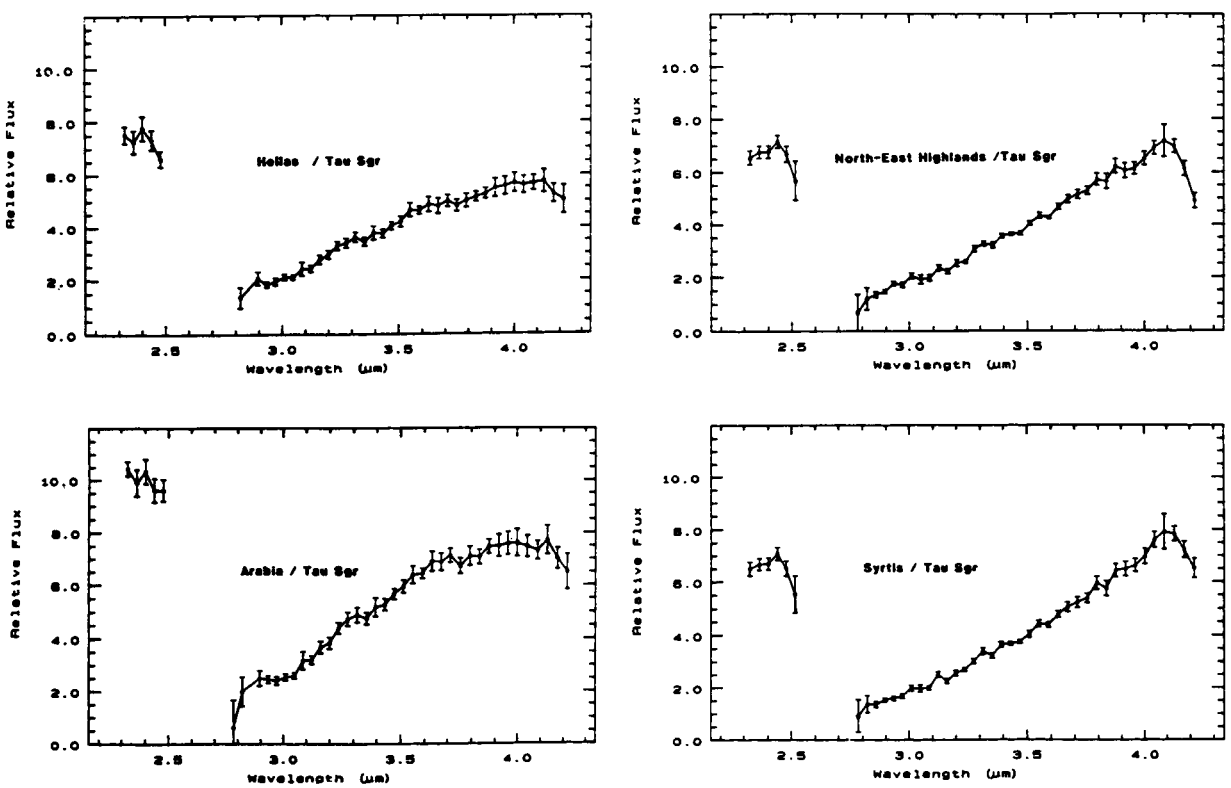

Figure 3. Reflectance spectra for four Mars regions designated Hellas, Arabia, Syrtis and North East Highlands. Tau Sagittarius was used as a calibartion standard. From Blaney and McCord 1987.

S6-91
154-106
28

SB 89 9064
N88-29660

SELECTIVE WEATHERING OF SHOCKED MINERALS AND CHONDRITIC ENRICHMENT OF THE MARTIAN FINES M. B. Boslough, Sandia National Laboratories, Albuquerque, New Mexico 87185.

In a recent paper, Boslough and Cygan (1) reported the observation of shock-enhanced chemical weathering kinetics of three silicate minerals. Based on their own experimental data and on those of Tyburczy and Ahrens (2) for enhanced dehydration kinetics of shocked serpentine, they proposed a mechanism by which shock-activated minerals are selectively weathered on the surface of Mars. The purpose of the present abstract is to argue on the basis of relative volumes of shocked materials that, as a direct consequence of selective weathering, the composition of the weathered surface units on Mars should be enriched in meteoritic material.

To support the idea that shock-enhancement of weathering rates of crystalline minerals is an important process on Mars, it is necessary to compare both production rates and volumes of shock-activated minerals to those of shock-melted minerals. The volume of impact melt produced on Mars was estimated by Newsom et al. (3) to be equivalent to a global layer 46 meters thick. However, this estimate is probably too high owing to Newsom's (4) use of an expression of Lange and Ahrens (5) which relates the volume of impact melt to crater diameter. This latter expression was derived from the work of O'Keefe and Ahrens (6), which provides an expression that linearly relates volume of melt, as a fraction of meteoroid volume (V_m), to the kinetic energy of the impact. The linear melt volume-kinetic energy relation was obtained by using a finite difference code with an assumed equation of state for the target material to simulate hypervelocity impacts and is only valid for cratering due to impacts at velocities greater than about 15 km/sec. This impact velocity range is appropriate for present lunar or terrestrial cratering, but is too high for Mars for two reasons: 1) at the orbit of Mars collision velocities are lower, and 2) Mars has a lower escape velocity than that of earth. Also, the crater size distributions used by Newsom (4) were from the ancient (4 b.y. old) lunar highlands. During the period of early, heavy bombardment, the orbits of the infalling bodies were more circular, and the relative velocities were not as high. Hartmann (7) estimates the mean impact velocity at early times to be 5.6 km/sec on Mars. By using the melt-crater diameter relationship of Lange and Ahrens (5), the Newsom et al. (3) estimate is equivalent to assuming that each impact produced a volume of melt equal to 1.4 V_m for a gabbroic anorthosite impactor striking a planet of the same composition at 5.6 km/sec. However, the calculations of O'Keefe and Ahrens (6) show that at lower impact velocities the melt-kinetic energy ratio decreases. Extrapolating the two lowest velocity calculations gives an upper bound of 0.4 V_m for the volume of impact melt.

To estimate the lower-bound quantity of shock-modified but unmelted material generated on the surface of Mars by impacts, we use the near field attenuation rate of Kieffer and Simonds (8). The dissolution rate data obtained for the three minerals by Boslough and Cygan (1) imply that for shock pressures above 7.5 GPa the weathering rate is enhanced, so we let the critical pressure be 7.5 GPa. The amount of material shocked to pressures above 7.5 GPa is equal to 2.8 V_m. As indicated above, about 0.4 V_m of this is melt, so 2.4 V_m is modified crystalline material, i.e., about six times the volume of melt. The upper-bound quantity is determined similarly by using the far-field function of Kieffer and Simonds (8) appropriate for pressures much less than the bulk modulus of the target material (This is

true for 7.5 GPa and any reasonable rock bulk modulus). The upper bound of shock-modified crystalline material is 3.9 V_m--about ten times the melt volume. The total volume of shock-activated and melted material is 4.3V_m, so 23% is meteoritic. If the chemically altered material (soil) comes only from shock-activated and shock-melted sources, it should be chondritically enriched by the same fraction.

During the later stage of Martian bombardment, after the planetesimals were gravitationally scattered, the impacting bodies approached the orbital distributions observed today for asteroids and comets. Hartmann (7) estimated the current mean impact velocity for asteroidal bodies onto Mars to be 10 km/sec. An impact at this higher velocity gives a lower ratio of shocked crystal to impact melt. The melt-to-meteoroid-volume ratio obtained by interpolating O'Keefe and Ahrens (6) calculation is 3.7, only slightly less than the value 4.5, consistent with the Newsom et al. (3) estimate. The near-field and far-field attenuation functions of Kieffer and Simonds (8) give a total volume of material shocked above 7.5 GPa of 6.2 V_m and 11.6 V_m, respectively, so the unmelted but critically shocked crystal volume is 2.5 V_m to 8.9 V_m. The shocked crystal to melt ratio is thus 0.7 to 2.4. By the same argument as above, this leads directly to a chondritic enrichment of at least 8% in the Martian soil.

In order to arrive at an estimate of the ratio of glass quenched from melt to significantly shock-modified crystalline material, we need to determine: 1) how much of the impact melt recrystallizes before it can be altered, and 2) what fraction of shock-metamorphosed minerals are annealed to a state which is no longer chemically activated. One can ignore these quantities to first order by assuming that materials which experience similar thermal histories will be similarly modified. The high-speed ejecta will cool and quench rapidly, retaining the shock-induced defects in the solid and forming glass from the liquid fraction. The material that is deeply buried in the nearby ejecta blanket would tend to cool much more slowly, recrystallizing the melt (9) and annealing the defects in the solid by a process similar to that observed for shocked titania by Casey et al. (10). If the shocked material is well-mixed in the ejecta (8), the two quantities will be approximately equal. Their magnitudes can be estimated by considering observations at terrestrial craters. At the Ries crater in West Germany, Engelhardt and Graup (11) estimated that a volume of 4-5 km^3 was melted by the impact, with only 0.2 to 0.6 km^3 remaining as glass (12), and the rest recrystallizing. This implies that 6-15% of the shocked material remains in an activated state which can undergo an enhanced rate of chemical alteration. Newsom et al. (3) determined that the suevite outside the Ries crater rim contains about 15 weight percent clay, consistent with the high end of the estimate if most of the shock-activated material was altered. In Kieffer and Simonds' (8) scenario for impacts on Mars, ejecta is finely dispersed by the expansion of shocked volatiles. This process would be expected to increase the net fraction of shock-modified material by quenching a greater volume.

The above estimates ignore the existence of another component of ejecta, namely the high-density shock-generated "diaplectic glass". This type of glass (it is also called "thetomorphic glass" or "maskelynite" when it occurs in plagioclase) is produced to varying degrees in silicates by shocks in the pressure range from 25 to 55 GPa (13). Because the details of the mineralogy of the impacted Martian surface are unknown, a good estimate of the quantity of diaplectic glass produced is difficult, but we assume it is small compared to the volume of melt and shock-activated minerals.

However, this component is highly metastable and would be expected to be the first to form alteration products.

The above discussion also ignores the contribution from the large basin-sized craters. As pointed out by Newsom (4), this avoids excessive extrapolation of the melt production relation. The amount of melt generated by the largest basins may be more than 10 times that produced by all other impacts; however, according to Newsom (4), the interaction with water may be much less for the associated impact-melt sheets.

It should be pointed out that the argument for chondritic enrichment of the Martian soil is strong even if shock-activation of crystalline minerals were an insignificant process. If the quantity of melt of 1.4 V_m is used, that corresponds to 71% of the melt consisting of meteoritic material. If only shock glass is weathered, the regolith would be enriched by this amount.

There is some evidence from the Viking x-ray fluorescence data that the Martian fines have a large meteoritic component. Toulmin et al. (14) listed one of the best matches of possible mixtures as being composed of approximately equal fractions of average tholeiitic basalt and type I carbonaceous chondrites. However, this model was promptly dismissed as fortuitous, since at the time there was no known mechanism by which large amounts of undifferentiated material could be concentrated in the soil. The present selective weathering hypothesis provides such a mechanism, and estimates of fractional enrichment span the ~50% amount implied by the Toulmin et al. (14) mixing model.

References

(1) Boslough M.B. and Cygan R.T. (1987) Proc. Lunar Planet. Sci. Conf. 18th, in press.
(2) Tyburczy J.A. and Ahrens T.J. (1987) Proc. Lunar Planet. Sci. Conf. 18th, in press.
(3) Newsom H.E., Graup G., Sewards T. and Keil K. (1986) J. Geophys. Res., 91, E239-E251.
(4) Newsom H.E. (1980) Icarus, 44, 207-216.
(5) Lange M.A. and Ahrens T.J. (1979) Proc. Lunar Planet. Sci. Conf. 10th, 2707-2725.
(6) O'Keefe J.D. and Ahrens T.J. (1982) Proc. Lunar Planet. Sci. Conf. 8th, 3357-3384.
(7) Hartmann W.K. (1977) Icarus, 31, 260-276.
(8) Kieffer S.W. and Simonds C.H. (1980) Rev. Geophys. Space Phys., 18, 143-181.
(9) Engelhardt W.v., Stöffler D. and Schneider D. (1969) Geologica Bavarica, 61, 229-296.
(10) Casey W.H., Carr M.J. and Graham R.A. (1987) Geochim. Chosmochim. Acta., to be submitted.
(11) Engelhardt W.v. and Graup G. (1984) Geologischen Rundschau, 73, 447-481.
(12) Pohl J., Stöffler D., Gall H. and Ernston K. (1977) in Impact and Explosion Cratering (D.J. Roddy, R.O. Peppin and R.B. Merrill, eds.), pp. 343-404, Pergamon, New York.
(13) Stöffler D. (1984) J. Non-Cryst. Solids, 67, 465-502.
(14) Toulmin P. III, Baird A.K., Clark B.C., Keil K., Rose H.J., Evans P.H. and Kelliher W.C. (1977) J. Geophys. Res., 82, 4625-4634.

This work was performed at Sandia National Laboratories, supported by the U. S. Department of Energy under contract number DE-AC04-76DP00789.

DB 608495 N88-29661

INTERCRATER PLAINS DEPOSITS AND THE ORIGIN OF MARTIAN VALLEYS; G. R. Brakenridge, Department of Geography, Dartmouth College, Hanover NH 03755

Detailed geological mapping of portions of the Thaumasia Fossae and Aeolis Quandrangles has documented several interesting relationships between valley development and local geology. At a location 150 km south of Warrego Vallis in Thaumasia, V-shaped branching valleys or sub-parallel slope ravines (figure 1) partially dissect an isolated remnant of intercrater plains deposits (figure 2). Cross-cutting relations and superposition indicate that the valleys developed after: a) plains deposition, b) N-S graben, and c) post-graben, NE oriented faults, one of which exhibits left-lateral displacments of ca. 2.5 km. Although most graben displace the plains material, several do not; this suggests that the (Tharsis-related) graben began forming while plains deposition was still underway. After both styles of faulting, dark flow volcanism covered low-lying areas and partially filled many graben. These extensive, dark, lava-covered plains stretch northward to, and partially cover, the Warrego Vallis tributary channels. Finally, younger, unmodified craters are superimposed on the entire landscape.

When did the valleys form? The stratigraphic relations constrain them as post-graben (many debouch into graben, but they are not cut by graben), and pre-final cratering (some valleys are truncated by ~3 km diameter craters). They might have developed prior to the dark flow volcanics, which are not themselves modifed by fluvial activity. However, they could, as well, be coeval to the volcanism. As noted, nearby Warrego Vallis is partially blanketed by similar volcanic rock, indicating that valley development there was terminated by final extrusion of the flow volcanics. Volcanism, or high heat flow from plutonism prior to volcanism, may have first provoked valley development at Warrego, and then culminated in partial valley burial by lavas. Of relevance in this respect is the suggestion of reference 1 that small Martian valleys require ice-rich plains materials as substrata for their development. This emphasizes that the valleys shown in figure 2 could in fact be coeval to the local extrusive volcanism, with their absence on the latter bedrock being due to its lithology rather than to the cessation of a "valley forming" climatic interval.

On the steeper slopes of the plains remnant (and near the resolution limit of the image), light-dark internal stratification is visible. A relatively dark-albedo stratum crops out near the flat surface of the plains, and is both overlain and underlain by higher-albedo strata. The dark unit may be a sill (figure 2) and may represent lava extruded at the same time as the surface flows to the north of the remnant. Supporting this inference is the presence of small (<1 km diameter) dark hills on the remant surface, which may be cinder cones, and E-trending dark lineaments cropping out on its slopes and to the south, which may be dikes. Nearly all of the valleys visible in this image appear to have heads at the base of the dark stratum. These observations suggest that the dark unit acted as an aquiclude for heated waters which exited as springs along its base: valley development occurred by hot spring activity associated with sill emplacement into ice-rich material (see also reference 2). In contrast, an ancient ground water system due to a past warmer climate is not required,

and suffers from several difficulties, including the need to either percolate water down through the dark unit from the surface or force it up into the remnant from below.

Earlier work in Aeolis suggested that some valleys there are the result of impact melting of icy materials (3). Quandrangle-wide measurements on valley orientations and additional local mapping also indicate: a) strong preferred orientations for the valleys (of 299 valleys or valley segments measured, none were aligned NE, and NW orientations are dominant), b) an association, also described by reference 1, of valleys with intercrater plains deposits, c) internal stratification of these deposits (first noted by Malin, reference 4), and d) a probable major role for mafic plains volcanism near the end of the Late Heavy Bombardment in providing the release mechanism for valley development.

If the upland intercrater plains (the "rough plateau" unit of reference 5, p.67, and the "degraded deposits" of reference 1) do contain ground ice, then the origin of the vast majority of both channels and valleys on Mars (classes 1-3 on figure 1, plus many outflow channels) seems clear: they must have formed by surface flowage of water liberated from frozen groundwater reservoirs by various mechanisms of heating, and especially magmatism and plutonism. A major concern, however, has been how water was added to surficial regions of the Mars crust. In this respect, the inferences of Jakosky and Carr (6) are critical. These workers infer that the calculated pre-Tharsis enhanced obliquity of Mars would have caused ice condensation at low latitudes, where it is now unstable when in contact with the atmosphere. This results in a mechanism for the deposition of ice, perhaps mixed with loess, in the cratered highlands early in Mars history.

The geological principles of uniformitarianism and actualism require that we pay more attention to using the Mars present as a key to its past, rather than searching for terrestrial analogs. Ice-rich, stratified deposits are forming today in the polar regions of Mars. If enhanced obliquity did occur, then a large part of the original Mars endowment of water was probably deposited quite early as ice. It then would have been intermittently released by impact cratering and extensive volcanism as the Heavy Bombardment came to an end. The solar-heating mechanism also outlined by Jakosky and Carr may be less important, but such surface melting could be responsible for the "coarse, disordered texture", including numerous small channels, of the rough plateaus at high resolution (5, p. 67-68), as well as their low crater densities.

1. Wilhelms, D.E. and Baldwin, R.J., 1986: Abstracts, 17th Lunar and Planetary Science Conference, p. 948-949.
2. Squyres, S.W., Wilhelms, D.E., and Mossman, A.C., 1987: Icarus, v. 70, p. 385-408
3. Brakenridge, G. R.,Newsom, H.E., and Baker, V.R., 1985: Geology, v. 13, p.859-862
4. Malin, M.C., 1976: Ph.D. dissertation, California Institute of Technology.
5. Carr, M., "The Surface of Mars", Yale University Press, New Haven, 232 p.
6. Jakosky, B.M., and Carr, M.H., 1985: Nature, v. 315, p. 559-561.

ORIGINAL PAGE IS
OF POOR QUALITY

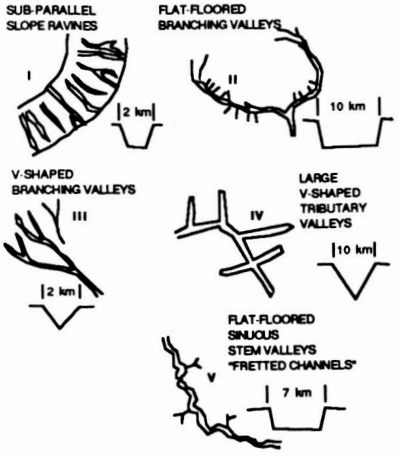

Figure 1 Valley Classification

Figure 2a Map of Viking 532A15

20 km

Faults and Dikes

Valleys

Young Craters

Sill Outcrops

N

Fv: Flow volcanics

Pr: Plains remnant

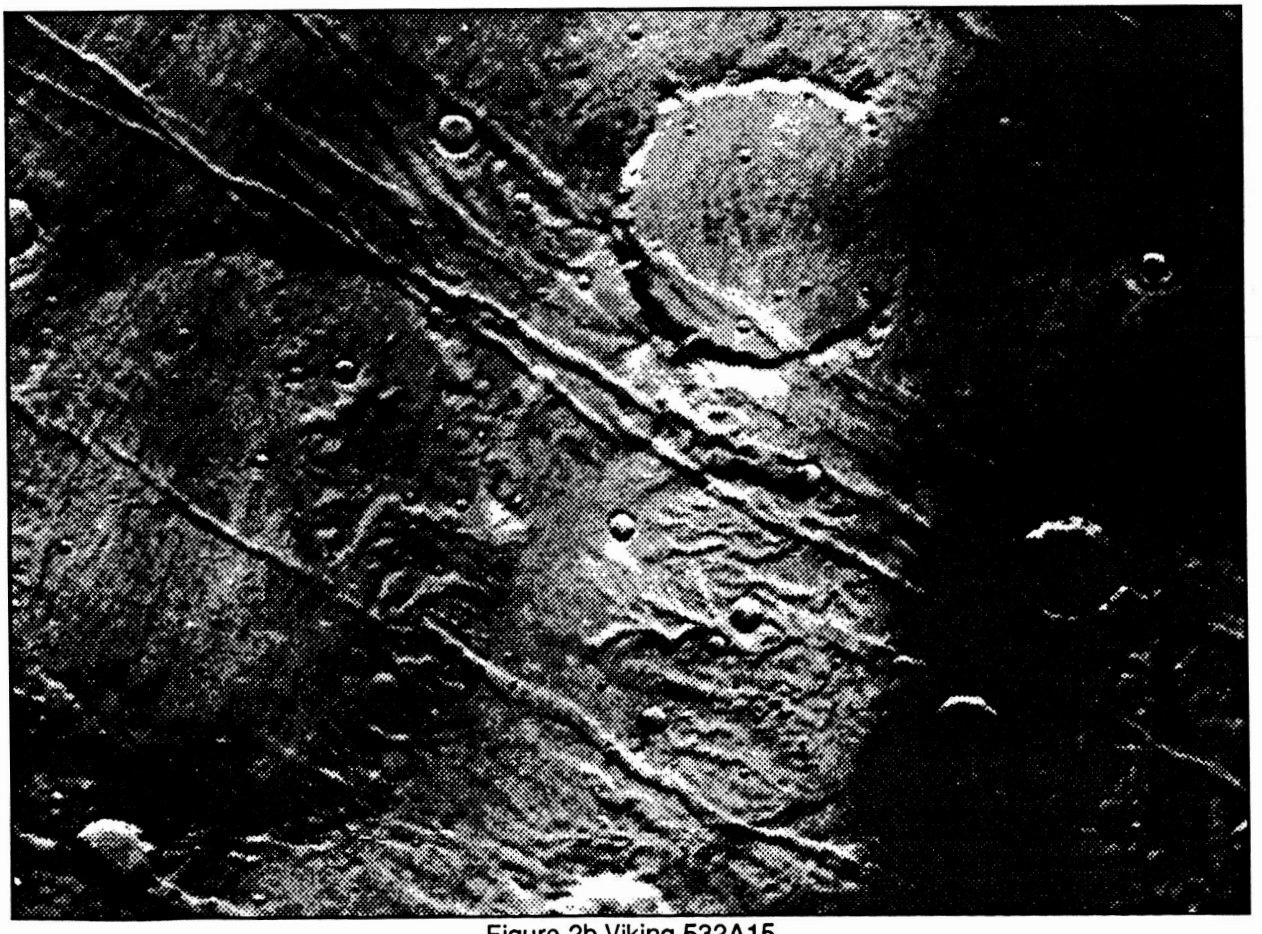

Figure 2b Viking 532A15

N88-11
151-23

N88-29662 MJ700802

WEATHERING OF SULFIDES ON MARS

Roger G. Burns and Duncan S. Fisher, Department of Earth, Atmospheric and Planetary Sciences, Massachusetts Institute of Technology, Cambridge, MA 02139.

Background. The presence of massive volcanoes in the Tharsis and Elysium regions, the distinctive petrology of SNC meteorites, and a compendium of results from the Viking Lander experiments all point to extrusive and plutonic mafic and ultramafic igneous rocks on Mars having analogies to terrestrial komatiites [1]. On Earth, the latter are associated with massive and disseminated sulfides containing pyrrhotite, pentlandite, and accessory pyrite and chalcopyrite [2]. Near-surface oxidation of these sulfides have produced conspicuous rust-colored gossans, which often betray the occurrence of unexposed ore deposits (**Figure 1**). Studies of gossans and sub-surface minerals [3-5] suggest pathways of oxidative weathering reactions that may be applicable to Mars.

Pyrite is pivotal to chemical weathering reactions of sulfides. It may occur as a minor constituent of primary igneous sulfides, or be formed by supergene reactions involving deep weathering of pyrrhotite (see equation **{1}** in **Table 1.**). At or near the water table, oxidation of pyrite by aerated groundwater occurs **{5},{6}.** Ferric iron liberated in this reaction, not only promotes the initial alteration of pyrrhotite **{1}** and of pentlandite **{2}** to secondary sulfides in the absence of dissolved oxygen, but also aids the dissolution of pyrite **{3}** below the water table. Supergene enrichment reactions also occur there **{4},{7}**, leading to high concentrations of Ni, etc. in secondary sulfides. Strongly acidic and sulfate-rich groundwater is produced which stabilizes dissolved ferrous iron and a variety of complex ferric ions [6] including those listed in **{11}** and **{12}**). At elevated temperatures, these complexes produce of a variety of hydroxo-ferric sulfate sols [7] (e.g carphosiderite **{11},{12}**), which may be the precursors to a number of ferric sulfate minerals [8] often found in gossans in arid regions. In less acidic environments above the water table, dissolved ferric ions and monodispersed sols are hydrolysed to poorly crystalline FeOOH phases (e.g. ferrihydrite, goethite **{8}-{10},{13},{14}**), which coexist with silica (opal, jasper) and the hydrated ferric sulfate minerals in gossans. The fields of relative stabilities of gossaniferous phases are depicted in the oxidation-acidity diagram shown in **Figure 2.**

The reactions formulated in **Table 1** demonstrate that groundwater in the vicinity of oxidizing sulfides is highly acidic. Such low pH solutions promote the chemical weathering of feldpars, pyroxenes and olivine in host igneous rocks [9], liberating dissolved silica, Al, Ca, Mg, Na and additional Fe ions, and producing secondary clay silicates (e.g. smectite) and iron oxyhydroxides. On Earth, seafloor basalts and gabbros erupting along submarine spreading centers have undergone extensive hydrothermal alteration by seawater circulating through underlying tectonically-fractured oceanic crust. As a result, the acidity of aqueous solutions is buffered by seawater-basalt interactions, leading to the slight alkalinity (pH 8.2) of present-day terrestrial oceans.

The oxidative power of atmospheric oxygen is the driving force in the weathering of sulfides (in the absence of bacterial activity). The dissolution of oxygen in groundwater and its migration to sulfide reaction centers involve diffusion processes and are probably rate-controlling. When the concentration of dissolved oxygen is very low and the supply of water is limited, oxidative reactions become sluggish and involve hydrogen peroxide. Furthermore, ferric-bearing solutions may liberate elemental sulfur. Thus, metastable sulfur is observed in pyrite-jarosite-sulfur assemblages associated with some ultramafic pyrrhotite-pentlandite deposits [10].

Martian Weathering. On Mars, where plate tectonic activity appears to have been insignificant, vast volumes of iron-rich basaltic magma has reached the surface of the planet via immense shield volcanoes. Fracturing associated with this volcanism, as well as impact cratering, facilitated deep-weathering reactions by permeating groundwater early in the history of Mars. However, the apparent absence of spreading centers and subduction zones, which cause recycling of the Earth's crust, has minimized acid-buffering of aqueous

ORIGINAL PAGE IS
OF POOR QUALITY

Table 1. Chemical Weathering Reactions Involving Sulfides

Oxidants:

-- at the surface: $O_2 + 4H^+ + 4e^- = 2H_2O$, or

$O_2 + 2H_2O + 4e^- = 4\ OH^-$

--below the water table: $Fe^{3+} + e^- = Fe^{2+}$

Primary Sulfides:

--pyrrhotite Fe_7S_8 {+/- pentlandite $(Fe,Ni)_9S_8$}

Deep-Weathering Reactions:

{1} Fe_7S_8 (pyrrhotite) + $6Fe^{3+} = 4FeS_2$ (pyrite) + $9Fe^{2+}$

{2} $(Fe,Ni)_9S_8$ (pentlandite) + $2Fe^{3+} = 2(Fe,Ni)Ni_2S_4$ (violarite) + $3Fe^{2+}$

Enrichment (Supergene) Reactions:

{3} $FeS_2 + 14Fe^{3+} + 8H_2O = 15Fe^{2+} + 2SO_4^{2-} + 4H^+$

{4} $(Fe,Ni)Ni_2S_4 + 2Fe^{3+} = Ni_3S_4$ (polydymite) + $3Fe^{2+}$

Near the Water Table:

{5} $2FeS_2 + 2H_2O + 7\ O_2 = 2Fe^{2+} + 4SO_4^{2-} + 4H^+$

{6} $4FeS_2 + 2H_2O + 15\ O_2 = 4Fe^{3+} + 8SO_4^{2-} + 4H^+$

{7} $2Ni_3S_4 + 2H_2O + 15\ O_2 = 6Ni^{2+} + 8SO_4^{2-} + 4H^+$

Above the Water Table:

{8} $Fe^{3+} + 2\ OH^- =$ FeOOH (ferrihydrite, goethite, hematite) + H^+

{9} $4Fe^{2+} + 6H_2O + O_2 =$ 4FeOOH (ferrihydrite, etc) + $8H^+$

{10} $3Fe^{2+} + 3H_2O + 2SO_4^{2-} + 3/2\ O_2 = [Fe_3(SO_4)_2(OH)_6]^-$ (jarosite)

Jarosite-Forming Reactions:

{11} $2FeSO_4^{1+} + FeOH^{2+} + 6H_2O = (H_3O)Fe_3(SO_4)_2(OH)_6 + 4H^+$

{12} $Fe(SO_4)_2^{1-} + 2FeOH^{2+} + 5H_2O = (H_3O)Fe_3(SO_4)_2(OH)_6 + 3H^+$

{13} $FeSO_4^{1+} + 2H_2O =$ FeOOH + $SO_4^{2-} + 3H^+$

{14} $(H_3O)Fe_3(SO_4)_2(OH)_6 = 3$FeOOH + $2SO_4^{2-} + 4H^+ + H_2O$

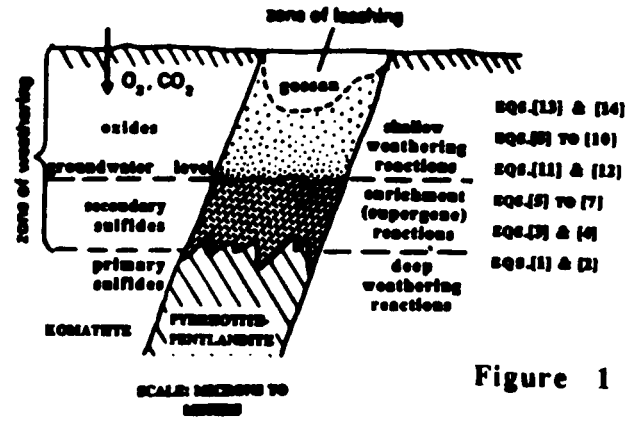

Figure 1

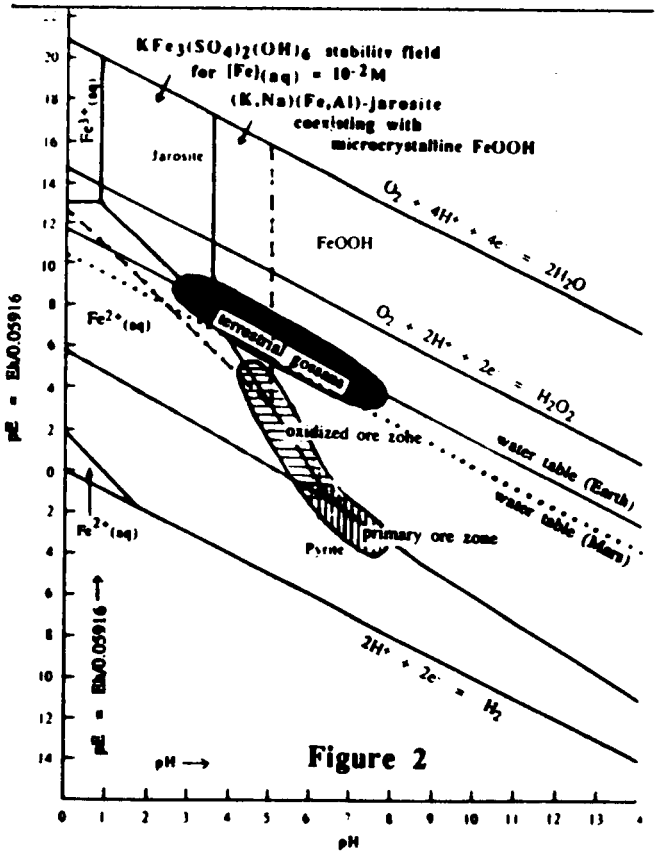

Figure 2

Figure 1 (top right). Zones of weathering associated with gossan formation above sulfide mineralization. The scale of the sulfide vein may be a few microns to several meters in diameter. Reactions {1} to {14} correspond to those in **Table 1.**

Figure 2 (bottom right). Caption is on the next page.

solutions by wall-rock alteration on Mars. Therefore, the acidity of groundwater, now permafrost, may have been maintained during the chemical evolution of the martian surface, thereby aiding the solubility and transport of Fe, Al, Mg, Ni, silica, etc. Geomorphological evidence attesting to the flow of water on Mars suggests that gossan-forming reactions may have occurred in the past. However, the present-day cold surface of Mars has impeded deep-weathering of sulfides in host basaltic rocks due to slow reaction rates and restricted access of dissolved oxygen or ferric iron to reaction centers. Nevertheless, some oxidative weathering may still be occuring in the frozen environment on Mars, as indicated by the oxidation of Fe and FeS phases observed in Antarctic meteorites [11]. When sublimation of martian permafrost occurs, species held in solution could be hydrolysed, precipitated as colloidal material and transported in dust storms..

Discussion. Evidence for gossan formation on Mars stems from several sources. First, remote-sensed reflectance spectral profiles are matched closely by ferrihydrite-silica gels and jarosite-bearing clay assemblages [12]. Second, jarosite which is so characteristically an oxidative weathering product of iron sulfides, may be present in SNC meteorites [13,14] believed to have originated from Mars. Third, the magnetic phase detected in the Viking magnetic experiment [15] may be remnant pyrrhotite which has been incompletely oxidized, particularly if the level of the water table has dropped on Mars. Finally, a limited supply of water and a low concentration of dissolved water, which favor the formation of hydrogen peroxide and promote the production of peroxide and superoxide phases, may account for results obtained in the Viking biology experiments [16].

Summary. Pyrrhotite-pentlandite assemblages in mafic and ultramafic igneous rocks may have contributed significantly to the chemical weathering reactions that produced degradation products in the martian regolith. By analogy with terrestrial processes, a model is proposed whereby supergene alteration of these primary Fe-Ni sulfides on Mars has generated secondary sulfides (e.g. pyrite) below the water table and produced acidic groundwater containing high concentrations of dissolved Fe, Ni and sulfate ions. The low pH solutions also initiated weathering reactions of igneous feldspars and ferromagnesian silicates to form clay silicate and ferric oxyhydroxide phases. Near-surface oxidation and hydrolysis of ferric sulfato- and hydroxo-complex ions and sols formed gossans above the water table consisting of poorly crystalline hydrated ferric sulfates (e.g jarosite), oxides (ferrihydrite, goethite) and silica (opal). Underlying groundwater, now permafrost, contains hydroxo sulfato complexes of Fe, Al, Mg, Ni, etc., which may be stabilized in frozen acidic solutions beneath the surface of Mars. Sublimation of permafrost may replenish colloidal ferric oxides, sulfates and phyllosilicates during dust storms on Mars. [17]

References.

[1] Baird, A.K. & Clark, B.C. (1981) *Icarus*, **45**, 113-123. [2] Guilbert, J.M. & Park, Jr, C.F. (1986) *The Geology of Ore Deposits* (W.H.Freeman). [3] Thornber, M.R. (1975) *Chem. Geol.*, **15**, 1-14 & 117-144. [4] Blain, C.F. & Andrew, R.L. (1977) *Minerals Sci. Engng*, **9**, 119-150. [5] Burns, R.G. (1987) *Lunar Planet. Sci.*, **XVIII**, 141-142; *Proc. 18th LPSC*, in press. [6] Sapieszko, R.S. *et al.* (1977) *J. Phys. Chem..*, **81**, 1061-1068. [7] Matijevic, E. *et al.* (1975) *J. Colloid. Interfac. Sci.*, **50**, 567-581. [8] Burns, R.G. (1987) *JGR*, **92** (B4) E570-574. [9] Siever, R. & Woodford, N. (1979) *Geochim. Cosmochim. Acta*, **43**, 717-724. [10] Nickel, E. (1984) *Mineral. Mag.*, **48**, 139-142. [11] Gooding, J.L. (1981) *Proc. 12th LPSC*, 1105-1122. [12] Sherman, D.A. *et al.* (1982) *JGR*, **87** (B12), 10169-10180. [13] Smith, J.V. & Steele, I.M. (1984) *Meteoritics*, **19**, 121-133.. [14] Gooding, J.L. (1986) *Geochim. Cosmochim. Acta*, **50**, 2215-2223. [15] Hargraves, R.B. *et al.* (1979) *JGR*, **84**, 8379-8384. [16] Huguenin, R.L. (1982) *JGR*, **87** (B12), 10069-10082. [17] Supported by NASA Grants NSG-7604 and NAGW-1078.

Figure 2 (previous page, bottom right). Eh-pH diagram at 25°C for pyrite and its oxidative products, including jarosite and FeOOH, occurring in gossans. Heavy lines correspond to 0.01M each of K, total Fe and total S dissolved species. The area bounded by dashed lines represents the approximate stability field of jarosite expanded by K-Na and Fe-Al atomic substitutions. Ranges of pE and pH measured in oxidized pyrrhotite-pentlandite assemblages are shown. Also shown are pE-pH curves for dissolved oxygen in equilibrium with the atmospheres of Earth and Mars.

N88-29663
51 380652
154909
38.37
59-91

MAPPING OF VOLCANIC UNITS AT ALBA PATERA, MARS

Peter Cattermole, Department of Geology, Sheffield University, Brookhill, Sheffield, S37HF, England.

Detailed photogeologic mapping of Alba Patera, Northern Tharsis, has been completed and a geologic map prepared. This is supplemented by a series of detailed volcanic flow maps for which quantitative data has been derived for a large number of volcanic flows. This has been used to study the morphometry of different flow types and analyse the way in which the volcano's behaviour has changed with time and also the manner in which flow fields developed in different sectors of the structure. The general geological map is shown in Figure 1.

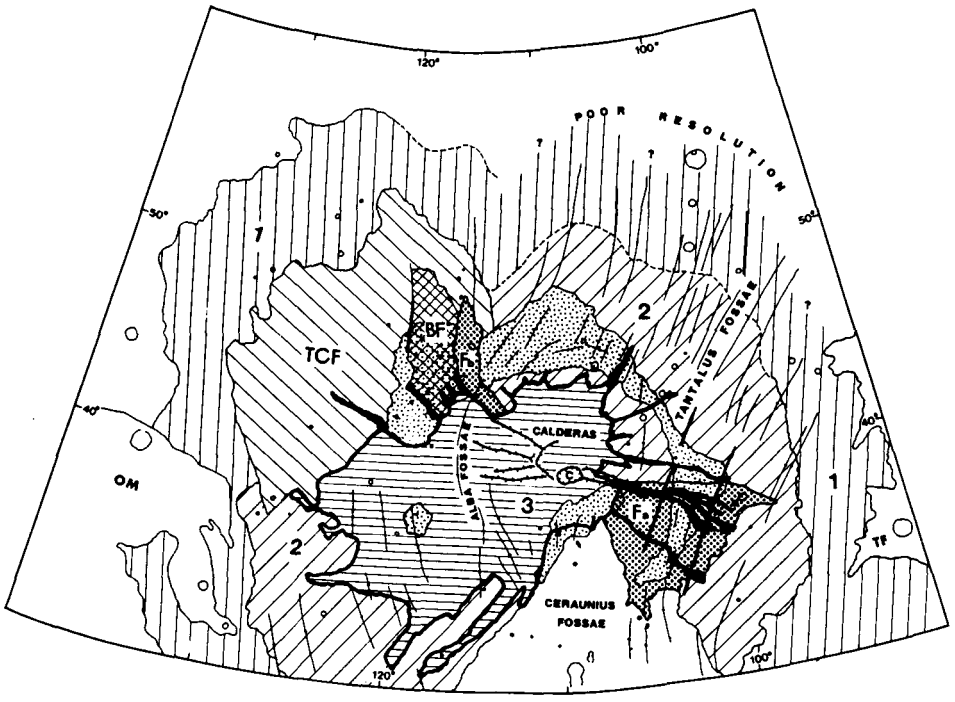

Figure 1. General geologic map of Alba Patera showing the principal units.

The geologic sequence is as follows:

Unit 1: massive flood-type flows, generally flat-topped and often seemingly composite. Also well-defined, narrower sheet lavas which have an approximately radial disposition with respect to the present summit. This unit is often heavily mantled, apparently by aeolian deposits which almost completely bury many impact craters. The most distal lavas extend 1400km from the present summit. On the basis of these being the most widely distributed flows, Alba's volcanic deposits can be said to extend over an area of as least as great as 1.8×10^6 km^{-2}.

Unit 2: a plethora of younger sheet flows (often 200-300km in length) and tube-fed lavas of high volume. The detailed distribution pattern is highly complex, as can be seen from the detailed map of a small area of the volcano's western flank shown in Figure 2 overleaf. The long

ORIGINAL PAGE IS
OF POOR QUALITY

sheet-style lavas often form multiple cooling units and in distal locations give rise to prominent flow scarps. Etched terrain amongst the flows is interpreted as pyroclastic material (e.g. ash or air-fall tuff).

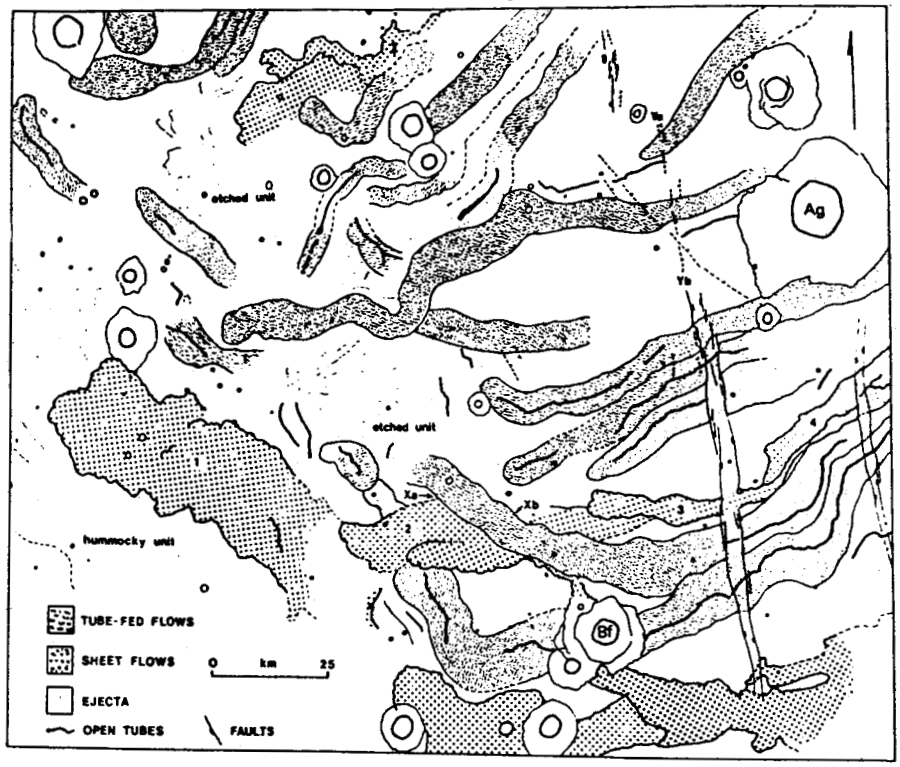

Figure 2. Detailed map of region on western flank of Alba Patera and within mapping unit 2. The massive sheet flows (1,2,3 etc) are usually overlain by tube-fed lavas in this region. The etched terrain may be pyroclastic in nature, possibly overlain by aeolian deposits.

Unit TCF: a broad field of massive tube-fed lavas which covers an area of 280,000km^{-2} on the lower western flanks. These 2-300km long flows are high volume lavas which may be up to 850m thick and have axial tubes/channels up to 250m across. The non-radial dispostion suggests these lavas emanated from fissures and linear vents on the western flanks prior to the eruption of unit 3 summit flows.

Units Fa and Fb: two massive sheet flow fields, both exceeding 15,000km^{-2} in area. These are amongst the best defined sheet flows on Alba. Their source regions are covered by younger lavas within the ringfracture zone.

Unit BF: is an area of complex tube-fed flows, faults and tear-shaped hollows which has been desribed as "etched terrain" by Mouginis-Mark et al (1) who interpret the textural grain as due to sapping of relatively non-resilient fragmental deposits. Another interpretation is that the hollows represent collapsed flow "buds" formed as the advancing tube-fed flows overspilled their marginal banks while flowing downslope. This unit is either coeval with or slightly older than Fb above.

Unit 3: the youngest summit-related flows. These can be divided into two groups: (i) long and relatively narrow sheet flows and lesser

numbers of tube-fed lavas, and (ii) shorter, narrow and often leveed flows which may be traceable to the caldera backwalls.

Channelled units: large areas within units 2 and TCF (including windows of unit 2 rocks within unit 3) show the development of dendritic drainage networks. These were noted by Carr and Clow(2) and have recently been described by Wilson and Mouginis-Mark (3). Their distribution is shown by stipple in Figure 1. The channels appear to be older than unit 3 but younger than unit 2.

On the basis of work completed to date, the earliest phase of Alba's eruptive cycle was characterized by eruption of extensive "plateau"style lavas(unit 1). Succeeding this was a period during which more strongly centralised eruption of high-volume sheet and tube-fed flows which spread down the lower flanks was interspersed with more explosive episodes which generated air-fall tuffs (or similar fragmental deposits) that became interbedded with the lavas (unit 2). A massive tube-fed flow field grew on the lower western flank and apparently was not related to the summit region. It is inferred that these huge flows emanated from linear vents or fissures. The later stages of the cycle saw eruption of relatively narrow sheet flows and lesser numbers of tube-fed lavas which centred on the caldera region at the summit.

Ongoing work addresses the problems associated with channellised units and the development of flowfields in different locations and at different periods in the volcano's evolutionary history.

References: (1) Mouginis-Mark,P.J.,Wilson,L.and Zimbelman,J.R. Submitted Bull.Volcanol.,1987. (2) Carr,M.H.and Clow,G.D., Icarus, 48, 91-117,1981. (3)Wilson,L. and Mouginis-Mark,P.J. Nature, 1987 In press.

510-91 134710
40

N88-29664

PH 956474

An Introduction to the Historical Records of China about Mars*

Chang Shuyen[1] Wu Zhongliang[2]
Peking University, Beijing, People's Republic of China

There are quite much information about Mars in the Chinese historical records across thousands of years. The rulers of ancient China believed in that stars had much to do with social life, so the historical records about various kinds of celestial phenomena were made systematically and completely. Of course, there are many elements of astrology and superstition in these records, but we don't think such records valueless because we can obtain some useful information from them through careful analysis.

China is one of the earliest countries which had historical records about Mars. Before Chou dynasty there were some descriptions about the occurrences and movements of Mars. As early as Tang dynasty, Chinese astronomers had already known is period and the changes of its orbits, which are

much close to their modern values. The name of Mars 荧惑 expresses its color and the complexity of its movements. In the ancient Chinese books we can find the descriptions about the eclipse of Mars and even the changes of its color .

Mars was also regarded as to be associatted with seasons and some natural disasters. Differing from the western nations, the ancient Chinese considered the so-called five planets as a whole system in which Mars could interact with other planets such as Venus, Jupiter, etc. and even with the Sun and the Moon.

Such records have been noticed by some Chinese scientists. Many historical records across a long period and wide range have been collected and analysed. Through this, we believe, some useful information could be obtained which at least could be a valuable reference in the researches on Mars.

1. Dept. of Geology, Peking University

2. Dept. of Geophysics, Peking University

* Co-workers:

Wang Lixing Beijing Observatary, Academia Sinica

Li Shujing Seismological Press, China

Chin Lizhao Institute of Space Physics, Academia Sinica

Gu Jicheng Institute of Geophysics,
National Seismological Bureau, China

MI 411305 N88-29665 S11-91
154911 43 10.

ELEMENTAL COMPOSITION OF THE MARTIAN SURFACE; Benton C. Clark, Planetary Sciences Laboratory (0560), Martin Marietta Astronautics, Denver, CO 80201

The Viking landers carried x-ray fluorescence spectrometers (XRFS) to the surface of Mars for direct *in situ* measurements of the elemental composition of samples that could be acquired by the surface sampler scoops. A total of 21 samples at the two landing sites were acquired and analyzed. In this review, I will discuss the constraints imposed on the design and operation of the XRFS; the accuracy and precision limitations of XRF; and the interpretation and extrapolation of results. The latter includes relevance of the investigation to martian geological processes, SNC meteorites, the formation and history of Mars, and future mission objectives/capabilities.

Design and operation. The Viking spacecraft originally had no geochemical analytical capabilities because it was thought that follow-on Viking missions would be designed to emphasize the geological exploration of the planet. Only through the efforts of certain individuals in the science community and NASA was the Inorganic Chemical Investigation added to the mission. The XRFS instrument design and integration concept was frozen in 1972: no deployment was allowed; 3 samples were to be acquired; weight, volume, and power were capped; the pulse-height analyzer mode was restricted; etc.

Accuracy/Precision. XRFS analytical results have been published with large error bars, reflecting the conservatism of the science team in the face of the lack of sample preparation. In laboratory XRF, geological samples are fine-ground and/or fused to achieve sample homogeneity and uniformity of grain size. In addition, reference samples with similar or identical matrix characteristics are measured before and after data taken on unknowns. None of this was possible on Viking, and the suite of 25 hard-rock characterization samples measured with the flight instruments prior to launch included *no* samples closely resembling the martian ones. However, for reasons that will be cited, certain estimated errors can be significantly reduced. End-to-end instrument calibration was assured by an on-board Ca+Al flip-in target, which proved invaluable in the difficult evaluation of anticipated K/Ca and Mg/Al overlaps. Precision of the measurements appears to have been very high; the accuracy of the measurements, though limited, is extremely powerful as a discriminator among compositional candidates; sensitivity limits were as anticipated, with a surprising detection of Br, but unexpectedly low Rb-Sr-Y-Zr signals from the martian materials.

Interpretations. Early interpretations of the XRFS elemental profile derived from its similitude with published geochemical analyses of nontronites. Currently, smectite clays and/or palagonite weathering products are widely discussed. These analogies are, in the author's opinion, not secure. The 21 samples of soil and inferred duricrust can now be understood in the context of silicate/salt variation diagrams. The silicate component is totally consistent with the elemental composition of certain SNC meteorites and related theoretical materials. The salt composition is consistent with isochemical weathering of a system comprised of silicates+volcanic gases. The martian megaregolith may be homogenized with respect to fines, presumably because of both physical and chemical homogeneity on the microscale, and eolian transport. The ubiquity of these "universal fines" is a major question for investigation.

Other extensions of the interpretations include the possible predominant geochemical and mineralogical nature of extrusives (Shergottite-like), rheology of martian lava, constraints on mantle composition, and the fate of martian volatiles. Each of these topics can be addressed in the context of the XRFS measurements, especially when combined with other relevant data.

Future mission objectives/capabilities. The Viking XRFS experience should be projected into future missions -- in terms of investigation design, operations requirements, and ground-based experimentation. The results affect both remote and *in situ* measurement strategies. Sample return missions should benefit greatly from simple geochemical screening techniques.

N88-29666

SUB-KILOMETER RAMPART CRATERS IN THE EQUATORIAL REGION OF MARS: POSSIBLE IMPLICATIONS FOR THE STATE AND DISTRIBUTION OF REGOLITH H_2O.

Stephen M. Clifford, Lunar an Planetary Institute, Houston, TX 77058, and Elizabeth Duxbury, Dept. of Earth, Atmospheric, and Planetary Sciences, Massachusetts Institute of Technology, Cambridge, MA 02139.

It has long been suspected that martian rampart crater ejecta morphology originates from an impact into a water or ice-rich crust [1,2]. This belief is at least partially supported by reports of a latitudinal variation of ejecta morphology [3,4] that may reflect the theoretically expected poleward increase in cryospheric thickness [5]. It is also supported by the tentative identification of rampart craters on at least one icy satellite, Ganymede [6]. If the H_2O-impact hypothesis is correct, then the occurrence of rampart craters at all latitudes, elevations, and in all types of terrain, implies that the distribution of regolith H_2O on Mars is global.

However, this picture of the distribution of subsurface H_2O on Mars has recently been complicated by the identification of another potential morphologic indicator of subsurface volatiles. "Softened terrain" is a term that has been used to describe the rounded or subdued appearance of martian landforms poleward of 30° latitude, an effect that has been attributed to the relaxation of topographic highs by ice-enhanced creep [7]. The absence of softened terrain at equatorial latitudes has been interpreted as an indication that the regolith in this region is ice-free, a conclusion that is consistent with the theoretical distribution of ground ice given a regolith in diffusive equilibrium with the atmosphere [5].

The absence of softened terrain between the latitudes of ±30°, and the ubiquitous presence of rampart craters in this same region, results in a major inconsistency in the distribution of subsurface H_2O inferred from these morphologies. In an effort to reconcile this apparent conflict it has been proposed that rampart crater ejecta morphology is a specific indicator of an impact involving groundwater, not ground ice [8]. In support of this explanation proponents cite current thermal models of the martian crust which suggest that the occurrence of groundwater in the equatorial region is restricted to depths in excess of 1 km [5]. They further note that excavation depths of this magnitude are consistent with the 3 km minimum rampart crater onset diameter reported in the literature [9]. By this line of reasoning the absence of softened terrain at equatorial latitudes is viewed as morphologic confirmation of the theoretically expected depletion of near-surface ground ice [10,11], while the presence of rampart craters indicates the survival of a much deeper body of groundwater [8].

To test this hypothesis we examined the occurrence of rampart craters at three locations within the latitude band of ±30° (specifically, within the ridged plains unit covered by MC-18). Working with the highest available resolution (8-10 m per pixel) 'clear' quality Viking Orbiter images, rampart craters with onset diameters between 0.6 km and 1.2 km were identified in all three areas (Figure 1). Several questionable candidates, at the very limits of resolution, have diameters as small as 0.4 km. Given the shallow depths of excavation expected of craters in this size range, it appears unlikely that their characteristic ejecta morphology can be attributed to impacts involving groundwater. This conclusion is based on the assumption that the climatic conditions that prevailed at the time of impact resembled those of today. Under such conditions, the occurrence of liquid water at depths as shallow as 100-200 m requires an unlikely combination of high geothermal heat flow, low crustal thermal conductivity, and the presence of strong freezing-point de-

ORIGINAL PAGE IS
OF POOR QUALITY

pressors. Therefore, if these smallest of rampart craters did indeed result from an impact into an H_2O-rich crust, that H_2O was almost certainly in the form of ice. This conclusion is in accord with that of another recent high-resolution study [12] which reported significant morphologic evidence for the entrainment of icy blocks within rampart crater ejecta but little evidence suggesting the involvement of groundwater.

Our analysis indicates that while few in number (approximately 1-2% of the crater population in this size range) rampart craters with diameters smaller than 3 km are indeed present at several locations within the equatorial region of Mars. This finding suggests that previous reports of a 3 km minimum onset diameter were artifacts of the resolution limits of the imagery used in those studies and not actual diameter-dependent changes in crater ejecta morphology. This finding appears to have significant implications for the inferred state and distribution of subsurface H_2O. In particular, it reaffirms the existence of a basic conflict between the distribution of ground ice inferred from the occurrence of rampart craters and that inferred from the occurrence of softened terrain. The resolution of this conflict appears to require that either: i) climatic conditions were very different at the time of rampart crater formation, or ii) that one (or both) of the candidate morphologic indicators is unrelated to the occurrence of ground ice. A more comprehensive analysis of the occurrence of sub-kilometer rampart craters is currently underway.

References: 1) Carr et al., JGR 82, 4055-4065, 1977; 2) Mouginis-Mark, P.J., Icarus 45, 60-76, 1981; 3) Johansen, L., NASA TM-80339, 123-125, 1979; 4) Blasius, K.R. and J.A. Cutts, BAAS 13, 709, 1981; 5) Fanale, F.P., Icarus 28, 179-202, 1976; 6) Horner, V. and R. Greeley, LPSC XII, 460-462, 1981; 7) Squyres, S.W. and M.H. Carr, Science 231, 249-252, 1986; 8) Squyres, S.W. and M.H. Carr, comments made during the MECA Panel Discussion on Martian Geomorphology and its Relation to Subsurface Volatiles, LPSC XVII, 1986; 9) Carr, M.H., Icarus 68, 187-216, 1986; 10) Clifford, S.M. and D. Hillel, JGR 88, 2456-2474, 1983; 11) Fanale et al., Icarus 67, 1-18, 1986; 12) Mouginis-Mark, P.J., Icarus 71, 268-286, 1987.

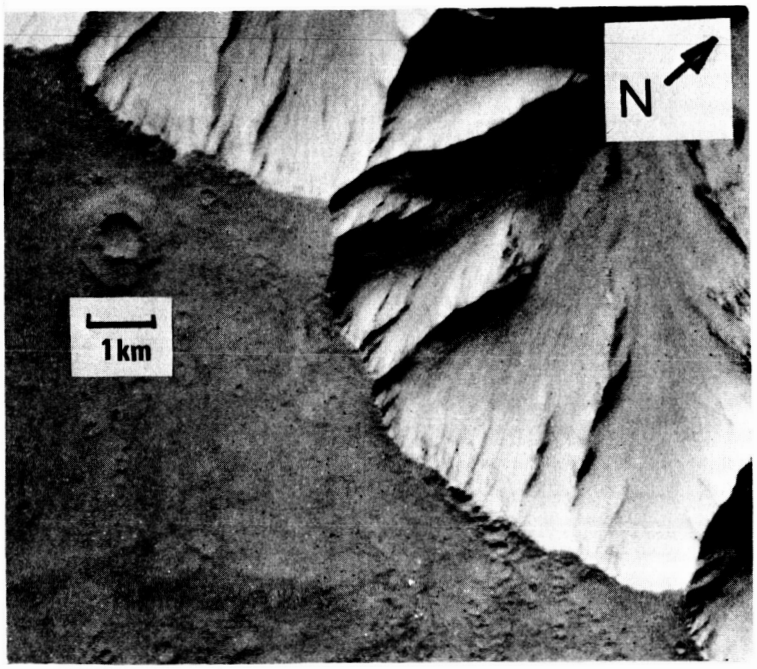

Figure 1. An example of a 0.6 km diameter rampart crater located at -13°, 69° (776A62).

SB 413977
HM 608620
SP 312460
N88-29667
NC473657

CHEMICAL AND SPECTROSCOPIC CHARACTERIZATION OF A SUITE OF MARS SOIL ANALOGS; L.M. Coyne[1], A. Banin[2], J. B. Orenberg[3], G. C. Carle[4], S. Chang[4] and T. W. Scattergood[5], [1]San Jose State University, [2]Hebrew University [3]San Francisco State University, [4]NASA-Ames Research Center, [5]S.U.N.Y. Stony Brook.

The National Aeronautics and Space Administration has begun preparations for the flight of the Mars Observer Mission in the early 1990's. This mission has several objectives: 1) to determine the global elemental and mineralogical character of the surface material; 2) to determine the spatial and temporal distribution , abundance, sources, and sinks of volatile material and dust; and 3) to explore the structure and circulation of the Martian atmosphere. These determinations will principally be made using a visual and infrared mapping spectrometer and a gamma-ray spectrometer. In order to evaluate those science objectives for this mission which are of importance to exobiology and to interpret the results of the mission, specifically reflectance spectra of the surface, an advance ground-based study is being conducted on a usefully limited suite of Mars Soil Analog Materials (MarSAM) intended to simulate the aeolian material that presumably covers much of the surface of Mars. A series of variably proportioned iron/calcium smectite clays have been prepared from a typical montmorillonite clay using the Banin method (Banin, 1973). Evidence has been obtained which supports the premise that these materials provide an exciting and unique model soil system for the Martian surface in that they are consistent with the constraints imposed by the Viking surface elemental analyses, the reflectance data obtained by various spacecraft instruments and ground-based telescopes, and the chemical reactivity measured by one of the Viking 'biology' experiments, the Labeled Release experiment. The modified clays also show evidence for a previously uninvestigated association between two structural moieties, surface iron and stored electronic energy, that are probably involved in catalytic properties of clays.

Whether or not clays are important constituents of the aeolian material is an important question for several reasons. First, the Viking surface analyses are consistent with clays constituting a significant portion of the Martian soil, but no information concerning the actual mineralogy could be obtained. Second, the presence of clays would be highly suggestive of abundant water on Mars existing sometime in the past. Third, only part of the water that is tied up in the clay structure would have been detected by the Viking instruments or remote observations and, hence, there could be much more water present on Mars than was found. Fourth, clays would be expected to contribute to the surface reactivity to a degree disproportionately greater than their abundance. Fifth, clays have a number of special properties which would suggest their capacity to store significant amounts of electronic energy that may affect both the reflectance properties of the clays and their surface reactivity, particularly in the presence of penetrating radiation (e.g. radioactivity or cosmic rays) or mechanical and frictional stresses (Coyne, 1985). Finally, clays are of particular interest to the exobiology community because of the role that they may have played in any surface chemistry and because of the hypothesis that clays may have been prototypic life forms providing templates for the prebiotic origin of simple life (Cairns-Smith, 1982).

A more specific hypothesis (Banin and Rishpon, 1978) that significant amounts of iron on Mars may have been associated with the postulated surface clays adds futher interest to the search for clays on Mars. Reflectance spectra of the Martian surface are not consistent with spectra of known crystalline iron oxides. Among several possible explanations for the weak iron absorption in the Martian spectra is that the iron may occur as both surface and structural cations in smectite clays. The absorption due to iron in both of these loci would be anticipated to be lower than expected based on overall iron abundance. Thus, as much as 33% of the Martian surface iron could be accommodated in clays. Also, iron as a surface constituent of a clay produces catalytic activity (for the decomposition of organic acids) which corresponds more closely to that found by Viking than does the iron in palagonite, another model for the Martian soil.

We discuss here the effect of increasing exchangeable iron on a diverse set of chemical and

spectroscopic properties of our suite of clays. In order to chemically characterize the MarSAM and to compare them with the Martian soil studied by Viking, our clays were analyzed for their major and minor elemental compositions by X-ray fluorescence and ion-coupled plasma techniques. The results of these analyses confirmed the compositional integrity of the materials after modification and the desired changes in iron (and calcium) content produced by the Fe-Ca exchange.

Initial results of the measurements of diffuse reflectance of the MarSAM are shown in Figure 1 (The spectra are offset for clarity). For comparison, a spectrum of a Martian high albedo region (McCord, et al., 1977) is also shown in the figure. Qualitatively, the match of the Martian spectrum with that of the 100% exchanged iron clay is quite striking, although not perfect. Iron is manifested most notably in the charge transfer region at wavelengths shorter than about 0.7 μm, however, absorptions of iron are also found at longer wavelengths. It should be noted that for this initial work, the clays were measured in room air and, hence, probably contained more adsorbed water than may be appropriate for the Martian soil. This additional water could explain the differences in the spectra for wavelengths longer than about 1.4 μm.

Results of initial studies on the relationship between surface iron and surface activity in simulations of the Viking Labeled Release experiment are shown in Figure 2. The profiles of chemical activity, as measured by the decomposition of sodium formate, with time are reasonably similar between the clays and the Martian soil. Note that the best match to the Viking LR results (from Levin and Straat, 1976) is obtained with the MarSAM with the highest amount of iron and the smallest amount of water. This particular clay also showed the best compositional agreement with the Martian soil as determined by Viking.

In Figure 3, the dependence of stored energy content, as evidenced by thermoluminescence, on amount of surface iron of natural and electronically excited materials is shown (Coyne and Banin, 1986). Note that marked changes in the light output from both the irradiated and non-irradiated clays occurs at about 0.2 mmole/g of surface iron, which corresponds to roughly 50% of the exchangeable cations. Non-linear behavior with increasing surface iron was also found for at least three other properties of the clays. The distribution of surface iron between exchangeable and acid-extractable fractions, the surface paramagnetism, and the surface chemical activity also exhibited non-linear increases with increasing surface iron. Of particular note is that changes in all of these properties appeared to level off at about the same amount of surface iron, that is, where iron accounts for about 50% of the exchange capacity of the clay.

We conclude that the surface iron has a complex and hitherto uninvestigated impact on the catalytic and spectroscopic properties of clays and on the ability of these materials to store energy. Such energy has been hypothesized to be an important structural moiety with respect to catalytic activity and spectral properties (Coyne and Banin, 1986). We believe that the MarSAM that we are investigating provide an exciting, unique, and appropriate model for the Martian aeolian material and that study of these MarSAM will reveal new insights into the catalytic activity of clay minerals. Also, these and future studies of the properties of suitably modified clays will provide a data base necessary for the proper interpretation of much of the reflectance spectra to be obtained by the Mars Observer, and that all of this information will be useful in determining the properties, past and present, of the soils on Mars.

References:

1. Banin, A.: 1973, 'Quantitative ion exchange process for clays,' U.S. Patent 3,725,528.
2. Banin, A. and Rishpon, J.: 1978, *Life Sci. and Spa. Res.*, **XVII**, 59.
3. Cairns-Smith, A.G.: 1982, The Genetic Takeover and the Mineral Origin of Life, Cambridge University Press, Cambridge.
4. Coyne, L.M. and Banin, A.: 1986, *Clays and Clay Minerals*, **34**, 645.
5. Coyne, L.M.: 1985, *Origins of Life*, **15**, 161.
6. Levin, G.V. and Straat, P.A.: 1976, *Origins of Life*, **7**, 293.
7. McCord, T.B., Huguenin, R.L., Mink, D., and Pieters, C.: 1977, *Icarus*, **31**, 25.

MARS SOIL ANALOGS

L.Coyne, A.Banin, J.Orenberg, G.Carle, S.Chang, T.Scattergood

REFLECTANCE SPECTRA OF MONTMORILLONITE CLAYS WITH VARIOUS LEVELS OF IRON SUBSTITUTION AND OF A BRIGHT REGION ON MARS

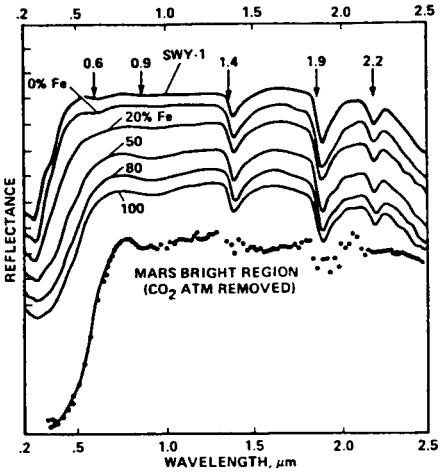

Figure 1.

DECOMPOSITION OF SODIUM FORMATE BY MARTIAN SOIL (VIKING LABELED RELEASE EXPERIMENT) AND BY THREE IRON-CALCIUM MONTMORILLONITE CLAYS AT TWO MOISTURE CONTENTS

Figure 2.

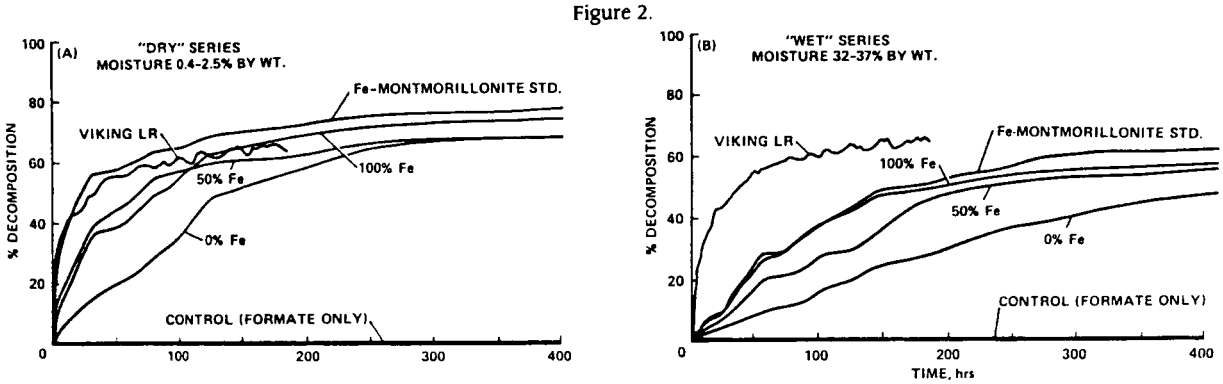

THERMOLUMINESCENT LIGHT YIELD AS A FUNCTION OF TOTAL SURFACE IRON

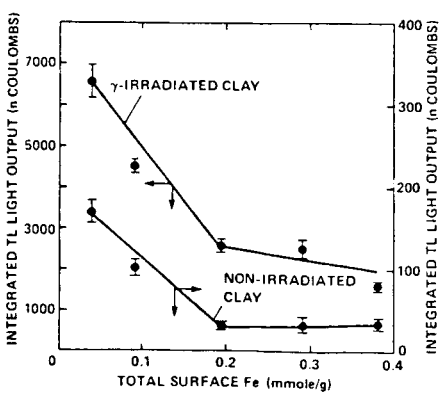

Figure 3.

GU 657484

N88-29668

SMALL MARTIAN VOLCANOES; Philip A. Davis and Kenneth L. Tanaka, U.S. Geological Survey, Flagstaff, AZ 86001

Various types of volcanoes have been identified on Mars, mainly on the basis of qualitative morphologic criteria such as relief, circularity, summit craters, and alignment with structural trends [e.g., 1-11]. Some of the volcano types thus far identified include shields, stratovolcanoes, silicic domes, table mountains, and cinder cones. We are currently conducting a survey of Viking Orbiter images to identify possible candidates for Martian volcanoes. Our selection is based on two criteria: the features have relief and a summit crater, and they are shown on images that have sufficient spatial resolution to allow acquisition of photoclinometric profiles across the features. The upper size limit for this survey is represented by tholi and paterae; the lower limit is dictated by Viking Orbiter image resolution. These two selection factors may allow features to be included in the database that appear similar to volcanoes because of fortuitous circumstances (e.g., an erosional mound that has a centrally located impact crater). However, we think that such circumstances will be rare and their effect on the database will be minimal. This survey and subsequent analyses will not include maars because they can be distinguished from impact craters only by their circularity [12], whose measurement for all such features would be very time consuming if not impossible, considering the spatial resolution of Viking Orbiter images.

The topographic profiles of the selected Martian volcanoes that are currently being acquired will be compared with tabulated data for terrestrial and lunar volcanoes [12-17] in an attempt to determine the types of volcanism that have occurred on Mars. Variation in volcanic style with age will also be examined. We hope that these analyses will also indicate clearly whether water or water-ice was involved in some periods of Martian volcanic history (such as in the production of tuff cones or table mountains).

An example of what may come from this study is the topographic data (Table 1) of a small volcano in northern Noctis Fossae (see Viking Orbiter frame 931A03), which we have already profiled. The topographic characteristics of this volcano (i.e., ratios involving volcano height and width and crater depth and diameter) are more similar to the average topographic characteristics of Icelandic lava shields than to those of all other types of terrestrial and lunar volcanoes reported in [12-14]. Of the 17 Icelandic-type lava shields reported in [13,14], the topographic data for the Baldheidi (Iceland) shield (Table 1) are most similar to those of this Martian volcano. Kilometer-sized volcanoes that occur elsewhere on Mars have been compared with terrestrial cinder cones [18,19]. However, the topographic characteristics of the Noctis Fossae volcano are very different from the topographic data reported for terrestrial cinder cones and tuff cones [13,14]. This observation may not hold true for the majority of the kilometer-sized volcanoes when more data are acquired. Also, we cannot exclude as yet the possibility that the Martian volcano is a pyroclastic deposit that differs from those on Earth because of degradation, incomplete evolution, or gravity scaling effects between the planets.

REFERENCES.

1. West, M. (1974) Icarus 21, p. 1-11.
2. Ward, C.A. (1979) Proc. Lunar Planet. Sci. Conf. 10, p. 2815-2840.
3. Scott, D.H., and Tanaka, K.L. (1981) Lunar Planet. Sci. XII, p. 952-953.
4. Greeley, R., and Theilig, E. (1978) Rept. Planet. Geol. Prog. 1979-1980, NASA TM 79729, p. 202.
5. Plescia, J.B. (1981) Icarus 45, p. 586-601.
6. Scott, D.H. (1979) Proc. Lunar Planet. Sci. Conf. 10, p. 3039-3054.
7. Plescia, J.B., and Saunders, R.S. (1979) Proc. Lunar Planet. Sci. Conf. 10, p. 2841-2859.
8. Pike, R.J., and Clow, G.D. (1981) Third Intern. Coll. on Mars, LPI Contrib. 441, p. 199-201.
9. Hodges, C.A., and Moore, H.J. (1979) J. Geophys. Res. 84, p. 8061-8074.
10. Scott, D.H. (1982) J. Geophys. Res. 87, p. 9839-9851.
11. Scott, D.H., and Tanaka, K.L. (1981) Proc. Lunar Planet. Sci. Conf. 12, p. 1449-1458.
12. Pike, D.J. (1980) U.S. Geological Survey Prof. Paper 1046-C, 77p.
13. Pike, D.J. (1978) Proc. Lunar Planet. Sci. Conf. 9, p. 3239-3273.
14. Pike, D.J., and Clow, G.D. (1981) U.S. Geological Survey Open-File 81-1038, 40 p.
15. Wood, C.A. (1980) J. Volcano. Geotherm. Res. 7, p. 387-413.
16. Wood, C.A. (1980) J. Volcano. Geotherm. Res. 8, p. 137-160.
17. Dohrenwend, J.C., Wells, S.G., and Turrin, B.D. (1986) Geol. Soc. Amer. Bull. 97, p. 421-427.
18. Scott, D.H. (1979) Proc. Lunar Planet. Sci Conf. 10, p. 3039-3054.
19. Frey, H., and Jarosewich, M. (1982) J. Geophys. Res. 87, p. 9867-9879.

Table 1. Topographic characteristics of a Noctis Fossae volcano and an Icelandic shield volcano.

	Crater Diameter (m)	Crater Depth (m)	Cone Height (m)	Flank Width (m)
Noctis Fossae	640±60	9±5	212±25	1107±60
Baldheidi[1]	600	10	240	2600

[1] Data from [13].

U5851425
S15-91
N88-29669/54915
30

THE MARTIAN SEDIMENTARY RECORD: R. A. De Hon, Department of Geosciences, Northeast Louisiana University, Monroe LA 71209.

On earth, layered sediments are normal occurrence at the surface, as sediments constitute 75% of the continents. Volcanic plains comprise over 60% of the entire surface, but they make up a small portion of the continental surface. The lunar experience emphasizes the recognition of nonsedimentary processes and the importance of impact and igneous processes on primitive bodies. Mars is somewhere between the earth and moon in terms of surface activity. The presence of large volcanic edifices and well-preserved volcanic flows readily attracts a large part of geologic curiosity. The relative importance of volcanic vs. sedimentary processes is not yet fully appreciated. Volcanic materials may comprise more than half the surface. The positive identification for some presumed regions of lava flows is clouded by the recognition that wrinkle ridges may form on surfaces other than lavas (1).

Terrestrial photogeologic mapping rests on distinctive patterns of depositional landforms and on distinctive characteristics of erosion. Significant sedimentary deposits are recognized as layered materials as revealed by their erosional characteristics. The most abundant sediments are shallow marine deposits which are laterally extensive but vertically limited. The earth is further characterized by a predominance of erosional forms produced by running water (streams). Only the high latitude regions where ice dominates and the most arid regions where water is lacking do nonfluvial processes dominate the landscape. Even mass-wasting involves significant water. In addition, the dominant erosional signature of running water is superposed on structural control produced by faulting and folding. Sedimentary layering and sedimentary sequences are revealed by tilted and folded sequences of rock which allow materials of different ages to be exposed at an erosional surface.

Mars, in contrast, exhibits little or none of the terrestrial style tectonics responsible for folding. Volcanic material is recognized by familiar primary landforms. Similarly, sedimentary materials that are present remain in original layer-cake stacking and must be observed either as pristine depositional surfaces or as revealed by erosional patterns. But, by earth standards, erosion is less ubiquitous on Mars. The photogeologist is faced with the interpretation of geologic history in terms of the most recent unmodified landforms and scant erosion of nearly flat-lying materials. Further problems are contributed by the limited resolution available through orbital imaging as opposed to unhindered ground observation.

The preceding is not an argument against sedimentary processes or sedimentary stratigraphy on Mars. It is merely a

warning as to the limitations of recognition of sedimentary deposits and thus the ability to interpret depositional history. It is the superposition of rock units that provides the most significant reading in the geologic record of a planet. Yet, on Mars, the pages are partially glued together.

Sedimentary processes are varied on Mars. Roughly half the surface of Mars is cratered upland which survives from the earliest period of martian history. Even that surface contains significant (albeit limited) evidence of fluvial, eolian, and possible glacial processes; hence, it does contain areas of sedimentary deposits. The polar regions are significant sedimentary sinks (2, 3). The layered materials are revealed by erosional processes that allow observation of layered eolian materials. The northern plains, on the other hand, are lightly cratered, at a low elevation, and provide a potentially significant sedimentary sink. A problem arises in the recognition of sedimentary materials in the scarcity of the familiar terrestrial erosional patterns, as well as a limited knowledge of pristine sedimentary depositional landforms.

Some sedimentary materials are readily identified on Mars by their landforms. Dune fields are apparent (4, 5, 6) and were obvious candidates for recognition in light of our previous knowledge of dust storms on the planet. Glacial and periglacial processes are suggested by the martian climate and landforms (3, 7, 8, 9). Fluvial sediments are less apparent but nevertheless important materials in light of the valley systems (10, 11). The presence of lacustrine and/or marine deposition is less well established due to the present ignorance as to the survival time of liquid water on the surface, but they are not ruled out.

Fluvial systems are recognized by distinctive patterns of erosion. Although deposition in the system is less readily apparent, it may be inferred to be present. The largest concentration of sediments in a fluvial system is in the alluvial fan or delta. Some sedimentary fans are identified on Mars (12), but even these forms are difficult to distinguish on low gradient surfaces. Point bar and bar deposits are recognized along some of the outflow systems (13).

Lacustrine sediments may be inferred, not by their unique depositional landforms, but by their lack of surface features and location in respect to channel systems. Hence, flat-floored basins along drainage lines and other places of natural entrapment may be presumed to be sites of pooling and sedimentation from temporarily impounded water. A few such sites have been proposed based on channel history and topography (13, 14).

Marine or glaciomarine sedimentation is suggested for much of the northern plains (15). Indeed, the apparent destruction of highland terrain along the highland scarp, the existence of the northern plains as a lowland sink, and the large outflow systems

(as well as other valley systems that could direct water to the plains) suggest that the northern plains comprise a large sedimentary basin. Recognition of the polygonally fractured terrain as megadessication cracks (16) provides evidence of clastic material of geologically significant thickness, as does identification of ablational moraine (17,18). Thus the largest and most significant sedimentary deposits probably exist in the northern hemisphere. These deposits may be the nearest likeness to marine sedimentation on Mars. Alternately, the northern plains may consist of many overlapping sedimentary fans imbricated with eolian debris, playa-like deposits, and volcanic materials.

A word of caution is offered. Not all plains-forming materials are volcanic. Significant sedimentary materials are present on Mars. Surface mapping reveals the more recent depositional patterns and the later processes modifying the surface, but much of the story may be buried. In future missions, radar sounding, active seismic systems, and on site deep drilling may be required to fully document the depositional history. For the present, identification of sedimentary layers must rest on localities of tectonic or erosional windows, detection of buried surfaces by indirect methods, and depositional superposition or off lap patterns of distribution.

REFERENCES

1. Plescia J.B. and Golombek M.P. (1986) Bull. Geol. Soc. Amer. 97, 1289-1299.
2. Cutts J.A. (1973) J. Geophys. Res. 78, 4231-4249.
3. Sharp R.P. (1973) J. Geophys. Res. 78, 4073-4083.
4. Cutts J.A. and Smith R.S.U. (1973) J. Geophys. Res. 78, 4139-4154.
5. Tsoar H. et al. (1979) J. Geophys. Res. 84, 8167-8182.
6. Breed C.S. et al. (1979) J. Geophys. Res. 84, 8183-8204.
7. Carr M.H. and Schaber G.G. (1977) J. Geophys. Res. 82, 4039-4054.
8. Squyres S.W. (1979) J. Geophys. Res. 84, 8087-8096.
9. Lucchitta B.K. et al. (1981) Nature 290, 759-763
10. Masursky H. et al. (1977) J. Geophys. Res. 82, 4016-4038.
11. Greeley R. et al. (1977) J. Geophys. Res. 82, 4093-4110.
12. Mutch T.A. et al. (1976) The Geology of Mars, Princeton Univ. Press, p.302.
13. Baker V.R. and Kochel R. C. (1979) J. Geophys. Res. 84, 7961-7984.
14. De Hon R.A. (1987a) Lunar Planet. Sci. Conf. 18, 227-228.
15. Parker T.J. et al. (1987) NASA TM-89810, 319-324.
16. McGill G.E. (1985) Lunar Planet Sci. Conf. 16, 534-535.
17. Grizzaffi P. and Schultz P.H. (1987) Lunar Planet. Sci. Conf. 18, 370-371.
18. De Hon R.A. (1987b) Lunar Planet Sci. Conf. 18, 229-230.

54

N88-29670

PROGRESS IN DETERMINING THE THICKNESS AND DISTRIBUTION OF VOLCANIC MATERIALS ON MARS

R. A. De Hon, Department of Geosciences, Northeast Louisiana University, Monroe LA, 71209.

Volcanic plains and constructs comprise over half the surface of Mars (1). Volcanism has ranged from the earliest period to the youngest rocks visible on the planet (2,3). The volume of volcanic materials provides important constraints to the history and structure of the planet. Volume estimates require sensible estimates of the surface area covered by volcanic materials and reasonable estimates of the thickness of volcanic materials. Estimates of the area of extent are provided by geologic mapping (2,4,5). Thickness estimates are provided by geophysical or photogeologic methods. One method of photogeologic estimation of lava thickness based on partial burial of craters (6) has been adapted for use on the moon (7) and Mars (8). Lacking sufficient topographic data, early martian estimates (8,9) employed crater geometric relationships based on lunar and Mercury observations (10,11), but improved observations based on Viking data allow a uniquely martian relationship (12) to be employed (13, 14).

Data for Mars based on partially buried craters must be used with caution. To construct reasonable isopachous maps, the surface on which the craters rest must be sufficiently cratered to provide an acceptable geographic distribution and point density. In addition, the craters must not be greatly degraded by erosional processes prior to burial. Further, the geologic contacts of the unit being mapped must be known. The contacts provide zero thickness-limits that are necessary for proper construction of isopachous maps.

Buried craters do not provide information 1) for regions in which the partially buried crater population is buried by later mantling materials; 2) for regions in which flooding is sufficiently deep to totally bury the pre-existing crater population; or 3) for regions of densely cratered volcanic terrain for which the initial volcanic plains character has been destroyed. Hence, the volume of materials within the large volcanic centers associated with Tharsis, Olympus Mons, and Elysium Mons cannot be estimated in this manner. Minimum estimates may be provided for these regions by simple geometric estimates of the positive topography of these regions, but subsurface volcanic materials can only be estimated by geophysical techniques. Even more difficult are estimates of presumed thick lenses of volcanics within basins such as Isidis or regions of extensive flooding prior to cessation of high impact rates.

Thickness of Volcanic Materials
De Hon, R.A.

The completion of 1:2M Viking photomosaics and a refined geologic map based on Viking photography (4,5) set the stage for improved thickness studies and volume estimates. Currently, a revised (but incomplete) data base of 740 partially buried craters has been compiled (Table I) using Mars photomosaics at 1:2M for initial identification and measurement. The revised crater-diameter to rim-height relationship (12) reduces thickness estimates reported earlier (9) by more than one-half. Most plains-forming materials have thicknesses ranging from 0.25 to 0.60 km. Because martian craters are probably degraded by various processes and because most craters used in this study possess rims that are incompletely buried, thickness estimates are probably maxima, and true thickness may be less than those recorded. Although a fluid volcanic process is probably responsible for most plains-forming materials reported here, some significant plains materials may be of sedimentary or ballistic origins.

These values are low but not unrealistic if viewed in comparison with terrestrial basaltic plains. On the earth, basalt thicknesses in excess of a kilometer are restricted to a very few centers of massive flood basalts. Many of the martian basalts represent eruptions of a localized nature. Only a few centers exhibit long lived activity, and these produced lava thicknesses too great to be measured by the buried crater technique.

REFERENCES

1. Greeley R. and Spudis P.D. (1981) Rev. Geophys. Space Phys. 19, 13-41.
2. Scott D.H. and Carr M.H. (1978) U.S. Geol. Misc. Inves. Map. I-1083.
3. Greeley R. (1987) Sci. 236, 1653-1654.
4. Scott D.H. and Tanaka K.L. (1985) U.S. Geol. Sur. Misc. Inves. Map I-1302A.
5. Greeley R. and Guest J.E. (1985) U.S. Geol. Surv. Misc. Inves. Map (in press).
6. Marshall C.H. (1963) Astrogeol. Stud. Ann. Prog. Rep., 1962, 19-31.
7. De Hon R.A. and Waskom J.D. (1976) Proc. Lunar Sci. Conf. 7th, 2729-2746.
8. De Hon R.A. (1982) J. Geophys. Res. 87, 9821-9828.
9. De Hon R.A. (1982) NASA Tech. Mem. 85127, 129-131
10. Pike R.J. (1977) in Impact and Explosion Cratering, 489-510.
11. Cintala M.J. (1979) Proc. Lunar Planet. Sci. Conf. 11, 2423-2436.
12. Pike R.J. and Davis P.A. (1984) Lunar Planet. Sci. Conf. 15, 645-646.
13. De Hon R.A. (1985) Lunar Planet. Sci. Conf. 16, 171-172.
14. De Hon R.A. (1985) Lunar Planet. Sci. Conf. 16, 173-174

TABLE I
CURRENT STATUS OF THICKNESS ESTIMATES BY QUADRANGLE

QUAD	NO. OF POINTS	MAXIMUM VALUE	MINIMUM VALUE	QUAD	NO. OF POINTS	MAXIMUM VALUE	MINIMUM VALUE
2NW	3	0.34	0.34	14SE	4	0.28	0.18
2NE	1	0.24	0.24	15NE	8	0.36	0.19
2SW	10	0.96	0.23	15SW	5	0.34	0.19
2S-C	6	0.36	0.20	15SE	10	0.67	0.24
3NW	7	0.53	0.25	16NW	3	0.46	0.40
3NE	2	0.30	0.29	16NE	2	0.32	0.22
3SW	2	0.31	0.27	16SW	11	0.40	0.24
3SE	1	0.19	0.19	16SE	14	0.56	0.22
4NW	2	0.44	0.39	17NW	5	0.34	0.16
4SW	10	0.49	0.24	17NE	4	0.41	0.16
4S-C	6	0.71	0.25	17SW	9	0.55	0.16
4SE	2	0.57	0.36	17SE	4	0.60	0.20
5NE	4	0.43	0.33	18NW	7	0.63	0.15
5SW	3	0.51	0.34	18NE	12	0.57	0.27
5SE	2	0.34	0.34	18SW	6	0.56	0.21
6NW	2	0.39	0.31	18SE	10	0.49	0.19
6SW	8	0.38	0.18	19NW	8	0.50	0.26
7NE	5	0.42	0.34	19NE	8	0.42	0.23
7S-C	3	0.29	0.22	19SW	9	0.53	0.30
7SE	19	0.61	0.22	20NW	31	0.64	0.19
8NW	23	0.96	0.18	20NE	16	0.55	0.27
8SW	17	0.80	0.19	20SW	8	0.47	0.20
8SE	3	0.37	0.34	20SE	13	0.45	0.24
9NW	2	0.27	0.21	21NE	6	0.40	0.28
9NE	5	0.24	0.15	22NW	7	0.31	0.25
9SW	1	0.27	0.27	22SW	15	0.46	0.23
9SE	2	0.27	0.24	22SE	23	0.49	0.23
10NW	5	0.43	0.20	23NW	7	0.46	0.20
10NE	11	0.51	0.18	23NE	6	0.38	0.18
10SW	11	0.66	0.18	23SW	9	0.40	0.19
10SE	12	0.62	0.31	23SE	12	0.55	0.31
11NW	12	0.51	0.29	24N-C	37	0.59	0.20
11NE	6	0.55	0.30	24NE	27	0.40	0.19
11SW	6	0.52	0.38	25NW	7	0.65	0.20
11SE	8	0.54	0.33	25NE	6	0.58	0.27
12NW	7	0.40	0.25	26NW	6	0.58	0.28
12NE	4	0.44	0.25	27NW	4	0.45	0.33
12SW	25	0.53	0.20	27N-C	8	0.43	0.31
12SE	4	0.46	0.30	27NE	5	0.44	0.24
13NW	5	0.47	0.19	27SE	12	0.53	0.28
13NE	4	0.30	0.22	28NE	9	0.64	0.23
13SW	3	0.53	0.23	29NW	12	0.28	0.27
13SE	8	0.43	0.16	29N-C	2	0.44	0.22
14NW	11	0.46	0.20	29NE	3	0.31	0.25
14NE	2	0.35	0.30	29SW	4	0.53	0.30
14SW	3	0.44	0.34				

--Thickness values in km--

N88-29671

GAMMA-RAY/NEUTRON SPECTROSCOPY FROM THE MARS OBSERVER*

P. Englert, San Jose State University, San Jose, CA 95192.
R. C. Reedy, D. M. Drake, W. C. Feldman, Los Alamos National Lab., Los Alamos, NM 87545.
S. W. Squyres, Cornell University, Ithaca, NY 14853.
L. G. Evans, Goddard Space Flight Center, Greenbelt, MD 20771
W. V. Boynton, University of Arizona, Tucson, AZ 85721.

The Gamma-Ray Spectrometer (GRS) experiment on the Mars Observer will measure gamma rays and neutrons that escape from Mars. The intensities of gamma-ray lines and of the thermal and epithermal neutrons can be used to study many problems related to martian volcanism and volatiles. The results of theoretical calculations for the production and transport of gamma rays and neutrons indicate that the GRS should be able to determine the abundances of many elements and the amounts and stratigraphy of H_2O and CO_2 on and in the top meter of the martian surface.

The galactic cosmic rays (GCR) produce many secondary neutrons in a planetary surface (1). These neutrons travel fairly far and undergo several types of nuclear reactions. Some reactions, such as scattering from hydrogen and carbon, rapidly reduce the neutrons' energies (2,3). Many neutrons eventually escape from Mars into space, and most of these leakage neutrons reach the orbital altitude of the Mars Observer spacecraft. Gamma rays are made by many types of nuclear reactions induced both by the primary GCR and secondary particles. The most important gamma rays for orbital remote sensing of elemental abundances are those made by nonelastic-scattering and neutron-capture reactions. Gamma rays are also made by the decay of the naturally-occurring radioelements K, Th, U, and their daughters (4,5). The gamma rays that escape from the planet without undergoing an interaction allow the emitting nucleus to be identified. The Apollo GRS mapped the abundances of natural radioactivity, iron, magnesium, and titanium in the moon (6).

The Mars Observer GRS detector will be a high-purity n-type germanium (hpGe) diode with a 56-mm diameter and a 56-mm length. It will be cooled to 100 K by a passive radiator. The hpGe will be surrounded by a plastic scintillator, and the GRS's electronics will reject any signals in the hpGe detector that are in coincidence with a signal in the plastic scintillator, eliminating background signals from the passage of charged cosmic rays through the hpGe detector. Signals from the hpGe for energies from ~0.2 to ~10 MeV will be processed in a pulse height analyzer. An entire gamma-ray spectrum (about 10,000 channels) will be transmitted every 20 seconds.

Thermal ($E < \sim 0.1$ eV) and epithermal ($E = \sim 1\text{-}1000$ eV) neutrons will be detected using a boron-loaded plastic scintillator for the anti-coincidence shield. The $^{10}B(n,\alpha)^7Li$ reactions of these low-energy neutrons in the borated plastic will produce a unique signal in the plastic scintillator's output (7). Because the spacecraft moves at a velocity slightly faster than that of a thermal neutron, the low-energy-neutron count rates in each of the four faces of the anti-coincidence shield (which is shaped like a pyramid and remains fixed relative to the spacecraft's velocity) can be used as a Doppler filter to determine the fluxes and spectral shapes of thermal and epithermal neutrons (8).

One of the most important design considerations has been the elimination of materials in the instrument that could create signals that mask signals of interest from the martian surface. This consideration led to the choice of Ti over Al for many of the major structural components of the instrument. Al is sufficiently important as a rock-forming element that its abundance must be known to calculate absolute abundances of all other elements. Moreover, it is an important diagnostic element for aluminosilicates such as feldspars. While the ubiquitous martian dust has a composition most consistent with weathering from a mafic source, its primary production mechanism may have been hydrothermal alteration of mafic volcanics in Mars' younger terrains. If this is the case, then we may have essentially no data at the present that bear on the elemental composition of the ancient highlands. Detection of Al will aid in the search for non-mafic lithologies there. Detection

of Al will also be important for searching for sialic volcanism; *e.g.*, evaluating the hypothesis that fine-grained deposits in Amazonis Planitia are ignimbrites.

We have done many calculations on the nuclear reactions that should occur in the martian surface, studying especially the production and transport of neutrons and gamma rays. The equilibrium distributions of neutrons in Mars were calculated using the ONEDANT (9) and the ANISN (10) neutron-transport codes. The ONEDANT code was modified to include the effects of gravity and the neutron's beta decay (11). All calculations assumed a 16-g/cm^2-thick atmosphere and the compositions of the atmosphere and soil determined by the Viking landers or estimated from the composition of SNC meteorites (see Table 1). Many special cases involving variable amounts of and depths for subsurface H_2O or thicknesses of CO_2 frost on the surface were run.

We found that the thickness of the martian atmosphere and the presence of H_2O in or CO_2 on the martian surface significantly affect the distributions of neutrons (9-11). Hydrogen rapidly thermalizes neutrons and shifts their depth distributions towards the surface. Because of its low absorption cross section, CO_2 builds a large reservoir of low-energy neutrons that can leak back into the surface (9,11). The count rates expected in the GRS's anti-coincidence shield are high enough (11) to allow a rapid determination of the concentrations of H_2O and CO_2 in and on the surface from the observed fluxes and spectral shapes of the thermal and epithermal neutrons (9). The depth that H_2O is below the surface can often be determined from the neutron data (9).

The fluxes from the ANISN neutron-transport calculations were used to determine the production rates of gamma rays by nonelastic-scattering and neutron-capture reactions (10). The gamma rays made by these reactions and by the natural decay of K, Th, U, and their daughters were transported through the martian surface and atmosphere to get fluxes at the spacecraft. To calculate the sensitivity of the GRS for determining elemental concentrations in the martian surface, the backgrounds determined by the Apollo GRS (6) were also used. The gamma rays most suitable for detecting 13 elements in Mars are given in Table 1, along with the amount of time necessary to get their abundance with 10% (1σ) uncertainty. These elements include most of the major rock-forming elements expected. Their determination should aid in identification of the major rock types present (using, *e.g.*, Si, Fe, Mg, Al), the degree of local and global refractory enrichment (using, *e.g.*, Al/Si and Ca/Si), *etc.* We should be able to identify various types of volcanic materials, ranging from the mafic types represented in the SNC meteorites to more sialic ones that may be present in the southern highlands or in ignimbrites. We can also detect elements such as S and Cl that might be present in surface precipitates. Besides elemental abundances, the gamma-ray data can also be used to study the distribution of hydrogen and CO_2 in Mars by comparing gamma rays made by both nonelastic-scattering and neutron-capture reactions with one element (10,12).

The data obtained from the gamma-ray and neutron modes of the Mars Observer GRS complement each other, and their use together will considerably improve the scientific return. For example, the elemental results from the gamma-ray spectra are needed to help interpret the transport of the leakage neutrons. The measured neutron fluxes can help to infer the presence of certain elements not directly observed in the gamma-ray spectra, such as relatively high amounts of neutron-absorbing gadolinium and samarium. Finally, the intensity of the leakage thermal neutrons can be used with the fluxes for the neutron-capture gamma rays from hydrogen (ratioed to Si or Fe) to determine information about the stratigraphy of H_2O in the top $\sim$100 g cm^{-2} of the martian surface. Figure 1 shows results for H_2O-rich soil buried below a layer of dry soil. Using the two data types together, we can in many cases solve for both the depth to the H_2O-rich layer and its water content.

References: (1) Reedy R. C. and Arnold J. R. (1972) *J. Geophys. Res.* **77**, 537-555. (2) Lingenfelter R. E., Canfield E. H., and Hess W. N. (1961) *J. Geophys. Res.* **66**, 2665-2671. (3) Lingenfelter R. E., Canfield E. H., and Hampel V. E. (1972) *Earth Planet. Sci. Lett.* **16**, 355-369. (4) Reedy

R. C., Arnold J. R., and Trombka J. I. (1973) *J. Geophys. Res.* **78**, 5847-5866. (5) Reedy R. C. (1978) *Proc. Lunar Planet. Sci. Conf. 9th*, pp. 2961-2984. (6) Bielefeld M. J. *et al.* (1976) *Proc. Lunar Sci. Conf. 7th*, pp. 2661-2676. (7) Drake D. M., Feldman W. C., and Hurlbut C. (1986) *Nucl. Instru. & Methods* **A247**, 576-582. (8) Feldman W. C. and Drake D. M. (1986) *Nucl. Instru. & Methods* **A245**, 182-190. (9) Drake D. M., Feldman W. C., and Jakosky B. M., *J. Geophys. Res.*, submitted. (10) Evans L. G. and Squyres S. W. (1987) *J. Geophys. Res.* **92**, 9153-9167. (11) Feldman W. C. *et al.*, in preparation. (12) Haines E. L. and Metzger A. E. (1984) *Nucl. Instru. & Methods* **226**, 509-516. * This work was supported by NASA. The work at Los Alamos was done under the auspices of the US DOE.

Table 1. Elements most readily measured by the Mars Observer GRS, model abundances of that element in the martian atmosphere and soil, source (mode) and energy of the gamma-ray line, and time necessary to determine that element's model abundance with a 10% 1-σ uncertainty.

Element	Model Composition (%) Air, Soil	Mode[a]	Energy (MeV)	Time (Hours)
H	–, 0.1	C	2.223	300
C	26.0, 0.6	S	4.438	4.4
O	71.3, 46.6	S	6.129	5
Mg	–, 3.7	S	1.369	21
Al	–, 4.1	C	7.724	1040
Si	–, 21.5	S	1.779	1.2
S	–, 3.0	C	5.424	210
Cl	–, 0.7	C	6.111	15
K	–, 0.12	R	1.461	4.0
Ca	–, 4.4	C	6.420	440
Fe	–, 13.5	C	7.632	7.6
Th	–, 0.45[b]	R	2.614	40
U	–, 0.13[b]	R	0.609	500

[a]S = inelastic scatter, C = neutron capture, R = natural radioactivity. [b]Parts per million by weight.

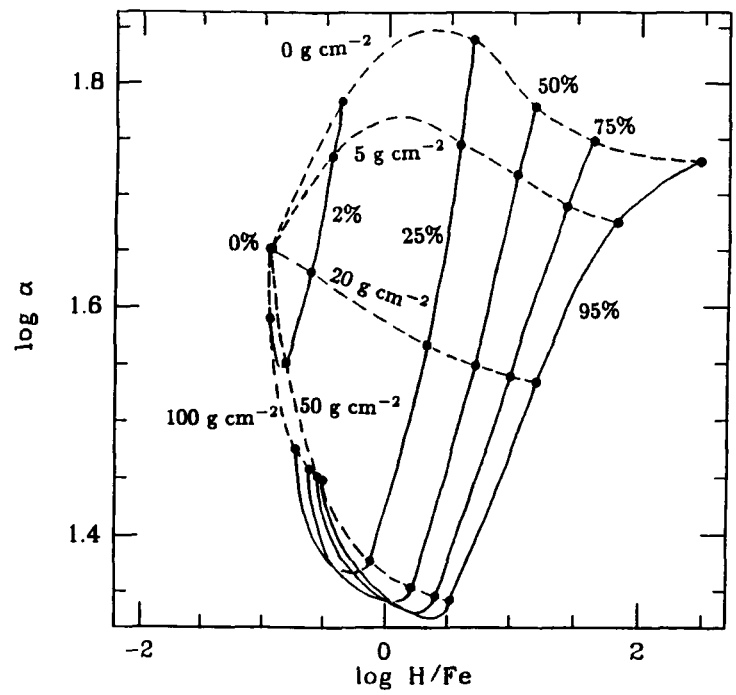

Figure 1. The relative flux of leakage thermal neutrons (α) versus the ratio of the neutron-capture gamma-ray fluxes from hydrogen and iron (H/Fe) can be used to determine the depth (dashed contours in g cm^{-2}) below which H_2O is present and its concentration (solid lines in weight %) below that depth. The hydrogen content above that depth was assumed to be 0.1%.

53-91
60 164913
7.0

L-84929
N88-29672

Variability in spectral signatures of terrestrial volcanic rocks and implications for volcanology on Mars. P.W. Francis, Lunar and Planetary Institute, 3303 NASA Road 1, Houston, Texas 77058.

Landsat Thematic Mapper (TM) studies of 2.2 my old ignimbrites in a test area around the Cerro Galan caldera, N.W. Argentina, show that the ignimbrites exhibit a remarkable range of spectral characteristics dependant both on intrinsic properties (welding, iron oxidation) and extrinsic properties resulting from aeolian weathering processes, notably deflation of low density pumic and glass and surface concentration of dense minerals and lithic clasts.
The TM has a spatial resolution of 30 m and is equipped with sensors working in seven spectral bands:

Band 1	0.45 - 0.52	micrometers
Band 2	0.53 - 0.61	"
Band 3	0.62 - 0.69	"
Band 4	0.78 - 0.91	"
Band 5	1.57 - 1.78	"
Band 6	10.42 -11.66	"
Band 7	2.08 - 2.35	"

The Cerro Galan caldera is an elliptical structure 35 km x 20 km. Ignimbrites erupted from the caldera totalling 1.2 km in thickness form the 6000m high resurgent center, while ignimbrites of the outflow facies are generally less than 100m thick but are exposed over 2-3,000 km^2 and extend radially to distances over 100 km from the caldera. Ignimbrites of the caldera facies are densely welded, while those of the outflow facies are lighlty welded or unwelded. Total volume of erupted ignimbrite exceeds 1000 km3. Chemically, it is a homogenous dacite (SiO_2 = 69%), composed of pumice clasts, shards, and phenocrysts of plagioclase, sanidine, quartz, biotite and magnetite.

Spectral profiles of the ignimbrite in four contrasted enviroments were constructed using 6 TM bands. (Fig.1) Fresh unwelded ignimbrite (A) has a high albedo with a marked spike in band 5, probably due to a surface film of oxidised iron minerals, goethite and hematite. Fresh welded ignimbrite (B) is much darker and resembles lava; it has only a very slight spike in Band 5; in places however, for reasons not fully understood, the welded ignimbrite is apparently highly oxidised, with a prominent spike in Band 5 (C). Most significant, however, is the contrast between fresh, unwelded ignimbrite (A) and the characteristic surface outcrop of such ignimbrites (D) over hundreds of square kilometres. The spectrum is very flat, resembling welded ignimbrite or lava.

Field studies show that such surfaces are lag gravels; covered by lithic clasts eroded out of the ignimbrite, all of the low density pumice and shards having been blown away. Heavy mineral concentrations are also locally important. Lithic clasts form only a small proportion by volume of the ignimbrite, of the order of 1%. In places, more than 30 m thickness of ignimbrite appears to have been blown away to leave the lag gravel concentrated on the surface. Thus, over most of its outcrop, the ignimbrite has a spectral signature which is unrelated to its bulk composition, but which is due to its least important component.

Spectral signatures of ignimbrites
P.W. Francis

The textural and structural characteristics of ignimbrites on Mars have been evaluated earlier (Francis and Wood 1982). Coupled with the conclusions made in the earlier study, the implications of the present observations are clear: it is impossible to identify unequivocally ignimbrites from remote sensed data, even in a well-studied terrestrial setting, without a detailed understanding of their environment. Although extremely extensive areas of ignimbrites have been mapped on Mars, e.g. in the Amazonis area (Scott and Tanaka, 1982) and the Olympus Mons aureole (Morris, 1982), only the most tenuous evidence to support their identification has been produced. For the most part, this relies on superficial morphological similarities between known terrestrial ignimbrites and postulated Martian examples. In the absence of young, well preserved source calderas or other vent structures unambiguously associated with them, suggestions of ignimbrites on Mars should be regarded as speculative. Few detailed spectral data are available at present for different units on Mars. When it does become available, it will have to be analysed cautiously. The lag gravels and heavy mineral concentrations observed at Cerro Galan also emphasize the need for care in interpreting the spectral characteristics of lithological units in areas where extensive aeolian erosion takes place.

References: Francis, P.W. and Wood, C.A., J. Geophys. Res., 87, 9881-9889,1982. Morris, E.C. J. Geophys. Res.; 87, 1164-1178, 1982. Scott, D.H. and Tanaka, K.L., J. Geophys. Res. 87, 1179-1190, 1982.

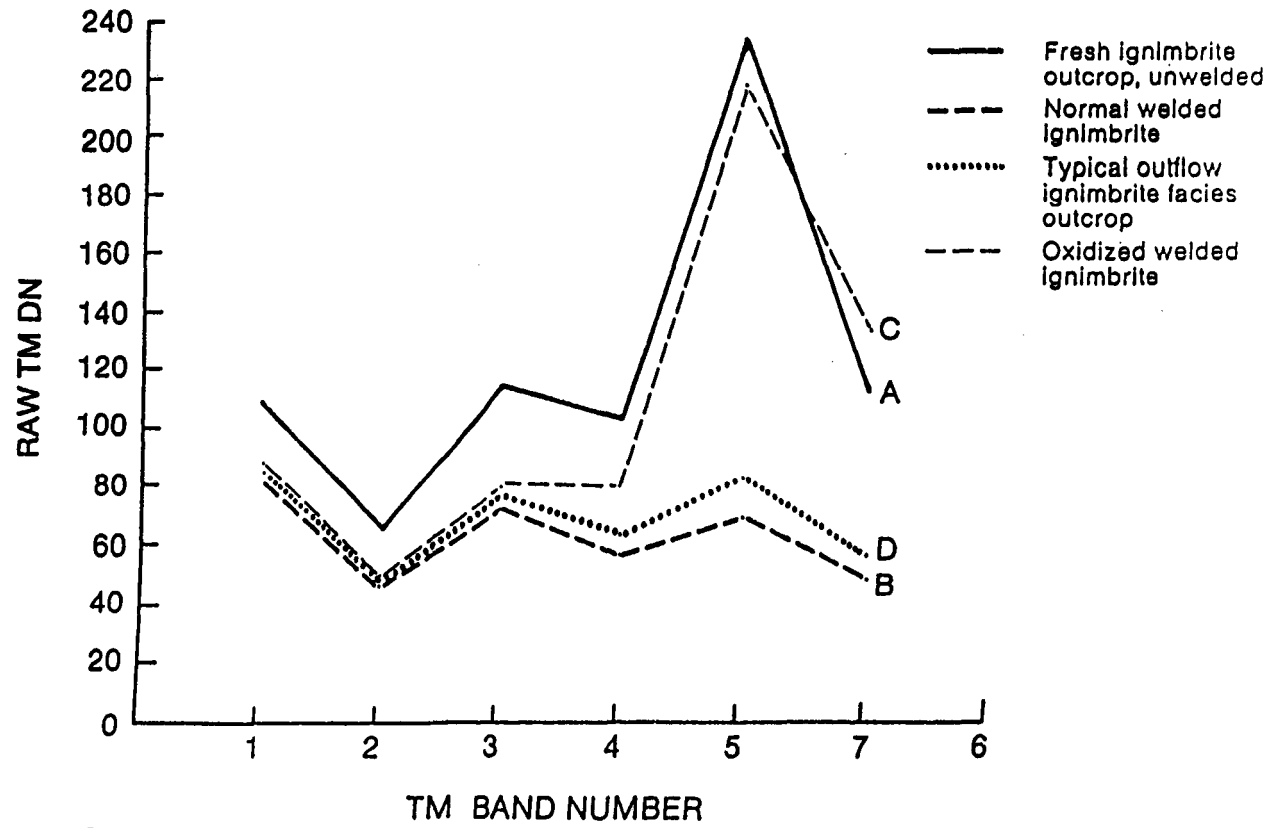

Figure 1

S13-91
62 1549
ND 185000
N88-29673

AQUEOUS ALTERATION IN S-N-C METEORITES AND IMPLICATIONS FOR WEATHERING PRODUCTS ON MARS. J. L. Gooding, SN2/Planetary Materials Branch, NASA/Johnson Space Center, Houston, TX 77058.

Introduction. If shergottite, nakhlite, and chassignite (SNC) meteorites are rocks propelled to Earth by large meteoroid impacts on Mars [1], then it is possible to deduce much about Martian igneous petrology and geochemistry [2]. Because SNCs are igneous rocks, however, it has not been obvious that they could reveal much about sedimentary and soil petrology and low-temperature geochemistry of Mars. It is important, though, that at least four of eight SNCs carry evidence for low-temperature, extraterrestrial "weathering product" phases. This paper reviews evidence for Martian weathering and alteration products in SNCs (Table 1) and outlines possible inferences for volatile/regolith interactions, regolith mineralogy, and sinks for the putative hidden volatiles on Mars.

In the strict sense, *weathering* refers only to processes by which rocks interact with planetary atmospheres, including meteoric water [3]. *Secondary minerals* (those that form by processes other than igneous crystallization) in SNCs might include authigenic phases formed during weathering, deuteric alteration, or sedimentary diagenesis. Distinguishing terrestrial from extraterrestrial alteration products in SNCs is a significant problem for those specimens that have been recovered as finds, including possibly the most interesting SNC, the Elephant Moraine shergottite [4].

Amphiboles. Chassigny and Shergotty comprise the only reported occurrences of amphiboles in meteorites of any type. Textures of the SNC occurrences, as inclusions in other igneous phases, prove that these hydrous silicates are extraterrestrial in origin [5,6]. Apparently, the SNC parent body fostered production of water-bearing magmas so that we should not be surprised to find evidence of deuteric alteration in these and other SNCs.

Secondary Minerals. Observed phases form two categories: (a) discrete grains of known minerals and (b) enigmatic occurrences of unidentified minerals or mineral(oid) mixtures. Most current evidence falls within the latter category. Nakhla has been long-recognized as a rusty rock but the origin of its rust has remained unsettled [7,8]. Structural-formula calculations for Nakhla (and Lafayette) "iddingsite" support its presumed identity as a mixture of chlorite or smectite with iron oxides [9], the latter of which may account for the ferric iron content of bulk Nakhla [10]. Pyrolysis of bulk Nakhla produces substantial release of CO_2 [11, 12], suggesting the presence of, as yet, unidentified carbonate minerals.

No grains of nontronite or other phyllosilicate have been confirmed in SNCs. Evidence for salt formation on the SNC parent body is reasonably strong, though. Discrete grains of Ca-carbonate and Ca-sulfate occur as relict crystals in glassy inclusions in the Elephant Moraine shergottite [13]. At least one variety of the calcite possesses a carbon stable-isotopic composition that closely resembles that of CO_2 extracted from Nakhla [14]. Even in those specimens where salt grains have not been identified, pyrolysis of bulk samples shows clear gas-release evidence for sulfates [12].

Implications for Martian Regolith Mineralogy. If Nakhla and Elephant Moraine are both from Mars, then existence of carbonates on Mars has been confirmed. Based on the SNC evidence, though, it is not clear whether carbonates are major components among Martian weathering products. First, the

SNC carbonates might be deuteric alteration products which did not form under surface conditions. Second, sulfate production may have predominated over carbonate production. There has been no measurement of the *inorganic carbon* content of Martian materials (Viking GCMS experiment could not have detected calcite, for example) but it is clear that the sulfur is abundant in fines (3% S [15]). In most SNCs, sulfate exceeds carbonate in abundance [12].

Although no relict smectites have been found in SNCs, hydrous clay-mineral formation readily occurs in shergottites under Antarctic conditions [16], including uptake of 0.2% H_2O in $< 10^6$ y [12]. In a Martian regolith of 10 m thickness, 0.2% H_2O would correspond to global abundances of 4 cm H_2O. In addition, extraterrestrial gypsum in Elephant Moraine [13] would be consistent with mineralogically bound water in the regolith of the SNC parent planet. Occurrence of all sulfur in Viking surface fines as gypsum in a 10-m regolith would be equivalent to a global abundance of 60-70 cm of H_2O. Accordingly, both the known relict alteration products and the observed terrestrial weathering behavior of SNCs supports the concept that products of rock weathering on Mars should be important sinks for Martian volatiles.

References: [1] Wood C. A. and Ashwal L. D. (1981) Proc. Lunar Planet. Sci., 12B, 1359-1375. [2] McSween H. Y. Jr. (1985) Rev. Geophys., 23, 391-416. [3] Gooding J. L. (1986) In M. G. Kivelson (ed.), The Solar System: Observations and Interpretations, Prentice-Hall, 208-229. [4] Gooding J. L. (1984) Lunar Planet. Sci. XV, Lunar and Planetary Institute, Houston, 310-311. [5] Floran R. J. et al. (1978) Geochim. Cosmochim. Acta, 42, 1213-1229. [6] Treiman A. L. (1983) Meteoritics, 18, 409-410. [7] Bunch T. E. and Reid A. M. (1975) Meteoritics, 10, 303-315. [8] Ashworth J. R. and Hutchison R. (1975) Nature, 256, 714-715. [9] Gooding J. L. (1985) Lunar Planet Sci. XVI, Lunar and Planetary Institute, Houston, 278-279. [10] Viera V. W. A. et al. (1986) Physica Scripta, 33, 180-186. [11] Carr R. H. et al. (1985) Nature, 314, 248-250. [12] Gooding J. L., Aggrey K. and Muenow D. W. (1987) Program for 50th Meeting of the Meteoritical Society, Newcastle, England, July 19-24, p. 69. [13] Gooding J. L., Wentworth S. J. and Zolensky M. E. (1987) Lunar Planet. Sci. XVIII, Lunar and Planetary Institute, Houston, 345-346. [14] Wright I. P. et al. (1987) Lunar Planet. Sci. XVIII, Lunar and Planetary Institute, Houston, 1106-1107. [15] Clark B. C. et al. (1982) J. Geophys. Res., 87, 10059-10067. [16] Gooding J. L. (1986) Geochim. Cosmochim. Acta, 50, 2215-2223. [17] Smith J. V. and Steele I. M. (1984) Meteoritics, 19, 121-133. [18] Gooding J. L. and Muenow D. W. (1986) Geochim. Cosmochim. Acta, 50, 1049-1059.

Table 1: Alteration Products and Hydrous Minerals in S-N-C Meteorites

Meteorite[a]	Effect Reported	Basis[b]	Ref.
Allan Hills A77005 (S)	Fe, S, Cl-rich patches in olivine and Cr-spinel	SEM/EDS, EPMA	[17]
Chassigny (C)	Kaersutite inclusion in glass	OM, EPMA	[5]
Elephant Moraine A79001 (S)	S, Cl-rich aluminosilicates in glass	SEM/EDS	[18]
	Occluded "sulfate" in glass	PYR, MS	[12,18]
	Calcite and gypsum in glass	SEM/EDS, XRD	[13]
Lafayette (N)	"Iddingsite"	OM, EPMA	[7]
Nakhla (N)	"Iddingsite"	OM, EPMA	[7]
	Ferric iron	MBS	[10]
	Carbonate	PYR/COM, MS	[11,12]
	Sulfate	PYR, MS	[12]
Shergotty (S)	Kaersutite inclusion in glass	OM, EPMA	[6]

[a] S = shergottite, N = nakhlite, C = chassignite. [b] COM = combustion, EDS = energy-dispersive X-ray spectrometry, EPMA = electron probe microanalysis, MBS = Mossbauer spectroscopy, MS = mass spectrometry, OM = optical microscopy, PYR = pyrolysis, SEM = scanning eletron microscopy, XRD = X-ray diffractometry.

50-91
64

N88-29674

DISTRIBUTION AND TIMING OF THICK TRANSIENT AIR-FALL DEPOSITS IN ELECTRIS: IMPLICATIONS FOR THE NATURE OF THE UPLAND PLAINS; J.A. Grant and P.H. Schultz, Geological Sciences, Brown University, Providence, RI 02912

INTRODUCTION: A large area in the Electris region of Mars is (or once was) covered by an unconformable and etched deposit. Although interpreted as lava filling volcano-tectonic depressions (1) or fluvial deposits filling large degraded craters (2), more recent work has shown the deposit is more likely the result of air-fall deposition (3,4). Crater densities on both the surface of the deposit and on exhumed, underlying ridged plains indicate that the deposit was emplaced and eroded over a relatively short time. These crater statistics also demonstrate that the relative age of the Electris deposit is similar to those obtained for other unconformable deposits, thereby suggesting they may be related.

OBSERVATIONS: The Electris deposit is unconformable and occurs irregularly over both ridged plains and cratered upland surfaces. Remnants of the deposit extend over an area of approximately 1.8 X 10^6 km^2 (from 160°W to 200°W and 30°S to 47°S), but the presence of partially filled craters to the immediate south of this region suggests initially broader coverage. The deposit has an estimated volume of 900,000 km^3 with average thickness ranging from 300+ m in the east up to 700+ m in the west (based on shadow measurements). The thickest deposits occur as chaotic unconformable material (2) filling degraded 50 to 200 km craters. Deposits in some craters display thick, poorly defined layering (10's - 100's of m), there is an absence of regular, thin layering.

Valley networks head within the Electris deposit and partially dissect its surface; however, they do not appear to incise the underlying ridged plains unit. Other characteristics of the deposit include a heavily eroded dome located at 79°W, 36.5°S in the northeast portion of the deposit and several examples of inverted topography (e.g. 190.5°W, 40°S).

Four classes of the Electris deposit have been identified. In some locations the deposit grades from mantled to unmantled areas. A second, slightly thicker class resembles gullied cuestas that form partial rings around the inside of degraded impact craters at constant elevation. The third class of deposit forms irregular promontories and mesas that are 300 m to 400 m thick and bounded by scarps lacking basal talus accumulations. The thickest class of the deposit resembles chaotic terrain and is found in large degraded craters (2). The irregular blocks comprising this class of the deposit are 400 m to over 700 m thick and typically grade into exhumed or only thinly mantled ridged plains. In contrast to some other areas having thick unconformable deposits (4,5), pedestal craters in the Electris region are uncommon.

DISCUSSION: Consideration of the characteristics of all four classes of the Electris deposit suggests that it is: A) the result of air-fall deposition; and B) volatile rich (3). The occurrence of the deposit over both high-relief cratered uplands and low-relief ridged plains strongly favors air-fall accumulation. It seems unlikely that extrusion of flood basalts, fluvial processes, or other processes could account for emplacement over such a range in relief. In addition, the low density of valley networks/area exhumed, an absence of flow-related features, and a deficiency of talus at the base of most scarps, demonstrate that eolian processes dominate erosion of the deposit. Efficient eolian erosion indicates the presence of fairly uniform fine grained material, consistent with an air-fall deposit. A locally high volatile content within the deposit is indicated by: A) relatively young valley networks that head within the deposit; B) observed atmospheric

water concentrations over the deposit even in the winter (6); and C) the daily winter occurrence of Electris clouds over the most dissected portion of the deposit (thought to be composed of CO_2 (7), but may be H_2O ice).

It is unclear whether current disparities in thickness of the deposit reflect original depths and/or variations in the rate of removal. Thin deposits may reflect low strength volatile poor zones and/or zones not thick enough to have undergone overburden welding and that underwent direct eolian deflation. Thicker deposits may be higher strength volatile rich zones that have undergone overburden welding and were dominated by scarp retreat and mass-wasting. Deposits inside craters resembling gullied cuestas and chaotic material are perhaps remnants of higher strength layers deposited on lower strength material that have undergone differing amounts of erosion and/or collapse. The thick layered appearance in some large craters suggests that several periods of burial may have occurred. A paucity of pedestal craters and the similarity between crater densities on both the deposit and exhumed ridged plains surfaces (Fig. 1) indicates rapid deposition and subsequent erosion of the Electris deposit.

The eroded dome in the northeast portion of the deposit has been described as a volcanic edifice (1,8). If this assessment is correct, it may have provided a source for the deposit. However, several characteristics of the dome suggest it was not a source: A) its isolated nature; B) large deposit volume compared to the dome size; C) large deposit volume compared to terrestrial deposits associated with volcanoes (9); D) apparent singular history; E) eroded style compared to adjacent deposits; and F) similarity with other types of non-volcanic terrestrial domes (e.g. diapiric).

Crater statistics indicate that emplacement of the ridged plains took place soon after formation of Sinai, Syrtis Major, and Hesperia Planum (Fig. 1). This was rapidly followed by formation of the Electris deposit and its subsequent modification by erosion (Fig. 1). Emplacement of the Electris deposit nearly coincided with the formation of similar unconformable deposits in Sinus Meridiani and Isidis basin (10), the thicker unconformable sequences of Arabia and Mesogaea (4), and the end of a peak in geomorphic activity identified in the Margaritifer Sinus quadrangle (11). The major outflow channels formed soon after these events (Fig. 1).

IMPLICATIONS: The Electris deposits appear to be representative of a period when unconformable deposits were widespread and geomorphic processes were high (11). While the Electris and other debris mantles in Sinus Meridiani and Isidis were emplaced and removed in a relatively short time, thicker accumulations occurred over a longer time in Arabia and Mesogaea. All deposits are believed to reflect an epoch when atmospheric volatiles were in abundant supply, whether from primary exogenic (12) or endogenic sources (13). Sources for volatile release and global deposition of these volatiles include the finite thermal history associated with impact basins (14,15) perhaps amplified by processes such as polar wandering (4) and high obliquity prior to the development of Tharsis (16). Outflow channels forming soon afterwards may reflect a re-release of these trapped volatiles.

The nature of the Electris and other similar deposits document periods of gradation on Mars that affected widely separated regions of the surface. Their eroded expression and locally thick layering demonstrates that such deposits were originally more widespread and that several periods of deposition and erosion may have taken place. Volcanic plains in some areas of the cratered uplands may be deeply buried by or wholly due to such deposits, thereby increasing ambiguities in interpreting the nature of some upland plains.

ORIGINAL PAGE IS
OF POOR QUALITY

References: (1) Scott, D.H. (1982), J. Geophys. Res., 87, 9839–9851. (2) Lucchitta, B.K. (1982). NASA Tech. Memo. 85127, 235–236. (3) Grant, J.A. and Schultz, P.H. (1987), Lunar and Planet. Sci. XVIII, 355–356. (4) Schultz, P.H. and Lutz, A.B. (1987), Icarus, in press. (5) Scott, D.H. and Tanaka, K.L. (1982), J. Geophys. Res., 87, 1179–1190. (6) Huguenin, R.L. and Clifford, S.M. (1982), J. Geophys. Res., 87, 10227–10251. (7) Briggs, G. et al. (1977), J. Geophys. Res., 82, 4121–4149. (8) Scott, D.H. and Tanaka, K.L. (1981), Proc. Lunar and Planet. Sci. Conf. XII, 1449–1458. (9) Francis, P.W. and Wood, C.A. (1982), J. Geophys. Res., 87, 9881–9889. (10) Grizzaffi, P. and Schultz, P.H (1987), Lunar and Planet. Sci. XVIII, 370–371. (11) Grant, J.A. (1987), NASA Tech. Memo. 89971, 1–268. (12) Schultz, P.H. (1987), Kagaku, 57, 486–495. (13) Greeley, R. (1987), Science, 236, 1653–1654. (14) Wichman, R. and Schultz, P.H. (1987), Lunar and Planet. Sci. XVIII, 1078–1079. (15) Schultz, P.H. (1987), This volume. (16) Jakosky, B.M and Carr, M.H (1985), Nature, 315, 559–561. (17) Masursky, H.J. et al. (1977), J. Geophys. Res., 82, 4016–4038. (18) Baker, V.R. (1982), The Channels of Mars, Univ. Texas Press, 198p. (19) Neukum, G. and Wise, D.U. (1976), Science, 194, 1381–1387.

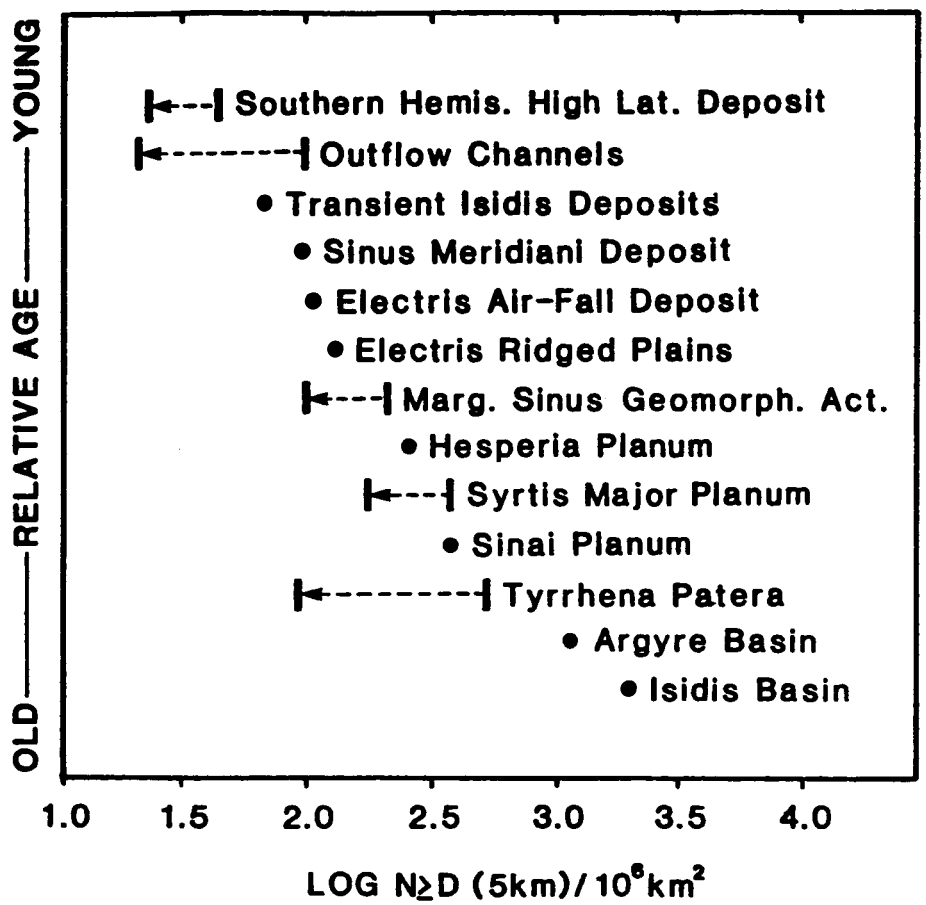

Figure 1. Relative ages of the Electris air–fall deposit, underlying ridged plains, and other selected surfaces and features, arranged by increasing age from top to bottom. Data for the outflow channels are from 17,18. Ages are given as the log of the number of craters ≥ 5 km, normalized using the Neukum and Wise standard crater curve for Mars (19).

AX 46679 N88-29675 551-91
154921

PHOTOGEOLOGICAL INFERENCES OF MARTIAN SURFACE COMPOSITION:

R. Greeley, Department of Geology, Center for Meteorite Studies, Arizona State University, Tempe, AZ 85287

Photogeological Mapping provides a systematic documentation of geologic observations and includes the identification of surface materials and structures (e.g., faults), and determination of their sequence of formation. Geologic maps enable the history for a region to be deduced and inferences to be drawn for the processes responsible for the evolution of the surface. In the absence of extensive field data, planetary mapping draws heavily on geomorphology, knowledge of geologic processes, and remote-sensing measurements.

Photogeologic mapping of planets began in the 1960s with the U.S. Geological Survey effort to place the surface of the Moon in a geological context (1,2). The principles were then applied to Mars using Mariner 9 data through a program involving U.S.G.S., university, and other geologists . These maps were synthesized to produce a global geologic map (3). With the acquistion of Viking data, many of the previous maps were revised and a new, 3-sheet global map was produced (4-6). These maps display about 90 units of different materials and/or ages and serve as a base for many current and future studies of Mars. Current mapping at a scale of 1:500,000 involves potential lander and sample collection sites, and topical studies.

Volcanic Materials. Mapping suggests that more than 50% of the martian surface involves volcanic materials (7), divided into two types based on morphology: **Central volcanoes** (shields, domes, highland and other paterae, and various small cones) which developed by prolonged eruption from point-source vents and various **volcanic plains** (simple flows containing mare-type ridges, complex flows displaying multiple flow lobes, and undifferentiated volcanic plains). Differences in primary morphology reflect the style of volcanism and the nature of the magma during eruption. Mapping shows that volcanism was important throughout the history of Mars and that the style of volcanism changed from predominantly plains-volcanism to central-vent volcanism, with a decrease in volumes of extrusion through time. This observation is consistent with a moon-like thermal history involving a thickening lithosphere.

Volcanic Morphology and the Compositional Connection. Morphology can be analyzed either for the total accumulation of volcanic products (the "whole" volcano) or for individual features such as flows. The potential relationship between morphology and composition has been of interest for more than 100 years (8-10). An assessment of terrestrial volcanoes vs. composition shows a potential correlation; simplistically, volcanoes composed of high-silica lavas have steep flanks. Silicic flows generally are viscous and tend to accumulate close to the vent, whereas mafic flows are more fluid and spread farther from the vent. Thus, volcanic domes are usually composed of rhyolite or dacite whereas shields and lava plains typically are basaltic. However, there are exceptions to this simple correlation. Even for a narrow range of composition, a wide variety of morphologies may be found. For example, basalts can include not only lava plains and shields, but also stratovolcanoes, domes, and pyroclastic plains. Critical analysis shows that volcano morphology results from many complex, often interrelated parameters. As reviewed by Whitford-Stark (11), these include three groups: *planetary variables, magma properties controlling rheology, and intrinsic properties of eruptions.* Planetary variables include factors characteristic for a particular planet. For example, the distribution of tephra in explosive eruptions is partly governed by the presence or absence of an atmosphere, gravity, and the escape velocity. On the airless Moon, tephra would be widespread, whereas on Earth, ejection would be retarded by the atmosphere and higher gravity and would acculumulate near the vent as a cone. Eruption characteristics include rate of effusion, volume erupted, and vent configuration.

A different approach is to assess the morphology of individual flows as a function of the composition. Characteristics such as flow-front heights and widths of levees along channels may reflect lava properties governed largely by composition. Hulme (12) developed a predictive model for simple flows assuming a Bingham model; Moore et al., (13) extended the model to assess lava yield strength vs silica content for application to Earth, Moon, and Mars. Baloga and Pieri (14)

assessed this relationship and concluded that the morphology of individual flows is dependent on many parameters in addition to composition.

In conclusion, photogeologic mapping shows the presence of a wide range of materials on Mars, many of which appear to be volcanic. The knowledge of the composition of these materials is poorly constrained. Inferences drawn from the morphology of individual flows would suggest that most of the materials had rheological properties similar to basalt or other mafic magmas at the time of their emplacement. Until the controlling factors are better known, caution must be exercised in interpreting the compositions of martian volcanic materials based on morphology.

REFERENCES

(1) Shoemaker, E.M. and R.J. Hackman, 1962, Stratigraphic basis for a lunar time scale, *The Moon - International Astronomical Union Symposium 14,* A. Kopal and Z.K. Mikhailov (eds.), 289-300. New York: Academic Press.
(2) Wilhelms, D.E., 1972, Interagency report: Astrogeology 55 geologic mapping of the second planet, *Astrogeology 55,* NASA, 1-36.
(3) Scott, D.H. and M.H. Carr, 1978, Geologic map of Mars, *U.S. Geol. Sur. Misc. Inv. Map I-1083.*
(4) Scott, D.H. and K.L. Tanaka, 1986, Geological map of western equatorial region of Mars, *U.S. Geol. Sur. Mis Inv. Series Map I-1802-A,* scale 1:15,000,000.
(5) Tanaka, K.L. and D.H. Scott, (in press), Geologic maps of the polar regions of Mars: *U.S. Geol. Sur. Mis. Inv. Series Map I-1802-C,* scale 1:15,000,000.
(6) Greeley, R. and J.E. Guest, (in press), Geologic map of the eastern equatorial region of Mars, *U.S. Geol. Sur. Mis. Inv. Series Map I-1802-B.*
(7) Greeley, R. and P.D. Spudis, 1981, Volcanism on Mars, *Rev. Geophys, Space Phys., 19,* 13-41.
(8) Dana, J.D., 1849, United States Exploring Expedition, G. Putnum, New York, 756 p.
(9) Dana, J.D., 1891, Characteristics of Volcanoes, G. Putnum, New York, 399 p.
(10) Milne, J., 1878, On the form of volcanoes, *Geog. Mag., 15,* 337-345.
(11) Whitford-Stark, J.L., 1982, Factors influencing the morphology of volcanic landforms: An Earth-Moon comparison, *Earth Science Rev. 18,* 109-168.
(12) Hulme, G., 1974, The interpretation of lava flow morphology, *Geo. Jour., Royal Astro. Soc., 39,* 361-383.
(13) Moore, H.J., D.W.G. Arthur, and G.G. Schaber, 1978, Yield strengths of flows on the Earth, Moon, and Mars, *Lunar Planet, Sci. Conf. 9th,* 3351-3378.
(14) Baloga, S., and D. Pieri, 1986, Time-dependent profiles of lava flows, *Jour. of Geo. Res., 91,* B9, 9543-9552.

L 3724234 N88-29676
AA 000005
L949 150/
154922

LAVA FLOW-FIELD MORPHOLOGY - A CASE STUDY FROM MOUNT ETNA, SICILY.

J.E. Guest[1], J.W. Hughes[1] and A.M. Duncan[2], [1]University of London Observatory, Mill Hill Park, London, NW7 2QS, England. [2]Department of Science (Geology), Luton College of Higher Education, Park Square, Luton LU1 3JU.

The morphology of lava flows is often taken as an indicator of the broad chemical composition of the lava, especially when interpreting extra-terrestrial volcanoes using space-craft images. While it is true that at the two ends of the compositional spectrum mafic lavas tend to produce extensive sheets whereas silicic lavas tend to give rise to thick stubby flows, this is not an infallible way of interpreting the composition of a lava. Other factors such as temperature, gas content, degree of crystallisation on eruption and rate of effusion also affect the flow form independent of composition. For example, basaltic magmas can erupt to give short thick flows analogous to those usually produced by more silicic lavas.

The historical lavas of the active volcano Mount Etna in Sicily provide an excellent opportunity to examine the controls on flow-field morphology. Virtually all the historical flows are of similar composition, being hawaiites. Though the lavas are typically porphyritic, preliminary investigations have not revealed any clear relations between major differences in crystallinity and flow morphology for lavas erupted over the last 200 years. On Etna there are a large variety of different planimetric flow-field forms, ranging from extensive sheets of mainly pahoehoe textured lava, through simple and compound flows with well developed lava channels and tube systems, to thick short flows with ogives.

In this study we restrict ourselves to those flows produced by flank eruptions after the middle of the 18th Century (a total of 30 eruptions). Prior to the 18th Century, Mount Etna underwent a period of high overall output, characterised by the extrusion of large volume, highly porphyritic lavas (1). Since 1750, the output from flank eruptions has been broadly constant, suggesting that the internal plumbing conditions have remained unchanged (2). The majority of flow-fields developed during post 1750 flank eruptions have either been long, narrow flows (e.g. 1981 eruption) or relatively wide, complex flows consisting of numerous flow units (e.g. 1983 eruption) (3).

Examination of the flow-field distribution shows that the complex flows occur only in the eastern sector of the volcano, centred around the Valle del Bove. This distribution correlates with the observation of Wadge (4), that long duration (i.e. greater than about 50 days) flows occur only in this sector. This sector is also characterised by low average effusion rates, generally less than 30 $m^3 s^{-1}$, and by large volumes. All the large volume flows, greater than 60 x $10^6 m^3$, occur in this region. Elsewhere on the volcano, the flows are of a simple nature, characterised by durations less than 25 days, effusion rates greater than 30 $m^3 s^{-1}$, and volumes less than 60 x $10^6 m^3$.

There thus appear to be two different flow-field populations, possibly the same populations observed by Kilburn and Lopes (5), which are related spatially to regions of the volcano where eruption conditions are different (Figure 1). This in turn suggests that the near surface plumbing of the volcano is different in the eastern sector compared with elsewhere on the volcano. It may be significant that this eastern sector is the unsupported sea-ward flank of the volcano and is subject to sliding under gravity (6).

In conclusion, the final form of a flow-field may be more indicative of the internal plumbing of the volcano, which may control such factors as the effusion rate, duration of eruption, volume of available magma, rate of de-gassing and lava rheology. Different flow morphologies on Etna appear to be a good indicator of differing conditions within the volcanic pile. Thus the spatial distribution of different flow types on an extra-terrestrial volcano may provide useful information about the plumbing conditions of that volcano, rather than necessarily providing information on the composition of material erupted.

References

(1) Wadge, G., Walker, G.P.L. and Guest, J.E. 1975 Nature, Lond., 255, pp.385-387

(2) Guest, J.E.; Duncan, A.M.; 1981 Nature, 290, pp.584-586

(3) Guest, J.E.; Kilburn, C.R.J.; Pinkerton, H.; Duncan, A.M.; 1987 Bull.Volcanol. 49: pp.527-540

(4) Wadge, G.: 1977 J.Volcan.Geo.Res. 2 pp.361-384

(5) Kilburn, C.R.J.; Lopes, R.M.C. 1987 (in press)

(6) Guest, J.E.; Chester, D.K. and Duncan, A.M. 1984 J.Volcanol.Geotherm. Res.21: pp.1-23

Figure 1

Sketch map of Mount Etna, Sicily, showing areal distribution of historical lava flows since 1750. Bold lines represent flows with volumes greater than 60×10^6 m^3, while narrow lines represent flows with volumes less than 60×10^6 m^3. A dashed line indicates that the flow has since been buried by younger lavas.

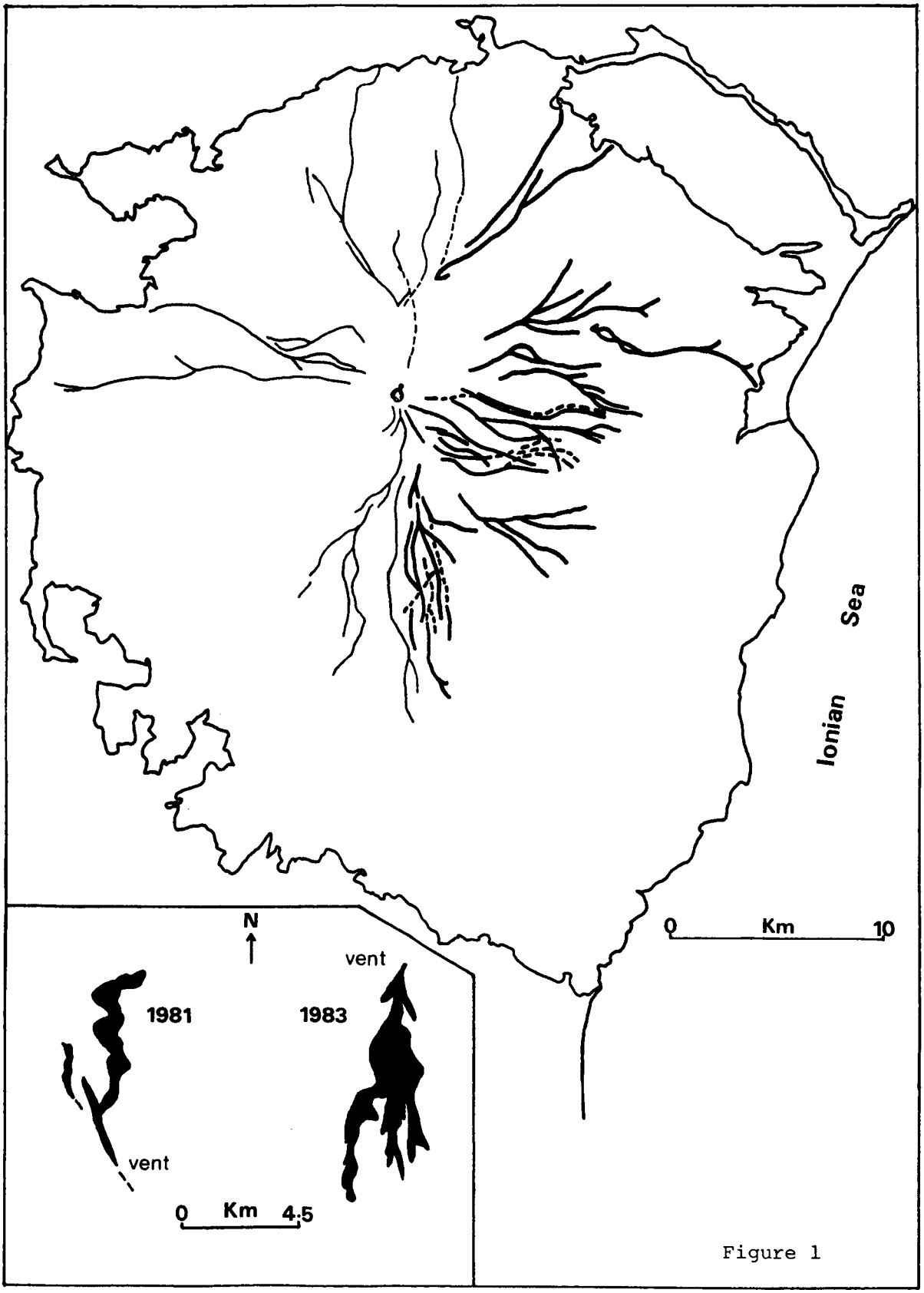

Figure 1

N88-29677

HOW DIRTY IS MARS' NORTH POLAR CAP, AND WHY ISN'T IT BLACK?;

Hugh H. Kieffer, U.S. Geological Survey, Flagstaff, Arizona 86001

Global studies of Mars seem to indicate conclusively that the seasonal polar caps are CO_2, that the residual north polar cap is H_2O, and that the north polar region is an annual net source of water vapor. More detailed observations show the late-summer north polar cap to be composed of bright icy areas with interspersed darker layered terrain (lanes), presumably composed of dust. However, simple models suggest that old dirty ice should be nearly as dark as, or darker than, the layered terrain.

Well-established observations are that in mid-summer, (1) the bright north polar material has an albedo near 0.41 and a temperature near 210 K; (2) the dark material has an albedo near 0.24 and a temperature near 235 K [1]; (3) the column water-vapor abundance in the north polar region is 30-100 precipitable microns; (4) the atmosphere over the cap is virtually saturated with water vapor; and (5) water-vapor abundance decreases away from the edge of the polar cap, definitely toward the equator, and probably toward the pole as well [2,3,4].

Viking Lander measurements indicate that the average visible opacity of the Martian atmosphere is on the order of unity and that the average annual global dust content of the atmosphere, by mass, is comparable to the average annual global water-vapor content [5]. Although there is considerable uncertainty as to just how and when water vapor and dust are carried into the seasonal polar cap, the average global values indicate deposition of a few milligrams/cm^2 of each in the seasonal polar cap, corresponding to a visual opacity in the deposit due to dust alone of approximately 10.

The dust and H_2O must initially be fine grained because they are transported into the polar region in suspension, probably as nuclei of CO_2 snow grains. The H_2O grain size cannot change significantly until the seasonal CO_2 is gone, because the metamorphism rate of H_2O at 145 K is negligible [6]. Thus, the expected composition of material residual from the current seasonal cycle is a mix of fine dust and H_2O in comparable abundance. In fine-grained ice-dust mixtures, even a 0.001 mass fraction of dust is sufficient to lower the visual reflectance to approximately 0.4 [7]. Metamorphism during the summertime warming of the residual cap will further lower the albedo by decreasing the surface area of H_2O grains while not affecting the surface area or spatial dispersion of the dust grains.

If the residual north polar cap is undergoing net annual sublimation, late summer observations should be of old dirty ice. Gradual metamorphism over many annual thermal cycles is calculated to result in H_2O grain sizes on the order of 100 microns. Ice of this granularity containing 50 percent fine dust has a reflectivity similar to that of dust alone.

The brightness of the icy areas conflicts with what would be expected for a residual cap deposited by an annual cycle similar to that observed by the Viking mission and aged for thousands of years. A possible explanation for the brightness of the residual cap is that the bright areas are accumulating frost in the late summer, while the dark areas are losing water vapor. This is not unreasonable, because the atmosphere is virtually saturated, and the

bright areas are about 25 K cooler than the dark areas and are probably at a temperature below the atmospheric frost point. This accumulation could be "clean," in that atmospheric dust need not be carried into the deposit (as occurs for CO_2 frost), and there is no obvious constraint on the grain size of H_2O noar frost.

Another possible explanation is that dust is a minor component of the residual H_2O cap, which implies that the material now at the cap surface formed in an atmosphere far cleaner than the present one.

The high thermal inertia observed for the residual north polar cap [8] is near that expected for bulk water ice and is suggestive of older, coarse-grained ice. The amount of water and dust deposited in one season is too small to influence the thermal inertia significantly, even if the material remains extremely fine grained and of low thermal conductivity. Hence, the last year's H_2O-dust deposit could significantly influence the brightness of the cap, but not its thermal inertia.

If we are observing an annual process, the dominant source of any H_2O accumulating on the residual caps in summertime must be the H_2O that was incorporated in the seasonal CO_2 cap and that was residual on the dirt surface when the CO_2 disappeared. By the end of the summer, the upper few centimeters of the dark lanes are probably desiccated down to a level at which diffusion inhibits the net removal of water [4].

The dichotomy of terrains in the north polar region may thus be stronger than generally realized. In the current climate, the bright areas may have net volatile accumulation while the dark lanes are depleted of perennial volatiles, at least near the surface. The net polar source of water implies that the bright areas are shrinking laterally. "Old" volatiles may be inaccessible to sampling of the north polar region; they may have either retreated below the surface of the dark terrains or been buried beneath young water ice in the bright areas.

The composition and annual budget of the residual caps and the local volatile transport suggested here should be well addressed by the complement of nadir-looking instruments on the Mars Observer spacecraft.

[1] Kieffer, H. H., S. C. Chase, Jr., T. Z. Martin, E. D. Miner, and F. D. Palluconi (1976) Science 194, p. 1341-1344.
[2] Farmer, C. B., D. W. Davies, and D. D. LaPorte (1976) Science 194, p. 1339-1341.
[3] Farmer, C. B., and P. E. Davis (1979) J. Geophys. Rev. 84, p. 2881-2888.
[4] Jakosky, B. M. (1983) Icarus 55, p. 1-18.
[5] Pollack, J. B., and O. B. Toon (1982) Icarus 50, p. 259-287.
[6] Clark, R. N., F. P. Fanale, and A. P. Zent (1983) Icarus 56, p. 233-245.
[7] Clark, R. N. (1982) Icarus 49, p. 244-257.
[8] Paige, D. A., and A. P. Ingersoll (1985) Science 228, p. 1160-1168.

N88-29678

SOME PROBABLE CHARACTERISTICS OF THE MARTIAN REGOLITH; Elbert A. King, Department of Geosciences, University of Houston, University Park, Houston, Texas 77004

A number of Mars' surface environmental factors seriously affect the properties of the martian regolith. The result is a regolith that is rather different from that of the Moon. Some of the anticipated differences are:

Weathering and lack of old glass - The abundance of volatiles on Mars, both at present and in the past should have resulted in devitrification of glasses that have been exposed to water and other volatiles for long periods of time. The fact that these volatiles are and have been present is supported by the existence of the present atmosphere, icy polar units and polar caps, and the large outflow channels and numerous small sinuous channels. Some stratigraphic units such as the ancient "hilly and cratered material" mapped in the southern highlands of Mars as Hellas Basin ejecta in MC-21 and MC-22 (1, 2) have abundant small channels superposed on them, indicating a long history of interactions with surface and near-surface volatiles, probably during aqueous fluvial processes. Greeley (3) has estimated that amount of juvenile water released in association with volcanism on Mars is equal to a planet-wide layer 46 meters deep, and furthermore that most of this water was released during the first 2 billion years of martian history. This figure probably is a minimum for water on Mars, but in itself is sufficient to promote much devitrification and hydration. It may be that parts of the martian regolith will be enriched in palagonite, montmorillonite, bentonite, smectite, amorphous gels and nontronite as a result of hydrous devitrification of volcanic and impact glasses. On the Earth, similar processes have led to the observation that glass older than Jurassic is quite rare. On Mars, as on the Earth, many rocks may show evidence of partial oxidation, alteration and/or hydration.

Desert varnish - One or more surfaces of regolith rocks may have a coating of desert varnish. Various studies of the colors of martian surface rocks have shown that in some fields of view the rocks show little color variation. This may be partly due to partial coatings of desert varnish on exposed surfaces. Conditions on Mars are near-ideal for distributing fine layers of dust on the tops of rocks and for precipitating volatiles out of the atmosphere that can react with the dust to form desert varnish.

Lack of micrometeorite impact products - The martian atmosphere, although only about 6 millibars total average pressure, is adequate to protect the surface rocks from small meteoroids. Small impact craters ("zap pits") should be absent as should the glassy spatter produced by micrometeorites. The regolith should not contain abundant glassy agglutinates.

Abundance of meteorite fragments - The thin martian atmosphere is adequate to slow down meteorites of as much as several hundred grams, such that they should reach the surface relatively intact. This fact, together with the anticipated greater flux of small meteoroids in the vicinity of Mars, probably causes a much greater amount of meteoritic debris to be preserved and/or weathered in the martian regolith than on the Moon.

Different grain size characteristics - Because of the non-ballistic sedimentation processes that operate on the martian surface, it is virtually certain that many regolith samples will have different grain size frequency distributions from lunar regolith. Some martian samples should be better sorted, more leptpkurtic, have lesser standard deviations and may generally be finer than lunar regolith. This type of sample also is suggested by the geo-

morphology of some parts of the martian surface, e.g. dune forms. In addition many of the anticipated weathering products mentioned above are produced in very fine grain sizes. Also, the mix of different sedimentation processes on Mars is expected to produce sediment and regolith samples that are multimodal.

References:
(1) Schaber, G. (1977) USGS Map I-1020 (MC-21).
(2) King, E. A. (1978) USGS Map I-1073 (MC-22).
(3) Greeley, R. (1987) Science 236, p. 1653-1654.

76
154525

YE 661058
N88-29679

WHAT SNC METEORITES TELL US ABOUT MARTIAN MAGMATISM.

John Longhi & Vivian Pan, Dept. of Geology & Geophysics, Yale University, New Haven, CT 06517

Although proof positive awaits a sample return from Mars, a sufficiently persuasive case has been made in favor of a martian origin for the SNC (Shergottite - Nahklite - Chassignite) suite of meteorites (1,2) that it is worthwhile to accept the premise tentatively and examine the implications for martian composition and evolution.

Petrography - Most SNC meteorites are igneous cumulates or partial cumulates. This means that the compositions of their parental liquids are different from their bulk compositions and can only be determined indirectly. One sample, EETA 7001, contains a fine-grained basaltic lithology, but its bulk composition is compromised by the presence of about 15% xenocrystic olivine and orthopyroxene (3). Variations in the proportions of the major cumulus phases -- olivine pigeonite, and augite -- serve as discriminants for the three classes of SNC meteorites: Shergottites = subequal proportions of pigeonite and augite ± olivine; Nahklites = augite with minor olivine; Chassignites = olivine with minor augite (4). The presence of plagioclase as a late-stage intercumulus or interstitial phase implies relatively low-Al_2O_3 liquids in contrast to the most common terrestrial lavas (Fig. 1). The composition of plagioclase (intermediate to sodic) distinguishes SNC's from mare basalts, most of which also have late crystallizing plagioclase. The prevalence of cumulus augite and a lower Mg/Fe ratio reflected in the presence of pigeonite (as opposed to orthopyroxene) distinguish SNC's from diogenites. Early-crystallizing Fe^{3+}-bearing chromite and late crystallizing titanomagnetite are common, although not ubiquitous, constituents of SNC's and indicate relatively high oxidation states, similar to terrestrial magmas. Trace amphiboles included in olivine and pyroxene plus apparently pre-terrestrial hydrous alteration indicate dissolved H_2O in the parent magma. The fact that olivines are not pervasively altered to hydrous minerals suggests that the H_2O concentrations were well below saturation and in the range of most terrestrial basalts.

Trace Element and Isotopic Composition - On a $\delta^{17}O$ - $\delta^{18}O$ plot SNC's lie on a mass fractionation curve distinctly higher (i.e., isotopically lighter) than those of the Earth, Moon, and eucrites, thus indicating a separate and probably single parent body that accreted from a different portion of the early solar system (5). Estimates of SNC-parent body abundances of siderophile elements, indicate stronger depletions than the Earth for siderophile elements that are also chalcophile, thus suggesting a sulfide-rich core (6). Ratios of volatile-incompatible to involatile-incompatible elements (e.g., K/La) suggest that the SNC parent body (Mars) is less depleted in volatile elements than the earth (7), in sharp contrast to the inferences made from measurements of surface K/U by the Soviet Mars 5 orbiter, which suggested that Mars was as depleted in volatiles as the Moon (8). Perhaps this discrepancy indicates that weathering preferentially removes alklalies from the Martian surface. Sm-Nd and Rb-Sr isotopic studies indicate that the source regions of the Nahklites and Chassignites were relatively depleted in the most incompatible elements (7), as are the mare basalt source regions and the Earth's upper mantle. There is no evidence of a negative Eu-anomaly, so no anorthosite formation was involved in the formation of the NC source regions. U-Pb studies indicate that the Nahkla source region was formed approximately 4.3 b.y. ago (9). Similar isotopic studies on the Shergottites, however, indicate enriched sources, formed 4.6 b.y. ago, similar in some respects to the Earth's crust. Given the mafic nature of the parental magma, the indication of an enriched source may actually be the signature of assimilated crust. The presence of small positive Eu-anomalies in some of the calculated parent magmas of the Shergottites, suggests an anorthositic component in the assimilated crust (7).

Because of complications introduced by shock metamorphism, estimates of the crystallization age of the Shergottites range from 1.3 b.y. to 160 m.y. (10,11,12). There is apparently little argument over the reported 1.3 b.y. age for Nahkla (9), however.

Major Element Composition - Fig. 1 illustrates that the inferred Shergottite parent

magma ("S" - 13) matches the Viking Lander soil analysis (14) more closely than any common lunar or terrestrial (MORB, flood, oceanic island) basalt type. The closest compositional match with martian soil, however, is with terrestrial boninites. These are relatively uncommon lavas associated with subduction zones that are believed to be generated by wet (possibly metasomatic) melting of depleted mantle. One important compositional difference not evident in Fig. 1 is Mg/Fe: boninites have unusually high Mg/Fe ratios for terrestrial basalts, whereas the martian soil value is relatively low. This difference may be nothing more than a reflection of a lower Mg/Fe ratio in the martian mantle. There is another important compositional difference, however, if the SNC s are martian. Boninites are commonly heavily altered -- a result of the reaction of the early-formed mafic minerals with magmatic water (estimated to be $\sim$2 wt%) released during crystallization -- whereas the hydrous alteration in SNC's is relatively minor, suggesting $<<1$ wt% H_2O.

An estimate of the composition of the liquid parental to Nahkla, based upon the composition of cumulus augite (Fig. 1b) coexisting with olivine, is depicted as "N". The parental composition of Chassigny cannot be estimated as simply because of extensive subsolidus equilibration of the augite (15). An alternative estimate of the Nahkla ("D") parental liquid (16), based upon a simple model of cumulus crystals and trapped intercumulus melt equalling the bulk rock composition, suggests (probably incorrectly) a highly unusual magma type. Calculated eruption temperatures for the SNC-parental liquids are in the range of 1200° - 1300°C with viscosities of 50 - 150 poise.

It is extremely unlikely that S and N represent primary magma compositions. Both probably were derived by prior fractionation of olivine and pyroxene. Without additional information it is not possible to estimate a depth of melting. However, by analogy with high pressure studies of lunar and terrestrial compositions, it is unlikely that any permissible parental liquid composition would have left a residual aluminous phase (plagioclase, spinel, or garnet) in a peridotitic source region. This fact plus the isotopic signature of a depleted source region in Nahkla, requires a complex melting event for the Nahkla parent magma, which apparently had a pattern of light-REE enrichment.

In many respects the SNC parental magmas are similar to fractionated samples of late Archean terrestrial magmatism ranging from basaltic komatiites ("K") to noritic dikes and sills ("L") both of which have late-crystallizing plagioclase (17). In fact a specific analogy has been drawn between Nahkla and komatiites based upon textures (18). The basaltic komatiites have a mantle isotopic signature and higher contents of the Wo component, analogous to the Nahklite and Chassignite parents, whereas the noritic dikes have crustal isotopic signatures and lower Wo components (due to the assimilation of granitic crust), analogous to the Shergottites.

Summary - The SNC meteorites record relatively recent ($\leq$1.3 b.y.) basaltic volcanism on a hydrous planet with a core. This much was known about Mars even before the Viking mission. The SNC's tell us that the basalts were unusually low in Al_2O_3 and, despite overall similarities in major elements, apparently sampled two isotopically distinct regions of Mars: one is relatively depleted in incompatible elements (Nahklite source) with a U-Pb model age of 4.3 b.y. and is probably a portion of the upper martian mantle, whereas the other is relatively enriched in incompatible elements (Shergottite source) with a 4.5 b.y. U-Pb age and is probably martian crust assimilated into the mantle-derived Shergottite magma. The SNC's also tell us that the overall abundances of moderately volatile elements, such as alkalies, are higher on Mars than the Earth. Given extensive volcanism and a depleted mantle, the present day absence of a thick atmosphere is more likely due to catastrophic removal of a primordial atmosphere than lack of degassing.

REFERENCES

(1) Wood C.A. and L.D. Ashwal (1981), Proc. Lunar Planet. Sci. Conf. 12th, p.1359-1375. (2) McSween H.Y. (1985) Revs. Geophys., 23, 391-416. (3) McSween H.Y. and E. Jarosewich

(1983) Geochim. Cosmochim. Acta 47, 1501-1513. (4) Stolper E.M., H.Y. McSween, and J.F Hays (1979) Geochim. Cosmochim. Acta 43, 1475-1498. (5) Clayton R.N. and T.K. Mayeda (1983) Earth Planet. Sci. Lett. 62, 1-6. (6) Dreibus G. and H. Wanke (1985) Meteoritics 20, 367-381. (7) Smith M.R., J.C. Laul, M.-S. Ma, T. Huston, R.M. Verkouteren, M.E. Lipschutz, and R.A. Schmitt (1984) J. Geophys. Res. 89, suppl., B612-B630. (8) Morgan J.W. and E. Anders (1979) Geochim. Cosmochim. Acta 43, 1601-1610. (9) Nakamura N., D.M. Unruh, M. Tatsumoto, and R. Hutchison (1982) Geochim. Cosmochim. Acta 46, 1555-1573. (10) Nyquist L.E., J. Wooden, B. Bansal, W. Wiesmann, and C.-Y. Shih (1984) Meteoritics 19, 284. (11) Jagoutz E. and H. Wanke (1986) Geochim. Cosmochim. Acta 50, 939-953. (12) Jones J.H. (1985) Lunar and Planetary Science XVI, 406-407. (13) Stolper E.M. and H.Y. McSween (1979) Geochim. Cosmochim. Acta 43, 1475-1498. (14) Clark B.C., A.K Baird, R.J. Weldon, D.M. Tsusaki, L. Schnabel, and M.P. Candelaria (1982) J. Geophys. Res. 87, 10,059-10,067. (15) Floran R.J., M. Prinz, P.F. Hlava, K. Keil, C.E. Nehru, and J.R. Hinthorne (1978) Geochim. Cosmochim. Acta 42, 1213-1229. (16) Treiman A.H. (1986) Geochim. Cosmochim. Acta 50, 1061-1070. (17) Longhi J., J.L. Wooden, and K.D. Coppinger (1983) J. Geophys. Res. 88, suppl. B53-B69. (18) Treiman A.H. (1986) Lunar and Planetary Science XVIII, 1022-1023.

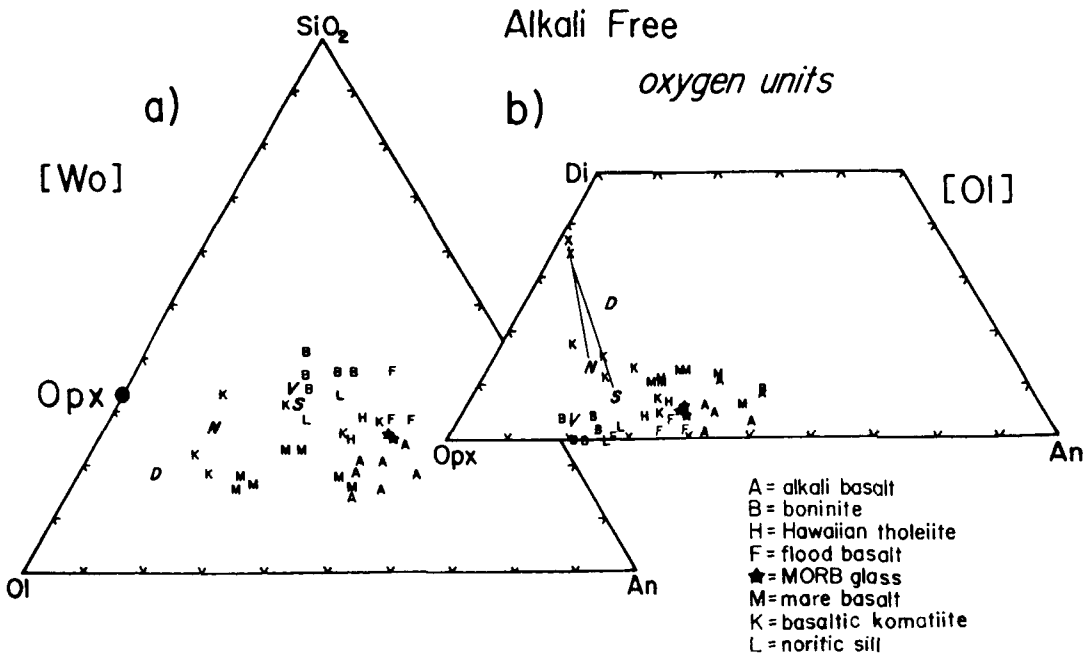

Figure 1. Depiction of basaltic compositions in terms of four mineral components: Ol = $(Mg,Fe,Mn)_2SiO_4$, An = $CaAl_2Si_2O_8$, Wo = $CaSiO_3$, and SiO_2. a) projection from Wo onto the Ol-An-SiO_2 plane; b) projection from Ol onto the Opx(Ol+SiO_2)-An-Wo plane. Alkalies are ignored in these projections in order to make basaltic compositions comparable to the Viking soil analysis ("V") which did not include Na_2O. Solid lines connect natural augite compositions with estimated parental magma compositions. S = Shergottite parental magma (13). D = Nahklite parent (16). N = Nahklite parent (this study).

G465-7484 N88-29680

SURFACE UNITS ON MARS: THE ASSEMBLAGE IN THE VALLES MARINERIS; B. K. Lucchitta, U.S. Geological Survey, Flagstaff, Ariz. 86001

The Valles Marineris system of troughs offers a unique opportunity to investigate Martian surface units in the third dimension. The troughs are more than 7 km deep in places and thus expose a significant portion of the Martian upper crust.

The geologic units within the Valles Marineris can be subdivided into three broad categories: wall rock, interior deposits, and surficial cover. The wall rock is exposed in the steep scarps bordering the troughs, in spurs projecting into the troughs, and in isolated erosional remnants. Wall rock is also found in the material reworked into landslide deposits. Interior deposits form free-standing, eroded mesas that locally lap up against or overlap eroded wall rock; they may also underlie parts of the Valles Marineris floor. Surficial cover forms blankets of variable thickness covering the other units.

Wall Rock

The wall rock has a layered cap and massive material in the lower slopes. The layers are clearly visible on the steep cliffs of the upper walls and are expressed by different albedos or different erosional resistances. Four layers are commonly visible, but as many as eight can be recognized in places. Many of the layers are extensive and some can be traced for hundreds of miles. The layers are probably composed of volcanic materials, most likely flood basalts (1), but the possibility that the upper 2 km of the wall are composed of other materials cemented by ice cannot be totally excluded.

The lower walls are massive; layers are visible only in a few places, for instance, an extensive bluish layer in the south wall of Coprates Chasma. The lower walls appear to be unstable; they have eroded to form deep gullies, generated debris flows, and collapsed readily into gigantic landslides. Thus, the material underlying the walls is apparently poorly consolidated. It is most likely composed of lunar highland-type breccia (2), and probably charged with ice and water at some depth behind the surficially desiccated walls (3). The wall material is probably similar to highland material elsewhere on Mars, which appears to be the primary reservoir for ground ice. Because of its ice content, this material gives rise to rock-glacial flow and terrain-softening features in mid-latitudes (4, 5) and to landslides in low latitudes (3).

Interior Deposits

The interior deposits reflect two episodes of deposition: an older one resulting in the layered sequences now standing as high eroded mesas that approach the elevation of the plateau surface, and a younger sequence deposited on a deeply eroded surface that has an elevation close to that of the present trough floors. The older layered sequence consists of alternating dark and light layers, the dark layers being generally thin and resistant to erosion and the light layers being more massive and highly susceptible to wind erosion. Volumetric constraints and observations associated with the younger set of interior deposits (see below) suggest that these older beds are largely of volcanic origin (6), even though deposition within a lake of wind-drifted or fluvial materials (7, 8) may have contributed in a minor way to the buildup of these deposits.

The younger interior deposits consist of (a) very dark, relatively blue patches with short stubby flows in places, occurring characteristically along faults; (b) thick, smooth, light-colored deposits that are locally associated with apparent volcanic craters; and (c) deposits with lobate fronts, layers in places, rough surface textures, and highly irregular albedos. These young deposits rest unconformably on older units and embay interior mesas, landslides, and tributary canyons. They are generally thin, but in western Candor Chasma they may reach thicknesses of 3000 m. These materials are probably volcanic, and the very dark patches may be mafic. As the albedo contrast between the dark and light units is not large, the light units could be palagonitic tuffs (9), a composition that also agrees with the reddish spectral signature of these units.

Some of the young interior deposits have surface characteristics, such as high-albedo, rolling, smooth surfaces and wind-eroded flutes, that are similar to those in the vast deposits of light materials in southern Amazonis Planitia. If the deposits in the Valles Marineris are indeed of volcanic origin, the similarity would strengthen the hypothesis that those in Amazonis Planitia are also volcanic (10, 11).

Surficial Cover

All units in the Valles Marineris are probably covered to some extent by fine-grained dust or wind-drifted sand. Smooth, light-colored materials on trough floors and mesa tops may be composed of thick blankets of light-colored atmospheric dust fallout, but this material cannot be distinguished visually from the underlying rock. Light materials on mesa tops have very low thermal inertia (J. Zimbelman, written communication), suggesting that the mesa tops are covered by this dust; the reddish spectral signatures of this material suggest a composition of iron-rich clays or palagonitic tuffs.

Dark surficial materials are relatively blue, suggesting mafic compositions. Streaks, dune forms, and entrapment in low areas or crevices suggest that the material moved by saltation or ground-hugging flow and therefore is probably composed of sand-sized grains. Small patches or thinly covered areas have no characteristic thermal-inertia signature, but more extensive patches (of which most show dune forms) have very high thermal inertia, suggesting abundant grains larger than 1 mm in size. The dark material inside the Valles Marineris troughs appears to be derived from local young volcanic vents (12) or older exposed dikes or sills.

The light, fine-grained material on mesa tops is probably similar in composition and grain size to materials found in many areas on the Martian surface; both most likely originated from atmospheric fallout of very fine grained material distributed by dust storms. The dark material in the troughs also has characteristics similar to dark materials elsewhere on Mars that occur as streaks or dunes or are trapped inside craters. Observations of the dark materials in the Valles Marineris suggest that some of the dark materials elsewhere may similarly be derived from young volcanic vents or older exposed sills or dikes. This contention is supported by the apparent preferential occurrence in the western hemisphere of dark material near fractured and faulted terrains that may have facilitated volcanism (these relations are seen on a color mosaic prepared by A. S. McEwen, U.S. Geological Survey).

Overall, the exposure of units in the Valles Marineris gives insights into surface units elsewhere on Mars: The observations tend to support the hypotheses that the highland material is charged with ice, that some light-colored, rolling, smooth deposits are of volcanic origin, and that dark dunes and streaks are composed of wind-blown mafic materials.

References

(1) Scott D.H. and Carr M.H. (1978) Geologic map of Mars: U.S. Geological Survey Miscellaneous Investigations Map Series I-1083, Scale 1:25,000,000.

(2) Carr M.H. (1979) Formation of martian flood features by release of water from confined aquifers: Journal of Geophysical Research, v. 84, no. B6, p. 2995-3007.

(3) Lucchitta B.K. (in press) Valles Marineris, Mars: Wet debris flows and ground ice: Icarus.

(4) Lucchitta B.K. (1984) Ice and debris in the fretted terrain, Mars: Lunar and Planetary Science Conference, 14th, Proceedings, Part 2: Journal of Geophysical Research, v. 89, Supplement, p. B409-B418.

(5) Squyres S.W. and Carr M.H. (1986) Geomorphic evidence for the distribution of ground ice on Mars: Science, v. 231, p. 249-252.

(6) Peterson Christine (1981) A secondary origin for the central plateau of Hebes Chasma: Lunar and Planetary Science Conference, 12th, Proceedings, Geochimica et Cosmochimica Acta, p. 1459-1471.

(7) Lucchitta B.K. (1982) Lakes or playas in Valles Marineris (abs.), in Reports of Planetary Geology Program--1982: National Aeronautics and Space Administration Technical Memorandum 85127, p. 233-234.

(8) Nedell S.S., Squyres S.W. and Andersen D.W. (1987) Origin and evolution of the layered deposits in the Valles Marineris, Mars: Icarus, v. 70, p. 409-441.

(9) Singer R.B. (1982) Spectral evidence for the mineralogy of high-albedo soils and dust on Mars: Journal of Geophysical Research, v. 87, no. B12, p. 10159-10168.

(10) Ward A.W. (1979) Yardangs on Mars: Evidence of recent wind erosion: Journal of Geophysical Research, v. 84, no. B14, p. 8147-8166.

(11) Scott D.H. and Tanaka K.L. (1982) Ignimbrites of Amazonis Planitia region of Mars: Journal of Geophysical Research, v. 87, no. B2, p. 1179-1190.

(12) Lucchitta B.K. (1987) Recent mafic volcanism on Mars: Science, v. 235, p. 565-567.

S27-91
82
N88-29681
GU6574
W 535 1617

MORPHOLOGIC CONTRASTS BETWEEN NIRGAL AND AUQAKUH VALLES, MARS: EVIDENCE OF DIFFERENT CRUSTAL PROPERTIES.

David J. MacKinnon, Kenneth L. Tanaka, *U.S. Geological Survey, Flagstaff, AZ 86001*, Philip J. Winchell, *Wittenberg University, Springfield, OH 45501*

We have made photoclinometric measurements of sidewall slopes in Nirgal and Auqakuh Valles and have interpreted these results in terms of the geologic setting and a simple geomorphic model to provide new insights into the physical properties of crustal materials in these areas. Nirgal has been interpreted to be a runoff channel and Auqakuh to be a fretted channel by [1]. Geomorphologic arguments for the sapping origin of Nirgal and Auqakuh Valles have been presented by [1] and [2]. The morphologies of the channels, however, differ greatly: the tributaries of Nirgal end abruptly in theater-headed canyons, whereas the heads of tributaries of Auqakuh shallow gradually. The plateau surface surrounding both channels appears to be covered by smooth materials, presumably lava flows; they are continuous and uneroded in the Nirgal area, but at Auqakuh they are largely eroded and several layers are exposed that total about 200 m in thickness. For Nirgal Vallis, our measurements show that sidewalls in the relatively shallow upper reaches of the channel (200-m to 400-m depth) have average slopes near 30 degrees and, in the lower reaches (500-m to 1000-m depth), sidewall slopes exceed 50 degrees. Auqakuh, on the other hand, has maximum sidewall slopes of 14 degrees and an approximate maximum depth of 1000 m. Faint, horizontal layering in portions of the lower reaches of Nirgal may indicate inhomogeneity in either composition or topography.

A key relation is whether these slopes are above, near, or below the angle of repose for loosely consolidated and noncohesive materials. (Such an angle of repose is about 30 degrees and is independent of gravity [3, 4, 5].) Slopes above the angle of repose may indicate competent rock, cemented fines, or compaction of poorly sorted materials [6]; slopes near the angle of repose may be composed of dry talus, soil, and other granular materials, and slopes below the angle of repose may suggest modification by volatiles. Selby [4, p. 200] and Moon [3] showed that equilibrium (stabilized) slope values are highly correlized with the strength of intact rock and spacing of joints; they tested models on scarps in Antarctica, New Zealand, and South Africa. Where soil formation is limited in "dry" climates and in mountains, slope angles reflect rock strength. We have extrapolated this correlation and its implied geomorphologic relation on Mars, along with our sidewall profiles and interpretation

of the geologic settings of Nirgal and Auqakuh Valles in order to understand the physical and hydraulic properties of their materials.

Nirgal Vallis:

Low slope angles (less than 30 degrees) in the upper 200 m of crust below the surface lava flows indicate a fairly well brecciated or fine grained material. This material is probably highly cratered: some low-rimmed craters are seen protruding through the caprock. The slope increases with depth, suggesting that the material becomes either less brecciated or more cemented with depth. In either case, the permeability and pore space would decrease with depth as well. This reduction in hydraulic capabilities indicates that, under present circumstances, only high discharges from a necessarily large volume of water-saturated material would be capable of removing materials to form the channel. Other possibilities include past climatic conditions that caused recharge of the ground water or surface flows sufficient to remove the materials.

Auqakuh Vallis:

The relatively gentle sidewall slopes for Auqakuh are not consistent with the "fretted" classification suggested by [1,2,5]. The sidewall slopes are, in fact, significantly below the angle of repose for unconsolidated material. Based on our model, this relation strongly suggests that the sidewall slopes were modified by periglacial mass-wasting, involving ground ice, as previously suggested by [1]. The surface lava flows are largely eroded, possibly by mass-wasting and wind, indicating that earlier processes had weathered the flows into relatively fine material. Below the flows, a lower layer of undetermined thickness (at least 600 m) appears to have a rough surface and is heavily cratered where exposed on the plateau. Because downslope processes have shed debris from the upper layers into the channel, it is uncertain whether this lower layer is actually exposed. The same downslope processes in the channel may have removed or subdued crucial indicators of Auqakuh's early formation. What is clear, though, is that an enormous volume of crustal material has been removed from the channel. If the material was fine grained and loosely consolidated, it was more readily removed by sapping and eolian processes than materials in Nirgal Vallis.

Future Considerations:

We have explored only one geomorphologic model that interprets crustal properties in Nirgal and Auqakuh Valles. Other aspects that need to be considered carefully include

apparently large differences in time of formation of the channels and variations in associate climate. Auqakuh, which is older than several heavily degraded craters, 10km diameter or greater, may have been initiated during the end of the heavy bombardment (it is about the same age as with other ancient valley systems) and later modified by surface volatiles and a colder climate. Nirgal, on the other hand, is only sparsely cratered and probably formed much later from subsurface aquifers (if such can be justified in terms of our earlier argument) after water from the surface layers was depleted. Its formation was possibly contemporaneous with the Tharsis tectonism that appears implicated in the formation of the large outflow channels east and north of Valles Marineris. Both may have even formed at nearly the same time if surface volatiles were never present at Nirgal Valles: each channel lies in a region roughly 30 degrees from the equator that is assumed to be transitional between an ice-poor and ice-rich regolith [8].

Clearly our interpretation of slopes needs to be more sharply qualified. For example, those slopes below the angle of repose for loosely consolidated materials may have been formed by landslides, eolian deposits, volatiles, earthquakes, or all of the above. We plan to produce more photoclinometric and stereophotogrammetric sidewall slope measurements of other channels and develop qualified geomorphologic models to obtain a broader understanding of the influence of crustal materials and climate on the formation of aquifer and channel systems on Mars.

References Cited:

[1] Baker, V. R., 1982, The channels of Mars: Univ. of Texas Press, Austin, 198 p.;[2] Sharp, R. P., and M. C. Malin, 1975, Channels on Mars: Geol. Soc. Amer. Bull., v. 86, p. 593-609; [3] Moon, B. P., 1984, Controls on the form and development of rock slopes in fold terrane, in Hillslope processes(edited by A. D. Abrahams):Boston, Allen & Unwin Ltd., p. 225-243;[4] Selby, M. J. 1982, Hillslope materials and processes: London, Oxford Univ. Press, 246 p.;[5] Terzaghi, K., and R. Peck, 1967, Soil mechanics in engineering practice, 2nd ed.: New York, John Wiley & Sons, 729 p.;[6] van Burkalow, A., 1945, Angle of repose and angle of sliding friction: An experimental study: Geol. Soc. Amer. Bull., v. 56, p. 669-708; [7] Carr, M. H., 1981, The surface of Mars: Yale Univ. Press, New Haven, 349 p.;[8] Fanale, F. P., J. R. Salvail, A. P. Zent, and S. E. Postawko, 1986, Global distribution and migration of subsurface ice on Mars: Icarus, 67, p. 1-18

GU 657484 N88-29682 53-91 34-325 3P

GEOLOGY OF SIX POSSIBLE MARTIAN LANDING SITES; Harold Masursky, A.L. Dial, Jr., M.E. Strobell, and D.J. Applebee, U.S. Geological Survey, Flagstaff, Arizona 86001

Thirteen detailed geologic maps of the first six (of ten) possible sites for a future lander/rover/sample-return mission to Mars are either nearing completion or in review. Base mosaics of all sites were available at 1:2 million scale. Mosaics at 1:1/2 million scale have been compiled for the Chasma Boreale (North Pole), Planum Australe (South Pole), Mangala Valles, and Kasei Valles sites; a new base at this scale has been compiled for the Olympus Rupes site and one is being prepared for the Memnonia Sulci site. Study is underway of four additional sites: Candor Chasma, Elysium Montes, Apollinaris Patera, and Nilosyrtis Mensae. In addition to preparing new base maps, we have generated special enhancements of computer mosaics and individual images that delineate the geologic units more clearly, and we have prepared photoclinometric profiles that allow us to measure the thicknesses of geologic units, the depth of channels, and the throw on faults. Topographic profiles and diffuse-scattering data, derived from Earth-based radar data, are being used to evaluate surface slopes and roughness parameters at the equatorial sites; Viking bistatic radar data are being used to determine roughness at the north polar site. Crater counts have been made for each geologic unit.

At the East and West Mangala Valles sites (the West Mangala site is shown in Fig. 1), terrain (unit Nc) is exposed that is thought to be very ancient because it is greatly degraded and does not show layering. Composition of this unit may be similar to lunar norites (ANT suite) or terrestrial granitoid-greenstones, the most ancient material on the Moon and Earth. In the eastern part of the map area, these ancient rocks are mostly covered by intercrater plains material (unit Hpi) that was deposited over a long period of time and is interpreted to be lava flows of possible basaltic or intermediate composition. For the first time, crater-density curves derived from this and other upland units, as we have subdivided them, yield relative ages that are consistent with stratigraphic relations shown by geologic mapping (Masursky et al., 1986, 1987). At the East Mangala site, an east-trending fault separates these upland rocks from a series of lava flows that comprise the northern lowland plains. They are thought, from their morphologic characteristics, to be basaltic in origin. These northern flows are overlain, in turn, by young volcaniclastic, probably pyroclastic, flows (unit Apt) that are thought from morphologic characteristics to be rhyolitic in composition. Three generations of fluvial channels (some young) are interspersed within these putative basaltic and volcaniclastic layered rocks; north-trending and east-trending fault zones cut all units except the young volcaniclastic material. These stratigraphic relations are clearly shown in computer-enhanced images.

Rock units in the Memnonia Sulci area are thought to be similar in age and composition to those recognized in the Mangala Valles area (D. H. Scott, written commun., 1987), but the stratigraphic relations are more clearcut at Memnonia. However, the Memnonia site has no channels.

The Olympus Rupes site is situated on smooth plains material (unit Aop) near the southeast flank of Olympus Mons. The gross shape of the volcanic shield and the shapes of individual flows indicate that the shield probably is basaltic but that composition may vary among the four recognizable units (E.C. Morris, written commun., 1987). The construct is

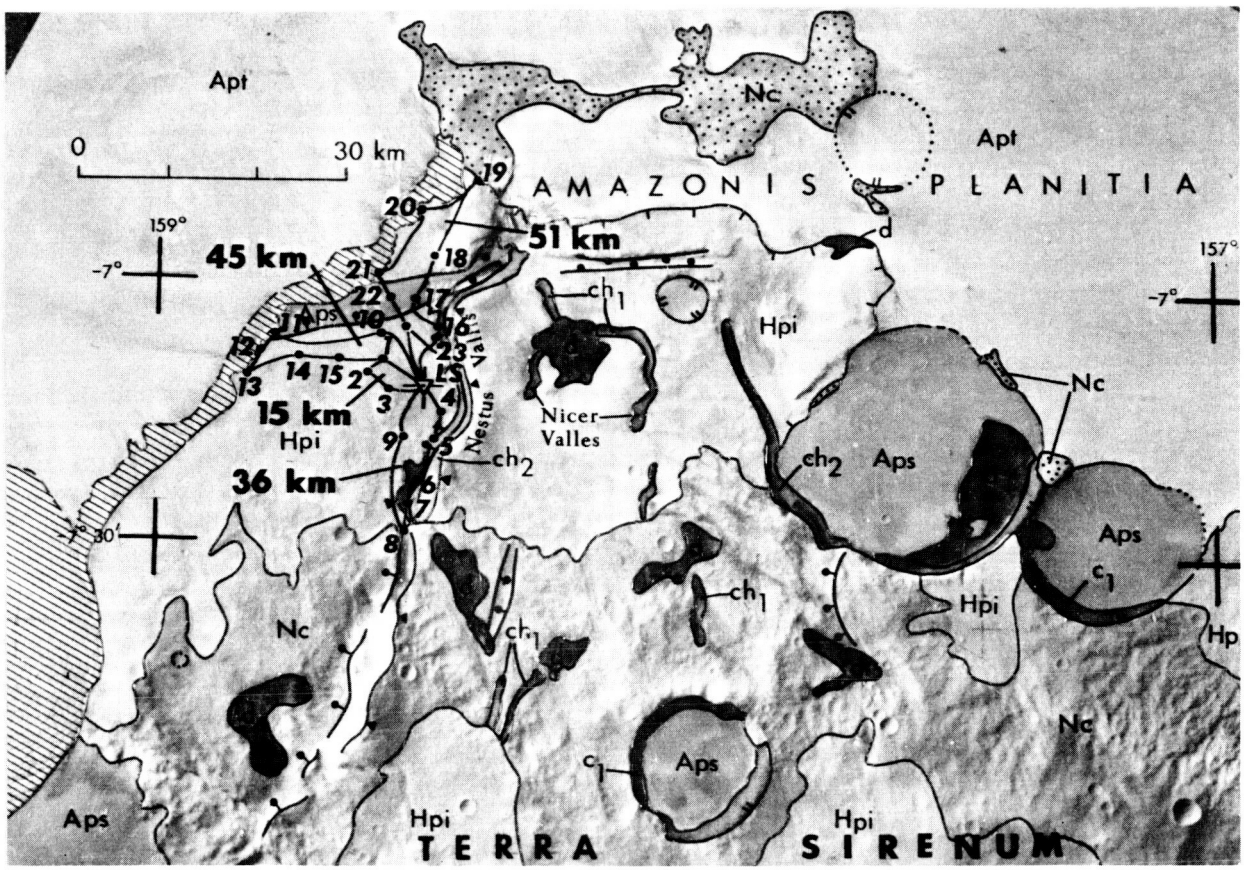

Figure 1. Geologic map and proposed rover traverse of the West Mangala Valles area, Mars.

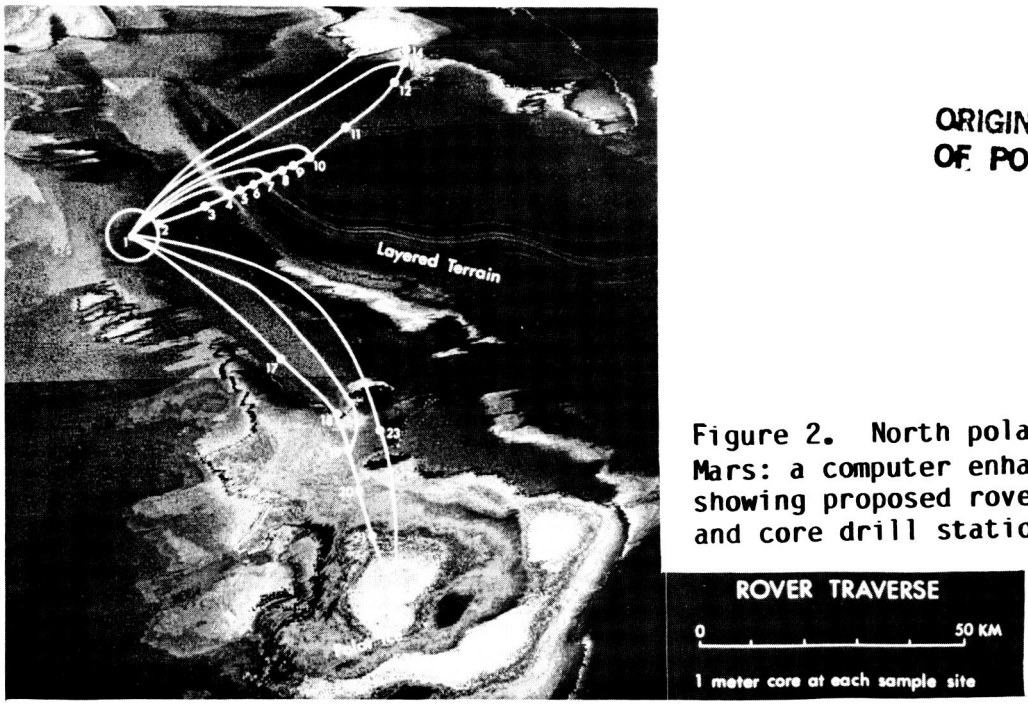

ORIGINAL PAGE IS
OF POOR QUALITY

Figure 2. North polar area of Mars: a computer enhanced mosaic showing proposed rover traverse and core drill stations.

bounded by a scarp--Olympus Rupes. At the base of the scarp, lobate flows that may also be basaltic in composition form a smooth plains unit; these flows appear to be younger than the flows that form the volcanic construct and are considered to be among the youngest flows on Mars (Scott et al., 1982). A few young flank flows cascade over the basal fault scarp and may overlie the smooth plains unit.

In the Kasei Valles area, a broad fluvial valley has been carved into layered plateau rocks of Lunae Planum that are of intermediate age. In the southern part of the Kasei site, the broad channel is buried by younger volcanic flows, probably basaltic in composition, that were emitted from sources to the west. Unfortunately, these flows are so widespread that a rover of limited range could not obtain samples of a variety of units. Farther north, where the broad Kasei channel bends and flows eastward, it is cut by a narrow inner channel. Small channels have furrowed the walls of the broad channel and constructed alluvial fans on the floor of the inner channel. Finally, a lava flow, probably basaltic, covered the inner channel and partly buried the fan deposits.

In the north and south polar regions, older rocks are buried by polar layered deposits. These deposits are interpreted by us and by many other investigators (e.g., Murray et al., 1972; Howard, et al., 1982) to be made up of a multitude of icy layers that contain lesser and greater amounts of dust. At both poles, the layered deposits are overlain by a brighter polar ice cap. In the north (Fig. 2), the cap is water ice; in the south, Viking observations suggest that the cap possibly may be water ice with a surface layer of carbon dioxide ice. Viking bistatic radar data show the north polar area to be one of the smoothest on the planet (Simpson et al., 1982). The north polar layered deposits are fringed by an enormous erg of dunes that are probably composed of sand grains resedimented as an aggregate of partly cemented silt- and clay-sized particles that move by saltation to form dunes. Similar dunes are common around playa lakes in Nevada. False-color sliced enhancements of polar images show that the ice caps also are layered. It should be possible to construct a complete section of the polar deposits by combining and correlating a series of meter-length cores obtained at many stations (Fig. 2).

We hope to learn as much about near-term climatic changes on Mars by studying the polar deposits as we have learned about the Earth's climatic changes by studying ice cores from Greenland and the Antarctic and deep sea cores. Also, we hope that study of samples from equatorial sites will elucidate the sequence of volcanic, tectonic, and fluvial events in that region and the effect of these events on the climate and geologic history of Mars.

The Mars Observer will image these areas with 10 to 40 times the present resolution and will also obtain geophysical and geochemical data; these data will be used to determine the geologic and engineering suitability of each candidate site.

References: Howard, A.D., Cutts, J.A., and Blasius, K.R., 1982: Icarus, 50, 161-215. Masursky, Harold, Chapman, M.G., Davis, P.A., Dial, A.L., Jr., and Strobell, M.E., 1986: 18th Lun. and Plan. Sci., 600-601. Masursky, Harold, et al., in A preliminary study of Mars Rover/Sample Return Missions conducted by the Mars Study Team: NASA Headquarters, January, 1987. Murray, B.C. et al., 1972: Icarus, 17, 328-345. Scott, D.H. et al., 1982: USGS Misc. Inv. Ser. Map I-1266. Simpson, R.A., Tyler, G.L., Harmon, J.K., and Peterfreund, A.R., 1982: Icarus 49, 258-283.

88 154729

N88-29683

SPECTRAL REFLECTANCE OF SNC METEORITES: RELATIONSHIPS TO MARTIAN SURFACE COMPOSITION

L. A. McFadden, California Space Institute, U.C.S.D., La Jolla, CA 92093-0216

The spectral signatures of each of the Shergottite-Nakhlite-Chassignite (SNC) meteorite types measured to date are unique among extraterrestrial materials. Reflectance spectra of dark regions of Mars show evidence of basaltic composition (1). Analytic analysis of absorption band positions and widths in reflectance spectra of SNC meteorites will permit comparisons with spectra from ~600 km-sized regions for which high-quality, near-IR spectra are available (2). Multi-spectral mapping data from orbital spacecraft is expected to provide the necessary spectra to determine basaltic compositions of smaller regions on Mars provided fresh, unaltered basalts can be observed or the effects of martian weathering can be understood and removed from the spectra. With modeling of spectral weathering and mixing of SNC meteoritic assemblages it should be possible with Mars Observer data to test for the presence of SNC analogues on the martian surface.

Reflectance spectra (0.33-2.6 μm) of powdered samples of Shergotty, ALHA77005, Nakhla, and Chassigny presented here were measured with the laboratory spectrometer facilities at the University of Hawaii's Planetary Geosciences Division (3) between 1979-1981. Absorption band minima are plotted on the pyroxene band-band plot (4) in Figure 1. The spectral features of these meteorites are presented as a starting point for an anlaysis that will eventually lead to some conclusions regarding the similarity in composition between martian basalts and SNC basalts.

The spectral reflectance of the Shergotty meteorite (Figure 2) is dominated by the signature of clino-pyroxenes, the dominant modal phase in this meteorite (5). The other major mineralogical component, maskelynite, is not expected to produce a spectral signature for two reasons: Smith and Hervig (5) report Fe_2O_3 contents for maskelynite but no FeO. Its diagnostic spectral signature at 1.25 μm is controlled by Fe^{2+}, not Fe^{3+}, therefore no 1.25-μm band is expected if the microprobe measurements are correct. Additionally, the loss of crystal structure in maskelynite compared to plagioclase reduces the probability of a transition and the absorption band is weaker and broader. Whitlockite, ilmenite, pyrrhotite, chlorapatite, baddeleyite and tridymite, all minor phases in Shergotty, do not have spectral features in the wavelength region covered in this spectrum. Other minor phases, fayalite, chromite and kaersutite are probably not present in sufficient abundances to produce detectable spectral signatures, however, their diagnostic features should be looked for in a numerically analyzed spectrum for absorption bands. The position of the 1 and 2 μm pyroxene band minima on the band-band plot of Adams (4) indicates that the mean pyroxene composition falls in the augite field. The band minima determined from this spectrum are in agreement with those determined by Feierberg and Drake (6). The overall albedo of Shergotty is lower than that of other basaltic achondrites which may be due to the presence of minor opaques in Shergotty, or to increased absorption from shock effects (7). The other notable spectral features in this spectrum are weak absorptions at 0.65 μm and shorter wavelengths superimposed on the strong UV charge transfer absorption. These features may be due to Ti, Cr, or both in pyroxenes. This band may be unique to Shergotty, although there are narrower, weak bands in this spectral region in some spectra of diogenites (8).

The spectrum of ALHA77005, (Figure 3) which is related to Shergottites (9) has a 1-μm absorption band that is weaker and broader than this band in the spectrum of Shergotty, indicating the presence of olivine. The 2.0 μm band is centered at a shorter wavelength than that in the Shergotty spectrum indicating a pyroxene chemistry of lower iron and calcium than found in Shergotty. It is superimposed on a reddened continuum which is also characteristic of a significant olivine component. The lower albedo of ALHA77005 (0.11 at 0.56 μm) relative to Shergotty may be due to the presence of large xenocrysts of chromite and/or shock effects. The maximum reflectance in the visible at 0.75 μm is longward of the 0.625 μm feature commonly seen in olivine. When the reflectance maximum is longward of the 0.625-μm feature, the olivine has a negligible nickel content and its petrogenesis is consistent with a metal-silicate fractionation history (10).

Spectra of the three lithologies of the shergottite EETA79001 which have no measured spectral reflectance to date, are anticipated to be different from the spectra of Shergotty and ALHA77005 in terms of the position and strength of the absorption bands due to mafic silicates of

olivine and pyroxene compositions (11). The differences will be subtle but detectable with band analysis routines. If the olivine signature is detectable in EETA79001's spectrum, a reflectance maximum in the visible shortward of 0.625 μm would be anticipated due to the high Ni content of the olivine (10, 11).

Of the three nakhlites (Nakhla, Governador Valderas and Lafayette) only Nakhla has a measured reflectance spectrum (12). It was measured again with an earlier version of the spectrometer where only interference filters and a photomultiplier tube were used from 0.33-0.7 μm. Figure 4 shows a spectrum where the 1.0 μm band is very broad and has a band minimum beyond 1.0 μm indicating the presence of a high-calcium, high-iron clino-pyroxene and olivine. The reflectance increases dramatically with increasing wavelength, a characteristic of a significant crystalline olivine component. The 2.0 μm band minimum is at 2.35 μm and supports the interpretation of the presence of augitic pyroxene based on Adam's pyroxene calibration (4). As the three nakhlites have different mafic mineralogy and textures (13), their reflectance spectra are anticipated to be slightly different and should be measured in the future.

The spectrum of Chassigny (12) which was measured again with the above-described configuration (Figure 5) shows the spectral signature of olivine with a strong UV absorption indicating a low -Ni olivine composition (10), a composite 1.0-μm band consisting of 3 overlapping bands between 0.8 and 1.3 μm and a high near-IR reflectance. The apparent band between 1.85 and 2.05 μm may be due to water vapor in the laboratory during acquisition of the spectrum or to a small orthopyroxene component which has a similar signature when present in small amounts with olivine (3). Examination of the meteorite sample and careful repetition of the measurement must be made to determine which interpretation is correct.

Before the relationship between the basaltic composition of units on Mars and the SNC meteorites can be addressed, it is necessary to analyze the absorption band parameters of the SNC reflectance spectra and to acquire high resolution spectral data on smaller regions of the martian surface.

1) Singer, R.B. (1985) Proc. of COSPAR Mtg., Graz, Austria. 2) Singer, R.B. and Roush, T.L. (1985) B.A.A.S. 17, 737. 3) Singer, R.B. (1981) J.G.R. 86, 1967. 4) Adams, J.B. (1974) J.G.R., 79, 4829. 5) Duke, M.B. (1968) in Shock Metamorphism of Natural Materials, Mono Books, Baltimore, p.613; Smith, J.V. and Hervig, R.L. (1979) Meteoritics, 14, 121; Stolper, E.M. and McSween, H.Y. (1979) GCA 43, 1475. 6) Feierberg, M.J. and Drake, M.J. (1980) Science, 209, 805. 7) King, T.V.V. (1986) PH.D. Dissertation, U. Hawaii. 8) McFadden et al. (1982) Mem. Nat'l Polar Inst. spec. issue 25, 188. 9) e.g. McSween, H.Y. et al. (1979) Science, 204, 1201. 10) King, T.V.V. and Ridley, W.I. (1987) J.G.R., 92, no. B11, 11,457. (11) Steele, I.M. and Smith, J.V. (1982) J.G.R. 87 supp. A375; McSween, H.Y. and Jarosewich, E. (1983) G.C.A. 47, 1501. 12) Gaffey, M.J. (1976) J.G.R., 81, 905. 13) Berkeley, J.L. et al. (1980) Proc. Lunar & Planet. Sci. Conf. 11th, 1089.

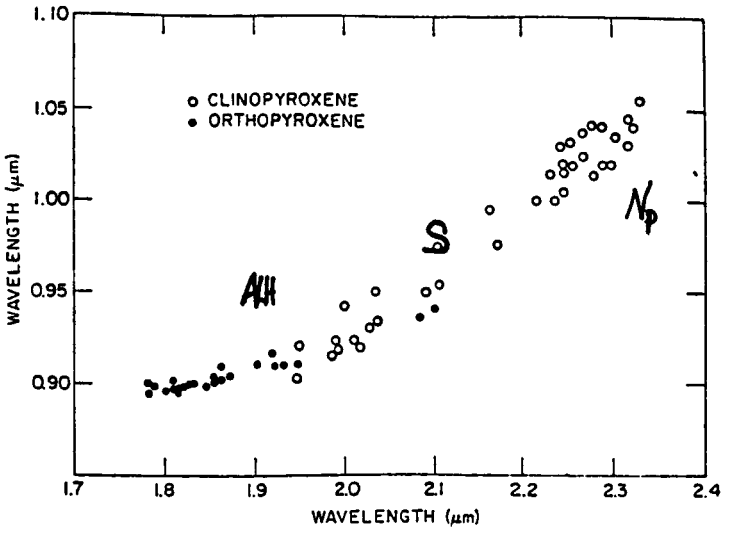

Fig. 1-Position of pyroxene absorption bands on Band-Band plot ref. 4. Shergotty (S), ALHA77005 (ALH) Nakhla pyroxene (Np)

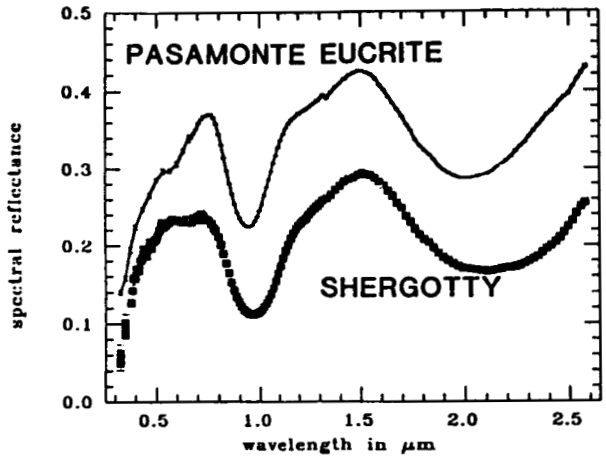

Figure 2 - Spectral reflectance of Shergotty and Pasamonte eucrite.

Figure 3 - Spectral reflectance of ALHA77005 plotted on 2X scale of figures 1,3 and 4.

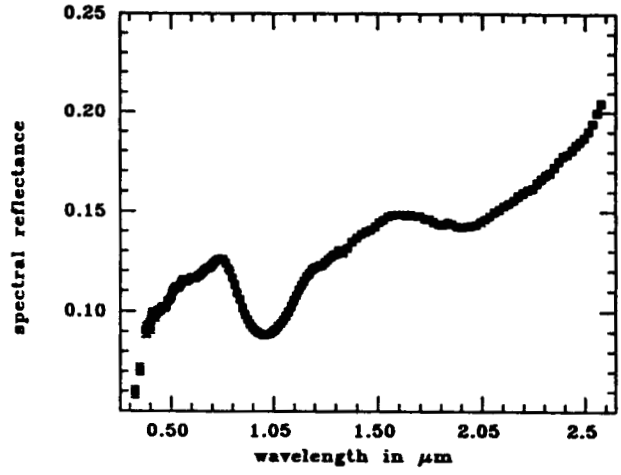

Figure 4 - Spectral reflectance of Nakhla meteorite.

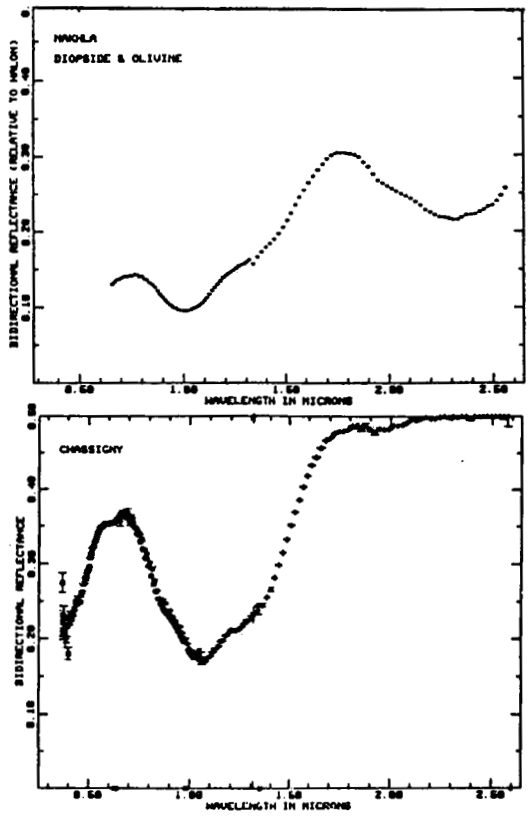

Figure 5 - Spectral reflectance of Chassigny meteorite.

MK 149394 N88-29684 30-91
38 154730 91

CONSTRAINTS ON THE ORIGIN OF FRACTURED TERRANE, NORTHERN MARTIAN PLAINS; George E. McGill, Department of Geology and Geography, University of Massachusetts, Amherst, MA 01003.

The terrane characterized by giant fracture systems that commonly define crudely polygonal patterns has received much attention because of its potential importance to such diverse problems as the amount and distribution of interstitial volatiles on Mars, the source of northern plains deposits, and the tectonic evolution of the northern plains. Several hypotheses have been proposed to explain the giant fracture systems, as reviewed by Pechmann (1); but, as originally proposed, most of these are mechanically unsound because of the orders-of-magnitude size differences between the martian features and suggested terrestrial analogues. However, if the nature of the surface upon which the fractured material was deposited is considered, the size problem can be overcome (2).

The crater age of fractured terrane material in Utopia Planitia falls within the range of ages for both major outflow channels and Elysium volcanism (2,3). Furthermore, the fracturing is temporally (and, by inference, causally) related to the deposition process, as indicated by superposition relationships with craters and with adjacent unfractured plains (2,4). These observations suggest that the fractured material was deposited as wet sediment or some type of volcanic. Either wet sediment or hot pyroclastics would possess properties compatible with the differential compaction plus shrinkage model proposed (2) to explain the giant fracture pattern (5). Nevertheless, determining which is most likely is extremely important to considerations of volatile content, and also important for our general understanding of the processes responsible for the deposits blanketing the northern third of Mars.

Lucchitta et al. (6) strongly advocate a sedimentary origin for the fractured material, an opinion that coincides with my own biases and, I suspect, the biases of most martian geologists who have given the matter serious thought. Even so, it is useful to consider the evidence relevant to the source of fractured material, because this evidence is somewhat equivocal.

Associated with the fractured terranes of both Utopia and Acidalia (2,7) are numerous small landforms resembling cinder cones, rows of pit craters aligned with grabens, and patches of material that may be remnants of pyroclastic flows. In the Utopia area, the cones are all external to the fractured terrane, and the other presumably volcanic features appear to be younger than the fracturing event of interest (2). In the Acidalia area, cones occur on fractured terrane (7), and at least some of them are unequivocally younger than the fracturing because they are superposed on the ejecta of craters that are superposed on the giant fractures. These volcanic features also seem pathetically small to be responsible for the areally extensive fractured terranes. Nevertheless, they are the only landforms associated with the fractured terranes of Acidalia and Utopia/Elysium for which an origin can be readily inferred. In the absence of any morphological characteristics of the deposits themselves supporting a sedimentary origin, one might argue that these small volcanic landforms represent the products of late-stage activity in a region with a long volcanic history. In fact, those of us favoring a sedimentary origin for the fractured terranes of Acidalia and Utopia/Elysium need to explain why there should be such an abundance of small volcanic landforms on and near these terranes. My tentative hypothesis is that this abundance is only apparent—an artifact of the great concentration of high-resolution Viking images in the Acidalia and Utopia areas (the small volcanic landforms commonly are not resolvable on typical mapping frames).

A long-standing problem has been the fate of the large volumes of sediment presumably transported by the large runoff and outflow channels on Mars, and the extensive fractured terranes provide a tempting sink because they are conveniently located

—Acidalia near the large channels debouching onto Chryse Planitia, and Utopia/Elysium near the channels draining the Elysium Mons area—and because they occur in topographic lows (6). Ideally, there should be a rough correspondence between the sizes of the channels and the volume of material deposited, and there should be some geomorphic evidence to support transport of sediment from channels to sinks. It is possible to make some headway with these constraints in the Utopia/Elysium area.

The channels draining the Elysium Mons area to the northwest gradually lose their definition in the disordered plains (8) that form an indentation into the fractured terrane (Fig. 3 in 6). But these channels appear to be younger than the fractured terrane (9), a conclusion supported by crater counts (Table 1) showing that disordered plains are the same age as the smooth plains clearly superposed on the fractured terrane of Utopia. On the other hand, fracturing and major erosion of the northern flank of Elysium Mons can be constrained by crater counts (10) to have occurred within a time span that includes the crater age of the fractured terrane. There is an excess of large craters on the disordered plains (Fig.1) suggesting that beneath the channels and volcanic (?) materials of the disordered plains there is a relict surface at least as old as the fractured terrane of Utopia. This supports speculations (6,10) that the present channels draining northwestward from Elysium Mons have, along with the widespread smooth plains, covered or obliterated evidence for the transport of large volumes of sediment from Elysium Mons to Utopia at an earlier date.

If the boundaries of fractured terrane in Utopia/Elysium are plotted on an orthographic projection centered near Utopia, the distribution appears to be roughly circular with a large indentation where disordered plains occur (Fig. 1 in 11). Assuming that the disordered plains are superposed on fractured terrane, then this roughly circular area contains (or contained) about 3.5 million square km of fractured terrane. The distribution of partially buried craters and ring fractures (Fig. 5 in 2) provides a clue to the thickness of this deposit. The smallest ring fractures are about 8 km in diameter, suggesting that the deposit is thick enough to mask the structural effects of all smaller craters. The complete burial of all craters less than 8 km in diameter implies that the deposit has an intercrater thickness of at least 300 m. Furthermore, there are some well defined, complete ring fractures up to 30 km in diameter, suggesting the burial of even larger craters and thus a deposit thickness greater than 300 m (because the larger craters may have been degraded before burial, it is not possible to be more precise than this). The absence of ring fractures in the northern part of the Utopia fractured terrane is probably due to the lack of complete crater rims of sufficient diameter to affect the surface of the deposit; consequently, there is no longer any control for estimating thickness. Assuming that there is no dramatic change in thickness where the control ceases, an estimate of 500 m for the average deposit thickness seems reasonable, and preliminary analysis suggests that this thickness is adequate to account for the fractures by bending related to differential compaction (5). This thickness leads to an estimate of 1.75 million cubic km of material within the circular area of fractured terrane in Utopia/Elysium. I believe that this is a very conservative estimate, because smooth plains are clearly superposed on fractured terrane peripheral to the circular area of exposure, suggesting a wider distribution of fractured terrane material in the subsurface. This is a lot of material, and it is not at all clear that the Elysium Mons area is large enough to provide it.

TABLE 1

Surface	Total n	n for D>5	N(5)
Smooth plains superposed on fractured terrane	378	24	90
Disordered plains	253	58	90
Fractured terrane of Utopia	118	35	115

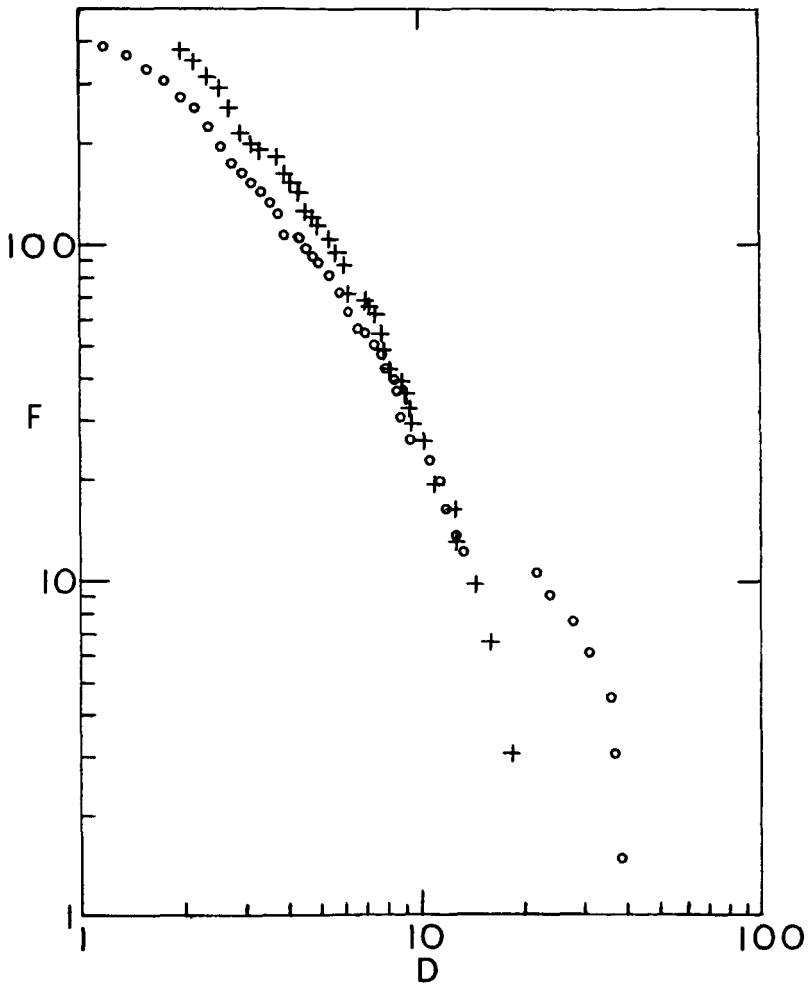

Fig. 1: Cumulative diameter/frequency plot for disordered plains (circles, n=253) and Utopia fractured terrane (crosses, n=118). F=cumulative frequency/million square km; D=crater diameter in km. Note excess large craters on disordered plains and gap between D=13 km and D=22 km.

REFERENCES CITED

(1) Pechmann, J.C., Icarus, 42, 185-210, 1980.
(2) McGill, G.E., Geophys. Res. Letts., 13, 705-708, 1986.
(3) Neukum, G., and Hiller, K., J. Geophys. Res., 86, 3097-3121, 1981.
(4) Helfenstein, P., and Mouginis-Mark, P.J., Lunar Planet. Sci. XI, 429-431, 1980.
(5) Hills, L.S., NASA Tech. Mem. 89810, 495-496, 1987.
(6) Lucchitta, B.K., Ferguson, H.M., and Summers, C., J. Geophys. Res., 91, E166-E174, 1986.
(7) Borrello, M.C., Lunar Planet. Sci. XVIII, 107-108, 1987.
(8) Carr, M.H., The Surface of Mars, 82-83, 1981.
(9) Tanaka, K.L., J. Geophys. Res., 91, E139-E158, 1986.
(10) McGill, G.E., Lunar Planet. Sci. XVIII, 620-621, 1987.
(11) McGill, G.E., Lunar Planet. Sci. XVIII, 622-623, 1987.

94

N88-29685

VIKING LANDERS AND REMOTE SENSING -- H.J. Moore, U.S. Geol. Survey, Menlo Park, CA, 94025; Jakosky, B.M., LASP, Univ. of Colorado, Boulder, CO, 80309; P.R. Christensen, Dept. of Geology, Arizona State Univ. Tempe, AZ, 85287.

Thermal and radar remote sensing signatures of the materials in the lander sample fields can be crudely estimated from evaluations of their physical-mechanical properties, laboratory data on thermal conductivities and dielectric constants, and theory. The estimated thermal intertias and dielectric constants of some of the materials in the sample fields are close to modal values estimated from orbital and Earth-based observations. This suggests that the mechanical properties of the surface materials of much of Mars will not be significantly different that those of the landing sites.

Three soillike materials, and rocks, occur in the sample fields: (1) drift, (2) crusty to cloddy, and (3) blocky [1]. Bulk densities near 1100 kg/m^3 were inferred for disturbed drift material [2]; those of porous clods of blocky material ranged between 1100 and 1900 kg/m^3 [3]. Angles of internal friction of crusty to cloddy and blocky materials (28-39°) are compatible with moderately dense soils (~1400 kg/m^3), while the angle of internal friction of drift material (~20°) is compatible with a loose soil (~1000 kg/m^3). Mineral grains in drift and crusty to cloddy materials are small (0.2 to 2 μm) [4,5]. All materials have cohesions and form fragments, clods, crusts, and weak lumps. Cohesions of crusty to cloddy and drift materials are several kPa and less, while those of blocky material are a few to as much as 10 kPa [1,3]. Cohesions of the rocks are probably of the order of MPas. Best estimates of bulk densities, cohesions, angles of internal friction, and the fractions of samplefield areas covered are listed in Table 1.

Thermal inertias, Is (10^{-3} cgs units), of materials in the sample fields can be estimated by assuming that the Is of the sample fields are the same as those determined from orbit [6] and two or three component models [7]. From orbit, I is 8±1.5 for Lander 2 [6]. A two-component model of rocks (I=40) and crusty to cloddy material (I=6.3) will yield an I of 8 for the entire sample field. From orbit, I is 9±0.5 for Lander 1 [7]. Lander 1 data requires, at least, a three-component model. Drift material is a loose porous powder with a fine grain size. The Is of loose porous powders in 7-9 mbar atmospheres should be near 2-4 [8,9,10] or lower [11]. Tentatively, I=3 is assigned to drift material. A three component model for Lander 1 would have drift material (I=3), rocks (I=40), and blocky material (I=9). Is for crusty to cloddy and blocky materials are larger than those expected for their bulk densities [10] so that cementation may contribute to their large Is [12].

Radar reflectivities may be interpreted as a dielectric constants [13], Es, which may, in turn, be interpreted as a bulk densities [14]. Two reflectivities reported for the area of the Lander 1 site from Earth-based radio echoes at 12.6-cm wavelength are 0.07 [13] and 0.13 [15], which imply Es of 2.9 and 4.5, respectively. An E of 3.3±0.7 was estimated for the Lander 1 site at 78.7-cm wavelength using the Lander-Orbiter relay links [16]. If the surface materials at the Lander 1 site behave like dry powders made from rocks with zero porosity, a bulk density of 2600 kg/m^3 and an E of 8 [14], the Rayleigh mixing formula gives bulk densities of 1400, 2000, 1600±300 kg/m^3 for the above values of Es. The predicted Es for the soillike materials are: 2.4 (drift), 3.3 (blocky), and 2.8 (crusty to cloddy). There are, of course,

other models. For examples, Es are near 2-2.5 for sandy to clayey soils with unspecified bulk densities at 3, 10, and 100-cm wavelengths [17]. Similar dry soils with bulk densities near 1300 kg/m^3 have Es of 2.5 at 1.15 and 3.8-cm wavelengths and 3.0 at 7.5 and 60-cm wavelengths [18].

Although the bulk Is and Es of the sites do not appear to be representative of Mars as viewed remotely [19], material components in the sample fields may be good analogs for the materials of much of Mars. As inferred here, the mechanical properties of drift (with I=3,E=2.4) and crusty to cloddy (with I=6.3,E=2.8) materials are probably not significantly different from those of the materials represented by the remote sensing modes of I=2, E=2 and I=5.5, E=2.9, respectively [19,20]. The I=9 of blocky material is large, but the E=3.3 is quite plausible.

There are uncertainties because the interpretations are model dependent. For example, moderately dense cohesionless sand (~300 μm) cannot be distinguished from moderately dense compacted fine soil on the basis of I and E alone. Is and Es depend not only on bulk densities (porosities), but also the chemical-mineralogical properties of the materials. Sensible interpretations require as much additional evidence as possible such as albedos, colors [21], and, especially, high resolution images.

Table 1. Estimated mechanical properties and remote sensing signatures of the surface materials in the sample fields of the Viking landers.

	Bulk density (kg/m^3)	Cohesion (kPa)	Angle of internal friction (degrees)	Fraction of area covered	Thermal inertia (10^{-3}cgs units)	Dielectric Constant
			Lander 1			
Drift Material	1,200±100	½ - 2	14-21	0.14	3	2.4
Blocky Material	1,600±400	2 - 9	27-32	0.78	9	3.3
Rocks > 3.5 cm	2,600 ±	1,500-50,000	40-60	0.08	40	8.0
Sample Field	1,620 ±	—	--	1.00	9	3.4
Remote Sensing	1,600 (1,290-1,845) 1,400 2,000	--	--	--	9±0.5	3.3±0.7 2.9 4.5
			Lander 2			
Crusty to Cloddy Material	1,400±200	½ - 5	28-39	0.85	6.3	2.8
Rocks	2,600 ±	1,000-50,000	40-60	0.15	40	d
Sample Field	1,580 ±	--	--	1.0	8	3.3
Remote Sensing	?	—	--	--	8±1.5	2.8-12.5

Reference List

[1] Moore, H. J. and others, 1982, A summary of Viking sample-trench analyses for angles of internal friction and cohesions: J. Geophys. Res., v. 87, p. 10,043-10,050.
[2] Clark, B. C. and others, 1977, The Viking X-ray Fluorescence Experiment: Analytical methods and early results: J. Geophys. Res., v. 82, p. 4577-4594.
[3] Moore, H. J. and others, 1987, Physical properties of the surface materials of the Viking landing sites on Mars: U.S. Geol. Survey Prof. Paper 1389, in press.
[4] Ballou, E. V. and others, 1978, Chemical interpretation of Viking Lander 1 life detection experiment: Nature, v. 271, p. 644-645.
[5] Oyama, V. I. and Berdahl, B. J., 1977, The Viking Gas Exchange Experiment results from Chryse and Utopia surface samples: J. Geophys. Res., v. 82, p. 4669-4676.
[6] Kieffer, H. H., 1976, Soil and surface temperatures at the Viking landing sites: Science, v. 194, p. 1344-1346.
[7] Kieffer, H. H. and others, 1977, Thermal and albedo mapping of Mars during the Viking primary mission: J. Geophys. Res., v. 82, no. 28, p. 4249-4291.
[8] Wechsler, A. E., and Glaser, P. E., 1965, Pressure effects on postulated lunar materials: Icarus, v. 4, p. 335-352.
[9] Fountain, J. A. and West, E. A., 1970, Thermal conductivity of particulate basalt as a function of density in simulated lunar and martian environments: Jour. Geophys. Res., v. 75, p. 4063-4069.
[10] Horai, Ki-iti, 1979, Loose and compacted soils: Two basic units composing the martian surface?: Lunar and Planet. Science X, p. 564-566.
[11] Jakosky, B. M., 1986, On the thermal properties of martian fines, Icarus, v. 66, p. 117-124.
[12] Jakosky, B. M., and Christensen, P. R., 1986, Global duricrust on Mars: Analysis of remote-sensing data: J. Geophys. Res., v. 91, p. 3547-3559.
[13] Tyler, G. L. and others, 1976, Radar characteristics of Viking 1 landing sites: Science, v. 193, p. 812-815.
[14] Campbell, M. J., and Ulrichs, Juris, 1969, Electrical properties of rocks and their significance for lunar radar observations: J. Geophys. Res., v. 74, p. 5867-5881.
[15] Harmon, J. K., and Ostro, S. J., 1985, Mars: Dual-polarization radar observations with extended coverage: Icarus, v. 62, p. 110-128.
[16] Tang, C. H. and others, 1977, Bistatic radar measurements of electical properties of the martian surface:Jour. Geophys. Res., v. 82, p. 4305-4315.
[17] Von Hippel, A. R., 1954, V. tables of dielectric materials, in Von Hippel, A. R., ed., Dielectric materials and applications, New York, John Wiley and Sons, Inc., 430 p.
[18] Hoekstra, P., and Delaney, A. 1974, Dielectric properties of soils at UHF and microwave frequencies: J. Geophys. Res., v. 79, p. 1699-1708.
[19] Jakosky, B. M., and Christensen, P. R., 1986, Are the Viking landing sites representative of the surface of Mars?: Icarus, v. 66, p. 125-133.
[20] Christensen, P. R., 1986, The spatial distribution of rocks on Mars: Icarus, v. 68, p. 217-238.
[21] Smith, M. O. and others, 1987, Viking Orbiter multispectral images linked to lander images and laboratory analogs: Lunar and Planet. Sci. XVIII, p. 934-935.

Hi 182556
LE 122961 N88-29686

VOLCANO EVOLUTION ON MARS; Pete Mouginis-Mark and Lionel Wilson*; Planetary Geosciences Divn., Hawaii Institute of Geophysics, Univ. Hawaii, Honolulu, HI 96822. *Also at Dept. Environmental Science, Lancaster Univ., Lancaster, Lancs., LA1 4YQ England.

INTRODUCTION: The diversity of volcanic activity on Mars throughout geologic time has been one of the major factors that has controlled the spatial distribution of surface mineralogies. The traditional view of martian volcanism is one in which effusive activity has dominated the entire preserved geologic history of the planet, with the minor exception of phreatomagmatic activity and associated volcano ground-ice interactions (cf., refs 1-3). However, two lines of evidence have made us reconsider this view, and have led us to study the possible role of explosive volcanism on Mars. First, detailed analysis of high resolution Viking Orbiter images has provided good evidence for explosive activity on Hecates Tholus (4) and Alba Patera (5, 6). Secondly, the problems believed to exist in associating explosive volcanism with silicic magmas on Mars, and the consequent unusual magmatic evolutionary trend for martian volcanoes from silica-rich to silica-poor (7), may now be circumvented by the consideration of basatic plinian activity similar in kind to terrestrial eruptions such as the 1886 Tarawera eruption (6, 8). Here we briefly review the morphologic evidence for an early phase of explosive activity on Mars and present a model for the emplacement of ash-flow deposits on martian volcanoes. The volcanoes Alba Patera and Olympus Mons are considered in this context, along with some of the older martian tholi and paterae.

PREVIOUS OBSERVATIONS: Pyroclastic (explosive) volcanism was first proposed for Mars from the analysis of low resolution (~1 km) Mariner 9 images (9, 10). These studies identified small cone-like hills that were believed to be cinder cones. A more detailed analysis of the volcanoes Hecates, Ceraunius, and Uranius Tholi and Uranius Patera (11) suggested that the channelized flanks of these volcanoes were created by volcanic density flows similar to terrestrial nuee ardentes (the melting of permafrost supplying the water required in base surge generation). Following detailed mapping using Viking Orbiter images (4) an alternative explanation was proposed for some of these channels, wherein the unconsolidated flanks of Hecates Tholus, formed from numerous air-fall deposits, had been carved by surface water released by sapping from the volcano's flanks. Recently, this arguement has also been used to explain the distribution of digitate channel networks on the flanks of Alba Patera (5, 6). Other, more enigmatic deposits in Amazonis have also been proposed to be ignimbrites (12). The key aspect of most of these recent investigations has been the attempt to associate volcanoes with channelized flanks to explosive activity; this attempt has of necessity been subjective, since it is difficult to recognize pyroclastic materials from orbit even for the Earth (7). For Hecates Tholus and Alba Patera, the connection between channelized flanks and pyroclastic materials depends on the assumption that the surface materials are more easily eroded than lava flows (since volcanoes such as Arsia and Ascraeus Montes display ample evidence for the eruption of lava flows, but lack the same kind of channelized flanks; refs. 4, 13), and that the most plausible alternative form of volcanic deposit would be pyroclastic materials created by explosive eruptions (either phreatomagmatic or initiated by juvenile volatiles).

VOLCANO TOPOGRAPHY: Hecates Tholus, Tyrrhena Patera and Alba Patera are all low-relief shields when compared to Tharsis Montes (5, 14, 15). Maximum elevations for the summits of these volcanoes are ~6 km for Hecates, 750 - 1,000 m for Tyrrhena, and ~ 2 km for Alba, while the Tharsis Montes may each possess 25 km of relief (cf. 16). These low elevations may not be coincidental, nor may the fact that they are all ~500 to 600 km in diameter (and so is the volcano Hadriaca Patera). For the case of Alba Patera, the constraint on maximum width of the volcano may be the run-out distance of pyroclastic flows (5), and such a model may also hold for these other low-relief martian volcanoes. Previous explanations for the low topography of these

shields were that they were made of very fluid lavas (10) but a volatile-rich martian mantle could also produce abundant pyroclastic volcanic materials capable of forming wide-spread ash-flow sheets (17). A new five-stage model for the evolution of Alba Patera (Fig. 1) has recently been proposed (5), which would account for the low-relief of the volcano by the emplacement of pyroclastic flows as the basement materials, their subsequent partial burial by younger lava flows, and the formation of the channels by melt water. It is not clear if this evolutionary trend is unique to Alba Patera, or whether it is simply easier to recognize at this location due to preservation of both explosive and effusive eruptive materials on the surface.

OLYMPUS MONS: The basal escarpment that surrounds Olympus Mons has as much as 9 - 13 km of relief (18, 19). Several origins for this feature have been proposed, including erosion of ash flow tuffs (20), which if correct would suggest that explosive volcanism characterized the early eruptive history of Olympus Mons. We are reconsidering this idea because if correct it would imply a diverse eruptive history for the volcano. If the materials underlying the Olympus Mons edifice are indeed pyroclastic units, then the subsidence associated with terracing on the upper flanks (21, 22) may have been associated with compaction of the ash layers due to the overlying denser lava flows. Alternatively, the erosion may have taken place within the pre-existing volcano substrate, rather than within materials erupted from the Olympus Mons vent (23). Gravity sliding and spreading of materials containing ground ice at low strain rates has also been proposed to account for the general morphology of the aureoles and the Olympus Mons basal escarpment (18, 24). Olympus Mons is unique in the extent of large-scale gravity spreading and basal scarps: perhaps such features, if they ever existed, have been buried by lava flows on other volcanoes, or perhaps their eruptive histories did not permit the development of such features.

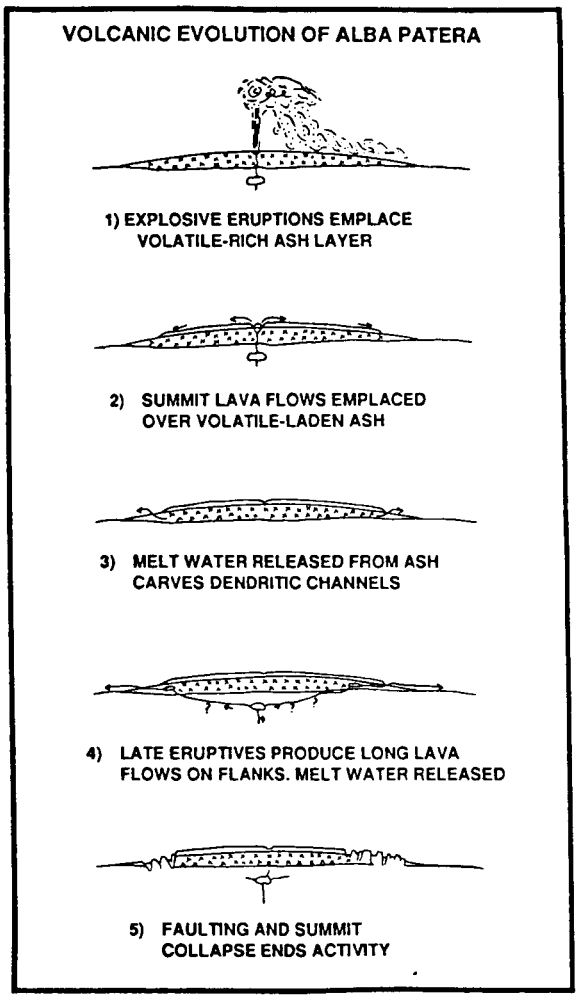

Fig. 1: Skematic 5-stage model for the evolution of Alba Patera proposed by Mouginis-Mark *et al.* (ref. 5).

CONCLUSIONS: Volcano morphology suggests that an evolution took place in the type of flank deposits that were produced at different times in martian history. Early in the preserved geologic record, explosive eruptions dominated, with the production of ash cones such as Hadriaca and Tyrrhena Paterae. These volcanoes probably experienced ignimbrite-forming eruptions of relatively volatile-rich magmas that produced low-aspect shields that were subsequently easily eroded by sapping of ground water. Ignimbrites do not necessarily imply silicic magmas, and an objective of the MEVTV Program should be to search for possible compositional variations between the flank deposits of these volcanoes and the lava-producing shields. Later in martian history, the more commonly cited effusive activity predominated, producing the lava flows observed on the Tharsis Montes, the Syrtis Major volcanoes, and Elysium Mons. Certain volcanoes, particularly Alba Patera, but also possibly

Olympus Mons, display morphologic evidence for the transition from an early explosive phase to later effusive eruptions. The implications of this evolutionary trend are two-fold: first magmatic evolution took place, from volatile-rich to volatile-poor, at a time when parts of the martian geologic record could be preserved until the present; and second this magmatic evolution would have dramatically affected climatic evolution on Mars, due to the decrease in magmatic gases which were liberated late in the planet's history (6).

SUGGESTIONS FOR FUTURE STUDIES: At this early stage in the MEVTV Program, there are obviously many unresolved problems pertaining to magmatic diversity and the morphologic interpretation of martian volcanoes. However, we offer some suggestions for research that can be carried out (with the existing data sets) that would complement the remote sensing studies that will be used to characterise the diversity of rock units on Mars:

1) Is there any latitudinal or elevation dependance to the ash cones that could be used to infer variations in near-surface volatiles (or juvenile volatiles) within the erupted materials?

2) It is possible that the base of Olympus Mons is made of pyroclastic material. Of interest is the question of whether we would see similar deposits on other martian shields had they not been buried by many large lava flows. It may not, for instance, be coincidental that Olympus Mons and volcanoes with channelized flanks are all ~500 - 600 km in diameter. Perhaps this size marks the maximum radial distance that early (basement-forming) pyroclastic flows could travel on Mars? Use of Earth-based radar topography or stereogrammetry may show subtle breaks of slope at the appropriate radial distances from the summits.

3) Is there any evidence for multiple episodes of explosive eruptions and channel formation on volcanoes such as Hadriaca and Tyrrhena Paterae, or was there only one period of explosive activity at each volcano?

4) How well can we determine the relative ages of these martian volcanoes? There is a need to refine the current age estimates based on crater frequencies (25) in order to see if some martian volcanoes experienced a transition in eruptive style before other volcanoes.

5) What role (if any) should we ascribe to volcano/ground ice interactions in controlling the large-scale morphology of martian volcanoes?

REFERENCES: 1) Greeley, R. and Spudis, P. (1981). Revs. Geophys. Space Phys., **19**, p. 13-41. 2) Mouginis-Mark, P.J. (1985). Icarus, **64**, p. 265-284. 3) Squyres *et al.* (1987) Icarus, **70**, p. 385-408. 4) Mouginis-Mark, P.J. *et al.* (1982). J. Geophys. Res., **87**, p. 9890-9904. 5) Mouginis-Mark, P.J., Wilson, L. and Zimbelman, J.R. (1987). Polygenic eruptions on Alba Patera, Mars: Evidence of channel erosion on pyroclastic flows. Submitted to Bull. Volcanol. 6) Wilson, L. and Mouginis-Mark, P.J. (1987). Volcanic input to the atmosphere from Alba Patera on Mars. Nature, in press. 7) Francis, P. and Wood, C.A. (1982). J. Geophys. Res., **87**, p. 9881-9889. 8) Walker, G.P.L. *et al.* (1984). J. Volcanol. Geotherm. Res., **21**, p. 61-78. 9) West, M. (1974). Icarus, **21**, p. 1-11. 10) Peterson, J.E. (1978). Proc. Lunar Planet. Sci. Conf. 9th, p. 3411-3432. 11) Reimers, C.E. and Komar, P.D. (1979). Icarus, **39**, p. 88-110. 12) Scott, D.H. and Tanaka, K.L. (1982). J. Geophys. Res., **87**, p. 1179-1190. 13) Mouginis-Mark, P.J. (1981). Proc. Lunar Planet. Sci. Conf., **12B**, p. 1431-1447. 14) Hord, C.W. *et al.* (1974). Pressure-altitude measurements on Mars - An atlas of Mars local topography. Lab. for Atmos. and Space Phys., Univ. Colorado, Boulder. 15) Wu, S.S.C. *et al.* (1986). Rpts. Plan. Geol. Geophys. Prog. 1985, **NASA TM-88383**, p. 614-617. 16) Carr, M.H. (1981). The surface of Mars. Yale University Press, 232 pp. 17) McGetchin, T.R. and Smyth, J.R. (1978). Icarus, **34**, p. 512-536. 18) Tanaka, K.L. (1985). Icarus, **62**, p. 191-206. 19) Wu, S.S.C. *et al.* (1984). Nature, **309**, p. 432-435. 20) King, J.S., and Riehle, J.R. (1974). Icarus, **23**, p. 300-317. 21) Hodges, C.A. and Moore, H.J. (1979). J. Geophys. Res., **84**, p. 8061-8074. 22) Lopes, R.M.C. *et al.* (1980). The Moon and Planets, **22**, p. 221-234. 23) Head, J.W. *et al.* (1976). Nature, **263**, p. 667-668. 24) Francis, P. and Wadge, G. (1983). J. Geophys. Res., **88**, p. 8333-8344. 25) Neukum, G. and Hiller, K. (1981). J. Geophys. Res., **86**, 3097-3121.

N88-29687

ORIGIN OF NORTHERN LOWLAND PLAINS: CONSTRAINTS FROM BOUNDARY MORPHOLOGY; Timothy J. Parker and R. Stephen Saunders, Jet Propulsion Laboratory, California Institute of Technology, Pasadena, CA

The origin of the surface units of the northern lowland plains of Mars, about one third of the planet's surface, remains unclear after 20 years of analysis of spacecraft data. Hypotheses that have been put forth to explain the morphologies and likely processes include: (I) Volcanic plains emplacement (1,2,3,4); (II) eolian blanketing (5). (III) emplacement of an ice-rich mantle (either eolian or fluvially derived) (1,6,7,8); and (IV) sediment deposition during periods of standing water (9,10,11,12,13).

The chief problem with constraining models of plains formation is that characterizing plains surface-forming processes is dependent upon the identification of distinctive landforms within the plains. Even with specific landforms, the processes inferred by different investigators can differ markedly. The most commonly cited examples of distinctive morphologies found within the northern lowlands include: wrinkle ridges; small domes; giant polygons; and curvilinear ridges and ground undulations.

Wrinkle ridges are common on many northern plains surfaces, particularly those at low latitudes (1). Because wrinkle ridges are common on the lunar mare volcanic plains, they have been taken to indicate volcanic material on Mars as well. Plescia and Golombek (14), however, were able to demonstrate, with convincing terrestrial analogs, that wrinkle ridge formation may be independent of surface composition.

Terrestrial analogs to small domes include volcanic cones and psuedocraters (2,3) and pingos (15). Both hypotheses are based on resonable morphological comparisons and the possibility, at least, of an association with other features of similar origin.

Giant polygons are common features in the northern lowland plains, being most concentrated in the central Acidalia and Utopia regions (9). They have been interpreted as giant dessication or compaction features in frozen outflow channel sediments (8,9) and as tensional fracture patterns formed by regional up-warping of the surface (16) or cooling of a lava plains surface (1).

Curvilinear ridges and ground undulations, most common within a few tens of kilometers of the lowland/upland boundary, have been interpreted by most investigators as primary or secondary sedimentary structures. Rossbacher (17) compared both types of morphology to terrestrial ground-ice features. Lucchitta et al., (9) compared curvilinear ridges to compressional and flow ridges in Antarctic coastal ice sheets. Parker et al., (10,11) compared the ridges to terrestrial lacustrine or shallow marine coastal spits and barriers. In the model of Lucchitta et al., the northern lowland plains materials would be comprised of outflow channel sediments deposited in a partially or completely frozen northern hemisphere ocean, whereas that of Parker et al. suggests a predominantly liquid water environment in which wave-generated currents are chiefly responsible for the development of the curvilinear ridges.

To further constrain the processes involved in the development of the northern plains, we are conducting a careful analysis of boundary morphology. Superposition relationships, erosional escarpments, crispness of boundary detail, and evidence of flow of plains material over adjacent terrain are characteristics of plains boundary morphology that should prove useful for inferring genesis. Plains units, whether volcanic or sedimentary in origin, are likely to be very thin at the margins, so boundary detail may not be obvious at typical Viking Orbiter image scales. Therefore, we have concentrated our efforts where high resolution (~50m/pixel or better) images are available at or just plainward of the lowland/upland boundary. Two areas that seem to typify plains boundary morphology are the southwest Cydonia Mensae - Acidalia Planitia region and the west Deuteronilus Mensae region. Several important aspects can be identified in these areas:

(a) In both regions plains units have sharp, crisply defined boundaries with adjacent plains units and elevated terrain (e.g., knobs, massif outliers). They are typically arcuate to sinusoidal with a distinct lack of small-scale irregularities.

(b) Plains boundaries are often parallel to the general trend of the lowland/upland boundary in the regional sense and are locally deflected around clusters of knobby terrain and several kilometers into fret

canyon reentrants in what appears to be a topographically conformal fashion (10,12).

(c) Superposition of surrounding terrain by plains units can be described as relatively simple or complex. In the simplest case, the plains material appears to onlap the surrounding elevated terrain or adjacent plains surface without exhibiting any obvious effect on the older surface beyond the contact. In the more complex examples, the boundary may exhibit both negative and positive relief relative to older terrain (11). In the more extreme examples of the former, highland remnants are surrounded by younger, low-lying plains materials, requiring that the uplands be eroded extensively - as much as several hundred kilometers southward - either prior to or contemporaneously with plains emplacement. Examples of boundaries exhibiting both positive and negative relief relative to adjacent terrain in southwest Cydonia Mensae are much lower in topographic relief, probably only a few meters at most.

The four processes for emplacing surface materials outlined in the first paragraph can be considered in light of the boundary morphology:

(I) (a) Volcanic plains emplacement could easily produce a sharp contact with adjacent terrain. Individual flow fronts have very irregular outlines, however. A smooth, sinuous boundary would probably require very low viscosities and a fairly smooth extant terrain surface - still not an impossible condition (18).

(b) Topographically conformal boundaries occur in the lunar mare and would be expected of volcanic plains on Mars.

(c) Erosion of adjacent terrain by lava, producing a smooth, arcuate escarpment, is unlikely. Similar morphology is not found at the margins of the lunar mare. In fretted terrains, the relief between uplands and lowlands is so great that an additional process of erosion is required prior to plains emplacement.

(II) Eolian blankets, most likely loess, would probably be the least likely to produce the observed boundary morphology.

(a&c) Loess blankets would likely thin gradually at the margins, thus making separation from adjacent material dependent mainly on available image resolution (19).

(b) Eolian deposits would not be confined to lower elevations as would low-viscosity lavas or water (either frozen or liquid), so would be unlikely to produce a topographically conformal boundary.

(III&IV) Fluvial emplacement of an ice-rich mantle (7,8) might produce most of the above characteristics if it remained fluid until erosional escarpments had been carved. Very high escarpments in fretted terrains, would require an additional event(s), however. Air-fall deposition of ice-rich sediment (6) might expectedly produce boundary morphology similar to eolian deposits, at least prior to ice removal.

Sediment deposition in a northern plains sea or ocean could produce the observed boundary morphology. Large scale erosional escarpments would be more easily produced in a dominantly liquid than in a frozen ocean environment, however. Freezing-through of a large body of water might expectedly carve drumlin-like forms upon expansion of the ice. Such morphology is decidely absent along the lowland/upland boundary. Possible periglacial forms become much more common farther plainward of the lowland/upland boundary above 30° latitude, which might indicate later freezing of a sea or ocean reduced in area by evaporation and loss to groundwater. Such a scenario requires a warm epoch relatively late in the planet's history, however.

REFERENCES:

(1) Carr, M. H., 1981, The Surface of Mars: Yale University Press, New Haven and London, 232 p.
(2) Frey, H., Lowry, B. L., and Chase, S. A., 1979, Pseudocraters on Mars: Journ. Geophys. Res. Vol. 84, p. 8075-8086.

(3) Frey, H., and Jarosewich, M., 1982, Journ. Geophys. Res., Vol. 87, No. B 12, p. 9867-9879.
(4) Wise, D. U., Golombek, M. P., and McGill, G. E., Journ. Geophys. Res., Vol. 84, p. 7934-7939.
(5) Soderblom, L. A., Kriedler, T. J., and Masursky, H., 1973, Journ. Geophys. Res., Vol. 78, p. 4117-4122.
(6) Grizzaffi, P. and Schultz, P. H., 1987, Icarus, In press, 58 p.
(7) Jons, H.-P., 1985, Lunar and Planet. Sci. - 16, Lunar and Planet. Inst., Houston, p. 414-415.
(8) McGill, G. E., 1985, Lunar and Planet. Sci. - 16, Lunar and Planet. Inst., Houston, p. 534-535.
(9) Lucchitta, B. K., Ferguson, H. M., and Summers, C., 1986, Journ. Geophys. Res., Vol. 91, p. E166-E174.
(10) Parker, T. J., Schneeberger, D. M., Pieri, D. C., and Saunders, R. S., 1986, In Symposium on Mars: Evolution of its Climate and Atmosphere, L.P.I. Tech. Rept. 87-01, Lunar and Planetary Institute, p. 96-98.
(11) Parker, T. J., Schneeberger, D. M., Pieri, D. C., and Saunders, R. S., 1987, Rept. Planet. Geol. Prog. - 1986, NASA Tech. Memo. 89810, p. 502-504.
(12) Parker, T. J., Schneeberger, D. M., Pieri, D. C., and Saunders, R. S., 1987, Rept. Planet. Geol. Prog. - 1986, NASA Tech. Memo. 89810, p. 319-320.
(13) Parker, T. J., Schneeberger, D. M., Pieri, D. C., and Saunders, R. S., 1987, Rept. Planet. Geol. Prog. - 1986, NASA Tech. Memo. 89810, p. 321-323.
(14) Plescia, J. B., and Golombek, M., 1986, Geol. Soc. Am. Bull., Vol. 97, p. 1289-1299.
(15) Lucchitta, B. K., 1981, Icarus, Vol. 45, p. 264-303.
(16) Pechmann, J. C., 1980, Icarus, Vol. 42, p. 185-210.
(17) Rossbacher, L. A., 1985, in Models in Geomorphology, Michael J. Woldenberg, ed., Allen and Unwin, Boston, p. 343-372.
(18) Basaltic Volcanism Study Project, 1981, Basaltic Volcanism On The Terrestrial Planets: Pergamon Press, Inc., New York, 1286 p.
(19) Zimbelman, J. R., 1987, Icarus, Vol. 71, p. 257-267.

HI 76256 N88-29688 S34-91
154934 103

EPISODIC VS. EPOCHAL RELEASE OF SO_2 ON MARS *S.E. Postawko, F.P. Fanale, and A.P. Zent, Planetary Geosciences Div., HIG, Univ. of Hawaii, Honolulu, HI 96822*

Erosion of the martian surface by the flow of liquid water has apparently taken place at different times and locations on the planet. Many attempts have been made to explain the valley networks seen on the martian surface by invoking a strong atmospheric CO_2/H_2O greenhouse early in the history of the planet (1,2,3). Recent calculations have shown that when reduced solar radiation is taken into account, it is necessary to have about 5 bars of CO_2 in the atmosphere in order for the mean global temperature to be above freezing (4). [Lesser amounts of CO_2 are required if only equatorial temperatures are to be above freezing. However, the valley networks are by no means confined to the equatorial regions (5).] It has been assumed that these large amounts of CO_2 would have disappeared mostly due to carbonate formation. However, carbonates have yet to be positively identified in martian spectra.

It is clear that volcanism has occurred throughout much of the history of Mars. Presumably gases such as SO_2 would have been released along with CO_2 and H_2O. Several studies have touched on the effects of SO_2 on martian climate (6,7). In our study, however, we have made estimates of amounts and rates with which SO_2 may have been released into the martian atmosphere, and how this may have affected global climate.

The amount of SO_2 released from terrestrial volcanoes varies greatly (cf., 8,9). For this study we have chosen 0.1 to 1 weight percent of SO_2 as reasonable bounds. The steady-state concentration of SO_2 is also dependent on its atmospheric lifetime. The lifetime of SO_2 in a volcanically perturbed martian atmosphere is somewhat difficult to assess. Settle (10) estimated the lifetime of SO_2 in a present-day martian atmosphere would be on the order of 6 [Earth] years. Terrestrial volcanoes, however, also release substantial amounts of water vapor, along with other gases. Since the concentration of odd hydrogen species in the martian atmosphere is directly proportional to the water vapor abundance, and the oxidation rate of SO_2 is directly proportional to the concentration of odd hydrogen species, increased atmospheric water vapor would decrease the lifetime of SO_2. Settle estimates the lifetime of SO_2 in a volcanically perturbed martian atmosphere would be comparable to, or somewhat greater than, the lifetime of SO_2 in the Earth's stratosphere. For our study we have chosen lifetimes of 1/4 year [approximate lifetime of SO_2 in the Earth's stratosphere (10)], and 1 year [a compromise between the lifetime in the present martian atmosphere and the lifetime in earth's stratosphere].

First let us consider an epochal time scale. Total magma erupted during each of 7 martian epochs was taken from Greeley (11). If volcanism had taken place uniformly through each epoch, then magma flux rates would have been between ~0.1 m^3/s and ~10 m^3/s, depending on the epoch. If the lifetime of SO_2 were on the order of 1 year, then for even 1 wt.% of SO_2 the steady-state concentration of SO_2 in the atmosphere would have been too low during each epoch to have significantly affected surface warming on a global basis.

Rather than continuous volcanism through each epoch, it is more likely that volcanism occurred episodically. We have chosen 2 magma flux rates for our study: 5×10^4 m^3/s, corresponding to a mid-range eruption rate for Alba Patera, Mars

(12); and 10^6 m^3/s, corresponding to some estimates for eruption rates of the Yakima Basalts of the Columbia Plateau (13), and for some flows on Alba Patera (14). For a 1 year lifetime and 1 wt.% of SO_2, these magma flux rates produce steady-state atmospheric SO_2 abundances which increase mean annual global surface temperature by about 5°K and 10°K, respectively.

While the effect of atmospheric SO_2 on very early martian climate is still quite speculative (calculations are under way to better estimate the lifetime of atmospheric SO_2 in a warmer, wetter early climate), it seems clear that SO_2 could have played a significant role in episodic warming of Mars even after an early thick atmosphere would have disappeared. This may have particular relevance to formation of features such as the layered deposits seen in the Valles Marineris. It has been suggested (15) that the nature of these layers is most consistent with formation by deposition of sediments in ice-covered lakes. Two of the processes which have been proposed to transport sediment down through an ice cover are 1) foundering, and 2) Rayleigh-Taylor instability (15). Among other parameters, the thickness of ice on perennially frozen lakes is dependent on the yearly average surface temperature (16). If all other parmeters remain constant, a 10°K increase in surface temperature could decrease the thickness of the ice by up to ~20%. Thus, the effeciency of both the above processes may be increased by even a small atmospheric warming.

It is possible that under certain circumstances SO_2 could have contributed even more to surface warming. Although the above magma flux rates are probably as high as possible, the steady-state atmospheric abundance of SO_2 could be significantly increased if the SO_2 lifetime were greater than 1 year. This may occur, for example, during periods of low obliquity when polar cold trapping acts to keep the atmosphere very dry. In addition, because early volcanic terrain may have been extensively covered by more recent volcanic activity, the amount of volcanism early in martian history may be much more extensive than indicated. Studies are continuing on effects of SO_2 and other volcanic gases on martian climatic history.

References

(1) Pollack, J.B. (1979), *Icarus,* **37,** 479-553. (2) Cess, R.D., V. Ramanathan, and T. Owen (1980), *Icarus,* **41,** 159-165. (3) Toon, O.B., J.B. Pollack, W. Ward, J.A. Burns, and K. Bilski (1980), *Icarus,* **44,** 552-607. (4) Kasting, J.F. (1986), In *Mars: Evolution of Its Climate and Atmosphere,* LPI Tech. Rpt. 87-01, Lunar and Planetary Inst., Houston, TX. (5) Carr, M.H. and G.D. Clow (1981), *Icarus,* **48,** 91-117. (6) Postawko, S.E. and W.R. Kuhn (1986), *J. Geophys. Res.,* **91,** D431-D438. (7) Kondratyev, K.Y., N.I. Moskalenko, and S.N. Parzhin (1986), *Earth, Moon, and Planets,* **35,** 13-18. (8) Anderson, A.T. (1975), *Rev. Geophys. Space Phys.,* **13,** 37-54. (9) Meszaros, E. (1981), In *Atmospheric Chemistry: Fundamental Aspects,* Elseiver Scientific Pub. Co., New York, pp 72-90. (10) Settle, M. (1979), *J. Geophys. Res.,* **84,** 8343-8354. (11) Greeley, R. (1987), *Science,* **236,** 1653-1654. (12) Baloga, S.M., D.C. Pieri, J. Plescia, and P. Davis (1987), *Proc. Lunar and Planet. Sci. Conf. XVIII,* Lunar and Planetary Institute, Houston, TX, pp 42-43. (13) Swanson, D.A., T.L. Wright, and R.T. Helz (1975), *Am. J. Sci.,* **275,** 877-905. (14) Cattermole, P. (1986), *Proc. Lunar and Planet. Sci. Conf. XVII,* Lunar and Planetary Inst., Houston, TX, pp105-106. (15) Nedell, S.S. and S.W. Squyres (1986), *MECA Symposium on Mars: Evolution of Its Climate and Atmosphere,* LPI Cont. 599, 74-76. (16) McKay, C.P., G.D. Clow, R.A. Wharton, and S.W. Squyres (1985), *Nature,* **313,** 561-562.

MJ70080 N88-29689 S35-91 N125 ONLY 154735

CHEMICAL INTERACTIONS BETWEEN THE PRESENT–DAY MARTIAN ATMOSPHERE AND SURFACE MINERALS; Ronald Prinn and Bruce Fegley, Department of Earth, Atmospheric, and Planetary Sciences, MIT, Cambridge, MA 02139

Thermochemical and photochemical reactions between surface minerals and present–day atmospheric constituents (O_3, H_2O_2, OH, HO_2, O_2, CO, CO_2, H_2O, NO_x, etc.) are predicted to produce microscopic effects on the surfaces of mineral grains. Relevant reactions hypothesized in the literature include conversions of silicates and volcanic glasses to clay minerals, conversion of ferrous to ferric compounds, and formation of carbonates, nitrates, and sulfates (see e.g. Gooding, 1978; Huguenin, 1982; Sidorov and Zolotov, 1986; and references therein).

These types of surface–atmosphere interactions are important for addressing issues such as chemical weathering of minerals, biological potential of the surface environment, and atmospheric stability in both present and past Martian epochs. We emphasize that the products of these reactions will be observable and interpretable on the microscopic surface layers of Martian surface rocks using modern techniques (SEM/EDS, EPMA, TEM/AEM, INAA, XPS, transmission spectroscopy, etc.) with obvious implications for sample return from Mars.

Macroscopic products of chemical weathering reactions in past Martian epochs are also expected in Martian surface material. These products are expected not only as a result of reactions similar to those proceeding today but also due to aqueous reactions in past epochs in which liquid water was putatively present. It may prove very difficult or impossible however to determine definitively from the relic macroscopic product alone either the exact weathering process which led to its formation or the identity of its weathered parent mineral. The enormous advantages of studying Martian chemical weathering by investigating the microscopic products of present–day chemical reactions on sample surfaces are very apparent: the relevant atmospheric, surface, and solar radiation environments leading to chemical alteration of the minerals and glasses and the identity of the material being weathered can all be precisely defined.

References:

Gooding, J. (1978). *Icarus* **33**, 483-513.

Huguenin, R., (1982). *J. Geophys. Res.* **87**, 10,069-10,082.

Sidorov, Yu, and M. Zolotov, (1986). In *"Chemistry and Physics of Terrestrial Planets"* (Springer-Verlag, NY) pp. 191-223.

Acknowledgements: Supported by NSF (grant ATM-8710102) and NASA (grant NAG9-108).

S36-91
AM84-1926
GU 6574 N88-29690

STRATIGRAPHY OF THE KASEI VALLES REGION, MARS

Mark S. Robinson, *University of Alaska, Fairbanks, Alaska, 99775, and* **Kenneth L. Tanaka**, *U.S. Geological Survey, Flagstaff, Arizona, 86001*

Introduction

We identify and describe thicknesses and geomorphology of the two principal stratigraphic units exposed in Kasei Valles to aid in interpreting (1) the nature of crustal materials and (2) the history of the channeling events in the area. Previous studies of Kasei Valles have related the channel landforms to glacial flow *[Lucchitta, 1982]*, catastrophic flooding *[Baker, 1982]*, and large-scale eolian erosion *[Cutts, 1978]*.

The two units (an upper and a lower unit) form thick sheets, each having distinct geomorphologic features. Thicknesses of the units were determined through preliminary stereogrammetric profiles taken across many sections of western Kasei Valles and shadow measurements taken of scarp heights from calibrated Viking images having sun angles less than 25°; DN values were examined to confirm that true shadows were observed.

Description and Interpretation of Upper and Lower Units

The upper unit is capped by ridged plains material. Along the margins of the unit (where it was partly removed by channeling), either steep-walled scarps *(A in Fig. 1)* or chaotic terrain *(B)* have formed. At the bases of the scarps are extensive talus slopes and debris aprons, and narrow moats *(C in Fig. 1)* border the chaotic terrain at the northwest edge of the Kasei Valles area. Carved into the upper unit are low-relief, streamlined forms *(D, E)* in high-standing, scoured interchannel areas. The upper unit is also incised by Sacra Fossae *(F)*, large fretted valleys that mostly trend northwest and northeast. Shadow measurements and stereogrammetry show the upper unit to have an average thickness of 1000 m ± 200 m west of long 59° and to thin or dip down to the east.

The ridged plains material is apparently underlain by more friable material. Where exposed by channeling, the upper unit has been eroded by the sapping of ground water or ground ice to form the fretted valleys, debris aprons, and chaotic terrain (the streamlined forms at *D and E (Fig. 1)* did not reach this lower layer of the upper unit). At the east edge of Lunae Planum, the ridged plains material embays cratered plateau material. We therefore interpret that the more friable lower layer consists largely of impact breccias. Our thickness measurements correspond to De Hon's *[1982]* estimates of the thickness of ridged plains material and Battistini's *[1984]* estimate of the depth to a mechanical discontinuity.

The lower unit, where exhumed, has a smooth, flat surface. The unit is eroded mainly by channeling; no mass-wasting features formed from it. In lower channel reaches, low scarps formed in the unit, indicating that it consists of a series of thin, resistant layers. Etched into the unit's surface is an extensive series of subparallel striations *(G and H in Fig. 1)* that, on a regional scale, follow the course of the Kasei Valles channel. Teardrop-shaped forms *(I and J in Fig. 1)* occur in the unit throughout the channel system; some appear to be depositional while others may be erosional. Locally, the unit is extensively fractured by sets of cracks that trend northeast and northwest; the cracks have been widened by processes of uncertain nature. In places, small, widely dispersed channel networks *(H and I in Fig. 1)* that cut the lower unit do not follow the regional stream course but follow local gradients. Where the channel cuts through the top of the lower unit, its elevation drops abruptly *(K, L)*. Wrinkle ridges on the lower unit are rare and somewhat degraded (e.g., at lat 26°, long 62° and lat 29.5°, long 58°).

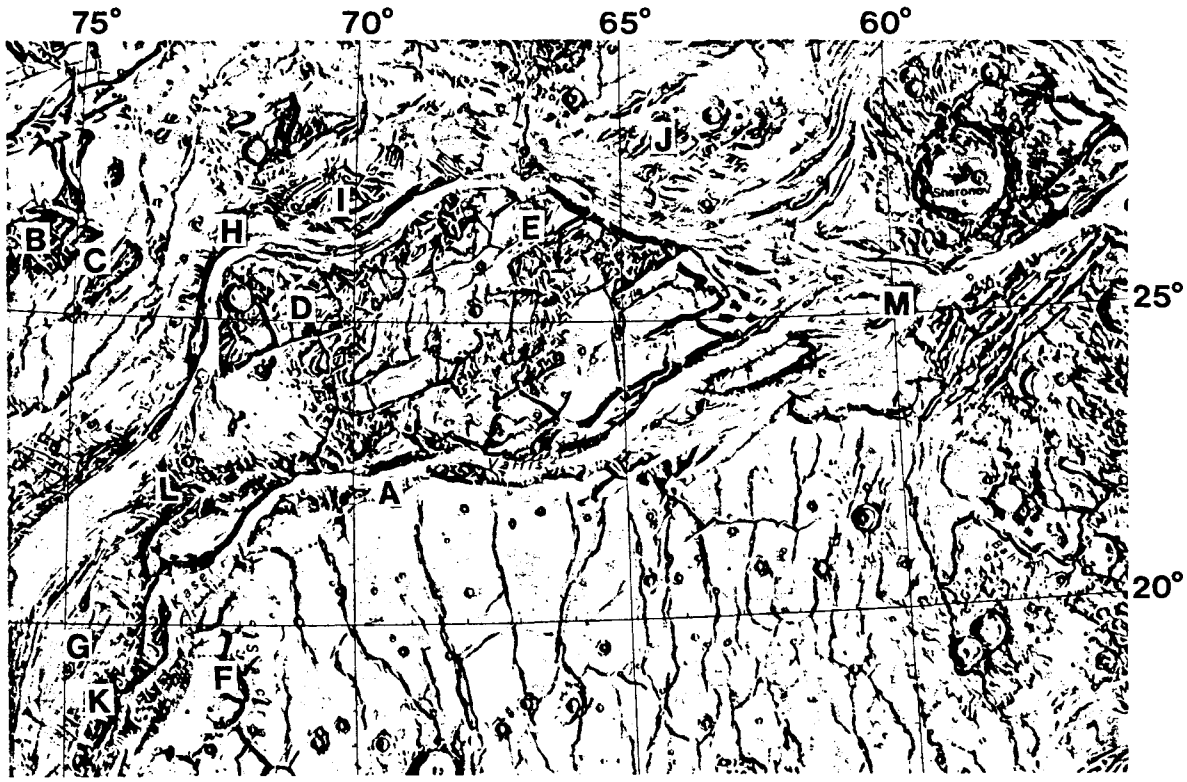

Figure 1. Shaded relief map of Kasei Valles; letters indicate locations referred to in text.

The lower unit occurs at depths ranging from about 1 km to at least 3.5 km. It therefore consists of material that is generally much lower in stratigraphic position than most exposed materials on Mars, including cratered plateau material. Its competence, layering, and low stratigraphic position indicate that it consists of a sequence of lava flows that correspond to basement material, which locally forms basin rims and massifs on Mars *[Scott and King, 1984]* of Early Noachian age *[Tanaka, 1986]*.

Channeling

Streamlined channel forms in Kasei Valles occur predominantly within the lower unit and outside the deeply incised main channels. The streamlined forms of the lower unit commonly exhibit first-order length-to-width ratios (the form of a group of bars) of 3 to 4 and second-order length-to-width ratios (the form of an individual bar) of 2 to 3. The first order ratios indicate high discharge rates, and the second-order values indicate waning discharge rates *[Baker, 1978]*. Within the upper unit no groups of bars are present, but the streamlined forms of individual bars on the upper unit *(e.g., D in Fig. 1)* have length-to-width ratios exceeding 3. The apparent sequence of events is as follows: (1) streamlined forms are carved into the ridged plains material that caps the upper unit; (2) the lower, friable material of the upper unit is removed by channeling, and streamlined forms and striations are cut into the surface of the lower unit; (3) the channel scarps continue to erode by mass wasting; and (4) the main channels are cut into the lower unit, which locally is fractured and channeled.

Preliminary stereogrammetric measurements show a rise of about 500 m in the floor of the main north channel where it turns to the northeast *(at H in Fig. 1)*. Striations etched into the lower unit veer out from and leave the main channel in the area where the channel floor begins to rise. The major flow of the eroding substance apparently did not follow the course of the main channel, but rather it turned less sharply to the east and dispersed on the exhumed surface of the lower unit.

Heights of scarps in the lower unit in the south channel of Kasei Valles show a gradual decrease from west to east, and the lower unit is not incised between long 61° and 63°. Goldstone radar profiles indicate that the ridged plains material is nearly flat in northern Lunae Planum (lat 20°). These observations indicate that the contact between the upper and lower units rises eastward. Farther east, the channel floor steepens and again cuts through the lower unit. This steepening of the channel floor is reflected in the steeper channel walls *(M in Fig. 1)*, similar to those seen in the area of headward erosion where the channel cuts through the lower unit 850 km upstream *(K)*.

Future Work

We are continuing to analyze the stereogrammetry data to more accurately determine scarp heights, slope angles, and stratigraphic thicknesses in Kasei Valles. The 500-m rise in the north Kasei channel is currently under investigation. Detailed study of the channel walls, streamlined forms, and elevation relations will help to determine the nature of the exposed crustal materials, the history of Kasei Valles, and processes involved in the channeling that has shaped them.

References

Baker, V. R. 1978. *Proc. Lunar and Plan. Science Conf.* 9^{th}, pp. 3193–3203.

Baker, V. R. 1982. The Channels of Mars: Austin, Texas, University of Texas Press, 132–139.

Battistini, R. 1984. *Earth, Moon, and Planets.* 31:49–91.

Cutts, J. A. 1978. *Abstracts Lunar Science Conference,* 9^{th}, pp. 206–208.

De Hon, R. A. 1982. *Journal of Geophysical Research.* 87:9821–9828.

Lucchitta, B. K. 1982. *Journal of Geophysical Research.* 87:9951–9973.

Scott, D. H., and King, J. S. 1984. *Abstracts Lunar and Planetary Science Conference,* 15^{th}, pp. 736–737.

Tanaka, K. L. 1986. *Journal of Geophysical Research.* 91:E139-E158.

JJ574450

N88-29691 S37-91

154937 P109

TOPOGRAPHY OF LARGE CRATERS ON MARS: IMPLICATIONS FOR THE HIGHLANDS RESURFACING HISTORY; L. E. Roth and R. S. Saunders, Jet Propulsion Laboratory, California Institute of Technology, Pasadena, California 91109.

The results of a point-by-point examination of the Goldstone topography data (1) in the martian highlands suggest that, at the 100-m range resolution, the rims of large craters are barely distinguishable against the surrounding terrain (Figs. 1-4). While on the moon topographic expression of a crater may extend to distances of at least one crater radius from the rimcrest (2), the topographic expression of craters in the Goldstone sample rarely extends beyond the immediate vicinity of the crater cavity. Thus the low or non-existent exterior relief appears to constitute the general characteristic of large martian craters. The often-noted shallowness (3,4) of these craters is perhaps not so pervasive since even some rimless structures (e.g., basin Ladon, Fig. 1) have preserved relatively deep depressions. Low rims in small martian craters may be genetically related to an impact into a volatile-rich upper crust (5). Excavation of large craters into a volatile-poor lower crust should not result in anomalously low rims. An advanced stage of structural adjustment of large craters would presumably be accompanied by the simultaneous loss of much or all of both the interior and the exterior relief (6,7). Since it is mostly the exterior relief that has been lost, while the interior relief, although reduced, has been largely retained, neither the rapid post-impact rebound nor the protracted relaxation are the likely principal contributors to the present rimless appearance of the large martian craters. Eolian-erosion induced disappearance of the competent exterior relief appears to be improbable (8,9). Likewise, fluvial erosion is an unlikely agent of the exterior relief suppression (10). Thus, while martian craters were certainly subjected to the action of all the commonly considered modification processes, the emergence of a rimless, flat-floored crater is probably related to a specific class of events, associated with the intermittent plains-resurfacing episode/episodes (11,12). A scenario in which pre-plains, late heavy bombardment-related large crater degradation is followed by post-plains degradation quiescence (13) apparently has to include an intermediate, co-plains, degradation-intense stage (12), nonuniform with respect to space and perhaps also time. If the relatively well-preserved exterior relief of basin Huygens is viewed as a marker, then intercrater-plains deposits to an average depth of perhaps as much as 1 km can be inferred. These conclusions, considered tentative, underscore the need for a reliable topographic information when attempting to reconstruct the geologic history of terrestrial planets.

References: (1) Downs, G. S. et al. (1975) Icarus 26, 273. (2) Settle, M. and Head, J. W. (1977) Icarus 31, 123. (3) Murray, B. C., Soderblom, L. A., Sharp, R. P. and Cutts, J. A. (1971) J. Geophys. Res. 76, 313. (4) Pike, R. J. (1971) Icarus 15, 384. (5) Cintala, M. J. and Mouginis-Mark, P. J. (1980) Geophys. Res. Lett. 7, 329. (6) Ramberg H. (1963) Bull. Geol. Inst. Uppsala 42, 1. (7) Danes, Z. (1965) Astrogeol. Stud. Ann. Prog. Rep. (8) Arvidson, R. E. (1986) Lunar Planet. Sci. XVII, 17. (9) Aubele, J. C. and Crumpler, L. S. (1987) Lunar Planet. Sci. XVIII, 36. (10) Baker V. R. and Milton, D. J. (1974) Icarus 23, 27. (11) Chapman, C. R. (1974) Icarus 22, 272. (12) Chapman, C. R. and Jones K. L. (1977) Ann. Rev. Earth Planet. Sci. 5, 515. (13) Malin, M. C. and Dzurisin, D. (1977) J. Geophys. Res. 82, 376.

ORIGINAL PAGE IS
OF POOR QUALITY

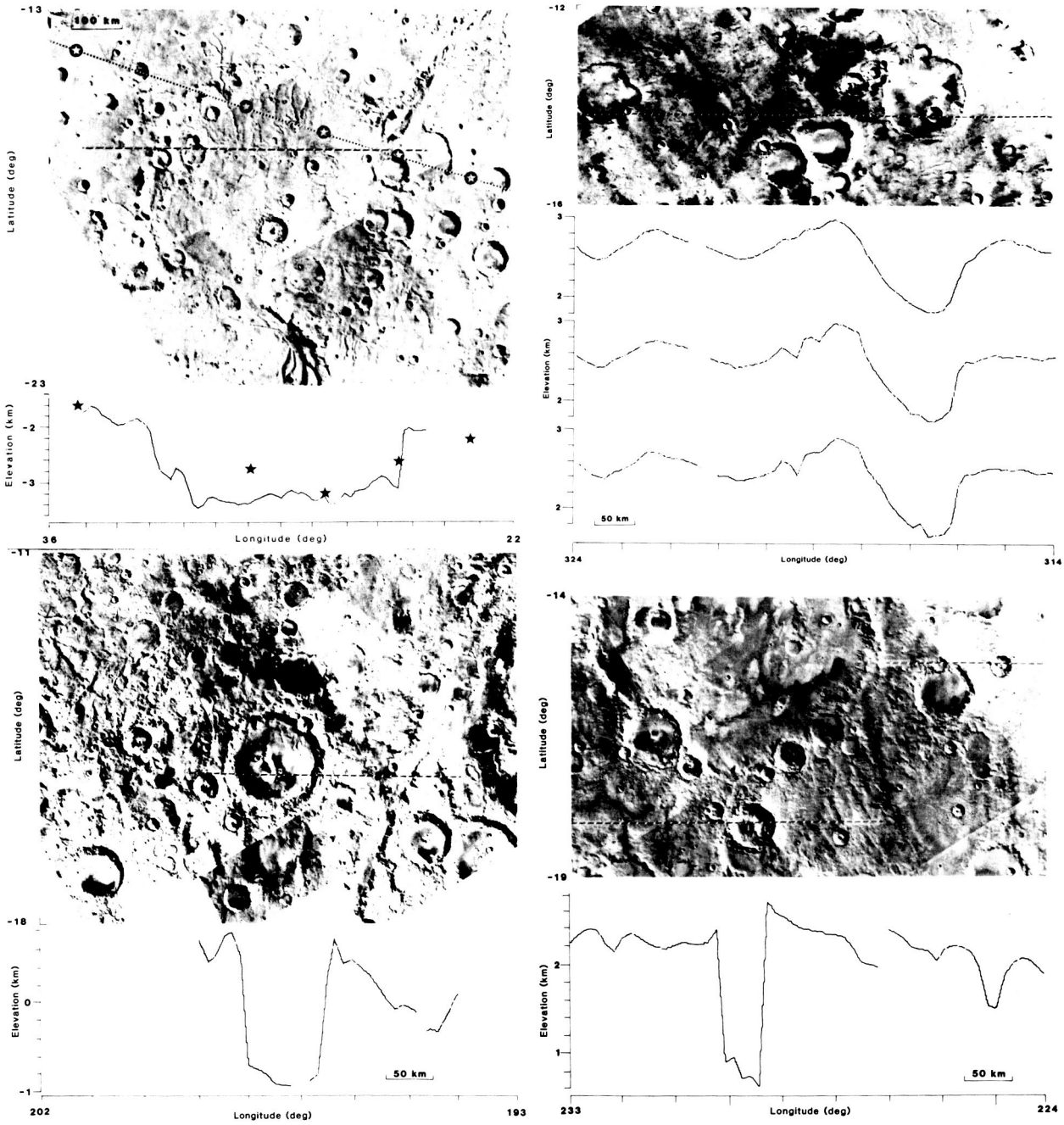

Elevation profiles of large martian craters. Clockwise from the top, left: Fig. 1. Basin Ladon (28.0°, -17.8°, 475 km) in Margaritifer Sinus. Fig. 2. Unnamed crater (317.0°, -13.7°, 95 km) in Sinus Sabaeus. Fig. 3. Two unnamed craters (229.6°, -18.0°, 55 km; 225.1°, -15.3°, 25 km) in Mare Tyrrhenum. The latter object is the smallest impact crater positively identified in the Goldstone Mars altimetry. Fig. 4. Crater Boeddicker (197.3°, -15.0°, 110 km) in Aeolis.

ORIGINAL PAGE IS
OF POOR QUALITY

NC 473657
AX 852975
Ai 782556
N88-29692
S38-91
154138
38.

PRELIMINARY ANALYSIS OF RECENT 2.2-4.2μm TELESCOPIC OBSERVATIONS OF ELYSIUM, MARS: IMPLICATIONS FOR CRYSTALLINITY AND HYDRATION STATE OF SURFACE MATERIALS; T.L. Roush (NASA Ames Research Center, Moffett Field, CA 94035), E.A. Roush, R.B. Singer (U. Arizona), and P.G. Lucey (U. Hawaii)

Several recent studies have reported the reflectance of mafic silicates (1), crystalline clays (2,3), and non-crystalline weathering products of basaltic glass (2,3) in the 0.6-4.3μm wavelength region. This wavelength range includes fundamental absorptions of OH^- and H_2O, as well as overtones and/or combinations of these fundamentals. The experimental details of these laboratory spectroscopic studies are presented elsewhere (1,2,3) but the important aspects will be summarized here. Particulate samples were continuously maintained in a nitrogen environment and spectral data were acquired before sample dehydration and at several incremental steps in the dehydration process. These studies provide direct evidence concerning the spectral effects of H_2O and OH^- associated with each of these materials and thus provide a basis for comparison with recent telescopic observations of Mars, which included the 2.2-4.2μm wavelength region (4). Such a comparison can provide valuable information concerning both the composition and hydration state of martian surface components.

The telescopic observations used here are disucssed elsewhere (4). Figure 1 shows the reflectance spectrum of a classical martian bright region, Elysium. Data in the 2.2-2.45μm region were collected to provide spectral overlap with prior observations. In this wavelength range the spectrum is relatively flat and no strong absorptions indicative of crystalline clays (5) are obvious. The longer wavelength region (2.8-4.2μm) of the spectrum exhibits an increase of reflectance with increasing wavelength, which at wavelengths >3.5μm is due to increasing contribution of a thermally emitted component (6). Beyond 2.9μm the spectrum exhibits a broad absorption which has previously been attributed to "bound" water (6,7,8,9). The slope change at 2.9μm and strong reflectance gradient from 2.8 to 2.9μm is indicative of a narrow absorption super-imposed on the "bound" water absorption. Generally, a narrow absorption observed in this region is ascribed to crystalline material containing the OH^- ion within its structure (2,3,5). Previous studies have indicated that atmospheric CO_2 is expected to be highly absorbing between 2.6 and 2.85μm (6,7). Thus, we believe the 2.8-2.9μm absorption edge seen in the telescopic data is due partly, if not entirely, to surface materials.

Since the telescopic data contain a thermal contribution at the longer wavelengths, we have attempted to add a first order thermal component to our laboratory data. We assumed the laboratory samples were located on the martian surface, and the flux of each sample from the surface can be expressed as:

$$\frac{[\pi P(T) (1 - R)] + RF}{F}$$

where P(T) is the Planck blackbody function for a given surface temperature T, R is the measured reflectance of the sample, and F is the solar flux incident on Mars. Using the measured laboratory reflectance of a sample and assuming a martian surface temperature, we calculated the total flux from each sample as it would look if it were located on Mars. Because the Elysium data were collected at Ls=183 and after local noon, we used 273K and 283K as upper limits for surface temperature (10). Both the calculated and telescopic spectra are normalized at 2.405μm in order to provide a more direct comparison.

Hawaiian palagonites, weathering products of mafic volcanic glass, provide the best spectral analogs to martian soils and bright regions in the 0.3-2.6μm wavelength region (11). Figure 2 shows a comparison of the telescopic data of Elysium with the calculated spectrum of a Mauna Kea palagonite which has been dehydrated at 400°C. The reflectance of this sample in the 3μm region exhibits a broader "bound" water absorption than the telescopic data and shows no evidence of the 2.8-2.9μm absorption edge seen in the telescopic data. All hydration states of this sample exhibit the same spectral trends in the 3μm region, and hence fail to provide a good comparison for the telescopic data. Figure 3 is a similar comparison using a sample of Pahala Ash, which has been dehydrated at 400°C. This comparison provides a much better spectral match to the telescopic data in the 2.8-2.9μm region and throughout the 3μm region. Other hydration states of this sample do not provide as good a comparison. The spectral differences between these two samples have been attributed to a greater degree of crystallinity in the Pahala Ash (3,12). This supports recent analyses of the 1980 Mars telescopic data, based on the 2.35μm region (13). Comparisons of the Elysium data with spectra of more crystalline materials (not shown) yield similar trends to those of Pahala Ash. That is, all spectra of crystalline samples which exhibit a strong 2.8-2.9μm absorption edge and a broad "bound" water absorption are dehydrated relative to the terrestrial environment (2,3). The presence of major amounts of these crystalline minerals on the martian surface has been shown to be inconsistent with the 0.3-2.6μm telescopic spectra of martian bright regions (12). However, it is possible that minor amounts of crystalline materials could be mixed with amorphous palagonite. Such a mixture could remain consistent with the shorter wavelength spectral data (13) and could also explain the spectral behavior observed in the 3μm region.

In summary, comparisons of the telescopic reflectance spectrum of a martian bright region, in the 2.2-4.2μm region, with recent laboratory studies of materials in this same wavelength range are consistent with: (1)terrestrial materials which are dehydrated relative to the terrestrial environment, and (2)terrestrial materials which exhibit spectral behavior indicative of some degree of sample crystallinity which is greater than that of amorphous palagonites. This second conclusion is in agreement with recent suggestions concerning the martian bright regions (13). However, additional laboratory research is required in order to constrain: (1)the degree of crystallinity required to result in the 2.8-2.9μm spectral behavior seen in the terrestrial samples, and (2)the limit of crystalline material which can be accomodated in a mixture with amorphous palagonite and remain consistent with previously measured telescopic data of Mars (0.3-4.2μm).

REFERENCES: (1)Roush, T.L. et al. (1987) LPSC XVIII, p.854-855 (2)Roush T.L. et al. (1987) LPSC XVIII, p.856-857 (3)Bruckenthal, E.A. and R.B. Singer (1987) LPSC XVIII, p.135-136 (4) Singer, R.B. et al. (1986) Bull. Am. Astron. Soc., p.806 (5)Hunt, G.R. and J.W. Salisbury (1970) Mod. Geol., p.283-300 (6)Houck, J.R. et al. (1973) Icarus, p.470-480 (7)Pimental, G.C. et al. (1974) JGR, p.1623-1634 (8)Moroz, V.I. (1964) Astron. Zh., p.79-86 (9)Sinton, W.W. (1967) Icarus, p.222-228 (10)Kieffer, H.H. et al. (1977) JGR, p.4249-4291 (11) Singer, R.B. (1985) Adv. Space Res., p.59-63 (12)Singer, R.B. (1982) JGR, p.10159-10168 (13)Singer, R.B. et al. (1985) LPSC XVI, p.787-788

ORIGINAL PAGE IS
OF POOR QUALITY

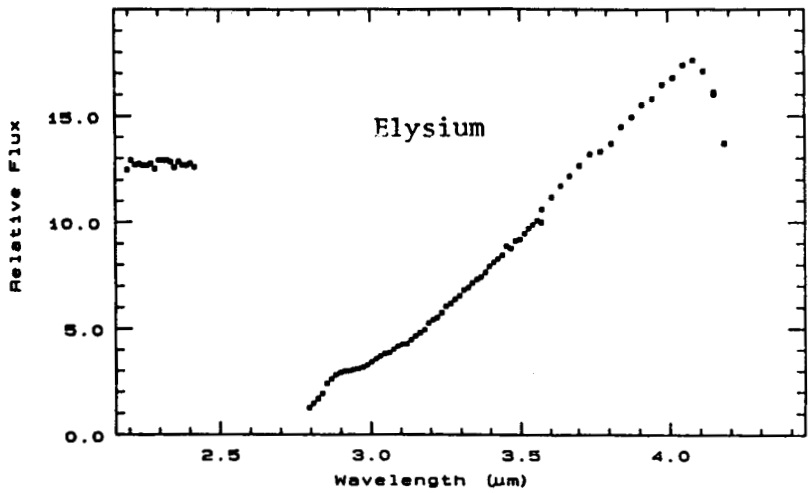

Figure 1. (left) Measured flux from the Elysium region on Mars relative to 16Cyg b, a solar analog. The broad absorption throughout the 3μm region is indicative of "bound" water and the superimposed absorption from 2.8-2.9μm is indicative of crystal strucutres which contain the hydroxyl ion.

Figure 2. (right) Scaled reflectance of Elysium compared with Mauna Kea palagonite and assuming surface temperatures of 273K and 283K. This illustrates a poor comparison for the absorptions seen in the telescopic data.

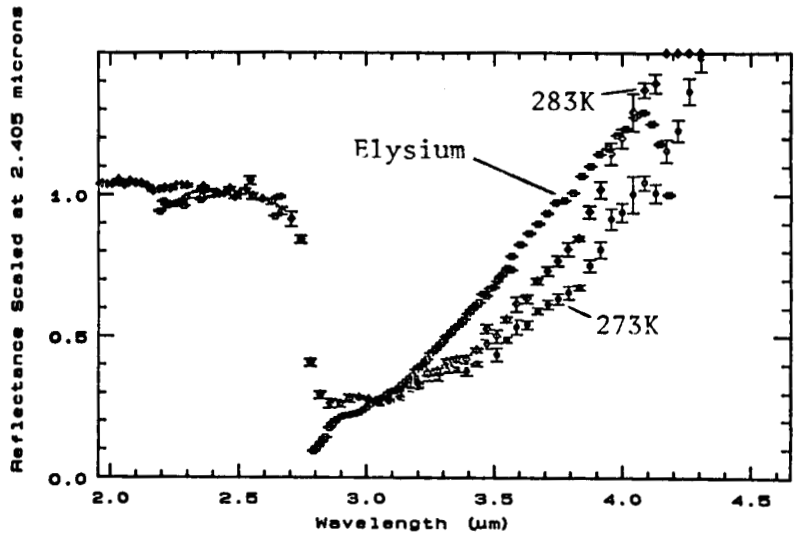

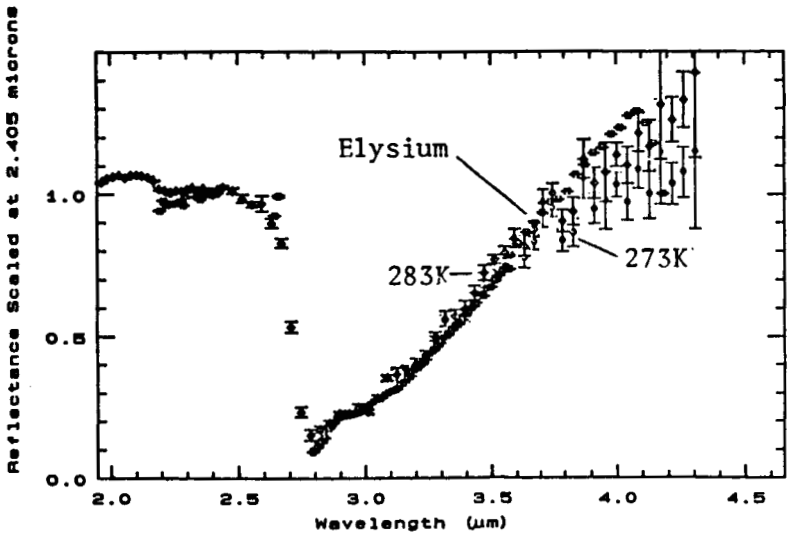

Figure 3. (left) Scaled reflectance of Elysium compared with Pahala Ash and assuming martian surface temperatures of 273K and 283K. This provides a relative good comparison with the telescopic data.

S39-71
B172051
N88-29693

ORIGIN OF SNC KAERSUTITIC AMPHIBOLE: EXPERIMENTAL DATA. M. J. Rutherford, Bruce Heine, and Marie Johnson, Dept. of Geological Sciences, Brown University, Providence, R.I., 02912

The SNC meteorites, a group of cumulus textured, fine grained diabases, pyroxenites and dunites, appear to have crystallized at relatively shallow depths on the same SNC parent body (McSween, 1985; review). Hydrous minerals generally are not present among the cumulus and intercumulus minerals in these meteorites except for some iddingsite alteration of olivine. However, a hydrous kaersutitic amphibole has been identified in melt inclusions in Chassigny olivine (Floran et.al., 1978), and in Shergotty and Zagami pyroxenes (Treiman, 1985). The nearly euhedral form of the amphiboles in these inclusions clearly indicates that they crystallized from a melt, and not from subsolidus recrystallization in the inclusion or from shock metamorphism.

The presence of hydrous magmatic amphibole in the SNC melt inclusions indicates that crystallization of the melt inclusions had to take place at significant pressure, probably greater than 1 kb based on previous amphibole stability data (Treiman, 1985). If experimental data for kaersutite amphibole were to be obtained, it should be possible to estimate this pressure more precisely than previously, and to estimate the volatile (H_2O) content of the parent magma. At this point, the factors controlling the chemistry and stability of high TiO_2, kaersutitic amphibole are not known, particularly for the iron-rich amphibole (Mg# = 35) found in the SNC meteorites. Kaersutite found in terrestrial rocks is much more Mg-rich, and is most commonly found in basic alkalic rocks. Many terrestrial occurrences of Mg-rich kaersutite are clearly of high pressure (mantle) origin.

In an attempt to determine the factors which control the stability and chemistry of TiO_2-rich amphibole, we have refined and extrapolated data from four experimental studies of amphibole-melt equilibria recently completed in this laboratory. At the same time, hydrothermal experiments have been carried out on a composition considered (Stolper and McSween, 1979) to be an early melt in the Shergotty magma liquid line of descent. The latter experiments were an attempt to reproduce crystallization of the amphibole-bearing melt inclusions.

EXPERIMENTAL RESULTS: Analysis of four recently completed experimental studies of amphibole-melt equilibria does reveal some of the factors which control amphibole stability and TiO_2 content. The experiments were done on andesite (Carroll and Rutherford, in press), dacite (Rutherford et.al., 1985; Rutherford and Devine, submitted), and quartz latite (Johnson and Rutherford, 1987, in prep.) bulk compositions, over a range of $P(H_2O)$ and T conditions and at pressures from 1 to 5 kb. Plagioclase, low-Ca pyroxene and Fe-Ti oxides coexist with amphibole and melt in all samples. The data show that the amphibole/melt D for TiO_2 increases from 3.5 to 9 ± 1.0 as the SiO_2 content of the coexisting melt increases from 60 to 70 wt% (Fig. 1). As SiO_2 increases from 60 to 70 wt %, Al_2O_3 in these melts decreases from 19 to 13 wt%. However, even though increased SiO_2 (and low Al_2O_3) in a melt result in a very high D for TiO_2, the absolute abundance of TiO_2 in the high SiO_2 melts was always very low and the coexisting amphibole never contained more than 2.5 wt% TiO_2 under any set of conditions.

The experimental data set for amphibole-melt equilibria supports two other conclusions which help to characterize the melt that crystallized the SNC amphibole. The data show that Al_2O_3 is regularly concentrated in the melt relative to amphibole, the D being 0.7 ± 0.1 for melt Al_2O_3 contents ranging from 12 to 20 wt%. Similarly, FeO is concentrated in the melt relative to the coexisting amphibole, the FeO/(FeO + MgO) of amphibole/melt ranging from 0.6 to nearly 0.8 in very iron-rich compositions (Fig. 2). These data applied to the amphibole found in SNC melt inclusions (Treiman, 1985) indicate the SNC amphibole crystallized from a melt with 20 wt% Al_2O_3 and an FeO/(FeO + MgO) ratio of 0.93.

The hydrothermal experiments done on the 2-pyroxene - plagioclase cotectic composition, SH-18 (Stolper and McSween, 1979) which approximates the Shergotty melt inclusion composition, do not yield a high-TiO_2 amphibole in the 2 to 3 kb pressure range. The FeO and TiO_2 in these experimental charges appeared primarily as Fe-Ti oxides. A low TiO_2 amphibole appears as a liquidus phase at 900°C after approximately 50% crystallization.

DISCUSSION AND CONCLUSIONS: The fine grained texture of the SNC meteorites and the near glassy mesostasis suggest that final emplacement of these rocks on the SNC parent body was shallow enough to allow relatively rapid cooling. The melt inclusions may have been entrapped earlier, at somewhat greater depth, but pressures much greater than 3 kb are difficult to envision. Hence, we are presently investigating possible low pressure origins for the SNC kaersutite assemblage. If none of these are satisfactory, it may be necessary to investigate higher pressure models.

The melt composition and conditions required to produce a TiO_2-rich amphibole similar to that found in the SNC melt inclusions is partially defined by data from the recent hydrothermal experiments. The melt would have to contain 20 wt% Al_2O_3 based on an amphibole/melt D of 0.7, and it would have to be very Fe-rich (FeO/(FeO+MgO) = 0.93). Although the amphibole-melt KD for TiO_2 approaches 10 for high SiO_2 melts, the highest TiO_2 amphiboles occurred in melts where the KD was about 4. Therefore, it is expected that the melt in equilibrium with the SNC amphibole would have approximately 2 wt% TiO_2.

Figure 3 shows that there is a large gap between any amphibole yet synthesized and the SNC composition. (There is also a significant gap between these two fields and the terrestrial kaersutites, but the latter generally appear to have a high pressure origin). It is possible that conditions still to be explored, i.e. very Fe-rich compositions, may yield SNC composition amphibole in equilibrium with plagioclase and pyroxenes. We do not consider this possibility very likely. Another model is that the high Al_2O_3 and the high TiO_2 in the SNC amphibole are the result of non-nucleation of plagioclase (Treiman, 1985). Experimentally, plagioclase nucleation easily can be suppressed making the non-nucleation of plagioclase in SNC melt inclusions an extremely intriguing possibility. Suppression of plagioclase nucleation would over-saturate the melt in Al_2O_3. The increased Al_2O_3 content of the melt would explain the observed hercynite overgrowths on magnetite, and it might affect amphibole chemistry. Suppression of plagioclase nucleation is now being investigated experimentally.

REFERENCES:

Caroll, M. and Rutherford, M. J. (1987, in press), *J. of Petrol.*
Floran, R. J. et al. (1978), *Geochem. Cosmochem. Acta, 42*, 1213-1229.
Johnson, M. and Rutherford, M. J. (1987), *EOS, 68*, 434.
McSween, H. Y. Jr. (1985), *Reviews of Geophy., 23*, 391-416.
Rutherford, M. J. et al., (1985), *J. Geophys. Res, 90*, 2929-2947.
Rutherford, M. J. and Devine, J. (submitted), *J. Geophys. Res.*
Stolper, E. and McSween, H. Y. Jr. (1979), *Geochem. Cosmochem. Acta, 43*, 1475-1498.
Treiman, A. H. (1985), *Meteoritics, 20*, 229-243.

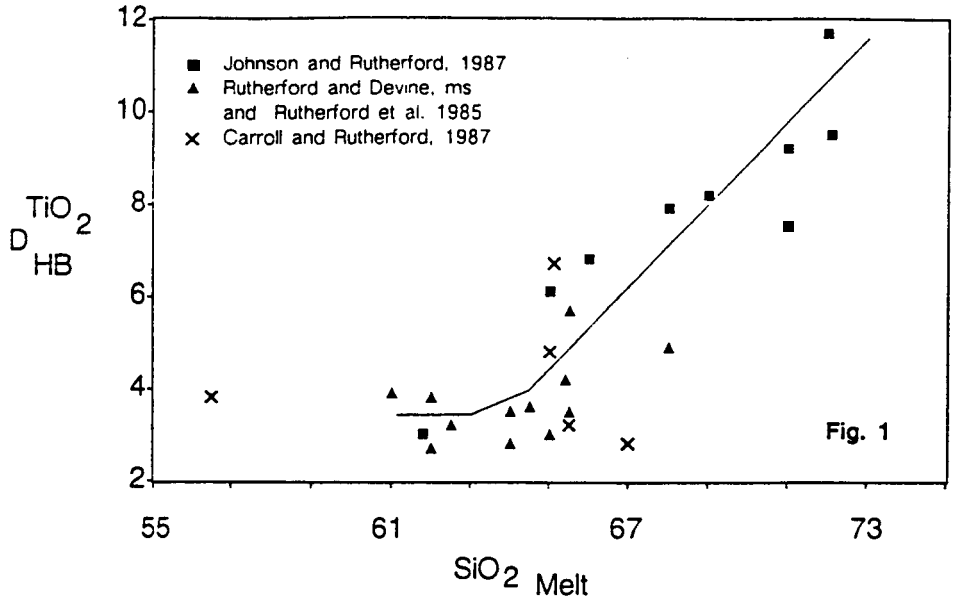
Johnson and Rutherford, 1987
Rutherford and Devine, ms
and Rutherford et al. 1985
Carroll and Rutherford, 1987
TiO2
D HB
12
10
8
6
4
2
55
61
67
73
SiO2 Melt
Fig. 1

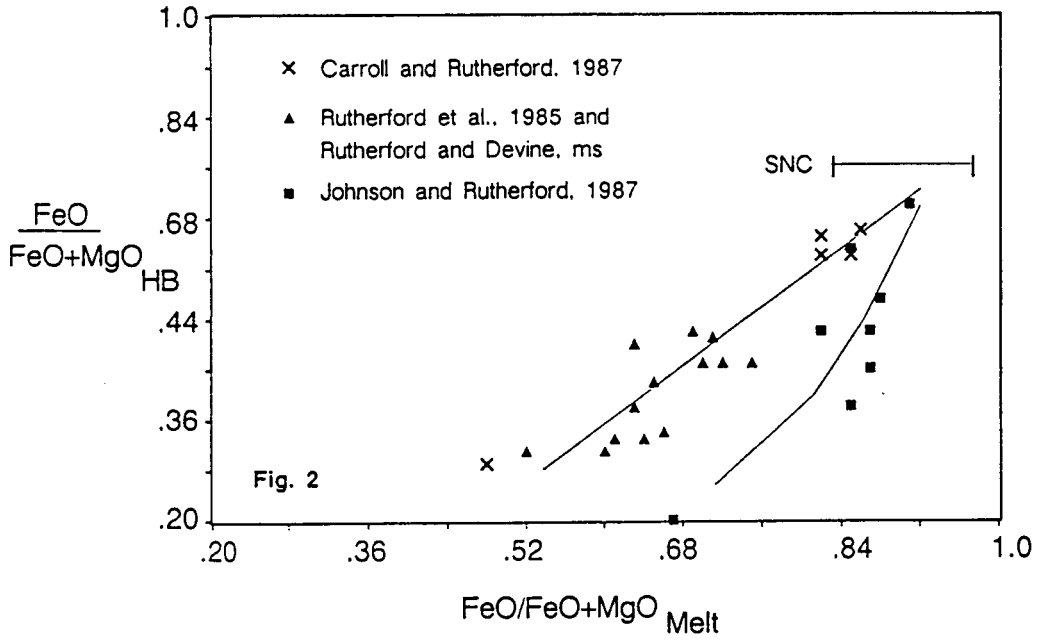
Carroll and Rutherford, 1987
Rutherford et al., 1985 and
Rutherford and Devine, ms
Johnson and Rutherford, 1987
SNC
FeO
FeO+MgO HB
1.0
.84
.68
.44
.36
.20
.20
.36
.52
.68
.84
1.0
FeO/FeO+MgO Melt
Fig. 2

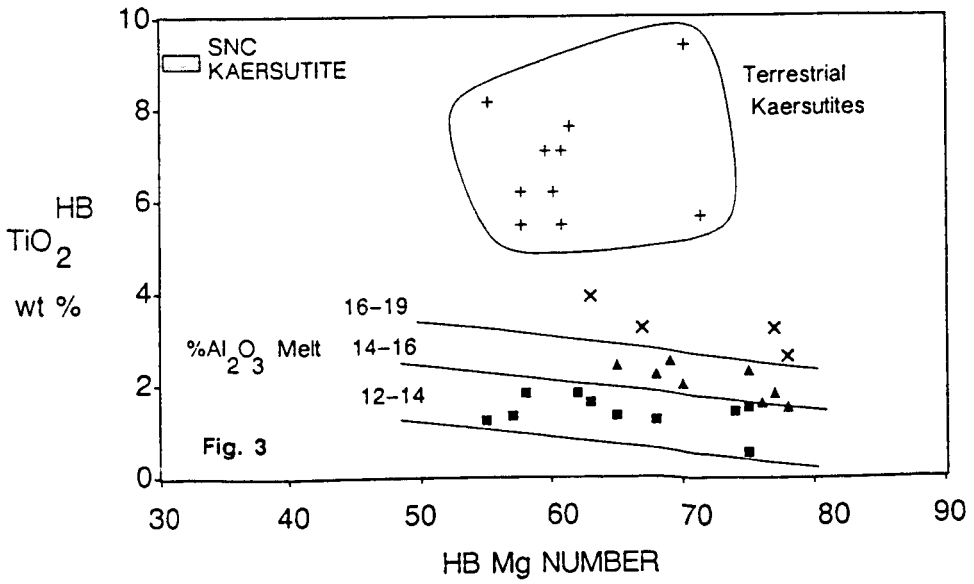
SNC
KAERSUTITE
Terrestrial
Kaersutites
HB
TiO2
wt %
10
8
6
4
2
0
%Al2O3 Melt
16-19
14-16
12-14
30
40
50
60
70
80
90
HB Mg NUMBER
Fig. 3

B1720314 N88-29694 540-91
154240
38

EARLY CRATERING RATES AND THE NATURE OF THE MARTIAN CRATERED UPLANDS;

P.H. Schultz, Dept. of Geological Sciences, Brown University, Providence, RI 02912

The cratered uplands of Mars represent a complex sequence of reworked crater ejecta, distant basin ejecta deposits, sedimentary (aeolian and fluvial) deposits, and possible volcanic plains. The heritage of the early period of impact bombardment is documented in the preserved cratering record where the areal density of large craters (>20 km) exceeds that of the Moon and subtle relicts of large impact basins remain. The cratering record provides a means to estimate the early impact flux on Mars, to constrain the direct and indirect effects of the impact process over various scales, and to evaluate the nature of the cratered upland surface materials. Four issues are addressed: the early martian cratering rate; the role of late-stage atmospheric accretion of volatiles; the relative effects of craters and basins on the global redistribution of crustal materials; and the indirect longer term effects of basin formation.

Early Cratering Rate: The cratering record of the martian uplands is partly masked by once more active erosional/depositional process and the possible global resurfacing by large impacts. An estimate of the early cratering rate must allow for or avoid such effects. One approach references the cratering record superposed on the youngest major impact basins, Argyre and Isidis, to subsequent martian units, thereby establishing a relative chronology. An absolute chronology requires referencing this history to the lunar time scale and can result in unacceptable surface ages, e.g., an age older than the planet if referenced to the estimates of the present-day flux. Another approach does not require a precise match over the entire martian time scale but only over a more limited time interval since basin formation. The total impact flux and change in impact flux over such time intervals provide explicit implications for the dynamical evolution of martian impactors and permit constraining the possible effects of impact cratering during early martian history.

Figure 1 compares the observed cumulative crater densities on Isidis, Argyre, the Elysium knobby terrains (relicts of dichotomy formation), and the old ridged plains of Hesperia on Mars with the cumulative crater densities on the lunar Imbrium and Orientale basins. The observed difference between crater densities on the youngest lunar and martian impact basins could reflect one or a combination of several processes: (a.) erosional enlargement of craters used in the statistics; (b.) an excessive number of large martian impactors; (c.) secondary impacts from post-Argyre, Isidis-size impacts now removed or buried (e.g., Tharsis region); (d.) martian basin ages much older than the last lunar basins; and/or (e.) a once higher impact flux on Mars. The first process cannot account for the observed difference alone since preserved relief of crater rims is inconsistent with excessive crater widening. Although the second suggestion is possible, it is difficult to prove. The third suggestion is also possible but there is no other evidence for such a feature (e.g., a regional gradient in the areal density of 20-50 km craters). If the lunar and martian impact flux of objects $< 10^{18}$ g were always the same, then time of formation of Isidis and Argyre would date from an unreasonably early epoch (4.5 by), even after correcting for the difference between lunar and martian gravity. The following discussions, therefore, focus on the consequence of the fifth possibility: the flux of objects $< 10^{18}$ g following the period of major basin formation on the Moon and Mars was different. Limits on how much they differ can be made by examining the consequences of two assumptions: the assumed age of a selected martian impact basin and the decay rate in the supply of martian impactors. If the Isidis basin on Mars dates to 3.78 by, about the age of Orientale impact on the Moon (1), then the last exposed major basin on Mars (Argyre) dates back to 3.67 by and the martian impact flux was 17 times the lunar flux at the time (after corrections for martian gravity and average impact velocity and an assumed Moon-like decay rate of impactors with a half-life of about 130 my). If the Isidis basin dates to 4.0 by, then Argyre dates to 3.88 by and the impact flux was 5 times the lunar flux. Figure 2 compares the consequences of different decay rates.

An important implication of such an approach is that the rate of surface processes acting to modify primary basin features or the subsequent cratering history can be largely constrained since small features from this epoch (e.g., narrow valley networks) remain preserved. If the observed fall-off in craters smaller than 18 km recorded in the massif/scarp annulus of Isidis reflects an early period of resurfacing, then the crater removal rate on Mars at this time approached the present terrestrial value given by Grieve (2). Although a longer half-life in the decay of post-basin impactors (e.g., 267 my) extends the time interval and decreases the inferred rate of crater removal, unreasonable constraints on the dynamical evolution of impactors and the absolute age of younger

geologic units result: the ridged plains such as Lunae Planum approaching 2.5 by and the impact flux equaling the present rate at 2.0 by.

Accretion, Erosion, and Release of Volatiles by Impact: Even the presently tenuous martian atmosphere shields the surface from impacts by small objects. Since the present atmospheric density on Mars at 80 km is comparable to the present terrestrial value at 100 km, atmospheric break-up prevents 50 m diameter craters from forming (3). Smaller mass objects (~ 1 g) are melted and vaporized during entry and essentially accreted by the atmosphere. On the Moon such impacts result in a net mass loss. If the incoming small mass were volatile-rich cometary material, a maximum equivalent of 15–30 precipitable meters (ppm) of water could have accreted in the 100 million years following Isidis (Figure 3). The post-Argyre accretion rate amounts to 4–11 ppm in the same time period but within 500 my this potential supply dwindled to less than 10 cm every 100 my. The values during and soon after the period of major basin formation approach estimates for water released by internal processes (4). The influx of cosmic volatiles would not result in rainfall but would become incorporated into the atmosphere or scavanged by atmospheric dust, thereby never directly affecting atmospheric pressure.

A competing process of atmospheric blow-off has been proposed (5) but the efficiency of the process remains in debate (6). Recent experimental studies (7) indicate that impact angle is very important in controlling target vaporization even at relatively low impact velocities (5 km/s). Impact vaporization may be more important in recycling (rather than removing) near-surface volatiles. From the derived impact rate, one 100 km-diameter crater would form in a 60,000 year interval (on the average) with less than 1 cm of ejected debris distributed globally. The Argyre impact basin, in contrast, would result in a global deposit 50–400 m with a 0.2–1.4 bar increase in atmospheric pressure if 1% of the excavated debris were released as volatiles. The catastrophic effects of a major basin therefore far outweigh the incremental effects of smaller and more frequent large impact craters. At basin scales, volatiles can be released not only by impact vaporization but also by distant ejecta re-entering the atmsophere, by ejecta impacting the surface, and by rapid devolatization of an exposed martian mantle. Released volatiles as well as suspended ejecta likely will be drawn back to the basin by strong recovery winds (as seen in the laboratory) and large thermal gradients created above the cooling basin cavity.

Recent comparisons of impact basin ages and associated plains-forming volcanism indicate that tectonism/volcanism persists only for a characteristic time following impact (8). It is proposed that volatiles released by the impact and collected within the basin, whether due to the initial atmospheric response to the impact or due to later orographic control of aeolian (and volatile) deposition, were subsequently recycled during basin-controlled volcanism. As the frequency of major basins decreased, the rate of recycling decreased until the re-trapping or escape rate of volatiles could not be offset by either internal or external sources (9) as illustrated in Figure 4.

Summary and Implications: The cratered uplands evolved not only from the local effects of large impact craters (20–200 km) but also from the global consequence of major basin formation. During the very late period of high impact bombardment (4.0 by), the martian crust may have received volatiles not only from internal heating but also from accretion of impactors too small to form impacts. Although impacts producing 100 km diameter craters are significantly more numerous than 1000 km impact basins, basin-scale impacts can be shown to have a much more important effect on the global redistribution of debris and the release of trapped volatiles perhaps expressed by a brief period of widespread unconformable deposits (10, 11) and the decrease in production rate of narrow-valley networks (12) before the development of the Tharsis volcanic constructs. The cratered uplands preserve this complex depositional history in a manner very different from the lunar highlands.

(1) Wilhelms, D. (1984) In *Geology of the Terrestrial Planets*, NASA SP-469, 107–197. (2) Grieve, R. (1984) *J. Geophys. Res., 89*, B403. (3) Gault, D. and Baldwin, B. (1970) *Trans. Am. Geophys. Union (EOS), 51*, 342. (4) Greeley, R. (1987) *Science 236*, 1653–1654. (5) Watkins, H. (1983) *The Consequences of Cometary and Asteroid Impacts on the Volatile Inventory of the Terrestrial Planets*, Ph.D. Dissertation, MIT, Cambridge. (6) Walker, J. (1986) *Icarus, 68*, 87. (7) Schultz, P. and Gault, D. (1986) In *Lunar and Planetary Sci. XVII*, Lunar and Planetary Institute, Houston, 779–780. (8) Wichmann, R. and Schultz, P. (1987) In *Lunar and Planetary Science XVII*, Lunar and Planetary Institute, Houston, 1978–1979. (9) Schultz, P.H. (1987) *Kagaku 57*, 486–496. (10) Grant, J. and Schultz, P. (1987) this volume. (11) Grizzaffi, P. and Schultz, P. (1987) submitted to *Icarus*. (12) Schultz, P. and Britt, D. (1986) In *Lunar and Planet. Sci. XVII*, Lunar and Planetary Institute, Houston, 775–776.

ORIGINAL PAGE IS
OF POOR QUALITY

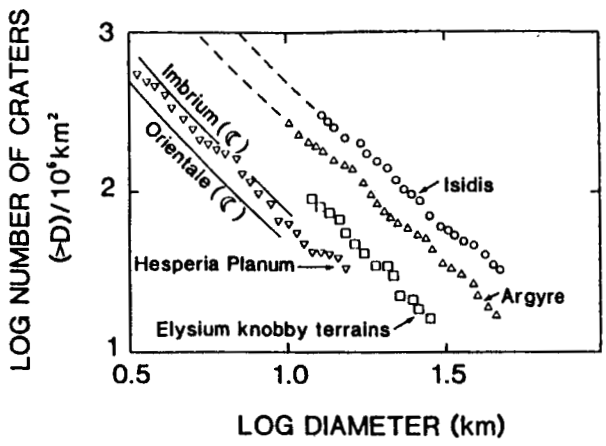

Figure 1. Relative crater densities on the last major martian impact basins (Isidis, Argyre), martian units, and the last major lunar impact basins.

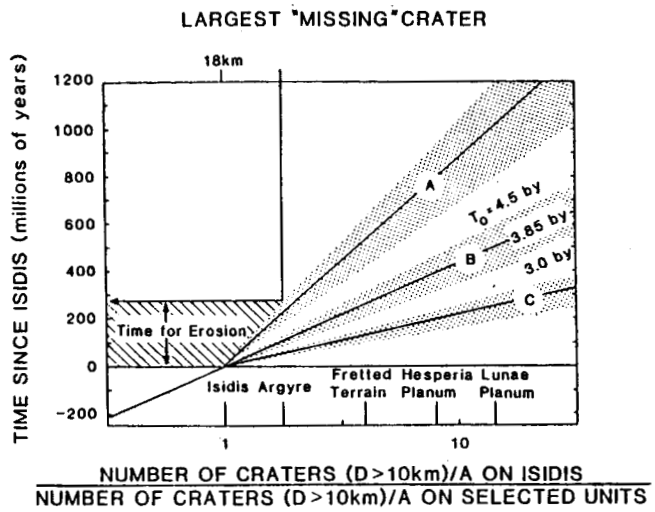

Figure 2. Absolute time intervals based on three different formation times of the Isidis impact basin (4.5, 3.85, 3.0 by) and three different exponential half-lives of impactors (A, B, C). Model A corresponds to a long half life (267 my); B, to a half-life comparable to post-basin lunar values (133 my); and C, to a very short half life (67 my). The inferred removal of 18 km diameter craters on Isidis but not on Argyre constrain the time for erosion.

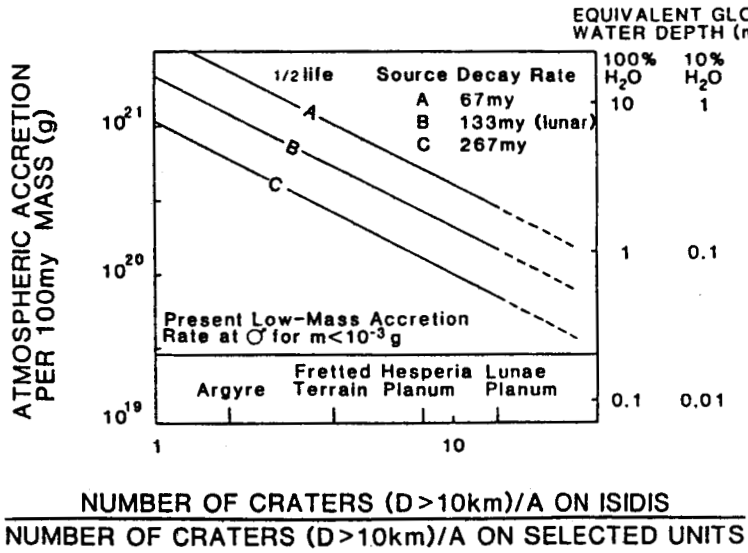

Figure 3. Atmospheric accretion of meteoritic material over 100 my for different assumed source decay rates corresponding to Figure 2 for an assumed age of Isidis equal to the lunar Imbrium basin. The potential depth of added exogenic water is indicated at right for different impactor types (cometary, 100%; C1 chondrites, 10%).

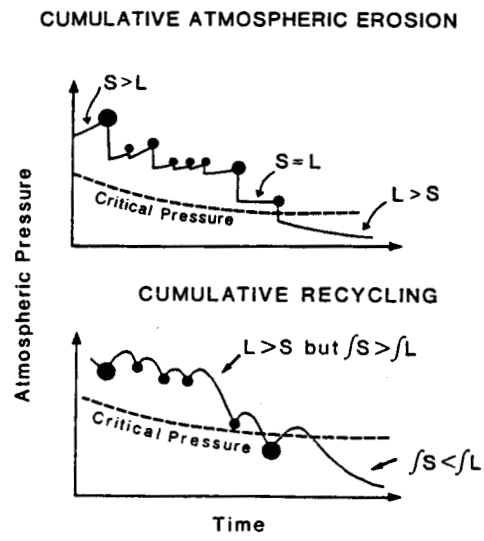

Figure 4. Two contrasting scenarios for episodic supply (S) and loss (L) of volatiles through time in response to formation of different size impact basins (dots of different sizes). In the model at top, the supply of volatiles to the atmosphere at first exceeds the natural loss rate (exospheric, regolith adsorption, etc.) punctuated by sudden impact-triggered losses. Eventually the loss exceeds the supply and the martian atmospheric pressure falls below a level allowing surface runoff of water. A different model (bottom) proposes atmospheric volatile losses generally exceeding the supply at a given time but basin-controlled impact release and hydrothermal recycling replenishes the atmosphere during a finite period of basin-controlled volcanism.

GU 65948

N88-29695

DOCUMENTING VOLCANO-TECTONIC EPISODES IN MARS' STRATIGRAPHIC RECORD;

David H. Scott and Kenneth L. Tanaka, U.S. Geological Survey, Flagstaff, Ariz.

INTRODUCTION

New global geologic maps of Mars at 1:15,000,000 scale [1,2,3] have been digitized to obtain accurate measurements of the areal extent of 90 geologic units. These data were used to determine the resurfacing history of Mars by volcanic, eolian, fluvial, periglacial, and impact processes [4]. We presently are extending this work to focus on the extent, magnitude, and duration of volcanism and tectonism (mainly faulting) throughout each of the three time-stratigraphic systems. This work involves detailed mapping to assess volcano-tectonic episodes in terms of their occurrence in eight epochs that represent subdivisions of Martian periods [5].

MAPPING TECHNIQUES

The global geologic maps of Mars consist of three sheets: (1) western equatorial region, (2) eastern equatorial region, and (3) north and south polar regions. For each of these map sheets, we have prepared three sets of maps (nine in all) showing the areal distribution of materials in the Amazonian, Hesperian, and Noachian systems. Individual faults or fault groups (too numerous to show separately) that originated during each Martian period were then mapped on each sheet. This task could be accomplished because the great majority of faults on Mars can be related to their transection, embayment, or overlap positions with respect to specific time-stratigraphic geologic units.

RESULTS AND GENERAL OBSERVATIONS

Results of the mapping show that structural deformation throughout Martian geologic history has been almost entirely confined to large elevated volcanic centers--Tharsis Montes, Syria Planum, Olympus Mons, Alba Patera, and the Elysium Mons. Faulting associated with Valles Marineris may be an exception. The Tempe Terra and Acheron Fossae regions are also highly faulted and have prominent, but relatively low relief, volcanic structures. The volcanoes of Tempe Terra lie on the northeast extension of the Tharsis Montes volcanoes. The large known impact basins on Mars, particularly Isidis Planitia, are ringed in places by concentric faults as are basins on the Moon. The Martian basins do not have complex (transverse, radial, and concentric) fault systems that are commonly seen around the large centers of volcanism and uplift on Mars.

The formational sequence of structural landforms in the Syria Planum region of Mars recently has been studied and documented in detail [6,7]. Our work will follow the analytic procedures used in the Syria Planum study for the other volcano-tectonic regions on Mars. In addition, our mapping procedures will allow the magnitude of tectonic deformation as expressed by faulting to be quantitatively measured for each Martian period and epoch. Faults, within fault systems, that have been reactivated during various time periods will be traced in order to estimate the duration and interplay of stress fields associated with the large tectonic centers.

Although our current studies have been restricted to structural dislocations of Mars' surface, other relations among features of probable tectonic origin can be documented further. The pervasive ridge systems, for example, that occur within lava flows of Noachian, Hesperian, and Amazonian age have trends and large-scale spatial distributions that commonly are nearly normal to extensional faults and grabens. It certainly will be important to

determine their relative times and modes of origin.

REFERENCES

[1] Scott, D.H. and Tanaka, K.L. (1986) USGS Map I-1802-A.
[2] Greeley, R. and Guest, J.E. (in press) USGS Map I-1802-B.
[3] Tanaka, K.L. and Scott, D.H. (in press) USGS Map I-1802-C.
[4] Tanaka, K.L. and others (in press) Proc. Lunar Planet. Sci. Conf. 18.
[5] Tanaka, K.L. (1986) Proc. Lunar Planet. Sci. Conf. 17, E139-158.
[6] Tanaka, K.L. and Davis, P.A. (1986) PLPSC 18 (abstract), 994-995.
[7] Tanaka, K.L. and Davis, P.A. (work in preparation).

AX 852975
N88-29696

THE SURFACE COMPOSITION OF MARS FROM EARTHBASED OBSERVATIONS

R.B. Singer, Lunar and Planetary Laboratory, Univ. of Az., Tucson, AZ 85721

This talk is intended as a tutorial about our current knowledge of the martian surface from earthbased spectral reflectance observations, and what we do (and don't) expect to be able to determine from orbital reflectance spectroscopy and spectral imaging. A companion tutorial is to be delivered about Viking Orbiter and Lander observations. It is hoped that these presentations will initiate significant discussion bridging the gap between remote sensing and more traditional geologic methods. The reader is referred to a review paper (1) for more information and detailed references. Because of space limitations only work since that paper is referenced in this abstract.

GENERAL

Much of our current information about the composition of Mars comes from earthbased spectral measurements. Like any other diagnostic tool, reflectance spectroscopy has strong and weak points. The sophistication of this technique is actively being improved, and along with this progress comes dissent, some failures, and occasional hype and over-sell. Nevertheless, the successes of reflectance spectroscopy for Mars and other planets are undeniable - it is not an accident that imaging spectrometers are important parts of most new scientific payloads.

To first order Mars has two classes of surface materials: bright, heavily altered materials and dark, less altered materials. It has been known for a long time that the distribution of bright and dark regions has no simple correlation with regional geomorphologic units. When observed spectrally, bright and dark surface regions on Mars show features which are indicative of certain important aspects of chemistry and mineralogy. Because these features are often combined and superimposed on the spectral continuum of the altered dust, they are more subtle and often more complicated to interpret than for "clean" minerals or rocks. This does not, however, mean that all diagnostic information is lost. On the scale of telescopic spatial resolution (>300km) regional variations have been observed within both bright and dark albedo classes, despite the large degree of surface-component mixing which certainly occurs within these large observational footprints.

The two major atmospheric impediments to reflectance spectroscopy of the surface are gaseous CO_2 and aerosol dust. The former has specific absorptions at well-documented positions which can either be bypassed for some analysis tasks or modeled out. Attempts at CO_2 modeling so far have not been very successful, in part because of the complicating effect of scattering from aerosol dust. The aerosol dust itself appears to be a fine-grained version of the brightest and reddest weathered soil material observed on the surface - its spectral properties are fairly well known. An operational procedure for modeling out the combined effects of dust and CO_2 is an important goal prior to Mars Observer. But to keep things in perspective, despite all of these problems, and without sophisticated corrections, we still detect quite real spectral features and differences which tell us a great deal about the surface composition of the planet.

SOILS AND DUST

Ferric Iron Fe^{3+} in some form has long been known from earthbased observations to be the "coloring agent" on Mars. All surface regions observed spectrally have an intense but relatively featureless absorption edge from about 0.75μm to the near-ultraviolet. The slope is steeper for bright regions than dark regions, indicating more ferric iron. This absorption edge is attributed to combinations of Fe^{3+} crystal-field and charge transfer absorptions. Spectroscopy in the UV and visible is very sensitive to Fe^{3+} and its mineralogic context. Well-crystallized ferric oxides and ferric-iron bearing clay minerals have distinct absorption features not seen for Mars - the best (but not perfect) spectral analogs are certain amorphous iron-silica gels (palagonites) which form by low-temperature alteration of mafic volcanic glass. (It is important to restate here that the term palagonite encompasses many somewhat different materials, and that only a limited subset of palagonites are good spectral analogs for Mars.) The assignment of the name "palagonite" somewhat sidesteps the issue of what the short-range mineral structure might be similar too. Recent work has indicated that very-fine-grained crypto-crystalline hematite might be responsible as the coloring agent (2). Somewhat separately, a number of Viking multispectral studies have indicated that ferric iron in typical martian soils may be slightly better crystalline than the terrestrial palagonite analogs, and that crystalline hematite might occur in some regions (e.g. 3,4).

During some observing years classic bright regions such as Arabia show a weak Fe^{3+} band near 0.87μm. Optically thick aerosol dust clouds appear spectrally almost identical. At other times the same or similar surface regions show a band at longer wavelengths indicative of some Fe^{2+} influence. There is a fairly good correlation between band position and surface dustiness, leading to the conclusion that at least some of the oxidized bright soils also contain less-oxidized Fe^{2+}-bearing components (mafic minerals, glass) which are are sometimes masked by temporary deposits of aerosol dust.

Bound Water and Structural OH - Clay Minerals The martian surface certainly contains some molecular water and OH, as attested to by the deep "3-μm" absorption envelope first observed decades ago. The surface is nevertheless quite dessicated relative to Earth. Structural OH and molecular water features near 1.4 and 1.9μm have not been seen for Mars. Although these spectral regions are complicated by atmospheric CO_2 absorptions, deep water/OH bands should be apparent if present. At 2.36μm there is a very weak absorption generally attributed to structural Mg-OH bonds, but with at least a factor of 3 less band depth than expected for a well-crystallized clay mineral. The conclusion from this is that either 1) crystalline clays are a minority phase mixed with other materials (e.g. palagonite), or 2) the bright soils are homogeneous but structurally intermediate between amorphous palagonites and crystalline clays. The martian atmosphere is essentially opaque at the location of the diagnostic OH vibrational fundamental near 2.75μm. New telescopic observations throughout the 3-μm region, however, define and differentiate the long wavelength edge of what is apparently a structural OH absorption from absorptions at slightly longer wavelengths due to bound H_2O (5). These results also indicate that observed soils on Mars are at least somewhat more crystalline than the most amorphous palagonite analogs. With some recently completed laboratory studies (6) and some additional work reflectance spectroscopy will be an effective tool for quantitatively determining surface water content on Mars.

Carbonates and Other Salts There has been much interest in the possible occurrence of carbonate minerals on Mars as indicators of a wetter climate and a much thicker CO_2 atmosphere in the past. Other salts, such as sulfates and nitrates, have also been suggested as likely secondary soil constituents. These phases are spectrally very active in the infrared longward of about 3μm, although weaker overtone bands occur at shorter wavelengths. Such overtone bands are not observed for Mars. Recent observing emphasis in the 3-5μm region (7,8) has also failed to detect absorptions attributable to salts, placing a very rough upper limit of a few weight percent carbonate in the regolith if uniformly distributed. The existence of small, spatially localized exposures of carbonate cannot readily be tested from Earth - the VIMS instrument on MO will be able do an excellent job of investigating these.

PRIMARY CRUSTAL MATERIALS

Much information about primary crustal materials is available in the near-IR, primarily due to Fe^{2+} crystal-field bands generally located near 1μm and 2μm. Diagnostic spectral information is controlled by the size and shape of the Fe^{2+} crystallographic site. Orthopyroxenes and clinopyroxenes are readily differentiable, and iron and calcium contents can be estimated fairly accurately. Olivine also has a very diagnostic band shape. Mafic glass has weaker and broader diagnostic bands than its crystalline counterparts, due to its irregular structure. The interpretive complications only arise when these components are mixed together, as in a basaltic rock. When additionally complicated by coating or mixture with fine-grained altered dust, most of this information is still not lost, but is much harder to extract correctly. Much effort has been expended to uniquely deconvolve overlapping absorption bands such as these - additional analytical techniques are currently being developed and evaluated. Much of the debate about interpretation of martian crustal chemistry revolves around the validity of these techniques.

The crust appears to be dominated by basaltic, but not necessarily ultramafic, rock. Much of this rock is crystalline and relatively unaltered, as evidenced by ubiquitous pyroxene absorptions in the 0.95-0.99μm region for dark region observations. In some dark regions a pyroxene band somewhat longward of 2μm has also been observed. If these spectral features are due primarily to a single pyroxene, their positions indicate a high-iron and low- to moderate-Ca clinopyroxene. If however there is a significant contribution from both CPX and OPX the compositions cannot be as well constrained at this time. Olivine and/or basaltic glass is also possibly evident in some of the dark region observations, although its presence is debated and must be confirmed. Clearly additional work needs to be done prior to Mars Observer. But the fact that evidence of mafic crustal components is obvious even with the large, well-mixed footprint observed from Earth indicates that orbital spectral measurements, with much higher spatial resolution, will sample "cleaner" crustal exposures, from which quite good interpretations will be possible.

(1) Singer, R.B., Adv. Space Res., v.5, #8, 59-68, 1985 (COSPAR). (2) Morris, R.V. et al., LPSC XVIII, 668-669, 1987. (3) Guinness, E., et al., J. Geophys. Res., v.92, #B4, E575-E587, 1987. (4) Soderblom, L.A., et al., Icarus, 34, 446-464, 1978. (5) Roush, T.L., et al., this abstract volume, 1987. (6) Roush, E.A. and R.B. Singer, Effects of Sample Dehydration on Reflectance Spectra..., submitted to J. Geophys. Res., June 1987. (7) Singer, R.B. et al., Bull. AAS., 18, 1986. (8) Blaney, D.L. et al., LPSC XVIII, 85-88, 1987.

JJ574450 S43-91
N88-29697 34943 28 125

MARS EARTH-BASED RADAR: 1986 RESULTS AND 1988-1990 OPPORTUNITIES

T. W. Thompson, Jet Propulsion Laboratory,
California Institute of Technology, Pasadena, CA 91109

Earth's orbit around the Sun is nearly circular, while Mar's orbit is slightly elliptical. When earth-based radars observe Mars, the echo strength is proportional to the inverse fourth power of the Earth-Mars distance. Thus, earth based radar observation are done near oppositions when the earth-Mars distance is less than 1.0 AU. Furthermore, radar echoes for the best oppositions near perihelion are about ten times stronger than the worst oppositions near aphelion. The 1986, 1988, and 1990 oppositions of Mars are near perihelion and provide excellent opportunities for earth-based radar observations of Mars. The last oppositions at perihelion occurred in the 1971 and 1973, while the next oppositions at perihelion occur in 2001, 2003 and 2005.

Earth-based radar coverage on Mars is along the subearth track, as these areas have the strong echoes which dominate the radar return. The subearth tracks for the 1986, 1988, and 1990 oppositions are south of Mars equator. The 1986, 1990 coverage is 0^{o} to 12^{o} south, while the 1988 coverage is 20^{o} to 25^{o} south. The 1971-1973 coverage was 14^{o} to 22^{o} south. Thus the combined coverage is from the equator to 25^{o} south which is 20 percent of the Mars surface and about one half of possible earth-based coverage. The coverages for oppositions for the mid 1990's opposition will be from the equator to 25^{o} north. Earth-based radar echo strengths and sub-radar latitudes for the next two decades are shown in Figure 1.

Mars observation in 1986 were made by the Goldstone Solar System Radar, the high power radars associated with 64m antenna operated by the Deep Space Network Complex north of Barstow, California. There were twenty-six 12.5cm wavelength and two 3.5cm wavelength tracks. These observations were conducted with the cw-spectra techniques used by Harmon et al. (1982 and 1985). A continuous tone was transmitted at Mars and the radar echo was sampled to obtain a Doppler-spread spectrum. Each received cycle was separated into polarized (opposite sense circular, OC) and depolarized (same sense circular, SC) periods.

Observed echo strengths have been converted to radar reflectivity and inferred bulk dielectric constant as shown in Figure 2. Coverage on Mars started at 8^{o} S in June 1986, travelled north toward the equator to 3^{o} S during August, and then migrated south to 14^{o} S for the last run in October 1986. These are new areas for earth-based radars. Longitudes 180^{o} to 90^{o} have low polarized (OC) reflectivities, high depolarized (SC) reflectivities and inferred bulk dielectric constants of 3.0-4.0. These values in general agree with those observed by Harmon et al. (1985) for the Tharis region north of the equatorat the same longitudes. In contrast, longitudes 75^{o} to 0^{o}, the Valles Marineris, have high polarized (OC) reflectivities, lower depolarized reflectivities and inferred bulk dielectric constants near 5.0. Longitudes 360^{o} to 180^{o} have intermediate values with inferred bulk dielectric constants of 3.5-4.5. Further analysis of the observed spectra will yield estimates of rms slopes.

MARS EARTH-BASED RADAR: 1986 AND 1988-1990 OPPORTUNITIES

T. W. Thompson

References:

J. K. Harmon, D. B. Campbell, and S. J. Ostro (1982), Dual-Polarization Radar Observations of Mars: Tharsis and Environs, Icarus, 52, 171-187.
J. K. Harmon and S. J. Ostro (1985), Mars: Dual-Polarization Radar Observations with Extended Coverage, Icarus, 62, 110-128.

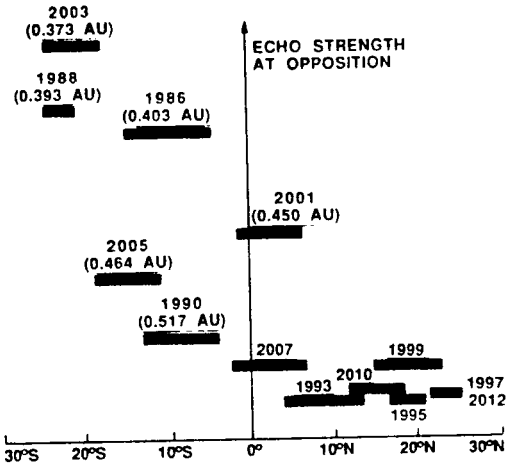

Figure 1 Mars Echo Strength versus Subradar Latitudes: 1986-2012

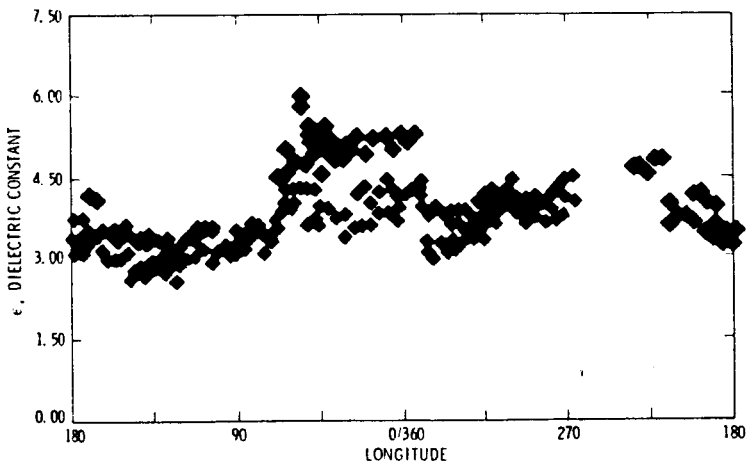

Figure 2. Mars Bulk Dielectric Constants versus Longitude: 1986

BU 370927 N88-29698 544-91 154944 127

CRYSTAL FRACTIONATION IN THE SNC METEORITES: IMPLICATIONS FOR SURFACE UNITS ON MARS

Allan H. Treiman, Geology Department, Boston University, Boston MA 02215

Almost all rock types in the SNC meteorites are cumulates, products of magmatic differentiation by crystal fractionation (addition or removal of crystals). If the SNC meteorites are from Mars' surface or near sub-surface, then most of the igneous units on Mars are differentiated. Basaltic units probably experienced minor to moderate differentiation, but ultrabasic units probably experienced extreme differentiation. Products of this differentiation may include Fe-rich gabbro, pyroxenite, peridotite (and thus serpentinite), and possibly massive sulfides.

The SNC meteorites include ten lithologies (three in EETA79001), eight of which are crystal cumulates [1]. The other lithologies, EETA79001 A and B, are sub-ophitic basalts. The cumulate lithologies ALHA77005 and EETA79001C have not been fully described and are not discussed here.

Shergotty and Zagami

The Shergotty and Zagami meteorites, diabases or fine-grained gabbros, are enriched in clino- and ortho-pyroxene relative to their parental magmas [2]. It has been suggested that the pyroxene enrichments arose through crystal settling [3], but this is unlikely. The parent magmas were basaltic, and thus had significant yield strengths. If the parent magmas had yield strengths like those of terrestrial basalts [4], the stress generated by a pyroxene crystal would have been below the yield strength of the magma (e.g. [5]). The pyroxene would not move.

Another fractionation mechanism, crescumulation, is more likely for Shergotty and Zagami. Crescumulates form at moderate undercoolings when new crystals nucleate at the walls of a magma body and grow inwards as elongate blades. The blades continue to grow as the melt among them is replenished by exchange with the bulk magma. As the blades grow wider, melt among them is "squeezed out". Typical features of crescumulates are: mild to moderate enrichment in the blade minerals; grains with quench morphologies; grains longer (greater aspect ratios) than usual for the mineral species; and moderate lineations of the elongate minerals without strong foliation [6-8]. Examples of crescumulates include spinifex zones in komatiites [6], harrissite in ultrabasic intrusions [7], and "Willow Lake textured" rock in gabbros and basalts [8].

Shergotty and Zagami have most of the petrographic features of crescumulates. They are mildly enriched in pyroxenes relative to their parental magmas [2]: Shergotty is 28% and Zagami is 45% cumulus pyroxenes. Some whitlockite grains in Shergotty are very elongate and rich in inclusions. [9], a typical quench morphology. Pyroxenes in Shergotty and Zagami are more elongate that typical basalt pyroxenes, which have aspect ratios <3; in Shergotty, aspect ratios range up to 7 or possibly 20 ([10], Fig. 1). The pyroxenes also show a preferred elongation direction [2, 10], which could be a lineation, a foliation, or both.

The compositions of crescumulates are generally not greatly different from those of the parent magma. An example is the Wabewawa flow, Kirkland Lake, Ontario. This hundred-meter thick basalt/gabbro flow has approximately 20 meters of crescumulate gabbro near its top, but otherwise shows no evidence of significant fractionation.

Nakhlites and Chassigny

The nakhlites and Chassigny are ultramafic igneous rocks, rich in augite and olivine respectively. They are cumulates, strongly enriched in crystals relative to their parental ultrabasic magmas [11-12]. The nakhlites and Chassigny are inferred to have formed through settling of crystals [11-13]; this inference is surest for the nakhlites because their cumulus augites form a grain-supported framework, and because the augites have preferred orientations typical of sediments [13]. Non-Newtonian behavior of the magma is unimportant because ultrabasic magmas have low yield strengths (e.g. [14]).

On Earth, ultrabasic flows and sills commonly differentiate to yield peridotite, pyroxenite, and Fe-rich gabbros [15, 16]. Petrographically, these pyroxenites and peridotites are almost identical to the nakhlites and Chassigny [17]. Uncommonly, enrichment in sulfide minerals occurs in such bodies [18], partly through interaction of magma and sulfur-rich wall-rock [19].

Conclusions

Almost all of the SNC meteorite lithologies are products of crystal fractionation; thus, many of the surface units on Mars may be strongly differentiated. Basaltic igneous bodies (e.g. sources of shergottites) may have experienced only moderate crystal fractionation. Enrichment in pyroxene (e.g. Zagami) or in plagioclase is possible, but formation of pyroxenite or anorthosite is unlikely. Ultrabasic igneous bodies (e.g. sources of nakhlites and Chasssigny) will have experienced extreme crystal fractionation. The products of fractionation (peridotite, pyroxenite, and Fe-rich gabbro) may be recognizable thorugh remote sensing, especially because Martian minerals are inferred to be rich in Fe (e.g. [1]). Peridotites (olivine rich) may have been altered to hydrous mineral assemblages (e.g. [20]). Sulfide-rich rocks and their alteration products might have distinctive reflection spectra, and might be sources of iron oxides in the regolith.

References

[1] McSween H.Y.Jr. (1985) Rev. Geophys. 23, 391-415. [2] Stolper E. and McSween H.Y.Jr (1979) Geochim. Cosmochim. Acta. 43, 1475- 1498. [3] Grimm R.E. and McSween H.Y.Jr. (1982) Proc. 13th Lunar Planet. Sci. Conf., J. Geophys Res. 87, A385-A392. [4] Basaltic Volcanism on the Terrestrial Planets, 1981, Pergamon Press. [5] Maaloe S. (1985) Principles of Igneous Petrology. [6] Donaldson C.H. (1982) 213-244 in Arndt & Nisbet eds, Komatiites. [7] Wadsworth W.J. (1985) Geol. Mag. 122, 549-554. [8] Taubeneck W.H. and Poldervaart A. (1960) Bull. Geol. Soc. Amer. 71, 1295-1322. [9] Jones J.H. et al. (1985) Meteoritics 20, 674-675. [10] Duke M.B. (1968) 613-621 in Shock Metamorphism of Natural Materials. (Mono Books). [11] Floran R.J. et al. (1978) Geochim. Cosmochim. Acta 42, 1213-1229. 12 Treiman A.H. (1986) Geochim. Cosmochim. Acta 50, 1061 1070. [13] Berkley J.L. et al. (1980) Proc. Lunar Planet. Sci. Conf. 11th 1089-1102. [14] Agee C.B. and Walker D. (1987) EOS 68, 437. [15] Arndt N.T. (1977) Can. J. Earth Sci. 14, 2620-2637. 16 Raudsepp M. and Ayres L.D. (1982) Can J. Earth Sci. 19, 837-858. [17] Treiman A.H. (1987) Lunar Planet. Sci. XVIII, 1022-1023. [18] Naldrett A.J. (1981) Econ. Geol. 75th Anniv., 628-685. [19] Ripley E.M. (1981) Econ. Geol. 76, 610-620. [20] Bunch T.E. and Reid A.M. (1975) Meteoritics 10, 303-315.

Hi 782 55 N88-29699 545-91 154945 30

MARTIAN SURFACE ANALOGS : LABORATORY SPECTRAL STUDIES IN THE MID INFRARED ; P. A. Walsh, D. L. Blaney, and T. B. McCord, Planetary Geosciences Div., Hawaii Inst. of Geophysics, U. of Hawaii, Honolulu, HI 96822

Ground-based telescopic reflectance spectra and analyses of Viking data have led to the conclusion that Martian surface fines are derived from a mafic to ultramafic source material[1,2,3], though the actual composition of these surface fines is still undetermined. A variety of possible compositions has been proposed by several authors, however, with salts, particularly sulfates and carbonates, as important components in many of these models. Although these salts are predicted components of the Martian surface, they have not been identified in telescopic reflectance spectroscopy observations to date[4,5]. One explanation for the absence of salts in these data is that they are not in quantities large enough to detect. This study was undertaken to determine the detectability of salts in various proposed Martian surface analog mixtures.

This study concentrates on the carbonate and sulfate spectral features in the 2.5 to 25 μm spectral range because of recent work showing the usefulness of weak bands in the mid infrared for the remote sensing of particulate planetary surfaces[6]. All measurements were made using a Nicolet 5SXC FTIR spectrometer with a bidirectional reflectance attachment, which uses an aluminum mirror as the background against which the sample is compared. The data were collected at two resolutions: at 64 cm^{-1}, which is comparable to that currently being collected by ground-based telescope instruments and at 32 cm^{-1}, which is comparable to the higher resolution expected from the Mars Observer VIMS.

The mixtures we examined are as follows:

a) Single and multi-component mixtures of salts in various weight percents in palagonite.

b) Stable gas-solid weathering products of a range of basalt compositions in thermodynamic equilibrium with the present Martian environment[7].

c) Stable gas-solid weathering products of a range of basalt compositions in thermodynamic equilibrium with the present Martian environment with metastable components [7].

d) Stable weathering products of a range of basalt compositions which have reached thermodynamic equilibrium with liquid water containing dissolved O_2 and CO_2 [7].

e) Stable weathering products of a range of basalt compositions which have reached thermodynamic equilibrium with liquid water containing dissolved O_2 and CO_2 with metastable components [7].

f) Mineralogic model components based on Viking XRF data[1,2].

g) Model compositions listed in b through f mixed in various weight percents with palagonite.

Palagonite is an amorphous iron-rich weathering product of mafic volcanic glass. Besides weathering, another way palagonite can be formed is by subglacial volcanic activity. Such activity, in which the interaction of hot basaltic lava interacts with glacial ice produces large masses of palagonite, has been well documented in Iceland[8]. A great

deal of palagonite should also be formed in the analagous situation of a mafic Martian lava erupting into the Martian permafrost[9]. Thus regardless of what the products of weathering on Mars are, they may still be mixed in a matrix of palagonite. In fact, palagonite is the closest known spectral analog to Martian dust and soil[10]. It is for this reason that we have run the other model mixtures both alone and mixed in palagonite.

The model with the fewest compositional components, and thus the simplest to interpret, is that with the single and multi-component mixtures of salts in various weight percents in palagonite. These samples were prepared by mixing palagonite from Mauna Kea, Hawaii, with various weight percent of a number of naturally occurring carbonate and sulfate salts. At the resolution of current telescopic instruments, individual salts can be detected with confidence at 5 wt%, and at 3 wt% with the increased resolution of VIMS (figure 1). Mixtures of two and three of these salts in palagonite yield similar detection limits. Since the spectral features of all carbonates in this region are primarily the result of the carbonate anion, they are differentiated by very small band shifts. Multi-component mixtures exhibit an average band position which appears to be linear with composition. The same trend seems to be true of the sulfates.

The effects of the more complex multi-component mixtures on salt detection will be discussed and the laboratory spectroscopic data presented.

References :

1) Baird A. K., Toulmin P., Clark B. C., Rose H. J., Keil K., Christian R. P., and Gooding J. L. (1976) *Science* 194, p.1288-1292.
2) Toulmin P., Baird A. K., Clark B. C., Keil K., Rose H. J., Christian R. P., Evans P.H., and Kelliher W. C. (1977) *J. Geophys. Res. 82,* p. 4625-4634.
3) Baird A. K., Weldon R. J., Tsusaki D. M., Schnabel L., and Candelaria M. P. (1982) *J. Geophys. Res. 87,* p. 10059-10067.
4) Houck J. R., Pollack J. B., Sagan C., Schack P., and Pecker J. A. (1973) *Icarus 18,* p.470-479.
5) Sinton W. M. (1967) *Icarus 6,* p.222-228.
6) Salisbury J. W., Hapke B., and Eastes J. W. (1987) *J. Geophys. Res. 92,* p.702-710.
7) Gooding J. L. (1978) *Icarus 33,* p.483-513.
8) Walker G. P. L. and Blake D. H. (1966) *Quart. J. Geol. Soc. London 122,* p. 45-61.
9) Clark B. C. (1978) *Icarus 34,* p.645-665.
10) Singer R. B. (1982) *J. Geophys. Res. 87,* p. 10159-10168.

Figure 1: Calcite in palagonite at 32 cm^{-1} resolution. a) Pure calcite b) 1 wt% calcite in palagonite c) 3 wt% calcite in palagonite d) 5 wt% calcite in palagonite e) Mauna Kea Palagonite

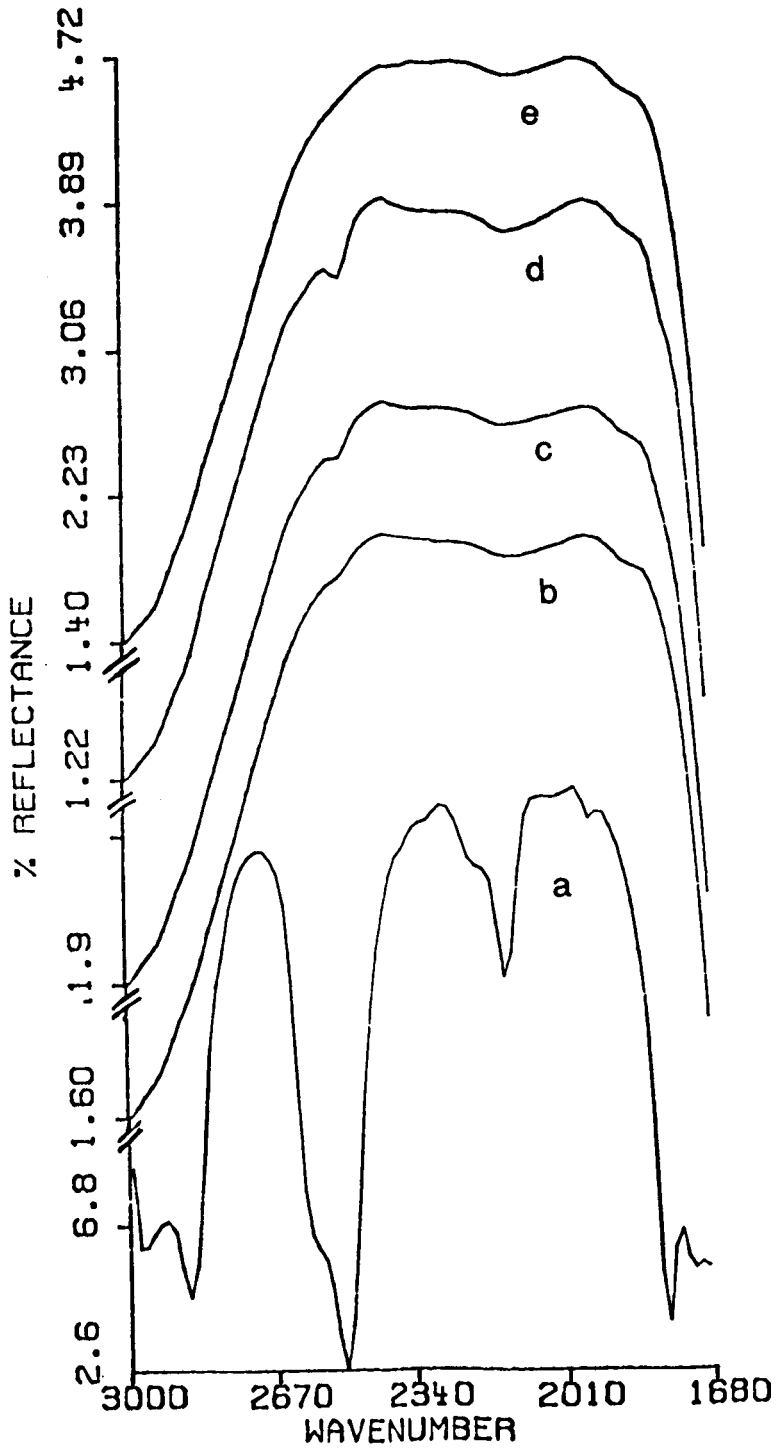

SD 413977
GU 717884 N88-29700

RIDGED AND GULLIED TERRAINS IN THE MARTIAN UPLANDS; D.E. Wilhelms and R.J. Baldwin, Geology Department, San Jose State University, San Jose, CA 95192 and U.S. Geological Survey (MS-946), Menlo Park, CA 94025

Two extensive types of geologic units in the martian uplands are ridged plains [1-3] and gullied ("valley-network") terrain [4-8]. The ridged plains, characterized by "wrinkle ridges" like those of the lunar maria, occupy depressions throughout the uplands. Gullied terrain is also widespread but is absent or rare in uplands dominated by plains or by large crater rims and basin rings [5,8]. The ridged plains are rarely gullied but the gullied terrain and other upland terrains are commonly ridged [9].

The gullies apparently have formed in a distinct type of geologic deposit that is superposed on the ejecta of old craters and that forms much of the intercrater terrain. The existence of this deposit in the study area (Fig. 1) is also supported by the very different appearance of areas where it is probably absent or thin, that is, the "primitive" crater-and-basin uplands [5,8]. The deposit probably consists of fragmental material (mostly impact debris and tuff) that acquired interstitial ice early in martian history when abundant water was being outgassed [7]. The deposit is Noachian, and the ridged plains Lower Hesperian, in Tanaka's martian stratigraphic scheme [10]. The Noachian-Hesperian boundary is 3.5 to 3.8 aeons old in the most likely calibrations of martian stratigraphy with that of the Moon [10].

A high density of craters in the gullied terrain has led to the assumption that the gullies themselves are old [4-7]. Many may indeed be almost as old as the deposit in which they occur. However, several very fresh-appearing crater rims and ejecta blankets are gullied (Viking Orb. 381S84). Also, our crater counts, in which superposed and buried craters are distinguished, suggest an overlap in age between the upper layers of the gullied deposit and the ridged plains (Fig. 1). This finding is somewhat subjective because of uncertain age assignments of some craters. Nevertheless, it means that some gullies are younger than commonly thought and probably approximate the ridged plains in age.

Three evident but heretofore inadequately explained geologic relations suggest that unexposed lateral extensions of the ridged plains lie topographically (though not stratigraphically) beneath the gullied deposit. (1) A generally common level of plains, for example in a crater floor and adjacent canyons, suggests a lateral continuity of the plains material in the subsurface. (2) Ridges in the gullied deposit, which by itself is probably too weak to deform into discrete narrow ridges, are reasonably explained as ridges that developed within the buried extensions of the plains material and that deform the overlying gullied deposit. (3) Transitional morphologies between the two types of terrain are likely to represent alterations of gullied terrain by the underlying plains. This is particularly evident where thin remnants of a gullied deposit lie on the surfaces of ridged plains, which otherwise have few gullies. Thus, the ridged plains are probably parts of extensive tabular units that happen to be exposed in depressions. The properties of the units are consistent with an igneous origin. The presence of extensive sills in the uplands is

also supported by dark layers visible in the walls of Valles Marineris and by dark flows that have emerged from the upland-lowland front [11].

We furthermore suggest that the gullies originated when the sills were emplaced. Subsurface flow of water, resulting in sapping of the surface material, is now widely accepted as the origin of the gullies [4-7]. The age similarities and the apparent "underplating" of the gullied deposit by extensions of the ridged plains material suggest that heat from the sills melted some of the interstitial ice in the overlying gullied deposit. The meltwater then seeped out and undermined the surface.

Thus, gullying apparently requires (1) the presence of an ancient (Noachian) ice-rich fragmental deposit and (2) later heating of the deposit from below. Most of the heating probably occurred when extensive sills were emplaced starting about 3.5-3.8 aeons ago. Many or most ridged plains, as well as ledges along steep scarps, are outcrops of the sill material. Other ridged plains are "hybrids" of gullied terrain somehow degraded by the underlying sills. Areal contraction resulting from cooling of the igneous material created ridges in the plains and, consequently, in overlying deposits of all types. Similar igneous activity may have begun earlier but was been obscured by cratering. Gullies cutting young crater rims and young crater-based ages of other gullies suggest that gullying continued long after the main gullying episode. This late gullying was probably the result of late intrusions.

We conclude that the cause of gullying was endogenic and not atmospheric. Furthermore, magmatic activity may have been almost as great in the martian uplands as in the lowlands; the difference is that the igneous rocks are mostly exposed as volcanics in the lowlands but mostly intruded as sills in the uplands.

---

[1] Scott D.H. and Carr M.H. (1978) USGS Map I-1083.
[2] Scott D.H. and Tanaka K.L (1987) USGS Map I-1802A.
[3] Greeley Ronald and Guest J.E. (in press) USGS Map I-1802B.
[4] Pieri D.C. (1980) Science **210**, p. 895-897.
[5] Carr M.H. and Clow G.D. (1981) Icarus **48**, p. 91-117.
[6] Mars Channel Working Group (1983) Bull. Geol. Soc. Amer. **94**, p. 1035-1054.
[7] Carr M.H. (1986) Icarus **68**, p. 187-216.
[8] Wilhelms D.E. and Baldwin R.J. (1986) Lunar Planet. Sci. **XVII**, p. 948-949.
[9] Raitala J.T. (1987) Lunar and Planet. Sci. **XVIII**, p. 814-815.
[10] Tanaka K.L. (1986) J. Geophys. Res. **91**, p. E139-E158.
[11] Squyres S.W., Wilhelms D.E. and Moosman A.C. (1987) Icarus **70**, 385-408.

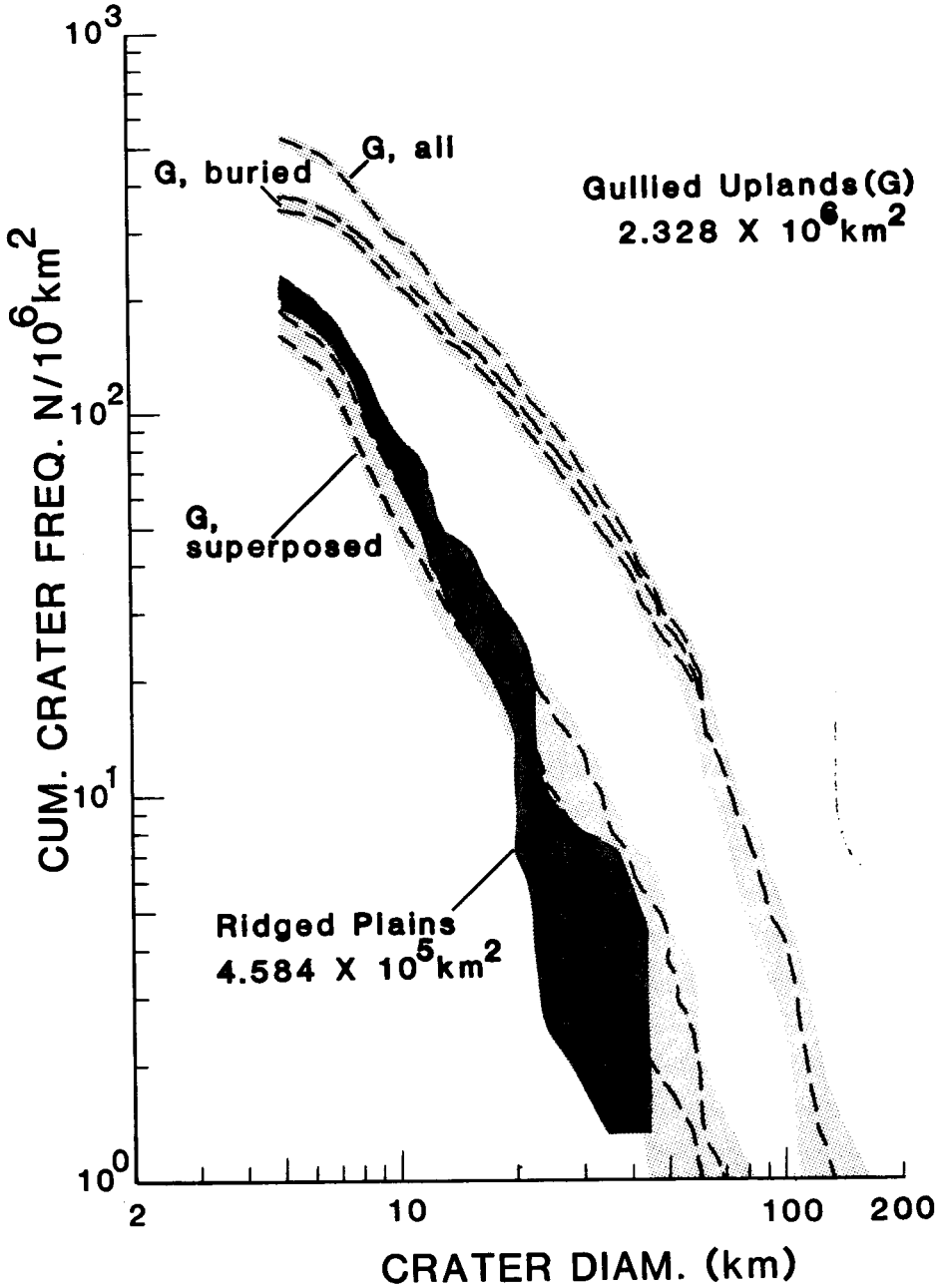

Fig. 1. Cumulative size-frequency distributions of >5-km craters in MC-22 NE, MC-23 NW, and MC-23 SW (lat. 0°-30° S., long. 202.5°-247.5° W.). Curve for ridged plains applies to craters superposed on the plains. Separate curves for the gullied terrain (G) show craters superposed on, and partly buried by, the gullied deposit. In each of these, the lower dashed line represents the craters whose relations are clear and the upper dashed line includes these plus a group that appears superposed but that is degraded and thus could be partly buried. The shaded envelopes of all curves are defined by 1-σ error bars.

H 2086781 N88-29701 S47-91 154947 30

VARIATION IN THE THICKNESS OF EJECTA COVER ON MARS WITH INCREASING CRATER DENSITY, A. Woronow, Geosciences Department, University of Houston, Houston, TX 77004.

Even relatively young surfaces on Mars have superposed craters and must carry a dusting of impact debris. For increasingly more ancient surfaces, deposits of ejecta generally increase in thickness, and the signatures of the geology beneath become more obscured. Although we can do nothing about this obscuration, we can describe these newer deposits, temporally and spatially, and thereby avoid falsely interpreting the geology beneath. We begin the task of temporal and spatial characterization by considering the areal variability of ejecta cover with increasing exposure to meteorite bombardment. This study establishes a baseline for evaluating the quality and distribution of exposures of strata lying temporally beneath the ejecta. Of special interest to this meeting is the distribution of ejecta overlying surfaces that have never sustained a direct impact by a large meteorite, for these retain the volcanic and sedimentary stratigraphy in its most pristine state.

Method

This simulation incorporates the effects of cratering only; as yet it includes no eolian erosion, no fluvial erosion, no tectonic nor volcanic processes. But cratering pervades the martian surface as it does the surface of the Moon and accounts for much of the structure and stratigraphy of their ancient terrains. The numerical density of preserved craters on the ancient terrains of Mars approaches that of the lunar highlands, and probably is only a vestige of an equal or greater barrage. Therefore, the ejecta deposits on Mars must be as extensive as those on the Moon, and their distribution also must be analogous to the Moon's.

An entirely new Monte Carlo simulation is under development along the lines of (1). It currently includes complex crater geometries (flat floor, inner rim, inward-sloping ejecta blanket, and exponentially decaying outward ejecta blanket) according to the parameters given by (2). Crater ejecta blankets extend to five radii from the crater center, conserve excavated volume, and so far mimic ballistic emplacement only. This simulation utilizes a variable-size, gridded target surface with an evolving topography interpolated between the grid points. The grid points serve too as sample points of ejecta thickness.

Crater diameters are selected at random from the production distribution function defined by (3) for craters greater than 8 km in diameter. Crater centers are located uniformly randomly on the surface at the instantaneous local elevation. A zone around this target surface can receive impacts and spray ejecta onto the target surface, but data are not retained on that extended zone.

Results

In applying these results, one must scrutinize the martian surfaces under study for both local and regional resurfacing. Resurfaced terrain will match the ejecta-cover conditions of the simulation of lightly cratered surfaces. But as the density of superposed craters increases, one might expect an orderly increase in the thickness of the ejecta cover. To some degree this is the case; however, the excavation into, and removal of, preexisting ejecta cover by later cratering complicates this overall trend.

Relatively lightly cratered surfaces, such as 0.5 times the observed lunar highlands density (OLHD), have distributions of ejecta thicknesses with more symmetry than those for higher crater densities, which are progressively more skewed toward greater ejecta thicknesses (compare Figure 1a with Figures 1b-d). The range of thicknesses, however, does not change rapidly with increasing crater density, although the upper limit of the ejecta thickness creeps upward slightly and steadily. The uncovered or thinly covered regions of the lightly cratered surfaces are gradually more deeply covered, but craters continually excavate through this cover, and provide fresh exposures so that the

percentage of surface showing through the ejecta dusting tends toward a constant with increasing exposure time (Figure 2). But with increasing crater density, the exposures through the ejecta cover become restricted to the crater walls and floors. Of interest are the regions having experienced zero impacts. Figures 3a-c illustrate the distribution of debris overlying these regions. In comparisons with their counterparts in Figure 1, the 0.5x OLHD case shows little difference--particularly in the critical thinly covered tail. But by 1x OLHD, this tail is being bobbed, and by 3x OLHD it is essentially gone. That is, by 3x OLHD the surface is so covered by ejecta that only crater floors and walls provide views to the strata below.

Conclusions

The surface of Mars must have sustained an impact flux at least as great as that of the lunar highlands. That cumulative flux has been estimated to be between 3x OLHD (4) and 5x OLHD (5). Although some regions will escape direct impacts even at these high cumulative fluxes, only very rare regions may have ejecta cover less than 1/2 km thick unless some other geologic process has stripped it away. The hope of observing very ancient, undisturbed strata on spacecraft images or even at the surface seems slight.

For younger strata (e.g. more recent lava flows), however, the ejecta cover becomes progressively less obscuring, and at even 0.5x OLHD original relief on the order of a few meters may reflect the original surface topography and morphology.

The proportion of surface that remains unimpacted will decrease when smaller craters are also considered, but the large craters dominate the mass of the ejecta cover so that the results given in Figures 1 and 3 will probably require only slight alterations.

REFERENCES

1. Cashore, J. and Woronow, A. (1985) Proc. LPSC XV, C811-C815.
2. Pike, R.J. and Davis, P.A. (1984) Abstracts of LPSC XV, 645-646.
3. Woronow, A., Strom, R.G., and Gurnis, M. (1982) Satellites of Jupiter (Morrison, ed.), 237-276.
4. Woronow, A. (1978) Icarus, 76-88.
5. Cashore, J.A. (1987) M.S. Thesis, University of Houston.

Figure Captions

1. The distribution of ejecta thicknesses with increasing cratering: a) 0.5x, b) 1x, c) 3x, and d) 5x observed lunar highlands density.
2. The percentage of surface area remaining unaffected by a direct impact with increasing cratering measured as multiples of the observed lunar highlands crater density.
3. The distribution of ejecta thicknesses with increasing cratering for surfaces that have not sustained a direct impact: a) 0.5x, b) 1x, and c) 3x observed lunar highlands density. Compare these to their counterparts in Figure 1.

FIGURE 1A

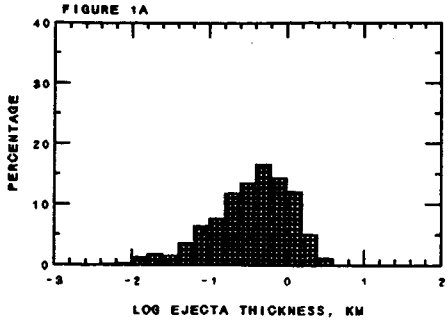

FIGURE 1B

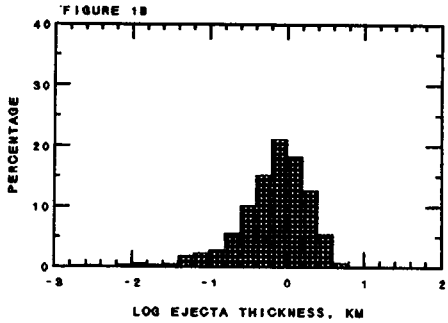

FIGURE 1C

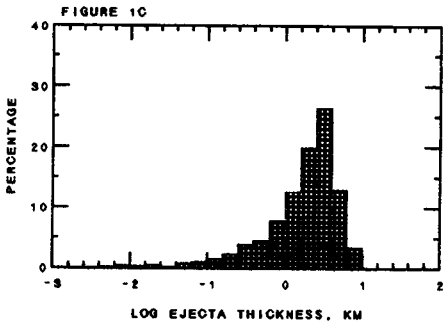

FIGURE 1D

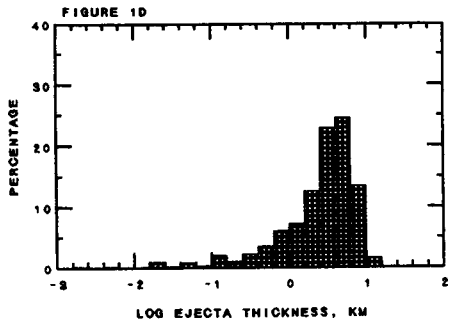

FIGURE 3A

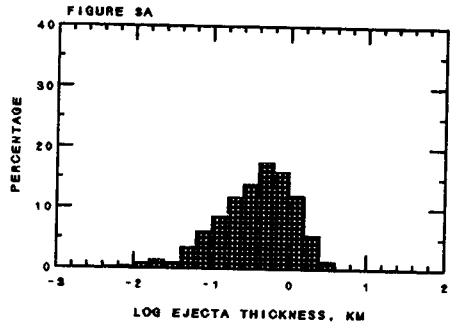

FIGURE 3B

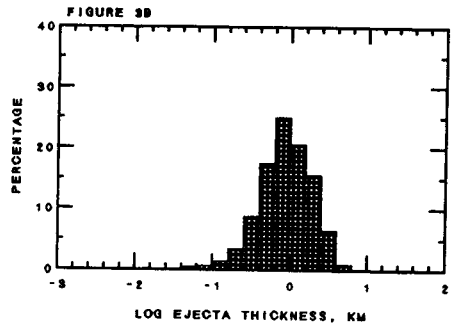

FIGURE 3C

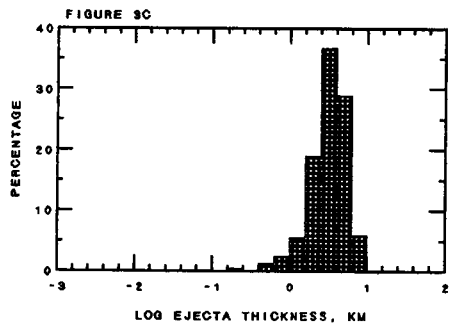

FIGURE 2

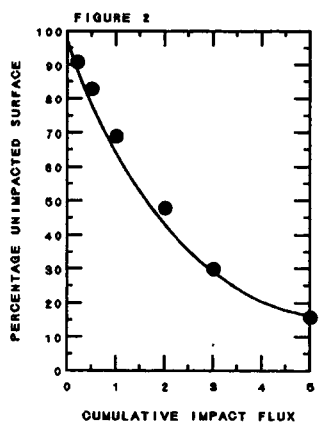

ORIGINAL PAGE IS
OF POOR QUALITY

N88-29702

COADSORPTION OF H_2O AND CO_2 ON THE MARTIAN SURFACE Zent, A. P., Planetary Geosciences Division, Hawaii Institute of Geophysics, University of Hawaii, Honolulu, Hi. 96822

The adsorption of both CO_2 and H_2O has been measured, under conditions of temperature and partial pressure similar to Mars, for a variety of adsorbents (1,2,3,4). Both adsorb at coverages that exceed a monolayer at their respective martian abundances. Clearly, their simultaneous presence in the martian atmosphere will result in coadsorption of both at concentrations that may differ greatly from those measured during separate measurements. To the best of our knowledge, no data exists on the coadsorption of both gases. We have begun to perform co-adsorption experiments and will report pertinent results.

In the meantime we are mathematically exploring the predicted behavior of such a system, as a compliment to our data, and to aid in its eventual interpretation. We report here some of the preliminary results of that effort.

The mathematical treatment of adsorption is exceptionally incomplete. As our primary concern has been volatile exchange between the atmosphere and regolith, we have limited our attention primarily to physisorption. Mathematically the simplest place to start is with the Langmuir isotherm. The derivation of the Langmuir isotherm involves assumptions that we expect to be violated at the the conditions of the martian surface. Specifically, it assumes that there is no more than one molecule of adsorbate per adsorption site, that there is no interaction between adsorbed molecules, and that all adsorption sites have the same adsorption energy. Nonetheless, it has the advantage of being tractable, and can be used to predict the adsorptive coverage of either H_2O or CO_2, separately, (up to a monolayer) with an accuracy of $\pm 50\%$. We note that results must be interpreted with the utmost caution.

We calculate the fraction of adsorption sites occupied by either H_2O or CO_2 by simultaneously solving

$$\theta_{CO_2} = \frac{a_1 p_1}{1 + a_1 p_1 + a_2 p_2}$$

$$\theta_{H_2O} = \frac{a_2 p_2}{1 + a_1 p_1 + a_2 p_2}$$

where the subscripts 1 and 2 refer to CO_2 and H_2O respectively, p is pressure, and a is found from

$$a = n_Q kT \exp\left(\frac{\mu_0}{kT}\right)$$

where μ_0 is the heat of adsorption, and n_Q is the quantum concentration. The heat of adsorption is calculated from adsorption isotherms of both H_2O and CO_2 on Vacaville basalt (1). The quantum concentration is the concentration associated with one molecule in a cube of side equal to the de Broglie wavelength. It is a function of molecular mass and temperature.

Typical results for a sample calculation are shown in Fig. 1. It is assumed that $P_{CO_2} = 7$ mb, and P_{H_2O} is equivalent to 10 pr μm. CO_2 is found to occupy a majority of adsorption sites at all temperatures. We anticipate that this result will apply to Mars as well. A very similar result can be found by relating the average adsorbed lifetime to the heat of adsorption

$$\tau = \tau_0 \exp\left(\frac{\mu_0}{RT}\right)$$

where τ_0 is a property of the solid, related to the frequency of vibration of the atoms in the solid. Typical values of τ_0 are on the order of 5×10^{-14} sec for solids (5). We find from the heats of adsorption calculated from the original isotherms, that $\tau_{H_2O} = 7 \times 10^{-5}$ sec at 200K, and that $\tau_{CO_2} = 9 \times 10^{-8}$ sec at 200K, a factor of ~ 700 shorter that the H_2O lifetime. The collision frequency of CO_2 with a wall is a factor of roughly 4.5×10^3 times greater than for H_2O. Unless the sticking coefficients are greatly different for H_2O and CO_2, (which may be true), then CO_2 should be some 5 times more abundant as an adsorbate than H_2O. Although simple, this calculation provides additional confidence in the result expressed in Fig. 1.

We should also expect that H_2O ice will compete more effectively for H_2O molecules at low temperatures. In Fig. 1, the pressure of H_2O was forced to equal the vapor pressure over ice at temperatures where 10 pr μm of H_2O vapor would be out of equilibrium with ice. This result is independent of assumptions

related to the Langmuir formulation, and should also be expected to hold on Mars.

A note of caution is in order. The calculations discussed above are based on heats of adsorption that were calculated from isotherms measured on basalt. Those basalt samples had been heated in vacuum, and hence adsorption was taking place on relatively clean silicate surfaces. Should the surface functional groups that are visited by physically adsorbed, and exchangeable molecules, be substantially different in character from the surface functional groups of the basalt, for example carbonate ions formed by CO_2 chemisorption, then the figures discussed above are invalidated. If there are two (or more) surface functional groups, and those different groups preferentially adsorbed different molecules, then once again, our results would not apply to the martian surface. Also, molecules that participate in chemical weathering reactions with the substrate must be expected to behave in a manner not consistent with our results.

REFERENCES

1. Fanale, F. P. and Cannon, W., 1971, *Nature* **230**, 502-504.
2. Fanale, F. P., and Cannon, W., 1974, *J. Geophys. Res.* **79**, 3397-3402.
3. Anderson, D. M., et al., 1978, *Icarus*, **34**, 638-644.
4. Zent, A. P., et al., 1987, *Icarus*, In Press.
5. Clark, A., 1970, The Theory of Adsorption and Catalysis, Academic Press.

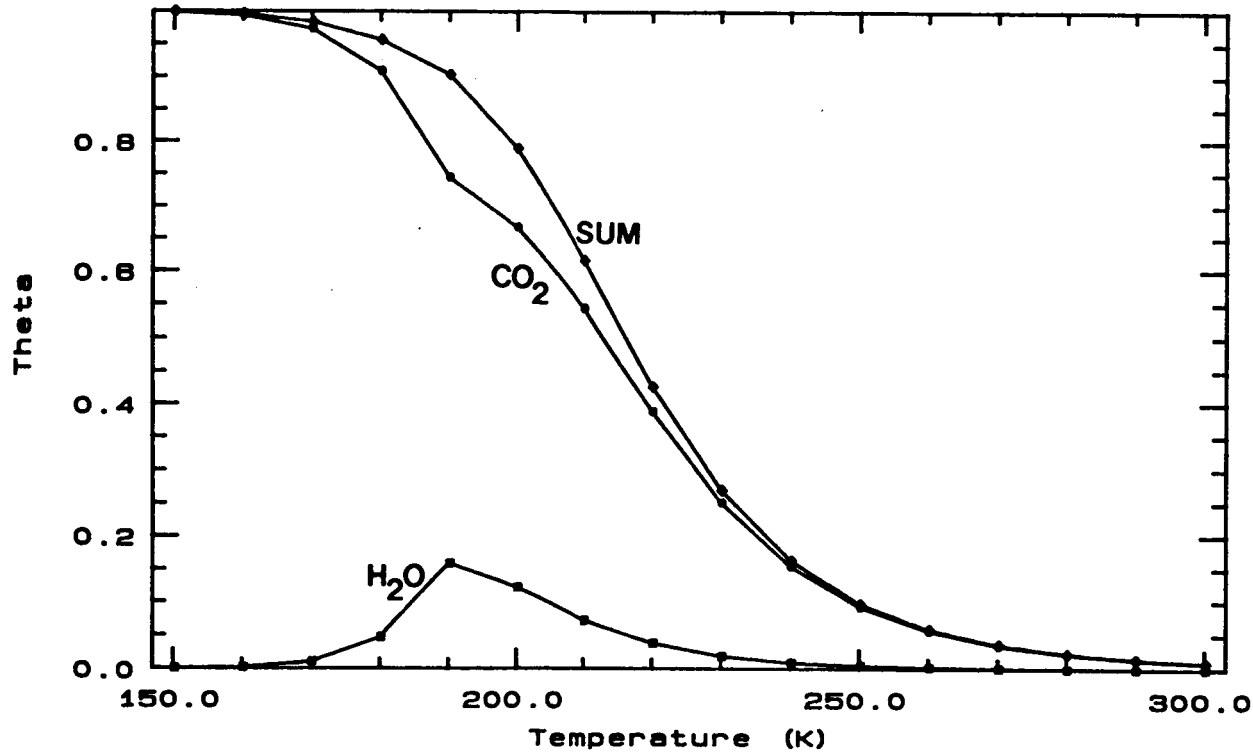

Fig. 1. Results of Langmuir isotherm calculation showing the fraction of adsorption sites filled by H_2O, CO_2, and the total fraction of occupied sites. P_{CO_2} is 7 mb, and the H_2O pressure is equivalent to 10 pr μm.

L 86 18932 9

88-29703

HIGH RESOLUTION VIKING ORBITER IMAGES: A USEFUL DATA SOURCE FOR TESTING THE VIABILITY OF GEOMORPHIC PROCESSES ATTRIBUTED TO MARTIAN LANDFORMS. James R. Zimbelman, Lunar and Planetary Institute, 3303 NASA Road 1, Houston, TX 77058.

The diversity of landforms visible in the Viking images of Mars have led to a proliferation of geomorphic agents proposed to be active in shaping the martian surface. While it is likely that numerous different processes have contributed to the geomorphology of Mars throughout martian history, it is important that proposed martian geomorphic agents be subjected to critical scrutiny by the scientific community. High resolution Viking Orbiter images represent a unique data set for investigating geomorphic processes on Mars.

Geologic mapping of Mars can take place at a variety of scales, utilizing a variety of image resolutions, but an interpretation of the history of individual landforms is dependent upon the best available spatial resolution. It has been shown that aeolian features evident at 9 m/pixel resolution are nondiscernable in images with >50 m/pixel resolution (1,2). Also, stratigraphic relationships important to the interpretation of surface history may be visible at 16 m/pixel resolution but not at 100 m/pixel resolution (3). Of the more than 51,500 Viking Orbiter images (4), only 5% of these images have <20 m/pixel resolution under relatively unhazy atmospheric conditions (3). These high resolution images provide the opportunity to examine proposed martian geomorphic processes.

Landforms inferred to be expressions of surface debris movement aided by creep of interstitial ice include "concentric crater fill" (centripital movement of material from crater rims) and "lobate debris aprons" (convex-profile accumulations at the base of steep scarps) (5,6,7). Fig. 1 shows a moderate resolution view of Utopia Planitia. At high resolution (Figs. 2 and 3), layered materials both outside and inside of a large crater are exposed along erosional scarps, indicating a pervasive presence of thin deposits that are currently subject to erosion. There is no indication of flow of surface materials away from the crater rim; instead, there is a sharp break in slope between the crater rim and the eroded materials surrounding the rim (Fig. 3). There is no clear indication of the origin of the layered (eroded) materials but they do not appear to be forcibly emplaced; a gentle superpositional emplacement seems likely. Lobate debris aprons are very common in the Deuteronilus Mensae region (Fig. 4). At high resolution (Fig. 5), a debris apron appears quite degraded. While there are some lineations in the apron parallel to the adjacent scarp, the lineations are secondary to the highly disrupted state of the entire apron surface. More importantly, there are no features oriented along the inferred direction of flow. A 500 m gap exists between the bulk of the debris apron and the base of the adjacent scarp, even within a crater breached by a scarp (Fig. 5). Since the debris apron is no thicker inside the crater than elsewhere on the apron, it is highly unlikely that concentric flow from the crater rim occured here. A crater on an upland area (Fig. 6) appears to be subject to erosional processes similar to those present in the Utopia area, although discreet layers are not exposed in the Deuteronilus Mensae area.

The high resolution images cast doubt on an ice-related flow origin for some concentric crater fill and lobate debris apron features. It is clear that researchers may not interpret features in the same way but it important that high resolution images of candidate features be made available to the scientific community so that a consensus can be reached. This procedure can provide a way to refine our understanding of geomorphic processes on Mars.

ORIGINAL PAGE IS
OF POOR QUALITY

REFERENCES: (1) Zimbelman, J.R., Lunar Planet. Sci. XVII, 963-964, 1986. (2) Zimbelman, J.R., Icarus 71 (in press), 1987. (3) Zimbelman, J.R., Mars Sample Ret. Sci. Workshop Abs. (in press), 1987. (4) Ezell, E.C., and L.N. Ezell, NASA SP-4212, p.423, 1984. (5) Squyres, S.W., and M.H. Carr, Science 231, 249-252, 1986. (6) Squyres, S.W., Icarus 34, 600-613, 1978. (7) Squyres, S.W., J. Geophys. Res. 84, 8087-8096, 1979.

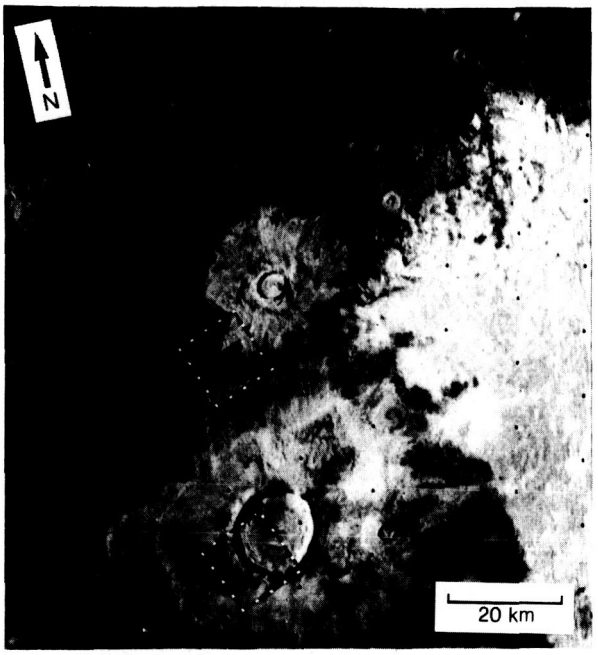

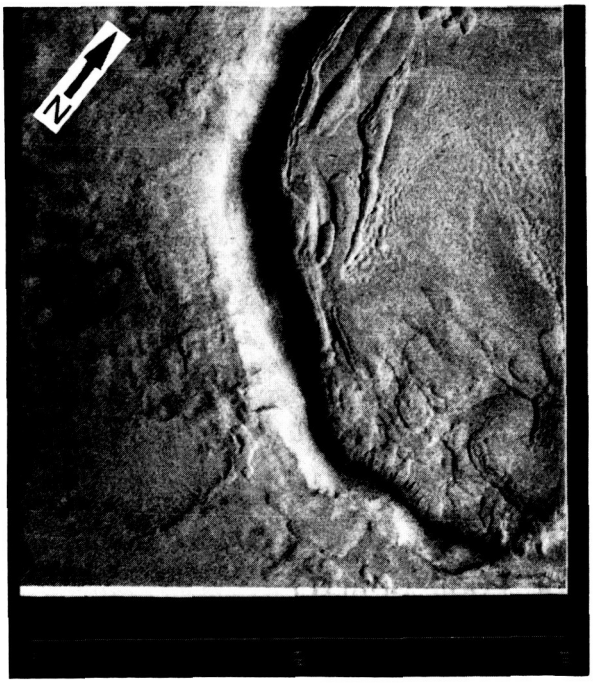

Figure 1 (upper left). Frame 10B42, 89 m/pixel, 45°N, 270°W. Utopia Planitia. Boxes indicate locations of Figs. 2 (top) and 3 (bottom).

Figure 2 (upper right). Frame 466B85, 10 m/pixel. Note layers exposed by erosion of smooth plains material.

Figure 3 (lower right). Frame 466B82, 10 m/pixel. Note layers exposed by erosion within crater (lower right).

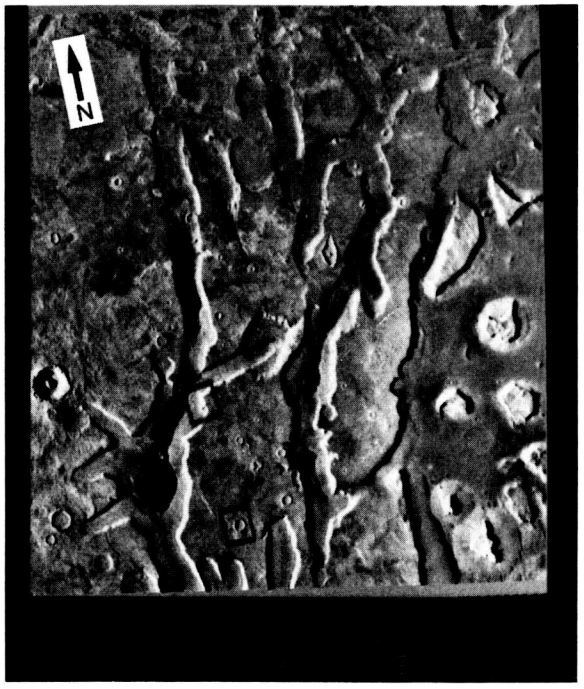

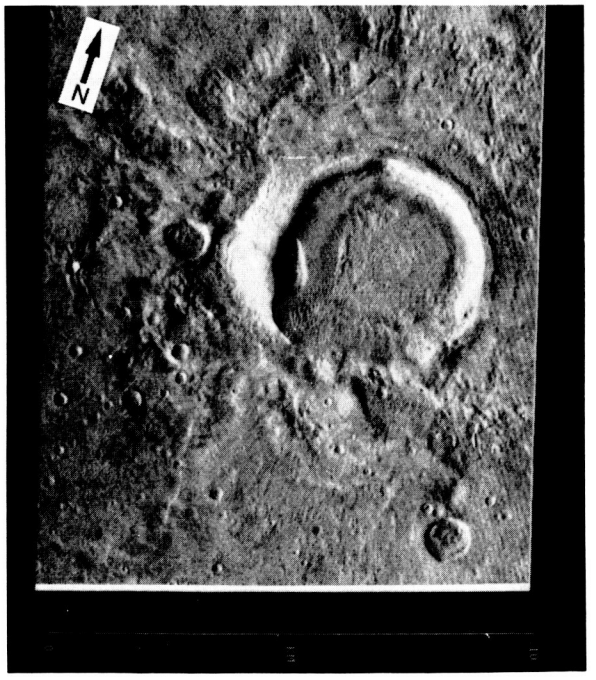

Figure 4 (upper left). Frame 675B59, 200 m/pixel, 46°N, 345°W. Deuteronilus Mensae. Boxes indicate locations of Figs. 5 (top) and 6 (bottom).

Figure 5 (upper right). Frame 458B46, 10 m/pixel. Note degraded appearance of apron surface and the 500 m gap between the apron and the scarp.

Figure 6 (lower right). Frame 458B42, 10 m/pixel. Note the erosion of material that overlies most of the surface and the small ridges (dunes?) within the large crater.

ORIGINAL PAGE IS
OF POOR QUALITY

END

DATE NOV. 15, 1988

Workshop Participants

John B. Adams
University of Washington

Raymond Arvidson
Washington University

C. Aubee
Brown University

Steve Baloga
Jet Propulsion Laboratory

Amos Banin
Hebrew University

Nadine G. Barlow
Lunar and Planetary Institute

Jim Bell
University of Hawaii

Diana Blaney
University of Hawaii

Mark B. Boslough
Sandia National Laboratories

Bob Brakenridge
Dartmouth College

Kevin Burke
Lunar and Planetary Institute

Roger Burns
Massachusetts Institute of Technology

Paul Butterworth
NASA Goddard Space Flight Center

Peter Cattermole
Sheffield University

Benton Clark
Martin Marietta, Denver

Stephen Clifford
Lunar and Planetary Institute

Lelia M. Coyne
San Jose State University

Joy Crisp
Jet Propulsion Laboratory

Larry S. Crumpler
Brown University

Rene De Hon
Northeast Louisiana University

Peter Englert
San Jose State University

Fraser Fanale
University of Hawaii

Bruce Fegley
Massachusetts Institute of Technology

William C. Feldman
Los Alamos National Laboratory

Peter Francis
Lunar and Planetary Institute

Friedeman Freund
NASA Ames Research Center

Herbert Frey
NASA Goddard Space Flight Center

James B. Garvin
NASA Goddard Space Flight Center

John Grant
Brown University

Ronald Greeley
Arizona State University

Robert Grimm
Massachusetts Institute of Technology

John E. Guest
University College of London

Edward Guinness
Washington University

John Holloway
Arizona State University

Bruce Jakosky
LASP/University of Colorado

Krikitt Johnson
Brown University

John Jones
NASA Johnson Space Center

Hugh Kieffer
U.S. Geological Survey, Flagstaff

Elbert A. King
University of Houston

John S. King
State University of New York, Buffalo

Michael Knight
University of Hawaii

Sam Kozak
Washington & Lee University

John Longhi
Yale University

Karen Love
University of Houston

Baerbel Lucchitta
U.S. Geological Survey, Flagstaff

Terry Martin
Jet Propulsion Laboratory

Ted Maxwell
Smithsonian Institution

Mike McCullough
FMC Corporation, San Jose

Lucy-Ann McFadden
University of California, San Diego

James McGee
U.S. Geological Survey, Reston

Kimberly McGeehan
Colorado State University

George McGill
University of Massachusetts

Albert Metzger
Jet Propulsion Laboratory

Henry J. Moore
U.S. Geological Survey, Menlo Park

Peter Mouginis-Mark
University of Hawaii

Scott L. Murchie
Brown University

James Orenberg
San Francisco State University

Frank Palluconi
Jet Propulsion Laboratory

Vivian Pan
Yale University

T. J. Parker
Jet Propulsion Laboratory

Roger Phillips
Southern Methodist University

Carle Pieters
Brown University

Patrick Pinet
GRGS/CNES, France

Susan Postawko
University of Hawaii

Bob Reedy
Los Alamos National Laboratory

Don Rendquist Jr.
FMC Corporation, Santa Clara

Ted L. Roush
NASA Ames Research Center

Mac Rutherford
Brown University

Martha W. Schaefer
University of Maryland

Peter Schultz
Brown University

Deborah Schwartz
NASA Ames Research Center

Dave Scott
U.S. Geological Survey, Flagstaff

Michael Sims
NASA Ames Research Center

Robert Singer
University of Arizona

David E. Smith
NASA Goddard Space Flight Center

Milton Smith
University of Washington

Sean Solomon
Massachusetts Institute of Technology

Ed Stolper
California Institute of Technology

Ken Tanaka
U.S. Geological Survey, Flagstaff

Ross Taylor
Australian National University

Thomas Thompson
Jet Propulsion Laboratory

Allan Treiman
Boston University

Donald Turcotte
Cornell University

James Underwood
NASA Headquarters

Thomas R. Watters
Smithsonian Institution

Don Wilhelms
San Jose State University

Alex Woronow
University of Houston

Aaron Zent
University of Hawaii

James Zimbelman
Lunar and Planetary Institute

Maria Zuber
NASA Goddard Space Flight Center